Synthesis and Characterization of Cyclopentadiene-fused Polyaromatic Hydrocarbon Radicals

Zur Erlangung des akademischen Grades eines

DOKTORS DER NATURWISSENSCHAFTEN

(Dr. rer. nat.)

von der KIT-Fakultät für Chemie und Biowissenschaften

des Karlsruher Instituts für Technologie (KIT)

genehmigte

Dissertation

von

M. Sc. Ali Samet Acan

aus Lübeck, Deutschland

1. Referent: Prof. Dr. Joachim Podlech

2. Referent: Prof. Dr. Stefan Bräse

Tag der mündlichen Prüfung: 18.12.2025

“How do you pick up the threads of an old life? How do you go on, when in your heart you begin to understand... there is no going back? There are some things that time cannot mend. Some hurts that go too deep, that have taken hold.”

— Frodo Baggins (The Lord of the Rings)

Declaration of Honesty

This work was carried out from March 2023 through November 2025 at the Institute of Organic Chemistry, Faculty of Chemistry and Biosciences at the Karlsruhe Institute of Technology (KIT) under the supervision of Prof. Dr. Joachim Podlech.
Die vorliegende Arbeit wurde im Zeitraum von März 2023 bis November 2025 am Institut für Organische Chemie, Fakultät für Chemie und Biowissenschaften des Karlsruher Instituts für Technologie (KIT) unter der Leitung von Prof. Dr. Joachim Podlech durchgeführt.

Parts of this work have already been published:

- Ali S. Acan, Jonas O. Wenzel, Frank Breher, Joachim Podlech, A Stable Carbon-Centered Radical Showing Six Amphoteric Redox States, *Chem. Eur. J.* **2025**, 31, e202403670.
- Ali S. Acan, Jonas O. Wenzel, Joachim Podlech, Cyclopenta-Fused Polyaromatic Hydrocarbon (CP-PAH) Radicals: Synthesis, Characterization, and Quantum Chemical Calculations, *Chem. Eur. J.* e02467.

Hereby I, Ali Samet Acan, declare that I completed this work independently, without any improper help and that all material published by others is cited properly. This thesis has not been submitted to any other university before.
Hiermit erkläre ich, Ali Acan, dass ich diese Arbeit selbstständig, ohne unzulässige Hilfe, angefertigt und alle fremden Quellen ordnungsgemäß zitiert habe. Diese Arbeit wurde bisher an keiner anderen Universität eingereicht.

Karlsruhe, November 4th, 2025
Ali Samet Acan

German Title of the Thesis:

Synthese und Charakterisierung von Cyclopentadien-haltigen Polyaromatischen Kohlenwasserstoff Radikalen

Table of contents

1 Abstract/Kurzzusammenfassung

Polycyclic aromatic hydrocarbons (PAHs) and polyarenes (PAs) have fascinated chemists for many years and have played a significant role in shaping the field of organic chemistry. In recent years, interest has resurged, particularly in non-alternant systems such as indenofluorenes (IFs). More recently, open-shell systems within this class of compounds have been found to be stable under ambient conditions, a key requirement for both their detailed investigation and potential applications. These radical species exhibit a range of promising electronic, optical, and magnetic properties, making them suitable candidates for use in organic electronics and organic magnets. Their intrinsic paramagnetic behavior opens opportunities in spintronics and could pave the path for the development of fully organic spintronic devices.

This study focused on the systematic exploration of IF-based PAH radicals with the goal of synthesizing compounds composed of alternating benzene and cyclopentadiene units with an odd number of five-membered rings, as these inherently adopt a radical nature in their fully conjugated state. A comprehensive investigation of their physical and spectroscopic properties using a combination of experimental measurements and quantum chemical calculations enabled to gain deeper understanding of the properties and to complement the experimental results. In most cases, the required kinetic stability is provided by mesitylene groups acting as bulky substituents, limiting the variability of different possible substituents. To address these limitations, one focus of this work was the development of a broadly applicable synthetic strategy and the incorporation of diverse substituents, to assess their influence and derive general principles for radical stabilization. As an increase in the size of the molecular scaffold is expected to lead to a decreased HOMO/LUMO gap, the extension of the π-system was pursued to investigate this effect. Most recent reported structures are mainly based on monoradical systems. Therefore, further investigation was conducted regarding increasing the number of potential radical centers and enabling the synthesis of compounds, potentially exhibiting triradical- or even pentaradical character.

Polyzyklische aromatische Kohlenwasserstoffe (PAK) und Polyarene (PA) haben Chemiker seit vielen Jahren fasziniert und eine wichtige Rolle in der Entwicklung der organischen Chemie gespielt. In jüngerer Zeit ist das Interesse insbesondere an nicht-alternierenden Systemen wie Indenofluoren (IFs) wieder gestiegen. In jüngster Zeit wurde entdeckt, dass offene Schalen-Systeme innerhalb dieser Verbindungsklasse unter Umgebungsbedingungen stabil sein können, eine entscheidende Voraussetzung sowohl für ihre detaillierte Untersuchung als auch für potenzielle Anwendungen. Diese Radikale weisen eine Vielzahl vielversprechender elektronischer, optischer und magnetischer Eigenschaften auf, wodurch sie sich für den Einsatz in der organischen Elektronik und in organischen Magneten eignen. Ihre intrinsisch paramagnetischen Eigenschaften eröffnen zudem neue Perspektiven in der Spintronik und könnten den Weg für die Entwicklung vollständig organischer spintronischer Komponenten ebnen.

Diese Arbeit widmete sich der systematischen Untersuchung von IF-basierten PAK-Radikalen mit dem Ziel, Verbindungen aus Benzol- und Cyclopentadien-Einheiten mit einer ungeraden Anzahl an Fünfringen zu synthetisieren, da diese im vollständig konjugierten Zustand eine radikalische Natur annehmen. Die physikalischen und spektroskopischen Eigenschaften wurden durch eine Kombination aus experimentellen Methoden und quantenchemischen Berechnungen analysiert, um ein tieferes Verständnis zu gewinnen und die experimentellen Ergebnisse zu ergänzen. In den meisten Fällen wird die nötige kinetische Stabilität durch sperrige Mesitylsubstituenten gewährleistet, was die Variabilität der möglichen Substituenten stark einschränkt. Daher lag ein Fokus auf der Entwicklung einer flexiblen Synthesestrategie sowie der Einführung unterschiedlicher Substituenten, um deren Einfluss auf die Radikalstabilität zu untersuchen und Prinzipien zur Radikalstabilisierung abzuleiten. Zusätzlich wurde die Erweiterung des π-Systems verfolgt, da ein größerer Gerüstaufbau eine Verringerung der HOMO/LUMO-Lücke erwarten lässt. Die meisten bisher beschriebenen Strukturen basieren überwiegend auf Monoradikalsystemen. Daher wurden weiterführende Untersuchungen zur Erhöhung der Anzahl potenzieller Radikalzentren durchgeführt, um Verbindungen zu erzielen, die möglicherweise Tri- oder sogar Pentaradikalcharakter aufweisen.

2 Introduction

PAHs and PAs have fascinated chemists for many decades and played a central role in shaping the field of organic chemistry during the 19th and 20th centuries.[1-2] These purely organic compounds consist of two or more fused aromatic rings and are composed exclusively of carbon and hydrogen. They are typically produced during the incomplete combustion of organic materials such as fossil fuels. PAHs are widely distributed in the environment, found in air, water, soil, and sediments, and are known for their environmental persistence and toxicological effects.[3] The study of PAHs began in the late 19th century with the large-scale production of artificial dyes. It reached its peak between 1950 and 1970, driven by the development of theoretical concepts of aromaticity. As a result, numerous aromatic compounds, including benzenoid PAHs and annulenes, were synthesized and studied. In connection with the increased popularity of organic electronic materials, this class of compounds has gained considerable interest in recent years, as they can be potentially utilized as materials for applications in areas such as field-effect transistors (FETs), organic light-emitting diodes (OLEDs), and organic photovoltaic cells (OPVs).[4-6] This reemergence is further supported by simultaneous advances in synthesis methodologies, analytical tools, and theoretical understanding. In additions, efforts to understand the reactivity of PAHs has led to the discovery of many new reaction mechanisms and catalytic pathways, which form the basis of modern physical organic chemistry.[7]

2.1 Alternating versus Non-Alternating Hydrocarbons

Unsaturated conjugated hydrocarbons can be divided into the following two classes: “alternating” and “non-alternating” hydrocarbons, with different typical properties. By definition, a conjugated unsaturated hydrocarbon is non-alternating when the carbon atoms cannot be divided into two sets in which each atom in the first group are adjacent only to atoms in the second group, and vice versa. As a result, any fully conjugated hydrocarbon that includes rings with an odd number of carbon atoms is inherently non-alternating.[8] Classic examples of alternating hydrocarbons include naphthalene, anthracene, and phenanthrene. In contrast, compounds such as pentalene, azulene, and heptalene are classified as non-alternating hydrocarbons. **Figure 1** highlights the contrast between the two classes by comparing naphthalene and azulene and further highlights their differences in their electronic structures. The comparison of naphthalene and

azulene reveals that both classes exhibit distinct electronic configurations and molecular orbital characteristics.[8-11] There are also significant differences in charge distribution between the two classes. Neutral alternating hydrocarbons exhibit a uniform charge distribution, leading to dipole moments that are zero or nearly zero. In contrast, non-alternating hydrocarbons generally have uneven charge distributions and exhibit large dipole moments.[12] This explains the relatively large dipole moment of 1.08 D for azulene in its ground state. Two aromatic ionic components, the cyclopentadienyl anion and the tropylium cation, are fused together and show pronounced reactivity toward both electrophilic and nucleophilic species.

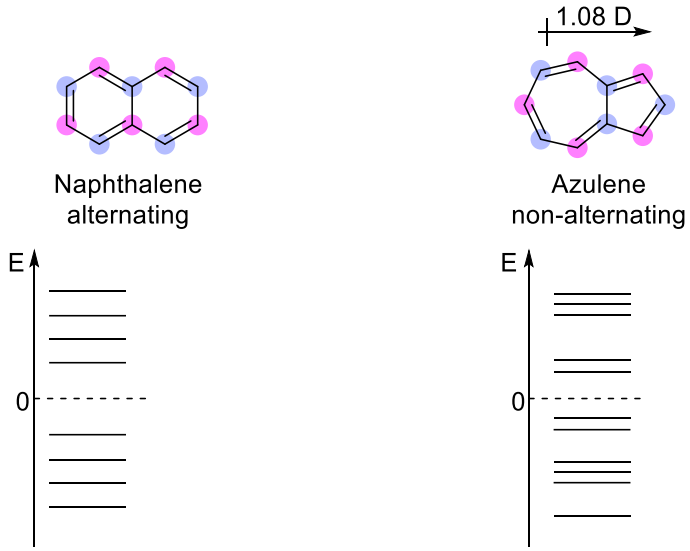

Figure 1: Comparison of Naphthalene and Azulene as alternating and non-alternating hydrocarbons, with their characteristic electronical structures and charge distributions.

In the *Hückel* approximation, alternating hydrocarbons exhibit symmetrical energies and coefficients between their bonding and antibonding orbitals. However, this symmetry is not present in non-alternating hydrocarbons, which leads to a significantly different absorption behavior (**Figure 1**).[12] This contrast is clearly illustrated by comparing the absorption spectra of azulene and naphthalene. A pronounced absorption maximum is observed for azulene at 585 nm, giving it a deep blue color, whereas its isomer naphthalene, with the same number of π-electrons, exhibits a distinct absorption maximum at 312 nm and remains colorless.[13]

2.1.1 Indenofluorenes

In the past few decades, interest in PAHs and PAs has risen again, mainly driven by advancements in synthetic methodologies and modern analytical techniques that have significantly improved the accessibility and characterization of these compounds.[6, 14-15] This renewed attention is primarily due to their unique optoelectronic properties, which are based on extensive π-conjugation and electron delocalization, making them valuable in a wider range of materials, such as organic semiconductors or organic field-effect transistors.[16-17] This resurgence has stimulated the development of various PAH subclasses, including higher order acenes[18-19] and condensed polycyclic aromatics.[4, 20-21] At the same time, PAHs containing five-membered cyclopentadiene rings (CP-PAHs), such as fullerenes,[22] have experienced rapid growth. Among these, indenofluorenes (IFs), a class of non-alternant hydrocarbons, have reemerged as a prominent class of CP-PAHs. As the term "Indenofluorene" suggests, these pentacyclic compounds can be described by the condensation of a fluorene unit with an indene unit, featuring a fully conjugated framework of alternating six- and five-membered rings similar to pentacene, which consists of five linearly fused benzene rings. The IF family consists of five structural isomers (**Figure 2**), which are difficult to distinguish in the literature, as different naming and numbering strategies have been applied over the last century to describe their shape and structure.[23]

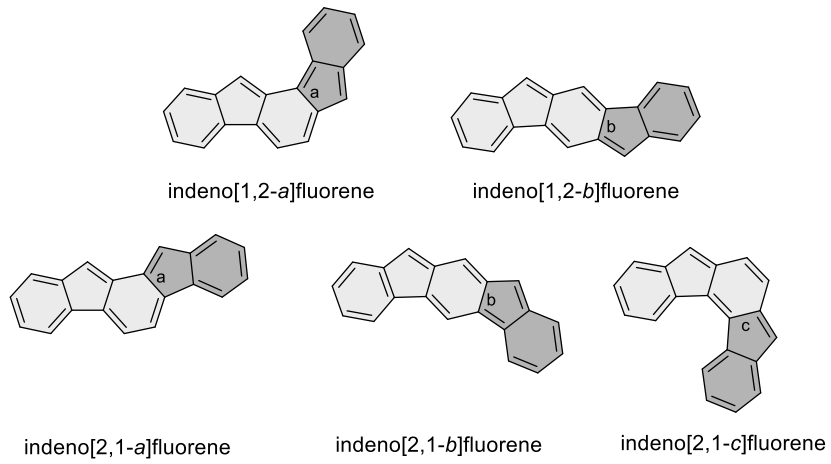

Figure 2: Five possible IF isomers. Isomers [1,2] exhibit an *anti* relationship between the methylene bridges of the five-membered rings, while isomers [2,1] display a *syn* relationship. The letter indicates the position of the ring fusion between the indene and fluorene units.

The current naming system for IF isomers utilize bracketed numbers and a letter to distinguish structural variations. The numbers indicate the orientation of the indene unit

relative to the fluorene core, while the letter indicates the position of the ring fusion between the indene and fluorene units. Isomers labeled [1,2] exhibit an *anti* relationship between the methylene bridges of their five-membered rings, whereas isomers labeled as [2,1] display a *syn* relationship.[24]

These IF isomers also differ in their molecular symmetry. The [1,2-*b*] isomer displays rotational symmetry, and the [2,1-*a*], [2,1-*b*], and [2,1-*c*] isomers each possess a mirror plane. As a result, each isomer presents a distinct ring topology, leading to significant differences in both structural and electronic properties.[24]

From a historical standpoint, the first synthesis of the IF framework dates back to the late 19th century, when *S. Gabriel* reported the synthesis of the [1,2-*a*]IF dione **4** by the condensation of phthalic anhydride **1** with ethyl acetoacetonate **2**, followed by a subsequent esterification (**Scheme 1**).[25]

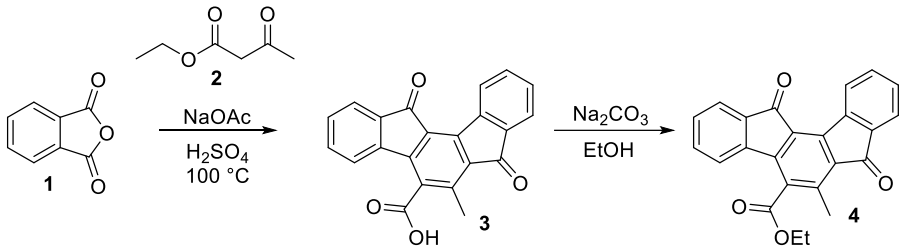

Scheme 1: Synthetic route reported by *S.Gabriel* to obtain [1,2-*a*]IF dione **4**.

Indenofluorenes remained a sporadically explored research topic for several decades, until *Chardonnens* and *Ritter* reported the synthesis of the corresponding parent dione **7** in 1955. By oxidative cleavage of benzo[*e*]acephenanthrylene **5** to generate 2-fluorenonylbenzoic acid **6**, followed by a subsequent acid-mediated ring closure, the IF scaffold **7** could be obtained (**Scheme 2**).[26] Further studies by *Chardonnens et al*.[27-29] resulted in additional condensation products, providing a pathway to various indenofluorene isomers.

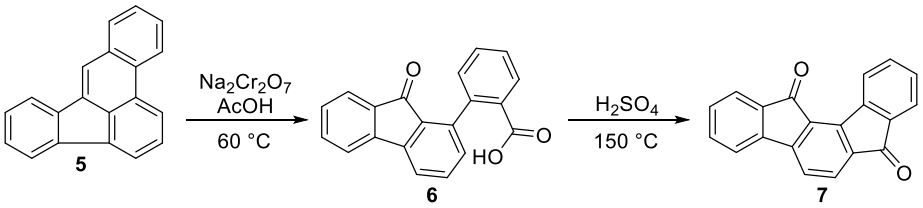

Scheme 2: Alternative approach by *Chardonnens* and *Ritter* to synthesize the unsubstituted [1,2-*a*]IF dione **7**.[26]

To gain access to the different isomers, further synthetic strategies were investigated. For example, the [1,2-*b*]IF scaffold can be obtained following the *Diels-Alder* approach reported by *Merlet et al*.[30] A [4+2] cycloaddition of cyclopentadienone derivatives with diphenylacetylene or phenylacetylene, followed by cheletropic elimination of CO, yields the diester **9**. Subsequent ester hydrolysis and *Friedel-Crafts* cyclization provided the [1,2-*b*]IF-dione scaffold **10** (**Scheme 3**).

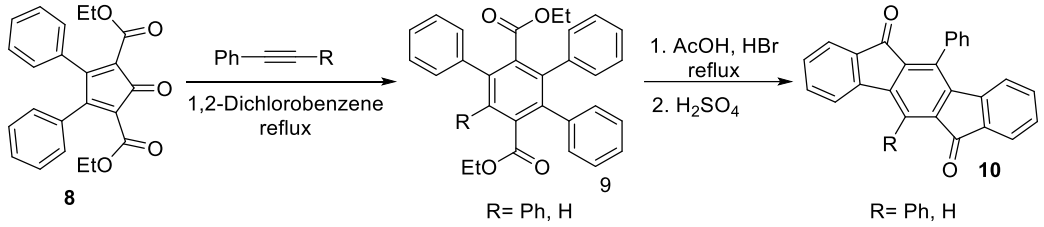

Scheme 3: *Diels-Alder* approach by *Merlet et al.* to generate the [1,2-*b*]IF scaffold **10**.[30]

Contributions towards the [2,1-*a*]IF core date back to 1939, when *Weizmann*[31] proposed the intramolecular *Friedel-Crafts* acylation of 3,6-diphenylphthalic anhydride **11** in refluxing CS_2. The generated fluorenone carboxylic acid **12** was then converted to the corresponding acid chloride, followed by the cyclization in concentrated sulfuric acid to the [2,1-*a*]IF dione **13** (**Scheme 4**). This synthetic approach was later repeated and confirmed by *Deuschel* in 1951.[32]

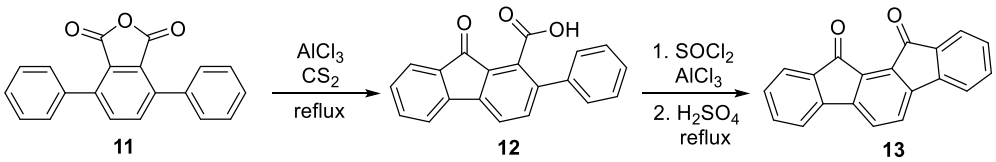

Scheme 4: Synthetic route reported by *Weizmann* to obtain [2,1-*a*]IF dione **13**.[31]

The first [2,1-*c*]IF scaffold was synthesized in 1961 by *Ginsburg* and *Altmann*.[33] They treated indanone **14** with Al-amalgam to obtain pinacol **15**. Elimination and cyclization with maleic anhydride **17** provided anhydride **18**. Decarboxylation produced **19**, which was finally oxidized to give the [2,1-*c*]IF scaffold **20** (**Scheme 5**).

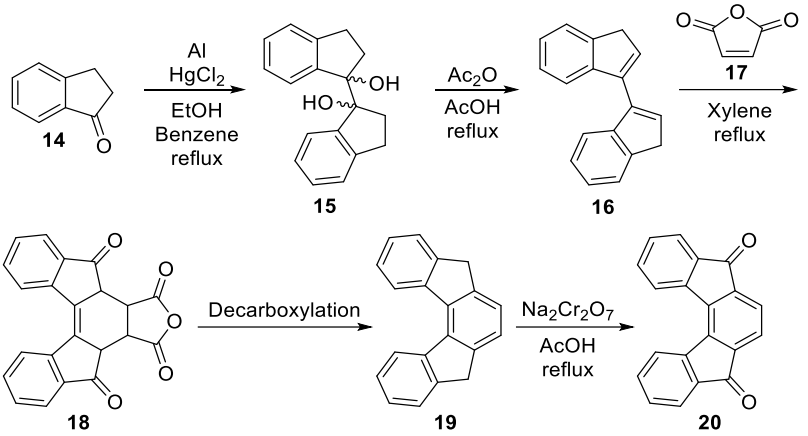

Scheme 5: Synthetic route reported by *Ginsburg* and *Altmann* to obtain [2,1-c]IF dione **20**.[33]

Due to the lack of modern spectroscopic and structural characterization methods at that time, early IF compounds could only be investigated to a limited extent, which ultimately led to a shift in focus away from this area of research.[7] However, interest in IF was revived roughly a decade ago, with the growing recognition of CP-PAHs as promising candidates for organic electronic materials, as recent research has increasingly focused on the use of π-electron-rich compounds in optical and electronic device applications [6, 14-15, 34-36] Among these, acenes like pentacene and its derivatives (**21**)[37-38] have received significant attention.[18-19] However, their susceptibility to oxidative degradation has driven interest in alternative acene-like structures.[39] One promising approach involves the incorporation of heteroatoms,[40] but more recent studies revealed the attractiveness of the [1,2-*b*]IF framework (**23-I** and **23-II**).[41] These pentacyclic compounds contain two fewer carbon atoms and thus two fewer π-electrons than pentacene, making them formally antiaromatic with a total of 20 π-electrons. This antiaromatic character contributes to a reduced HOMO/LUMO gap.[42] Although various compounds in the literature include the [1,2-*b*]IF core, most feature substituents at positions 5 and 11 that either introduce cross-conjugation or disrupt the π-conjugation entirely (**Figure 3**). [43-47]

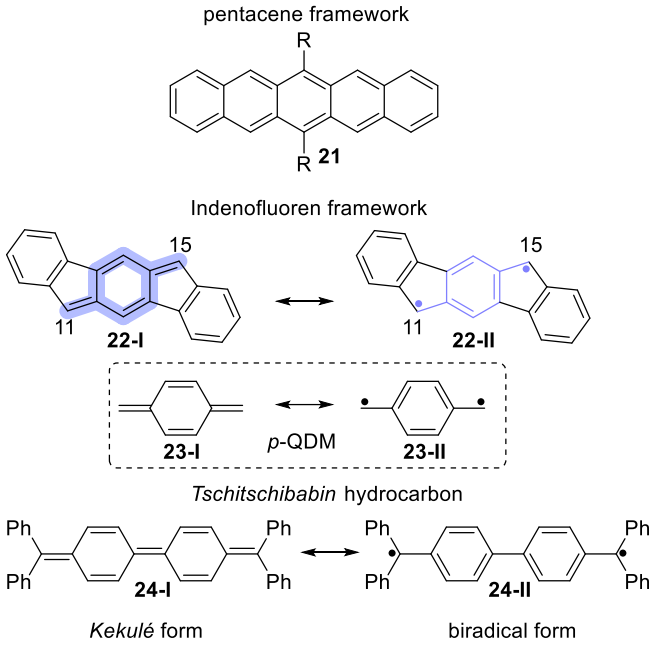

Figure 3: Structures of pentacene **21**, [1,2-*b*]IF in its closed-shell (**22-I**)and open-shell configuration **(22-II**); *p*-quinodimethane (**23-I** and **23-II**); *Tschitschibabin*'s hydrocarbon in the *Kekulé* form (**24-I**) and in its biradical form (**24-II**).

Structurally, these compounds feature a *para*-xylylene (*p*-quinodimethane (QDM); closed-shell configuration, **23-I**) as a subunit, that exists in equilibrium with its biradical form (open-shell configuration, **23-II**). Due to its high reactivity and strong tendency to undergo oligomerization or polymerization, it is typically too unstable to isolate.[48] A similar behavior is observed in the π-extended *Tschitschibabin* hydrocarbon **24-I**, which also exhibits an open-shell configuration **24-II**.[49-50] This *para*-xylylene unit allows for an open-shell configuration for the [1,2-*b*]IF scaffold and the formation of a biradicaloid species, which is further stabilized by the aromatization of the central six-membered ring.[51]

Until recently, examples of fully conjugated species were extremely rare, with only a handful of compounds known to date.[52-54] However, the group of *Haley* has highly contributed towards the synthesis and characterization of fully conjugated IFs in recent years, especially with respect to their biradical character.[55-59]

2.1.2 Organic Radicals

The first reported organic radical was synthesized and characterized by *M. Gomberg* in 1900 in the form of the triphenylmethyl radical (**25-I** and **25-II**). *Gomberg* observed the relatively high instability of the radical, which manifested in its relatively high reactivity and led to its dimerization to the corresponding *Gomberg* dimer **26** (**Scheme 6**).[60]

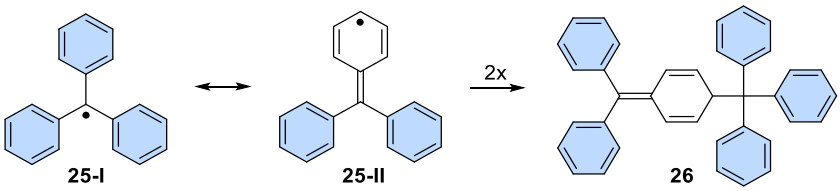

Scheme 6: *Gomberg* radical **(25-I** and **25-II**) and its dimerization to the *Gomberg* dimer **26**.[60]

In general, radical formation typically occurs through the homolytic cleavage of covalent bonds, in which each atom retains one of the shared electrons, resulting in two species with unpaired electrons. The ease of homolysis depends on the bond strength: Weaker bonds can undergo thermal cleavage, while stronger bonds may require high-energy photons to break.[61] In addition to photochemical and thermal methods, radicals can also be generated through ionizing radiation, such as X-rays, or via electrochemical processes involving oxidation or reduction.[62]

As discussed in the previous chapter, another property of IF is their classification as biradicaloid species. Most biradicaloids are typically characterized by QDM substructures, which can exist in three different types: *para*-quinodimethane (*p*-QDM), *ortho*-quinodimethane (*o*-QDM), and *meta*-quinodimethane (*m*-QDM, more accurately described as *m*-xylylene).

These subunits can be found in some of the IF scaffolds and thus enable the formation of the open-shell configuration with three *Clar* sextets. According to *Clar's* rule, the most important resonance structure of a polycyclic system is the one that contains the maximum number of aromatic sextets. This structure best represents the stability and electronic properties of the compound.[2] As a result, compound **28**, **29**, and **31** gain one additional benzene unit compared to their closed-shell configuration, while compound **27** and **30** gain two. This leads to a diradical character that is relatively weak in compound **28**, **29**, and **31**, but strongly pronounced in compound **27** and **30** (**Figure 4**).[23, 63-65] These

structural differences suggest that each isomer probably has different optical and electronic properties.[23]

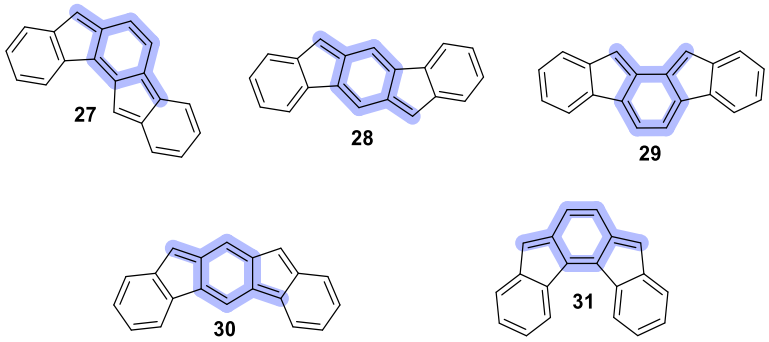

Figure 4: The five possible IF isomers **27**, **28**, **29**, **30**, **31** with their QDM substructures highlighted in blue.

The intrinsic reactivity of radical species can be modulated by delocalizing the unpaired electron density across multiple aromatic rings (as seen in systems like phenalenyl) and/or by providing kinetic stabilization through bulky substituents such as mesityl groups.[49] The extent to which a biradical resonance structure contributes to the overall electronic ground state is quantified by the biradical character index, y_0.

Natural orbitals (NOs) are fundamental in assessing biradical character, with their corresponding occupation numbers, natural orbital occupation numbers (NOONs), serving as a reliable indicator of singlet biradical character.[66] Specifically, the biradical nature can be estimated by examining the occupation numbers of the highest occupied natural orbital (HONO) and the lowest unoccupied natural orbital (LUNO). The natural orbital occupation numbers can be obtained through quantum chemical calculations by applying *Yamaguchi's*[67] scheme, which utilizes the orbital overlap T_0, to quantify the interaction between the frontier molecular orbitals (**Eq. 1**):[68-70]

$$y_0 = 1 - \frac{2 \cdot T_0}{1 + T_0^2}$$

Equation 1: Equation for the calculation of $\boldsymbol{y_0}$, with $\boldsymbol{T_0}$ describing the orbital overlap.

In an Unrestricted *Hartree-Fock* (UHF) approach, T_0 can be calculated with the occupation numbers n of the HONO and the LUNO, as obtained from an NBO (Natural Bond Orbital) analysis (**Eq. 2**).[71-72]

$$T_0 = \frac{n_{HONO} - n_{LUNO}}{2}$$

Equation 2: Calculation of $\boldsymbol{T_0}$.

The NBO analysis transforms the HF-MOs delocalized over the entire molecule into electron pairs that are localized on single atoms or between two atoms and thus links the orbital model with the *Lewis* representation. Ideally, a fully occupied NO has an occupation number of $n = 2$. The diradical character is then expressed by the index y_0. This index spans a continuum where $y_0 = 0$, corresponding to a fully closed-shell configuration, to $y_0 = 1$, representing a fully open-shell biradical. However, the y_0 value should be viewed with caution, as it is often overestimated.[73]

Although the class of biradicaloids represents a fascinating group of compounds, further research has led to the discovery of species that not only exhibit radical properties but are genuine radicals in their neutral ground state.[74]

Most radicals either have their radical center located on a heteroatom or are stabilized by heteroatoms or substituents derived from them. Only a few examples of carbon-centered stable radicals are known, particularly those that exist as pure hydrocarbons. These can be traced back to a small number of recurring structural motifs, which can be modified through variations in connectivity, substitution patterns, and the fusion of additional aromatic rings.[75-77]

Considered as one of the simplest members of the conjugated hydrocarbon radicals, the cyclopentadienyl radical has hardly been investigated and found only limited application due to its high reactivity.[76] However, sufficient stability can be achieved by protecting the positions of highest spin densities with bulky substituents such as mesityl groups, preventing possible side reactions emerging from the radical properties, *e.g.*, σ-dimerization.[78]

Interest in organic radicals has continued to grow, leading to the discovery and study of numerous carbon-centered hydrocarbon radicals. In addition to their intriguing structural features, these radicals possess a range of notable properties including electronic, optical, and magnetic characteristics, that make them suitable for applications in organic electronics[79] and nonlinear optics.[80] Their paramagnetic nature also allows possibilities for use in spintronics[81] and as organic magnets,[82] potentially paving the way for the development of fully organic spintronic devices.[83] Nearly all of them can be categorized into distinct categories based on their structural or electronic properties. These include triarylmethyl radicals, cyclopentadienyl-[84-86] and fluorenyl-based systems,[87] and radicals

embedded within electron-push-pull frameworks[88] or extended π-conjugated systems.[89] A selection from different classes is given in **Figure 5** and includes compounds based on the fluorenyl **32**,[87] **33**,[90] and the truxene motif **34**.[74] Another example is the phenalenyl radical **35**,[91] along with **36** as a hybrid structure combining both the phenalenyl and fluorenyl motifs.[92]

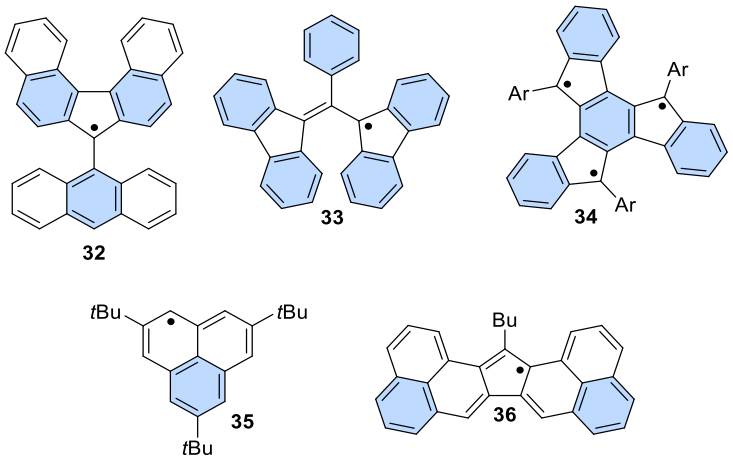

Figure 5: Selection from different classes of carbon-centered radicals, including structures based on the fluorenyl (**32** and **33**), truxene **34** and phenalenyl motif **35**, as well as the hybrid structure **36** containing both phenalenyl and fluorenyl motifs. Fully intact benzene units are highlighted in blue.

The radical based on the truxene motif (**34**) represents a particularly interesting system. It represents a CP-PAH with an odd number of five-membered rings. Motifs that exhibit this property are necessarily radicals in their neutral and fully conjugated state.[93-94] Furthermore, this radical is reported to be present in its triradical configuration in contrast to its monoradical configuration, which is represented by its quinoidal form and hence has two fewer intact benzene units.[74] Thus, the triradical state of this truxene should be the predominant in the ensemble of possible resonance formulas. However, investigations by quantum chemical calculations of similar systems have revealed, that the monoradical species has a more significant contribution in contrast to the triradical species.[93-94]

As previously introduced, the rule of *Clar* also provides a simple and effective way to estimate aromaticity, an important characteristic of fully conjugated polycyclic systems.[95] However, since it cannot be measured directly, it has been a subject of ongoing discussion among many scientists.[96]

The next chapter will explore the historical development of aromaticity and highlight the importance of this concept, in order to provide a deeper understanding of the chemistry of polycyclic systems and enable more precise conclusions.

2.1.3 Aromaticity

Until today, the precise definition of aromaticity remains a major challenge. Since there is no direct way to measure it, its definition and practical relevance continue to be the subject of ongoing discussion.[96] While originally associated with benzene and related compounds, the concept of aromaticity has broadened significantly to include a wide variety of molecules featuring two- or three-dimensional networks of delocalized electrons. Fundamentally, aromaticity describes the increased thermodynamic stability found in systems with cyclic electron delocalization. Such compounds typically retain their structural integrity during chemical reactions and exhibit characteristic features such as bond-length equalization, unique reactivity patterns, and distinct magnetic and spectroscopic behavior.[96] While aromaticity is often evaluated based on structural, energetic, or magnetic criteria, each comes with its own limitations and uncertainty, highlighting the complexity and richness of the concept.[96]

From a historical perspective, the discovery of benzene in 1825 by *Faraday*[97] can be considered as the starting point leading to the development of new theories and models in the concept of aromaticity. Later contributions by *Hückel* in 1931 offered a fundamental tool for the identification of aromatic compounds. According to *Hückel's* rule, molecules that are cyclic, planar, and fully π-conjugated with [4n+2] delocalized electrons are classified as aromatic.[98] *Dewar* and *Breslow* later formulated the [4n] π-electron rule to characterize antiaromatic compounds.[99-101]

Further research showed that not all systems can be characterized by these criteria. In 1924, *Heilbronner* discovered that large-ring polyenes can adopt a twisted topology, giving rise to what are now referred to as *Möbius* systems. This twisting introduces a phase inversion between adjacent p-orbitals, resulting in an odd number of nodes within the π-system. Consequently, *Hückel's* rule is effectively reversed in *Möbius* aromatics, which are stabilized by [4n] π-electrons rather than the [4n+2] required for *Hückel* aromaticity.[102-103] In addition to *Möbius* systems, there exists a class of compounds known as homoaromatic compounds. These molecules exhibit aromatic-like behavior

despite having a disruptive cyclic conjugation, typically caused by one or more saturated (sp^3-hybridized) atoms within the ring.[104-105] Examples of such systems are shown in **Figure 6** and include **37** *(Möbius* aromat) and the homotropylium cation **38** (Homoaromat).

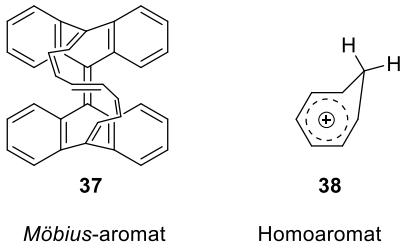

Figure 6: Aromaticity beyond the concept defined by *Hückel*; *Möbius* aromat **37** and homotropylium cation **38** (Homoaromat).

2.1.3.1 Criteria of Aromaticity

As already mentioned, there is no single parameter that directly quantifies aromaticity. However, numerous approaches have been proposed that suggest that the estimation of aromaticity should be based on a combination of experimentally measurable and theoretically calculable parameters. Neglecting one of these factors or moreover defining it as a purely theoretical concept without any experimental evidence, risks losing its practical significance. Yet, it remains unsolved, which parameters are best to describe these systems. One possible approach is to use stabilization energy as a parameter. But the aromatic stabilization energy (ASE) is not clearly defined and is highly dependent on the choice of system. Moreover, there is no absolute reference point for ASE, hence aromaticity is often evaluated indirectly through physiochemical properties. Overall, these obstacles challenge the reliability in determining ASE.[106-107] Another promising approach arises from the utilization of the magnetic and structural criteria, since both allow experimentally measurable evidence by NMR and X-ray crystallographic analysis. The magnetic criteria, in particular, allow great advantages in assessing aromaticity. In the presence of a magnetic field, aromatic compounds generate a diatropic (stabilizing) ring current, whereas antiaromatic systems exhibit a paratropic (destabilizing) ring current.[96, 108] These ring currents, along with their induced magnetic fields, can be easily detected using NMR spectroscopy, effectively bypassing the difficulties associated with selecting an appropriate reference system.[109] Although the induced ring currents in aromatic systems cannot be measured directly, their existence can be deduced from chemical shifts. For this purpose, the ring current model (RCM) can be utilized (**Figure 7**).[110]

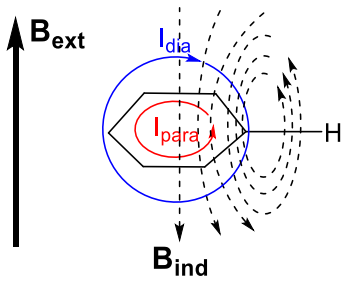

Figure 7: Ring current model displaying ring current and induced magnetic field in benzene.

In aromatic compounds, the application of an external magnetic field induces a diatropic ring current, which generates a secondary magnetic field opposing the external field at the center of the ring. This results in shielding of NMR-active nuclei inside the ring, causing their resonances to shift upfield (to lower δ values). In contrast, outside the ring, the induced magnetic field reinforces the external field, leading to deshielding of nearby nuclei and a downfield shift (to higher δ values). In antiaromatic systems, a paratropic ring current is induced, reversing this pattern, nuclei inside the ring become deshielded, while those outside experience shielding.[111] Although NMR spectroscopy is among the most direct experimental methods for detecting ring current effects, chemical shifts are influenced by multiple factors beyond aromaticity. Therefore, ^{1}H NMR chemical shifts should be considered only as a qualitative indicator of aromaticity.[96]

In recent years, computational methods based on density functional theory (DFT) have become powerful tools for analyzing and characterizing the aromatic or antiaromatic nature of molecules. Among the various approaches, the Nucleus-Independent Chemical Shift (NICS), originally invented by *Schleyer* and coworkers,[112] has proven especially valuable. NICS is defined as the negative value of the absolute magnetic shielding calculated at the center of a ring or at a strategically chosen point, typically positioned above the ring plane.[113] Rings with negative NICS values are considered aromatic, with increasingly negative values indicating stronger aromatic character. Non-aromatic systems generally tend to exhibit NICS values close to zero, while positive NICS values are characteristic of antiaromatic species.[114] Initially, NICS values were calculated at the center of the ring. However, it was later discovered that contributions from the σ-electrons can significantly influence these values. To minimize this effect, it was recommended to compute NICS values above the molecular plane, usually at the distance of 1.0 Å (NICS(1)) above the ring plane.[115] This method was later extended for the study of polycyclic systems for predicting global, semiglobal, and local ring currents.

Alternatively, in a NICS-XY scan, a series of NICS values were computed at a constant height (usually 1 Å above the molecular plane) along a predefined path that traverses the centers of all rings in the system. This method enables a more accurate assessment of aromaticity in fused polycyclic systems, with rings showing more than one current.[116]

Alternative quantum mechanical methods also allow for the direct visualization of induced ring currents (**Figure 8**). One particularly useful approach is the Anisotropy of the Induced Current Density (ACID) method, developed and established by *Herges* and coworkers. In this method, the ring current is visualized using vector arrows plotted on an isosurface. A clockwise circulation (diatropic ring current) is characteristic for an aromatic system, while counterclockwise circulation (paratropic ring current) signifies an antiaromatic system.[117-118]

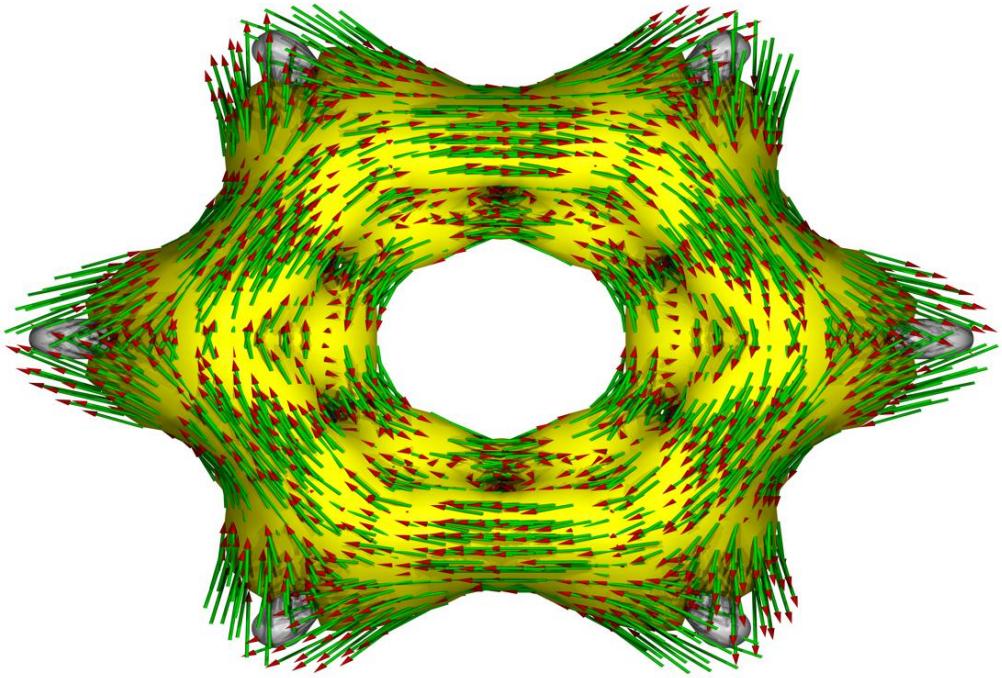

Figure 8: ACID plot of benzene. The ring current is visualized with vector arrows on the isosurface. The clockwise circulation (diatropic ring current) describes the aromatic system of benzene.

In addition to the magnetic criterion discussed, the molecular structure can be used to estimate aromatic character. The fundamental idea is that in aromatic systems, the cyclic delocalization of electrons leads to uniform bond lengths around the ring. This contrasts with non-aromatic polyene systems, where alternating single and double bond lengths are typically observed due to the lack of electron delocalization. Antiaromatic compounds,

such as cyclobutadiene, may also exhibit bond length alternation due to *Jahn-Teller* distortion, which allows the molecule to lower its energy by breaking symmetry in an otherwise electronically unstable configuration.[119-120] A commonly used structural measure is the HOMA index (Harmonic Oscillator Model of Aromaticity), which provides a quantitative evaluation based on bond length data.[120-121] In this model, the experimentally or computationally obtained bond lengths R_i are compared to the ideal bond length of benzene ($R_{opt} = 1.388$ Å). A normalization factor α = 258 Å^{-2} is applied to ensure that benzene gives a HOMA value of +1.00, while a localized *Kekulé*-type cyclohexatriene yields a value of 0.00. The HOMA index can be calculated using the following equation (**Eq. 3**):

$$HOMA = 1 - \frac{a}{n}\sum_{i=n}^{n}(R_i - R_{opt})^2$$

Equation 3: Calculation of HOMA.

The greater the deviation or alternation of the bond lengths R_i from the optimal value R_{opt}, the lower the resulting HOMA value will be compared to that of benzene. A significantly reduced HOMA value indicates that the corresponding ring system possesses non-aromatic or even antiaromatic character.

2.1.4 Quantum Chemical Calculation

The time-independent *Schrödinger* equation forms the foundation of quantum chemical calculations, and expresses the relationship between a chemical system's energy E and its wave function $\psi(r)$ (**Eq. 4**):

$$\hat{\mathrm{H}}\psi(r) = E\psi(r)$$

Equation 4: Time-independent *Schrödinger* equation.

The energy of a system can be obtained by applying the Hamiltonian operator $\hat{\mathrm{H}}$ to the wave function and consists of the operators for the kinetic and potential energies of the nuclei and electrons. The operators $\hat{T}$ and $\hat{V}$ represent the kinetic energies of the electrons e and the nuclei K, as well as their respective interactions (**Eq. 5**):

$$\hat{\mathrm{H}} = \hat{T}_K + \hat{T}_e + \hat{V}_{eK} + \hat{V}_{ee} + \hat{V}_{KK}$$

Equation 5: The Hamiltonian operator, composed of the operators for kinetic and potential energy.

Since atomic nuclei are much heavier than electrons, their motion is significantly slower. According to the *Born-Oppenheimer* approximation, nuclear motion can therefore be neglected, and their mutual repulsion treated as constant. This simplification leads to the definition of the electronic Hamiltonian, expressed as (**Eq. 6**):

$$\hat{\mathrm{H}}_{el} = \hat{T}_e + \hat{V}_{ee} + \hat{V}_{eK}$$

Equation 6: Electronic Hamiltonian, post *Born-Oppenheimer* approximation.

Despite the simplification, the resulting electronic *Schrödinger* equation can only be solved exactly for the two-particle systems. For more complex systems, further approximations are necessary.[122-124]

2.1.4.1 Hartree-Fock and DFT

One approach to approximate the desired wave function is based on the *Hartree-Fock* method, which aims to minimizes the systems total energy. In this method, the multi-electron wave function is constructed from a set of orbitals. Adjusting these orbitals changes the wave function and, consequently, the expected energy. The goal is to determine the optimal set of orbitals that yields the lowest possible energy, ideally as close as possible to the exact electronic energy of the system.[122-124]

According to the theorems established by *Hohenberg* and *Kohn*, the ground state energy E of a molecule can be determined from the electron density $\rho(\mathrm{r})$, instead from the wave function Ψ. This means that energy is expressed as a functional $E[\rho(\mathrm{r})]$, which forms the foundation of density functional theory (DFT). The electron density corresponds to the probability of finding an electron within a given volume element. Similar to the electronic *Hamilton* operator, the functional can be divided into its individual components including the kinetic energy of the electrons $T_e[\rho_0]$, the electron-electron interaction $E_{ee}[\rho_0]$, and the electron-nucleus attraction $E_{ek}[\rho_0]$ (**Eq. 7**):[122]

$$E_0[\rho_0] = T_e[\rho_0] + E_{ee}[\rho_0] + E_{ek}[\rho_0]$$

Equation 7: Density functionals in analogy to the electronic Hamiltonian operator.

The second *Hohenberg-Kohn* theorem establishes that the variational principle applies to the electron density and states that for any arbitrary electron density $\rho(\mathrm{r})_{Test}$, the resulting energies are greater than or equal to the exact ground-state energy E_0 (**Eq. 8**).[122]

$$E[\rho(r)_{Test}] \geq E_0$$

Equation 8: Variational principle.

One of the main advantages of orbital-free density functional theory (DFT) over wave function methods is that the energy depends only on the electron density. If the electron density is known, the energy of the system can be determined using the universal functional without the need for the wave function. According to the second *Hohenberg-Kohn* theorem, the minimum of this functional must be found with respect to the electron density in order to obtain the ground state energy. However, the exact functional that relates the electron density to the energy is unknown. This problem can be significantly prevented with the *Kohn-Sham* approach, in which a large fraction of the energy is determined in a wave-based approach using a *Slater* determinant with n spin orbitals φ_i.

In *Kohn-Sham* theory, the kinetic energy is calculated under the approximation of non-interacting electrons. The missing part of the exact kinetic energy, along with electron correlation and exchange energy, is included in the additional term $E_{XC}[\rho]$ in the DFT energy calculation. In addition, the *Coulomb* interaction is taken into account in the term $J[\rho]$ (**Eq. 9**).[122]

$$E_{DFT}[\rho] = T^{SD}[\rho] + E_{eK}[\rho] + J[\rho] + E_{XC}[\rho]$$

$$E_{XC}[\rho] = (T[\rho] - T^{SD}[\rho]) + (E_{ee}[\rho] - J[\rho])$$

Equation 9: Density functional and exchange-correlation term.

Since the exchange-correlation functional $E_{DFT}[\rho]$ cannot be determined exactly, the accuracy of a DFT calculation depends heavily on the made approximations for the calculation of this functional. This problem can only be addressed by solving the equation iteratively using the self-consistent field (SCF) method. The process begins with an initial guess for either the orbitals or the electron density. Based on this guess, the corresponding eigenvalue equation is solved. The resulting orbitals or densities are then used as input for the next iteration. This process is repeated until the input and output orbitals or densities differ by less than a predefined threshold.[122-124]

2.1.4.2 Functionals and Basis Sets

Ever since the development of density functional theory (DFT), a wide range of functionals have been introduced. *Perdew*'s "*Jacob's* ladder" provides a fundamental framework for

classifying these functions based on their degree of approximation and calculation principles. Common functionals such as B3LYP, PBE, and TPSS can be categorized into one of the following classes based on their computational principle: LDA, GGA, Meta-GGA, Hybrid, and Double-Hybrid. The *Jacob's* ladder is a conceptual model in DFT that illustrates the hierarchy of approximations that ascend step by step to the "heaven" of chemical accuracy.[122]

The simplest functional, the local density approximation (LDA), which is the most basic approximation, is located at the lowest level of the ladder. It assumes that the local electron density behaves like a homogeneous electron gas. For molecular systems, this approximation is often insufficient.

At the next level, the GGA functionals (Generalized Gradient Approximation) are located. These functionals consider not only the local electron density but also its gradient (the derivative of the density). Since there are various methods for calculating exchange and correlation energies, choosing the right functional is critical. In general, GGA functionals provide a significantly better description of chemical systems and their properties compared to the LDA method, making them especially popular for modeling large molecules.

The meta-GGA functionals are on the next level of the ladder. These functionals are extensions of the GGA functionals, taking into account not only the first derivative of the electron density, but also higher derivatives.

One step further are the hybrid functionals. In these functionals, the exchange-correlation energy is calculated only partially using density functional theory. The remaining exchange energy is described using *Hartree-Fock* theory, incorporating the *Kohn-Sham* orbitals. The most well-known hybrid functional is B3LYP, which generally provides good results for organic molecules.

The fifth step on the ladder is occupied by the double hybrid functionals. These computationally intensive methods are based on the hybrid functionals and also take into account virtual orbitals and explicit electron correlations.

Overall, it can be said that the accuracy of the various functionals on the *Jacob's* ladder has been significantly improved. However, this higher accuracy is associated with

considerable computational effort. Furthermore, different functionals within the same level can give different results. Some functionals are better suited for molecules, while others are better suited for solids. It is therefore important to carefully consider which functional is best suited for the investigated system.[122]

In addition to the choice of functional, the quality of the calculations also depend significantly on the electron wave functions, *i.e*. the spin orbitals φ_a or $\chi_\mu$in the HF approach. According to the LCAO model (Linear Combination of Atomic Orbitals), a spin orbital can be represented by a basis set defined as a linear combination of basis functions (**Eq. 10**):[122]

$$\varphi_a = \sum_\mu c_\mu \chi_\mu$$

Equation 10: Linear Combination of Atomic Orbitals.

This requires suitable LCAO coefficients c_μ to be calculated and varied iteratively using the SCF method until a set of molecular orbitals is found that optimally describes the investigated system. The atomic orbitals χ_μ on the other hand, are typically modeled as exponential functions that peak at the atomic nucleus and decay with increasing distance. Ideally, these would be represented by *Slater*-type orbitals (STOs), which closely resemble the true shape of atomic orbitals. However, due to computational efficiency, Gaussian-type orbitals (GTOs) are more commonly used in practice. While single *Gaussian* functions lack a cusp at the nucleus and decay too quickly, making them poor individual approximations of real atomic orbitals, a linear combination of several *Gaussian* functions can approximate *Slater*-type behavior quite well, resulting in a more accurate and efficient description of atomic orbitals. Such combinations of atomic orbitals form what is known as the basis set. The more atomic orbitals are available to describe a molecule, the more accurately the molecular orbitals or spin orbitals in the *Slater* determinant can represent the system. Similar to functionals, the computational effort increases with the number of basis functions, requiring a balanced approach between the quality of the results and the required computational resources.[122-124]

2.1.4.3 Applying the Concepts

The *Born-Oppenheimer* approximation enables the calculation of a molecular system's energy for a fixed arrangement of nuclei, using the quantum chemical methods described

above. Different configurations of the N nuclei yield different energy values $V(x)$, which together form the potential energy surface (PES) as a function of the 3N−6 internal coordinates for non-linear molecules. Of particular interest are the configurations corresponding to minima on the PES, representing reactants, intermediates, or products and saddle points, which correspond to transition states. These points are characterized by the fact that the first derivatives of $V(x)$ with respect to the nuclear coordinates x vanish. The nature of each point is determined by the Hessian matrix, which contains the second derivatives of the energy. A point is classified as a minimum if all eigenvalues of the Hessian are positive. If the Hessian has a single negative eigenvalue, the point is a first-order saddle point. Quantum mechanical calculations begin by locating such stationary points through geometry optimization. Starting from an initial guess that is ideally close to a minimum or saddle point, numerical methods iteratively refine the structure. Once optimization converges, a second step verifies the result by computing the Hessian matrix and analyzing its eigenvalues. Assuming the harmonic oscillator model, the eigenvalues of the Hessian are directly related to vibrational frequencies. This step, known as frequency analysis, also yields the IR and Raman active vibrational modes. A saddle point will display one imaginary frequency (*i.e.*, a negative eigenvalue), while multiple imaginary frequencies indicate an incorrect optimization. Once a valid minimum or saddle point is confirmed, important molecular properties such as bond lengths, total energy, and vibrational spectra are accessible. From the optimized geometry, additional properties can be calculated using specialized methods.[124]

3 Aim of the Project

Since the discovery of the triphenylmethyl radical, a wide range of stable carbon-centered radicals have been investigated. However, only a few demonstrate stability under ambient conditions, such as in the presence of air, moisture, and solvents, or show resistance towards dimerization and disproportionation. In recent years a number of CP-PAH radicals, such as truxene proposed by *Yang et al.,*[74] or the helical carbon-centered radical by *Herzog et al*.,[93] meeting these criteria have gained reasonable attention. These structures are intended to serve as templates and to contribute to the development of a flexible and broadly applicable concept to access further rare examples of carbon-centered radicals. The focus of this work is on the synthesis of compounds consisting of benzene rings and cyclopentadiene units containing an odd number of five-membered rings, as these necessarily must exist in the form of radicals in their fully conjugated state. Compounds with these structural features are likely to exhibit interesting physical properties, such as small HOMO/LUMO gaps. A comprehensive investigation of their physical and spectroscopic properties will be carried out using a combination of experimental measurements and quantum chemical calculations to provide further insight into the compounds properties to support and complement the experimental results. In most cases, the required kinetic stability is mostly provided by mesitylene residues as a bulky group, limiting the scope of different possible substituents. Furthermore, the reported radicals are generally based on relatively small molecular scaffolds. In addition, this work aims to establish criteria for the formation and stabilization of radicals.

To address the above-mentioned limitations, the study is divided into three main chapters. The first chapter will focus on the development of a broadly applicable synthesis strategy for the investigation of heptacyclic systems. Particularly, the focus will be set on the variation of substituents in order to assess their influence and derive general principles for radical stabilization (**Figure 9**).

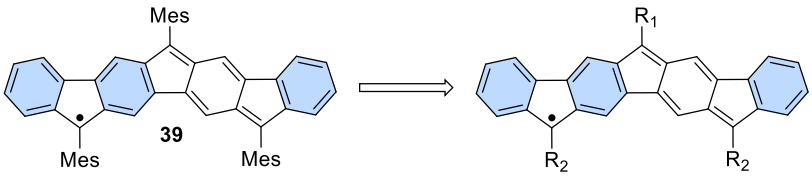

Figure 9: Substitution of the mesityl units on the heptacyclic scaffold.

As outlined in the introduction, an increase in the size of the molecular scaffold is expected to lead to a decreased HOMO/LUMO gap. To examine this effect, the second chapter will explore the extension of the π-system through the synthesis of nonacyclic systems (**Figure 10**).

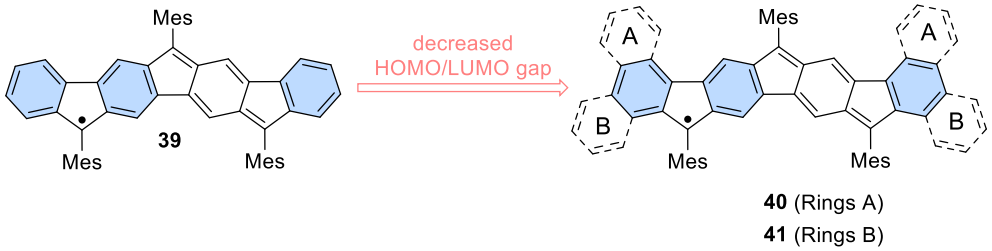

Figure 10: Increase of the molecular scaffold to achieve decreased HOMO/LUMO gap.

The compounds reported thus far are primarily based on mono- or triradical systems. Therefore, the third chapter will set its focus on increasing the number of potential radical centers (**Figure 11**).

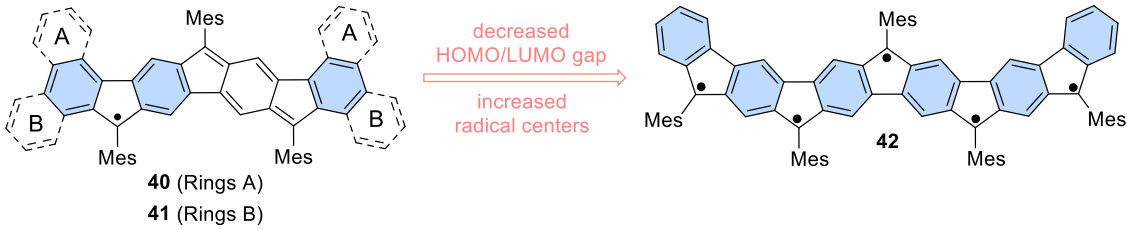

Figure 11: Further expansion of the molecular scaffold to induce a further decrease in the HOMO/LUMO gap; expansion of the radical sites.

As a complementary side project, the cyclopentadiene units in the heptacycles will be replaced with cycloheptatriene units, and the resulting target compounds fully characterized.

4 Results and Discussion

As previously mentioned, the main objective of this work is to develop a broadly applicable synthesis strategy to enable the preparation of a variety of novel compounds. In addition, it is of interest to establish criteria for the formation and stabilization of radicals. Therefore, the following chapter will outline the synthesis of a series of polyaromatic hydrocarbon radicals, while addressing the above-mentioned limitations and providing solutions.

4.1 Synthesis and Characterization of Heptacyclic CP-PAH Radicals

Theoretical considerations show that an alternating sequence of four six-membered and three five-membered rings allows 21 distinct structural arrangements. While all of these scaffolds are accessible through *ortho*-linkage, the synthetic realization of many of these structures is limited by the complexity of the required precursors or the difficulty of controlling regioselectivity during ring fusion. Nevertheless, some of these motifs can be efficiently realized through carefully designed synthetic strategies. Among these, linear or angled CP-PAH systems are particularly attractive (**Figure 12**) due to their readily available precursors, which not only enable the synthesis but also a detailed characterization of these motifs.

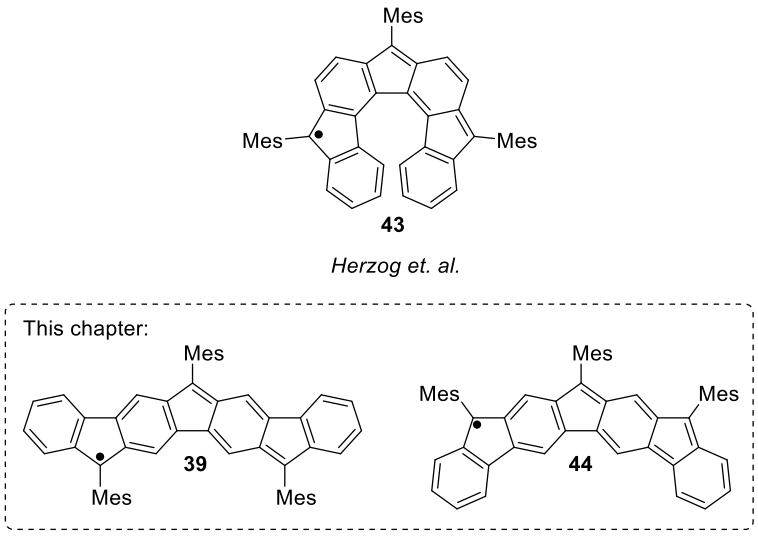

Figure 12: Various heptacyclic CP-PAH radicals, including the helical polycycle **43** and its linear (**39**) and angled (**44**) isomers.

Starting point of the synthesis was the conversion of commercially available 2,7-dibromo-fluoren-9-one (**45**) to the respective mesityl-substituted fluorene **46** following a *Lewis*

acid-mediated reduction/electrophilic aromatic substitution.[125] In contrast to the conventional *Grignard* reaction, where the substrate is first converted into an alcohol and then reduced to the corresponding fluorenone, this approach offers the advantage of a one-pot synthesis. The proposed mechanism shown in **Scheme 7** indicates a $FeCl_3$-catalyzed hydrosilylation, followed by a chlorination while cleaving a siloxane unit and a final *Friedel-Crafts* alkylation, to afford the targeted fluorene **46** in a yield of 74% (**Scheme 7**).[125]

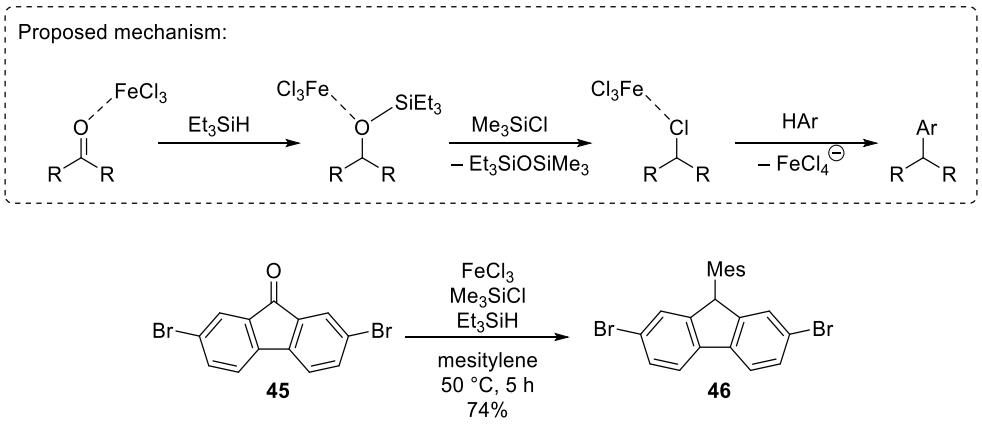

Scheme 7: Proposed one-pot mechanism and synthesis of the corresponding mesityl substituted fluorene **46**.[125]

Double *Suzuki* coupling of fluorene **46** with 2-formyl-phenyl boronic acid (**47**) resulted in the formation of the corresponding dialdehyde **48** in a yield of 72%. Following a published method by *Sharma et al*.,[126] **48** was reacted with the *Grignard* reagent MesMgBr. The quantitative obtained dialcohol **49** was transformed without further purification to the heptacyclic core **50** in a *Lewis* acid-induced *ortho* fusion in a yield of 93% over two reaction steps (**Scheme 8**). After column chromatography, several fractions were analyzed by ^1H NMR, revealing the formation of three diastereoisomers. Several attempts were made to separate the isomers by HPLC, but without success. Another potential complication in this reaction step is the unintended ring closure, which could result in the formation of regioisomers. However, as reported by Sharma *et al*.,[126] the steric hindrance provided by the mesityl groups should effectively prevent the formation of these regioisomers, as observed for the investigated system.

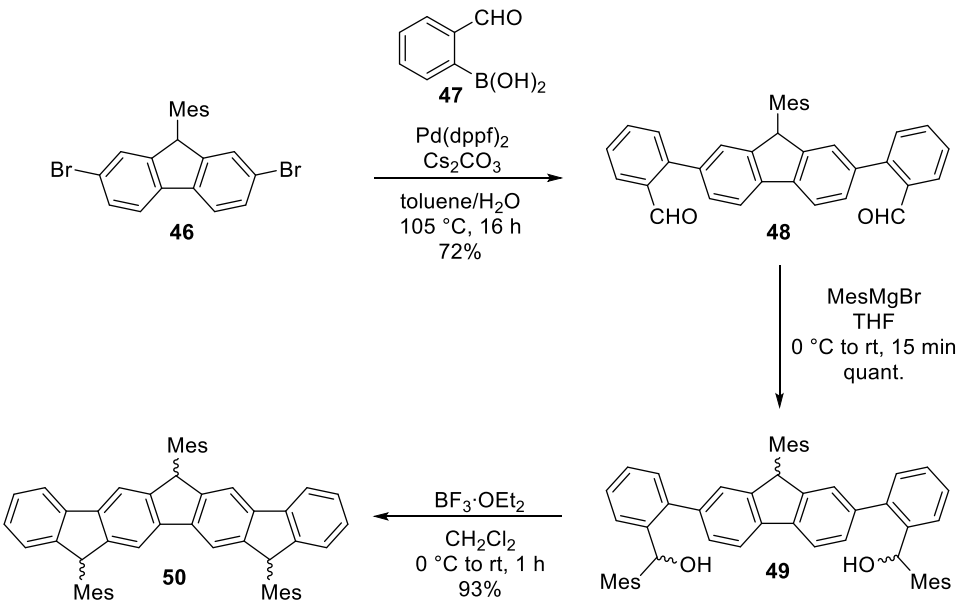

Scheme 8: Double *Suzuki* coupling of **46** with 2-formyl-phenyl boronic acid (**47**) to obtain dialdehyde **48**, followed by the *Grignard* reaction to the dialcohol **49** and a final cyclization to the heptacyclic core **50**.

Since the separation of the formed diastereoisomers could not be achieved, the mixture of isomers (**50**) was deprotonated with KO*t*Bu and immediately oxidized with *p*-chloranil furnishing the fully conjugated heptacyclic radical **39** in a yield of 69% as a dark green solid (**Scheme 9**). Further investigations revealed that the final oxidation step also proceeds under ambient oxygen atmosphere, albeit at a slower rate. Overall, the synthesis of the targeted structure **39** was achieved through five consecutive reaction steps in a total yield of 34%.

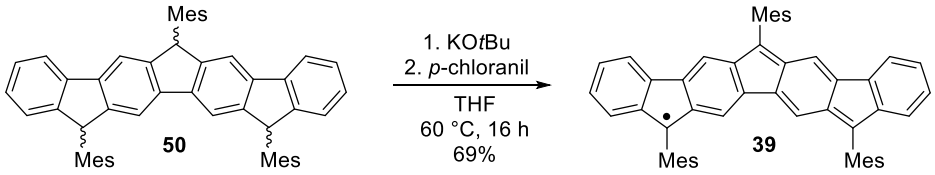

Scheme 9: Deprotonation of mixture of isomers and subsequent oxidation to obtain the fully conjugated heptacyclic radical **39**.

The obtained radical exhibited notable stability towards air, moisture, daylight, and dimerization, which was confirmed by the acquisition of ^{1}H NMR spectra over several weeks.

Conventional analytic methods such as mass spectrometry can provide a sufficient indication of the success of a reaction and allowed to proof the formation of the desired product. However, these methods are not able to confirm the structure of radical **39**. Therefore, X-ray crystallographic analysis was intended to verify the successful synthesis.

Numerous attempts were made to grow single crystals suitable for X-ray crystallographic analysis, but its tendency to form dendritic crystals or amorphous solid-state structures prevented a crystallographic structure determination. Fortunately, single crystals of its precursor **50**, isolated as the all-*cis meso* diastereoisomer, were obtained by liquid/liquid diffusion using a chloroform/ethanol solvent system, yielding colorless crystals suitable for X-ray analysis (**Figure 13**). This crystallographic data not only confirmed the constitutional framework of the polycyclic core of precursor **50**, but also for radical **39**, since the oxidation step to form the radical is anticipated to be inactive in means of skeletal modification of the polyarene, which is supported by previous results.[93] Therefore, the solid-state structure of precursor **50** is a strong evidence for the proposed linear anellation of the targeted compound **39**.

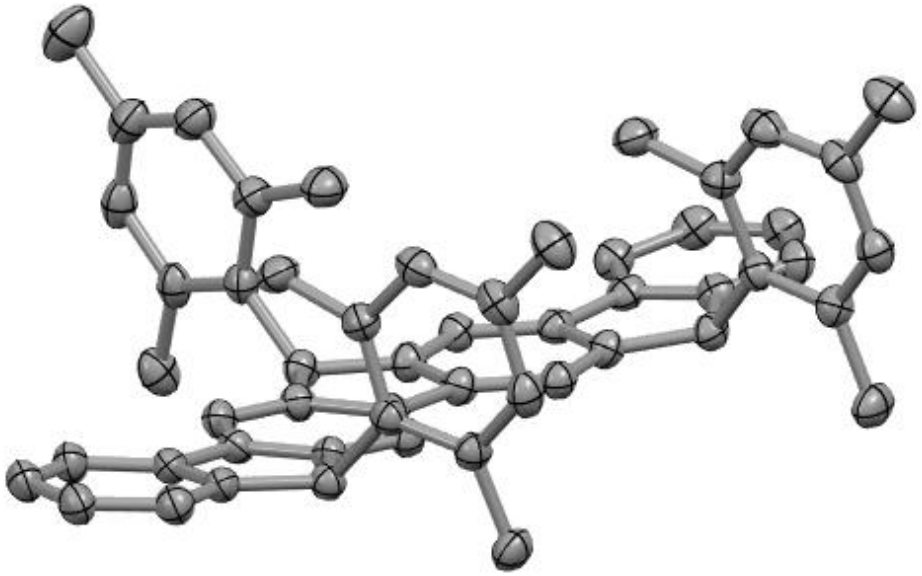

Figure 13: Molecular solid-state structure of all-*cis meso* **50** obtained by single-crystal X-ray diffraction. Hydrogen atoms and a co-crystallized $CHCl_3$ molecule are not shown for clarity. Thermal ellipsoids are drawn at the 30% probability level. Data was provided by Dr. *Jonas Wenzel*.[94]

In contrast to the described linear system, the synthesis of an angled heptacyclic core presents some challenges and requires strategic modifications. The ring closure to obtain the linear scaffold was carried out from the outside to inside, which was enabled by the bulky mesityl groups that prevented undesirable ring closure patterns and the formation of regioisomers. However, this approach is not readily possible for the angled heptacyclic core. One of these modifications involves the introduction of aldehyde moieties to facilitate nucleophilic addition of a mesityl *Grignard* reagent, enabling the ring closure to occur from inside to outside. To achieve this, building block **51** (**Figure 14**) reported by

Majewski et al.[127] should be utilized as a template. By replacing the ethyl units with a mesitylene unit and a hydrogen atom, the corresponding building block **52** can be generated, allowing the synthesis of the angled scaffold.

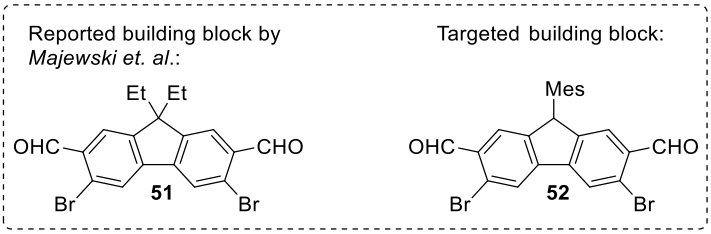

Figure 14: Building block **52** derived from the reported building block **51** by *Majewski et al*.[127].

The synthesis towards **52** was initiated by introducing nitro groups on the unsubstituted fluorenone **53**, obtaining the dinitrated species in a yield of 53%. Subsequent reduction with $SnCl_2$ in EtOAc afforded the diamino intermediate **55** in a poor yield of 10%. The amine functions enable a regioselective bromination at positions 3 and 6 provided by their electron donating nature. Therefore, **55** was subjected to a bromination reaction utilizing NBS. However, the desired product **56** could not be isolated (**Scheme 10**). Several challenges were encountered during the reaction sequence. The regioselectivity of the nitration was difficult to control, leading to the formation of undesired mono- and tri-nitrated byproducts alongside the target dinitro compound **54**. This competing substitution pattern significantly contributed to the low yield. Additionally, the poor solubility of the fluorenone core under the reaction conditions limited reaction efficiency and led to poor yields.

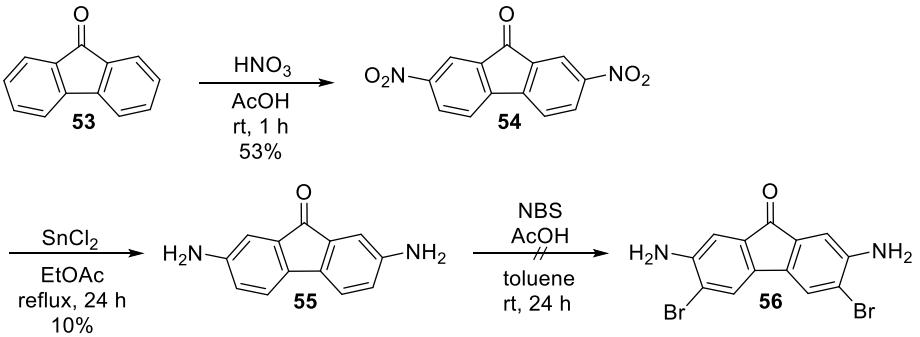

Scheme 10: Unsuccessful synthesis route towards building block **52**.

To address the abovementioned issues, an alternative synthetic route was explored using commercially available 2,7-dinitro-9*H*-fluorene **57**. This bifunctionalized compound (**57**) does not only ensured the presence of only two nitro functions, but also provided flexibility for different synthetic strategies, as illustrated in **Scheme 11**. The reduction of

57 to the corresponding diamine **58** was performed under standard reduction conditions (Pd/H_2), affording **58** in a quantitative yield. The oxidation to generate the fluorenone scaffold was performed on both the dinitro species **57** and the diamine **58**, resulting in **54** and **55** with yields of 47% and 69%, respectively. Following the protocol reported by *Majewski et al*.,[127] acetyl protecting groups were introduced to **55**, giving the protected species **60** in a yield of 43%. Alternatively, acetyl protection was performed on diamine **58** in a yield of 90% (**59**), followed by an oxidation to the fluorenone scaffold **60** in a yield of 70%. To address the solubility issue, an attempt was made to introduce mesitylene to **60** prior to bromination. However, the desired product could not be obtained, requiring an alternative synthetic strategy.

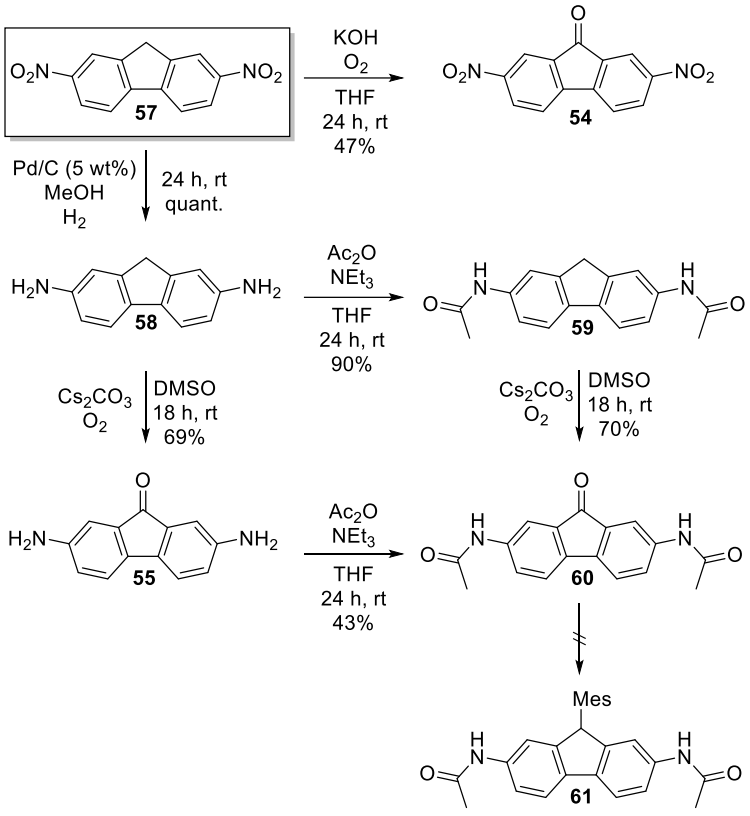

Scheme 11: Alternative synthetic route towards building block **52**.

A final approach involved the use of the previously synthesized building block **46**, which can undergo a *Buchwald-Hartwig* amination, thereby circumventing the described reaction steps in **Scheme 12**. However, analysis by ^1H NMR revealed the absence of the desired product **61**. In a parallel attempt, the *Ullmann* reaction was employed, which allows the copper-catalyzed coupling of a nucleophile (NH_3) with aryl halides. Yet again, this approach also failed to yield the target compound **62**.

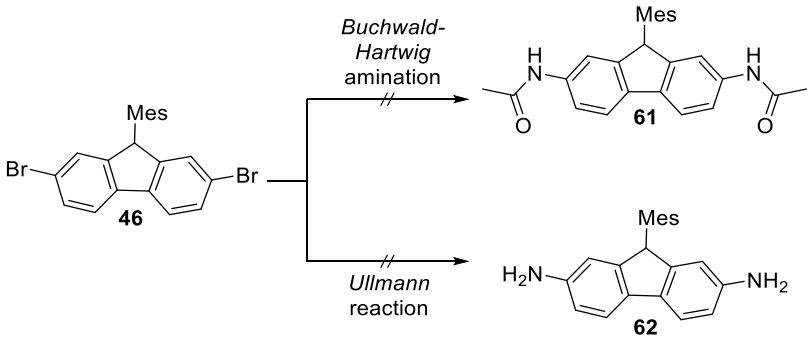

Scheme 12: *Buchwald-Hartwig* amination to generate **61**; *Ullmann* reaction to obtain **62**.

After the presented unsuccessful attempts to synthesize the desired building block **52**, a more similar approach to the synthesis of the linearly arranged heptacyclic core was applied. To obtain the required fluorenone **64**, commercially available dione **63** was reacted in a ring contraction reaction to obtain 3,6-dibromo-9*H*-fluoren-9-one (**64**) in a very good yield of 89% (**Scheme 13**).

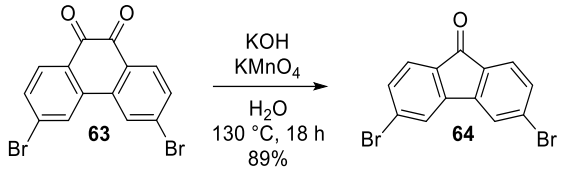

Scheme 13: Synthesis of 3,6-dibromo-9*H*-fluoren-9-one **64**.

In the following step, mesitylene was introduced in a one-pot approach, generating the mesityl-substituted fluorene **65** in a poor yield of 39% (**Scheme 14**). Several attempts were made to improve the yield, including extending the reaction time or increasing the amount of mesitylene used. However, none of these measures succeeded in an increase of the yield. Furthermore, analysis by TLC and ^{1}H NMR spectroscopy revealed that the majority of the starting material did not react during the reaction, possibly due to the poor solubility of fluorenone in mesitylene, which also acts as the reacting agent.

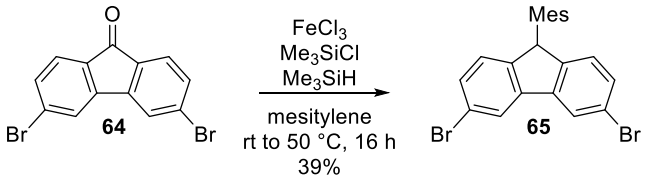

Scheme 14: One-pot approach to synthesize **65**.

Alternatively, **65** can be obtained in a two-step approach, following the reports by *Phan et al.*[128] In an initial step, intermediate **66** is generated in a nucleophilic addition of a mesityl *Grignard* reagent, followed by the reduction to the corresponding mesityl-

substituted fluorene **65** in a quantitative yield (**Scheme 15**). This approach led to a significantly higher yield of the desired product with virtually the same amount of time required, as the reduction can be performed on the obtained crude product.

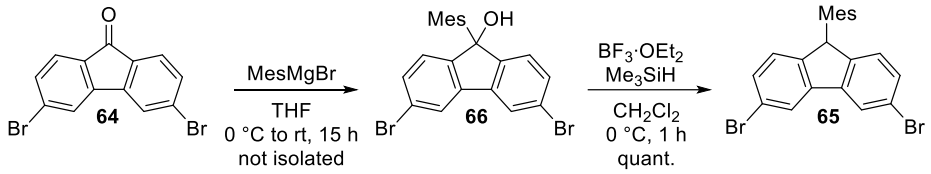

Scheme 15: Two-step approach to synthesize **65**, including the *Grignard* reaction to generate alcohol **66** and subsequent reduction to fluorene **65**.

Following the previously described synthetic strategy, compound **65** was subjected to a double *Suzuki* coupling with commercially available (2-formylphenyl)boronic acid (**47**), affording intermediate **67** in a very good yield of 83%. Subsequent nucleophilic addition of MesMgBr yielded diol **68**, which was converted without any purification to the angled heptacyclic core **69** in a *Lewis* acid-induced cyclization in a quantitative yield over two reaction steps. Theoretically, the regioisomer **70** can be formed during the cyclization, as shown within the box in **Scheme 16**. However, the formation of this regioisomer is considered very unlikely, since the obtained ^{1}H NMR spectrum displays additional splitting patterns compared to the linear precursor **50**. This may be attributed not only to the presence of diastereoisomers but also to hindered rotation between the mesityl units, leading to atropisomers. These observations strongly support the successful formation of the desired precursor.

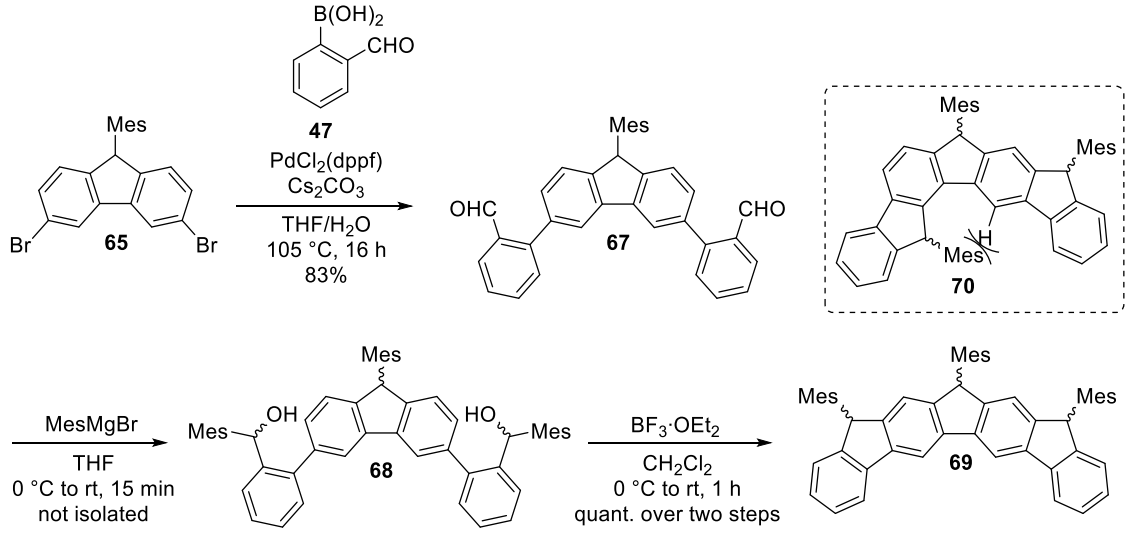

Scheme 16: Synthetic route towards radical precursor **69**; Structure inside the box displays the possible formation of the regioisomer **70** during the cyclization step.

In a finalizing step, the mixture of diastereoisomers of **69** were reacted with KO*t*Bu and oxidized immediately to obtain the angled radical **44** as a dark blue solid in a yield of 10% and the success of the reaction was confirmed by mass spectrometry (**Scheme 17**).

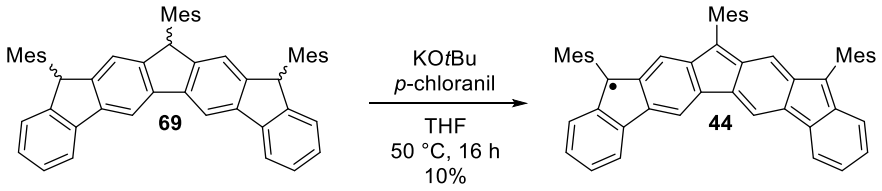

Scheme 17: Synthesis of radical **44**.

In summary, two novel heptacyclic radicals **39** and **44** were successfully synthesized and confirmed. A detailed examination of the radical nature of both radicals will be presented in the following chapter.

4.1.1 Radical Character of the Heptacyclic Motifs

The first evidence for the radical nature of compound **39** was provided by the absence of resonances in conventional frequency ranges (0–12 ppm) in the ^{1}H NMR spectra, which is typical for paramagnetic compounds. The absence of the signals in the spectra can be attributed to the interaction between the magnetic moment of the unpaired electron and the magnetic moments of nearby nuclei. This electron-nucleus coupling causes significant disturbances in the chemical shift (δ), resulting in substantial signal broadening, which ultimately prevents the acquisition of interpretable NMR spectra under standard experimental conditions.[129] Another evidence for the radical nature was provided by its EPR activity.[94] While NMR is primarily focused on the splitting of nuclear spin states in a magnetic field, EPR is related to the splitting of electronic spin states.[130]

A continuous-wave (cw) X-band (9.4214 GHz) EPR-spectrum of **39** (**Figure 15**) was measured in toluene (1 mM) at ambient temperature and showed a broad single line centered around g = 2.0029 without any discernible hyperfine couplings. The broad singlet can be explained by calculating the hyperfine coupling constants. These reveal that no strong coupling of individual protons is present, which would have resulted in a resolvable splitting pattern. Instead an equal participation of all protons is observed, leading to the broad signal.[94]

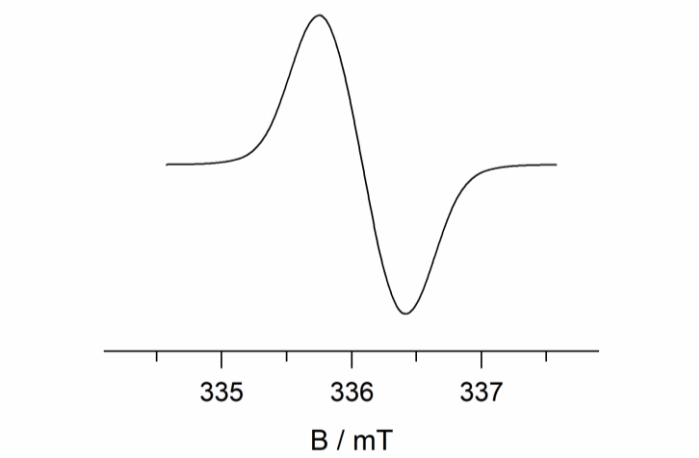

Figure 15: Cw X-band (9.4214 GHz) EPR spectrum of **39** in toluene (1 mM) at ambient temperature showing a single resonance signal centered at *g* = 2.0029. Data was provided by Dr. *Jonas Wenzel*.[94]

The *g* factor was determined from the measured magnetic flux density B = 336.55 mT, considering the exact measuring frequency ν = 9.4214 GHz, the *Planck* constant h = 6.626·10^{-34} J·s and the *Bohr* magneton μB = 9.274·10^{-24} J·T^{-1} (**Eq. 11**):

$$g = \frac{h \cdot \nu}{\mu_B \cdot B}$$

Equation 11: Calculation of the *g* factor.

Furthermore, the radical character of **39** provides for interesting discussion, as three distinct resonance structures can be proposed, each exhibiting different radical configurations (**Scheme 18**).

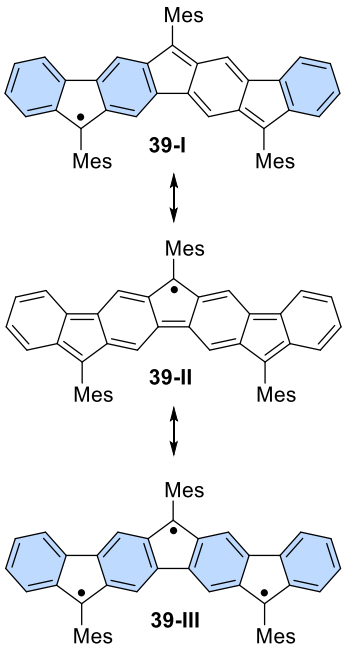

Scheme 18: Resonance formulas of radical **39**; Structure **39-III** exhibits triradical character, while **39-I** and **39-II** exhibit monoradical configuration. Fully intact benzene units are highlighted in blue.

Among these, structure **39-III** features four fully aromatic benzene units and represents a triradical configuration. Based on its stability described by the rule of *Clar*,[2] this structure is expected to be the most pronounced in the resonance ensemble. On the other hand, structure **39-I** comprises three intact benzene units and exhibits a monoradical state. In contrast, **39-II** should be the least pronounced in the ensemble with the unpaired electron positioned in the central five-membered ring, as it lacks any fully aromatic benzene rings.

These considerations suggest that either structure **39-I** or **39-III** is preferred, indicating that the radical species exists predominantly in a mono- or triradical form. To further quantify this, quantum chemical calculations of natural orbital occupation numbers (NOONs)[66] were conducted by applying *Yamaguchi*'s[67] scheme yielding a y_0 value of 0.24, strongly indicating the presence of a monoradical species. Additional experiments, including *Evans*' NMR method, further confirmed the negligibly small triradical character of **39**, which is in agreement with prior findings of its constitutional (helical) isomer **43**,[93] again confirming the monoradical state of **39**.

Similarly, the radical nature of the angled radical **44** was indicated by its paramagnetic behavior, which was confirmed by the absence of resonances in conventional NMR frequency ranges and its EPR activity. A cw X-band (9.4214 GHz) EPR spectrum (**Figure 16**) was measured in toluene (1 mM) at ambient temperature and showed a broad single line centered around g = 2.0041 without any discernible hyperfine couplings.

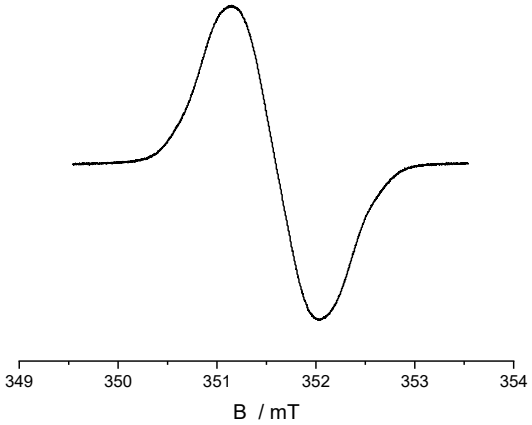

Figure 16: Cw X-band (9.4214 GHz) EPR spectrum of **44** in toluene (1 mM) at ambient temperature showing a single resonance signal centered at *g* = 2.0041. Data was provided by Dr. *Jonas Wenzel*.[94]

Again, three distinct resonance structures can be proposed, with one exhibiting triradical character and two exhibiting a monoradical configuration (**Scheme 19**). Generally, both structures **44-I** and **44-II** should contribute equally in terms of stability, since both feature

equal amount of intact benzene units, whereas structure **44-III** should again be the most stable in the ensemble of resonance structures by the rule of *Clar* with its four intact benzene units.

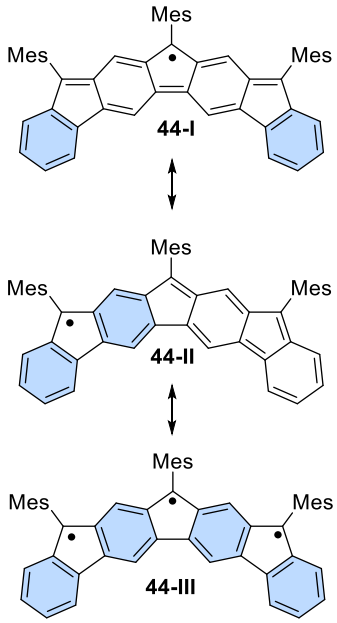

Scheme 19: Resonance formulas of radical **44** with structure **44-III** exhibiting triradical character, while **44-I** and **44-II** exhibit monoradical configuration. Fully intact benzene units are highlighted in blue.

In accordance, the NOON values were evaluated for the underlying system and a y_0 value of 0.66 was obtained. This result strongly indicates a triradical character for **44**. However, this rather unusual result does not correspond with previously obtained values (0.30 for **43** (helical) and 0.24 for **39** (linear). Since the change in geometry should not significantly affect the value, the discrepancy is unexpected. As previously mentioned, the y_0 values are often overestimated and should therefore be considered with caution. It is therefore assumed, that in this case, the obtained value is likely an overestimation.[73]

4.2 Influence of Diverse Substituents on the Radical Character

To date, a relatively narrow range of substituents have been investigated in these polycyclic systems, with mesitylene being the most commonly used. The phenyl (Ph) group has been explored only to a limited extent. *Frederickson et al*.,[51] introduced phenyl moieties on the IF scaffold and reported a rapid decomposition of the resulting compound under aerobic conditions. The decomposition could be suppressed to a certain degree under an inert atmosphere. In general, the instability of the core demands the use of a bulky residue and/or or those that are electron deficient.[51] As Ph residues does not fulfil the necessary criteria, this likely explains the observed instability. However, this influence was not further examined, and therefore the following section discusses the synthesis of the previously introduced linear scaffold with a phenyl group instead of mesitylene as a substituent in order to enable more accurate conclusions regarding stability. In addition, the substrate range is expanded by introducing various residues on the core in order to establish criteria for radical formation.

Starting point of the synthesis was the conversion of commercially available 2,7-dibromo-fluoren-9-one **45** to the respective phenyl substituted fluorene following a *Lewis* acid-mediated reduction/electrophilic aromatic substitution protocol,[125] obtaining **71** in a very good yield of 89%. Subsequent subjection to a double *Suzuki* coupling with 2-formyl-phenyl boronic acid (**47**) generated the dialdehyde **72** in an excellent yield of 93%. A following nucleophilic addition with a phenyl *Grignard* reagent yielded diol **73** in a quantitative yield,[126] which was transferred to the heptacyclic scaffold following a *Lewis* acid-induced *ortho* fusion protocol,[126] obtaining **74** in a fair yield of 56% over two reaction steps (**Scheme 20**).

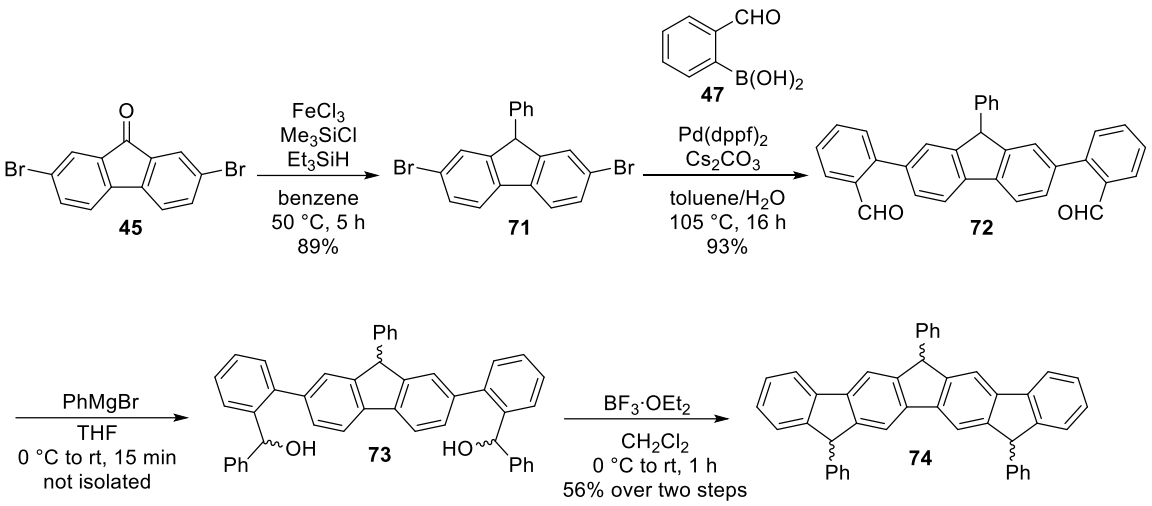

Scheme 20: Synthetic route towards precursor **74**.

As described for previous systems, the presence of more than one diastereoismer was again confirmed by ^{1}H NMR analysis. However, it remains unclear, whether only one regioisomer was formed during the cyclization step, as the phenyl groups offer reduced steric hindrance compared to mesitylene. The formation of an undesired regioisomer is therefore plausible, which would also result in a different conjugation pattern for its corresponding radical. However, this aspect was not explored in the scope of this work. The primary objective of the study remained the assessment of the feasibility of incorporating Ph as a substituent on the heptacyclic core and evaluate its influence on the stabilization of the radical system.

Nevertheless, the mixture of isomers of **74** were reacted with KO*t*Bu and immediately oxidized with *p*-chloranil, yielding a light-red solid. Initial analysis by ^{1}H NMR spectroscopy revealed resonances in conventional frequency ranges (0–12 ppm), which is untypical for paramagnetic compounds. Assuming the green color originates from the π-system, no change in color should occur, as the underlying molecular framework has not been modified. These observations strongly indicate that the radical was possibly formed but could not be stabilized sufficiently (**Scheme 21**).

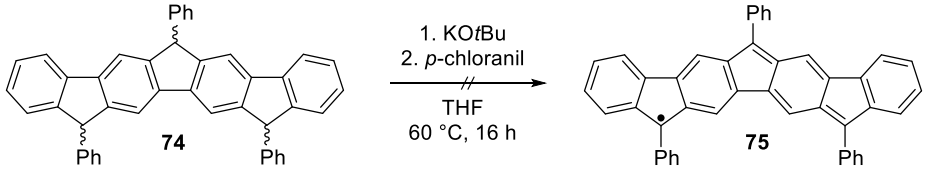

Scheme 21: Unsuccessful attempt to generate radical **75**.

One possible explanation for this outcome can be derived by considering the frontier orbitals (SOMO). **Figure 17** shows the SOMO of the mesityl-substituted radical **39**. It is clearly visible that nodal planes are present at the positions where the radical can reside.

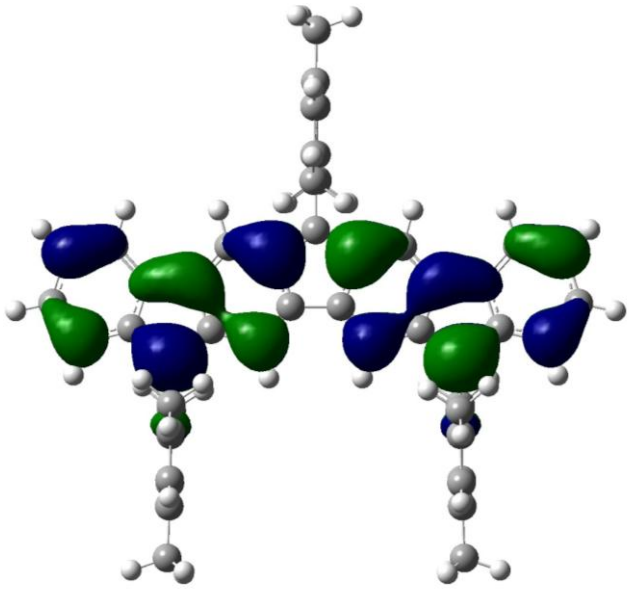

Figure 17: SOMOs of alpha and beta spins of **39**

As a result, interaction between the SOMO and the electron pairs of the mesityl substituents is not possible, hence no orbital overlap can occur. However, when examining the phenyl-substituted system (**75**), a strong similarity to the *Gomberg* radical (**25**) is evident (**Scheme 6**). Since the phenyl groups can rotate unhindered, orthogonal alignment is no longer guaranteed, and the nodal plane at the central five-membered ring should disappear. This enables interaction between the orbitals of the molecular skeleton and the substituents, which allows for the radical to delocalize in such a way that increased spin density can occur at the *para* positions of the phenyl rings. It is well established that phenyl-based radicals are very unstable,[131] typically leading to rapid follow-up reactions such as radical propagation[132] or, as observed with the *Gomberg* radical (**25**), dimerization through radical coupling.[133] *Prajapati et al*.[134] conducted similar investigations and reported that the equilibrium twist angle and the isomerization barriers of alkenes can be controlled by steric effects (**Scheme 22**). This is typically achieved by weakening the double bond, via oxidation, reduction or introducing a permanent twist to the molecules ground-state structure. The large twist induced by bulky substituents ultimately leads to increased bond lengths, a decrease in the electronic energy gaps and finally a reduction in the isomerization barriers, giving significant rise to

the resulting open-shell character. Applied to the present system, these insights provide a plausible explanation for the resonances observed in the NMR spectrum.

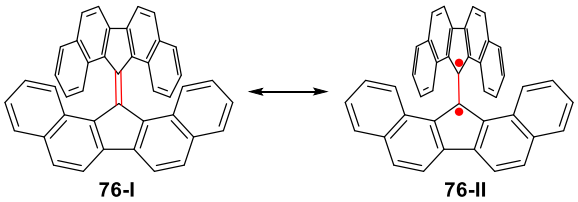

Scheme 22: Control of equilibrium twist angle and the isomerization barriers by steric effects. Bulky substituents induce large twists, increase bond lengths, reduce electronic energy gaps, lower isomerization barriers and enhance open-shell character.[134]

To gain insights into the spin distribution within the molecular scaffold of **39** (linear radical), or to identify the positions with the highest spin densities, DFT calculations can be employed to obtain *Mulliken* atomic spin densities. In this context, the spin density $\rho_s(r)$ is defined as the difference between the α and β electron densities (**Eq. 12**):[135]

$$\rho_s(r) = \rho_\alpha(r) - \rho_\beta(r)$$

Equation 12: Equation for the calculation of *Mulliken* atomic spin densities.

A closer look at the calculated *Mulliken* atomic spin densities for **39** (**Figure 18**) reveals the highest spin densities at the carbon atoms C-12 and C-15 with a value of +0.41. The carbon atom C-6 at the central five membered ring takes on a smaller, yet still significant value of −0.29. The negative value for the spin density at C-6 can be explained due to negative spin polarization of lower MOs.[94] In these fully populated MOs, the electron whose spin is aligned parallel to the spin of the electron in the SOMO favors the positions where the density of the unpaired electron is high. This can be explained by a reduced electrostatic repulsion due to the exchange interaction, which is also the basis of *Hund's* rule. The second electron of the occupied MO, which must be antiparallel to the electron of the SOMO according to the spin pairing, migrates to other positions and thus causes the negative spin density in the nodal planes of the SOMO.[135-136] Given the prior assumption that radical **39** is best described by resonance formula **39-I** (**Scheme 18**) (the monoradical configuration, where the radical is located at one of the outer five-membered rings) the highest probability of locating the radical would be at positions C-12 and C-15.

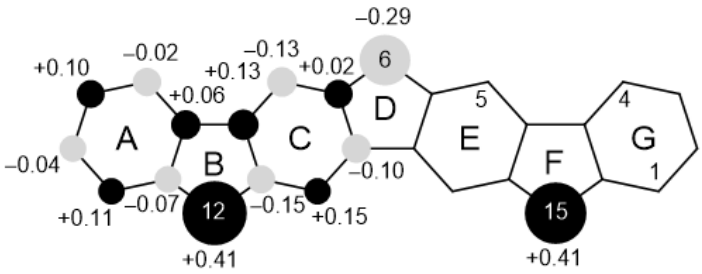

Figure 18 Calculated *Mulliken* atomic spin densities of **39**; Mes groups are excluded for clarity.

This raises the question of whether the framework can still incorporate a Ph group while retaining its radical properties. Precise modifications could achieve a structure with these characteristics. By using a MesMgBr *Grignard* reagent instead of PhMgBr, the desired product can be obtained. Therefore, synthesis was initiated by a double *Suzuki* coupling of fluorene **71** with 2-formyl-phenyl boronic acid (**47**) to generate **72**, followed by a nucleophilic addition with a mesityl *Grignard* reagent yielding diol **77**, which was then transferred to the heptacyclic scaffold in a *Lewis* acid-induced *ortho* fusion affording precursor **78** in a very good yield of 84% over two reaction steps (**Scheme 23**).

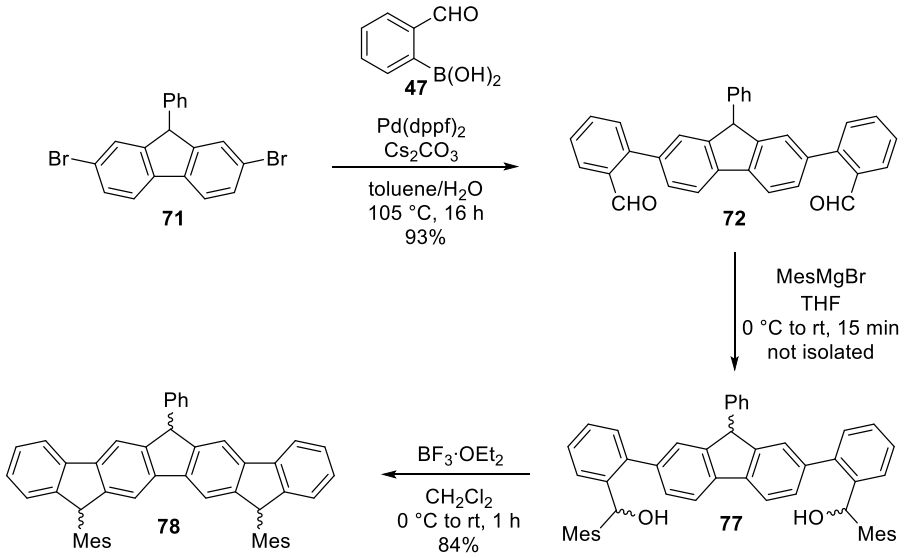

Scheme 23: Synthesis route towards precursor **78**.

Due to the absence of the bulky mesityl group at position C-6, there is no clear indication that only one regioisomer is formed. Interestingly, the comparison of the ^{1}H NMR spectra of **50** and **78** (**Figure 19**) show a high degree of similarity not only in the chemical shifts but also in the splitting patterns, strongly suggesting the presence of just one regioisomer. This is likely once again attributed to the steric hindrance provided by the mesityl groups.

Furthermore, the absence of more complex splitting pattern supports the absence of additional regioisomers.

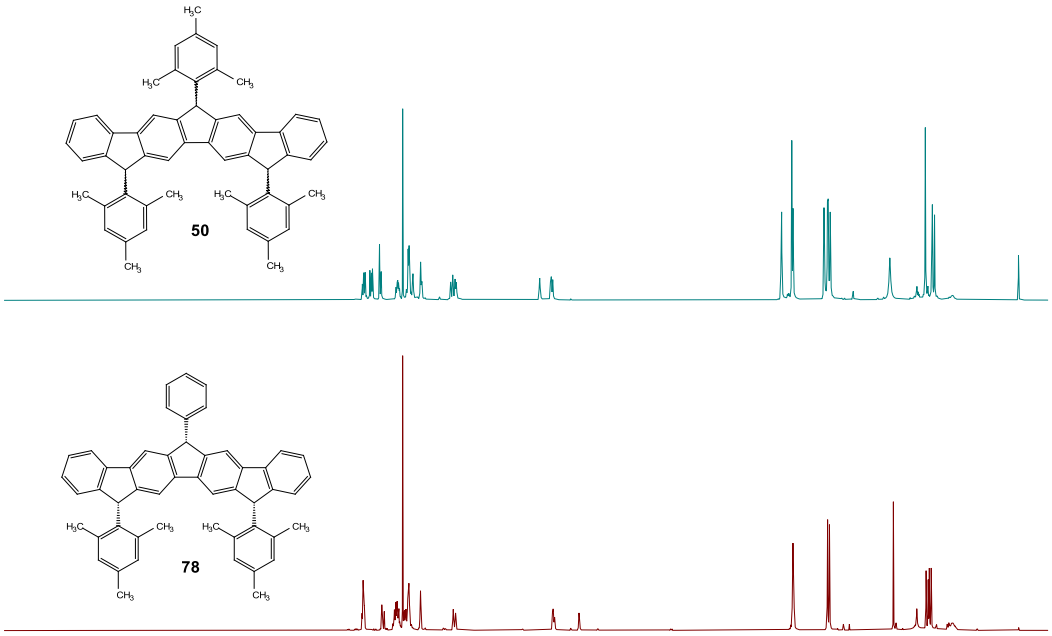

Figure 19: Comparison of the ^{1}H NMR spectra of radical precursors **50** and **78**.

Deprotonation of precursor **78** and subsequent oxidation was carried out analogously as mentioned above. Upon addition of the oxidizing agent, no color change was observed in the brown solution (**Scheme 24**). However, shortly after the beginning of the reaction, a green substance appeared at the edge of the flask, suggesting that the target species may have formed temporarily but was too unstable and decomposed rapidly.

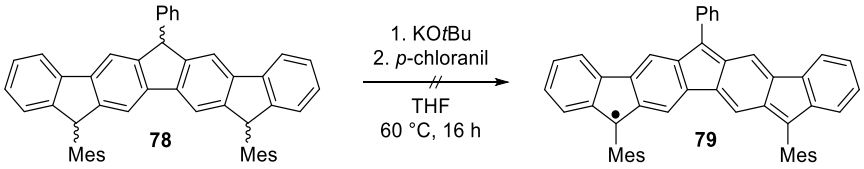

Scheme 24: Failed attempt to synthesize radical **79**.

Assuming the green species corresponded to the desired product, a second attempt was made with a significantly reduced reaction time of just 30 minutes. Upon addition of the oxidizing agent, a rapid change of color to green was observed. Given the presumed low stability of the product, all subsequent steps were carried out rapidly to minimize decomposition as far as possible. After purification by column chromatography, the target compound **79** was isolated as a dark green solid in a yield of 81% (**Scheme 25**) and its radical nature confirmed by the absence of resonances in the acquired ^{1}H NMR spectrum.

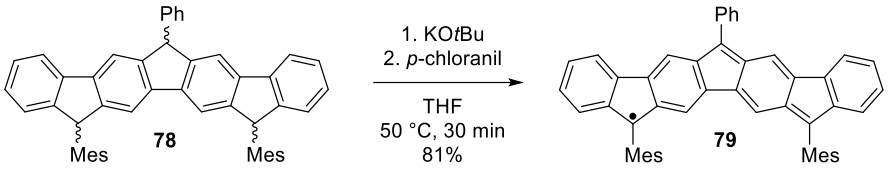

Scheme 25: Successful synthesis of radical **79**.

Further evidence for the compounds radical nature was provided by its EPR activity. A cw X-band (9.4214 GHz) EPR spectrum (**Figure 20**) was measured in toluene (1 mM) at ambient temperature and showed a broad single line centered around g = 2.0037 without any discernible hyperfine couplings.

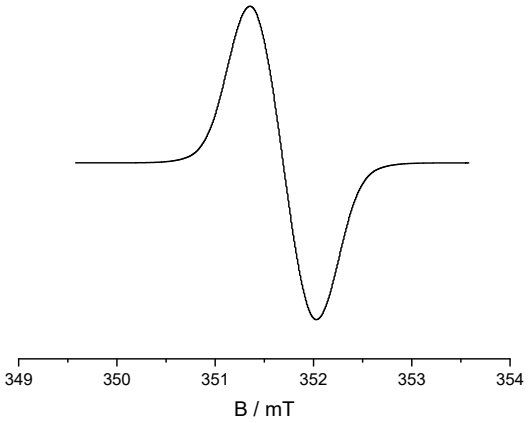

Figure 20: Cw X-band (9.4214 GHz) EPR spectrum of **79** in toluene (1 mM) at ambient temperature showing a single resonance signal centered at g = 2.0037. Data was provided by M. Sc. *Johannes Werner*.

Compound **79** demonstrates relatively stable behavior under ambient conditions, showing resistance to air, moisture and solvents. However, compared to compound **39**, a decreased stability for radical **79** is observed, particularly in solution, as the color changes from green to red, whereas such behavior is not observed for the other radicals. The successful synthesis of this compound also serves as experimental proof that the monoradical species shown in **Scheme 18** is the most significant. This suggests that the radical center is mainly located on one of the outer five-membered rings, as the radical could be isolated as a stable compound. This is also evident when examining the SOMOs of the alpha and beta spins of **79**, as the nodal plane in the central cyclopentadiene unit becomes apparent (**Figure 21**).

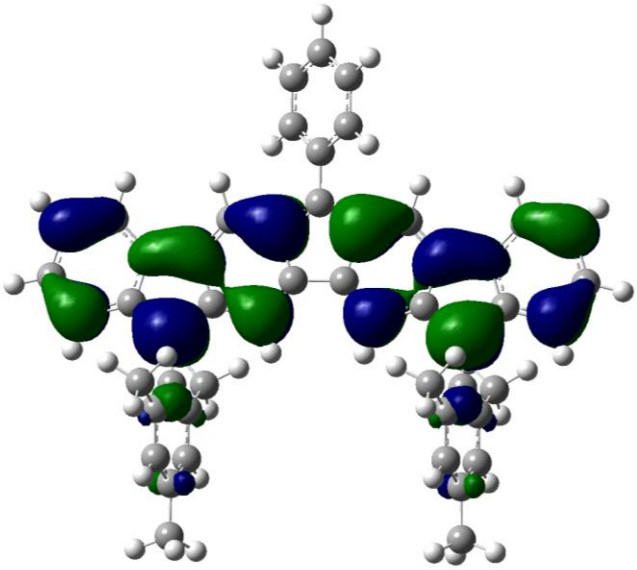

Figure 21: SOMOs of alpha and beta spins of **79**.

Although it was discussed that the triradical character of these compounds is relatively small, it is nevertheless present. Assuming a triradical configuration, the unrestricted rotation of the phenyl group could cause a rearrangement of the radical, which would lead to an increased spin density in the *para* position in the phenyl ring. And as already discussed, this can result in follow-up reactions, possibly explaining the observed reduced stability for **79**.

As previously mentioned in this chapter, bulky and electron-deficient residues play a key role in stabilizing the polyaromatic framework, allowing for the introduction and study of various functional groups. This can easily be achieved by the synthetic strategy outlined in **Scheme 8**. The aldehyde groups enable straightforward introduction of various residues via *Grignard* reactions.

For example, *Jiang et al*.[137] utilized 2-bromo-1,3-dichlorobenzene (**80**), which was also used in the present system. Unlike Ph, this substituent introduces significant steric hindrance at the *ortho* positions, thereby promoting restricted rotational freedom. Moreover, it was reported, that chlorine atoms further provide resonance stabilizing effects, leading to an overall increased stability.[74] Starting from dialdehyde **48**, 2,6-dichlorophenyl was introduced by a proposed *in situ* generated *Grignard* reagent, prepared from 2-bromo-1,3-dichlorobenzene (**80**) and ^{i}PrMgCl. Cooling the system to 0 °C ensured selective metal-halogen exchange at the more reactive bromide site. Subsequent

treatment of the resulting diol **81** with $BF_3{\cdot}OEt_2$ afforded precursor **82** in a fair yield of 65% over two reaction steps (**Scheme 26**).

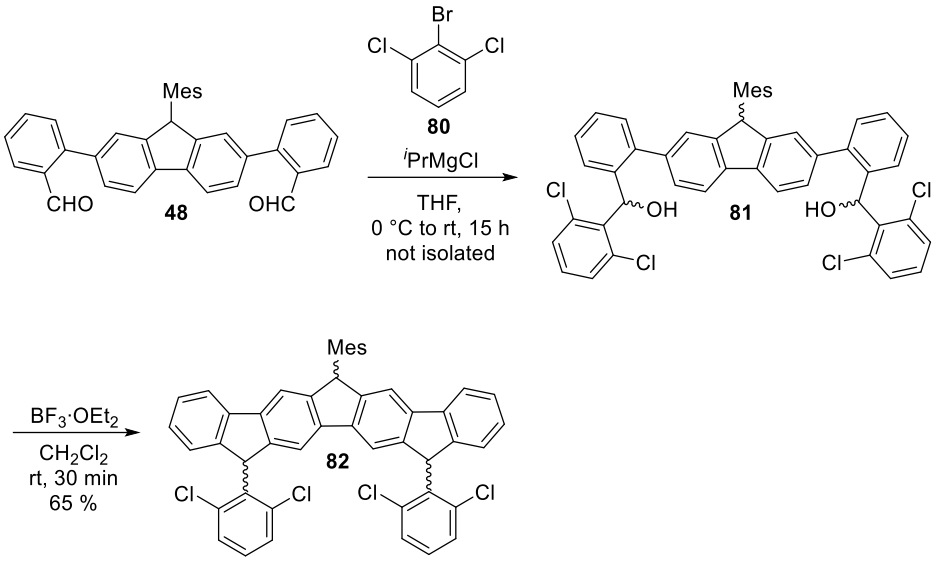

Scheme 26: Synthesis route to obtain precursor **82**.

Since the ^{1}H NMR Spectra did not fully allow to identify the product, the success of the reaction was confirmed by mass spectrometry. In a finalizing step **82** was deprotonated with KO*t*Bu and subsequently oxidized by *p*-chloranil to generate the fully conjugated radical **83** in a fair yield of 52% as a green solid (**Scheme 27**).

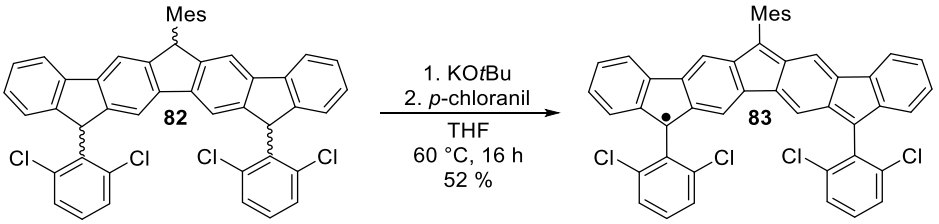

Scheme 27: Synthesis of radical **83**.

The absence of resonances in conventional frequency ranges in the recorded ^{1}H NMR spectra, proved the products radical nature. Again, the radical was confirmed to be stable under ambient conditions.

Similarly, a cw X-band (9.4214 GHz) EPR-spectrum (**Figure 22**) in toluene (1 mM) at ambient temperature showed a broad single line centered around g = 2.0038 without any discernible hyperfine couplings and confirmed the compounds radical nature.

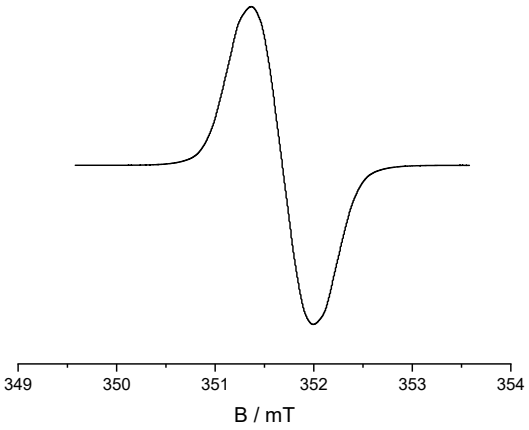

Figure 22: Cw X-band (9.4214 GHz) EPR spectrum of **83** in toluene (1 mM) at ambient temperature showing a single resonance signal centered at *g* = 2.0038. Data was provided by M. Sc. *Johannes Werner*.

Another interesting approach was made by *Sharma et al*.[138] by investigating symmetric, asymmetric, and benzo-extended [*1,2-b*]IFs. They successfully introduced C_6F_5 and $C_6H_3(CF_3)_2$ units to the IF core. However, their influence in open-shell systems remains unexplored, which motivated the incorporation of these units in the present system.

Two possible approaches are applicable for the incorporation of these residues. **Table 1** shows the respective reaction conditions and yields of the synthesis route shown in **Scheme 28**. The method by *Jiang et al*.,[137] allows a one-pot synthesis, combining the preparation of the *Grignard* reaction and the subsequent metal-halogen substitution. First, the *Grignard* reagent is formed *in situ* by slowly adding ^{i}PrMgCl to either 1-bromo-3,5-bis(trifluoromethyl)benzene (**88**) or 1-bromo-2,3,4,5,6-pentafluorobenzene (**89**) and stirring for 2 h. Subsequently, aldehyde **48** was added to the mixtures, and stirring continued for 15 h. The obtained diols **84** and **85** were then transformed in a *Lewis* acid-mediated *ortho* fusion to the heptacycles **86** and **87** in poor yield of 33% and 19% as pink solids.

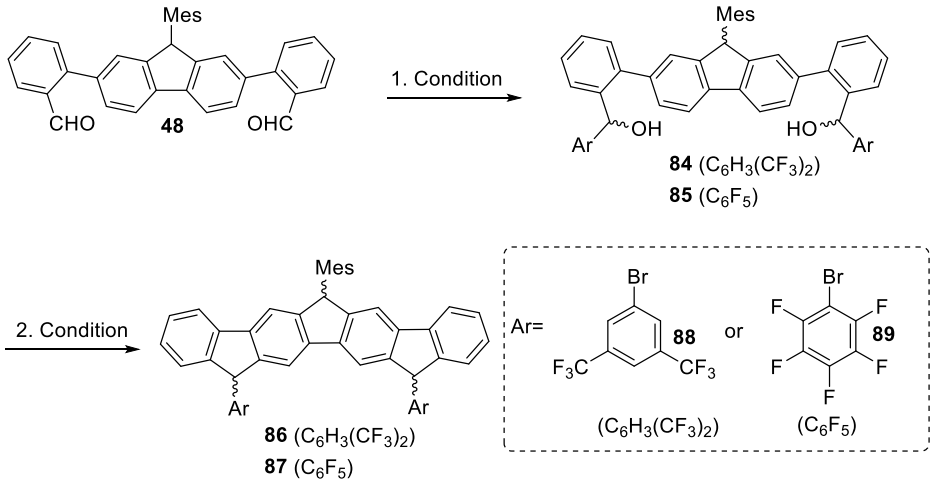

Scheme 28: Two possible approaches to introduce the substituents $C_6H_3(CF_3)_2$ and C_6F_5 and the subsequent cyclization to the heptacyclic framework. 1. Condition: **88** or **89**, ^{i}PrMgCl, THF,0 °C to rt, 15 h; 2. Condition: **84** or **85**, $BF_3{\cdot}OEt_2$, CH_2Cl_2, 0 °C to rt, 1 h. The results are summarized in **Table 1**.

In comparison, the approach by *Sharma et al*.[138] requires the prior preparation of the corresponding *Grignard* reagent. However, the reaction time is drastically reduced to only 15 min to yield dialcohols **84** and **85**. Subsequent treatment with $BF_3{\cdot}OEt_2$ afforded precursors **86** and **87** in poor yields of 30% and 43% as pink solids.

It is noteworthy that the yields achieved in the various reactions are in a similar range and remain relatively low, which highlights a general limitation in the efficiency of the conversion. Entries 1 and 2 illustrate that generating the *Grignard* reagent beforehand and adding it to the reaction mixture significantly shortens the reaction time compared to generating it *in situ*. This improvement may be due to the more efficient and fast metal-halogen exchange. This is also observed for entries 3 and 4, with the *in situ* generated species leading to substantially higher yield.

Table 1: Comparison of reaction conditions for the *Grignard* reaction showcased in **Scheme 27**.

Entry	Ar	1. Condition	2. Condition	Overall yield
1	$C_6H_3(CF_3)_2$	**88**, ^{i}PrMgCl, THF 0 °C to rt, 15 h	$BF_3{\cdot}OEt_2$, CH_2Cl_2, 0 °C to rt, 1 h	33%
2	$C_6H_3(CF_3)_2$	**88**, THF 0 °C to rt, 15 min	$BF_3{\cdot}OEt_2$, CH_2Cl_2, 0 °C to rt, 1 h	30%
3	C_6F_5	**89**, ^{i}PrMgCl, THF 0 °C to rt, 15 h	$BF_3{\cdot}OEt_2$, CH_2Cl_2, 0 °C to rt, 1 h	19%
4	C_6F_5	**89**, THF 0 °C to rt, 15 min	$BF_3{\cdot}OEt_2$, CH_2Cl_2, 0 °C to rt, 1 h	43%

Nevertheless, the precursors **86** and **87** were deprotonated with KO*t*Bu and immediately oxidized with *p*-chloranil to yield red solids (**Scheme 29**). As previously established, assuming the green color for the radicals originates from the π-system of the framework, no change in color should occur, as the underlying molecular framework has not been modified. The appearance of a red species strongly indicates that the radical was generated during the reaction but could not be sufficiently stabilized as similarly observed for the all-phenyl-substituted compound **75**.

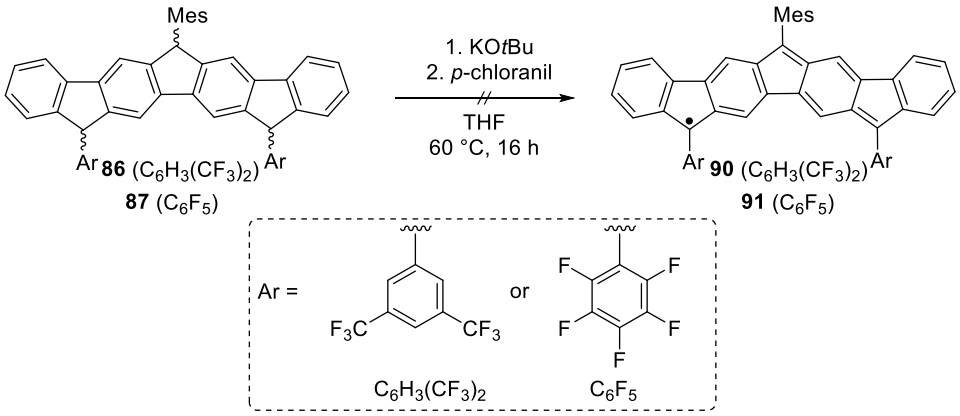

Scheme 29: Unsuccessful attempts to obtain radicals **90** and **91**.

A rather unnatural behavior was observed during the analysis of the corresponding ^{1}H NMR spectra. No signals were detected, which would typically indicate paramagnetic properties. However, analysis by mass spectrometry did not confirm the expected radicals. As previously discussed for the all-phenyl-substituted framework **75**, a closer examination of the molecular scaffold could provide valuable insights into the failure of the reaction.

Both residues (**90** and **91**) exhibit the same structural feature as the phenyl-substituted system, the ability to rotate unhindered. In the case of **90**, the steric hindrance provided by the CF_3 moieties is not sufficient enough. Moreover, the absence of sterically demanding moieties in *ortho* positions, as in case of mesitylene, results in a possible rotation. This enables a co-planar alignment between the substituent and the core, potentially increasing the spin density at the *para* position. Such an arrangement can facilitate secondary reactions, such as dimerization, similar to what has been described for the *Gomberg* radical. A similar pattern can be observed for structure **91**.

These valuable insights enable us to establish potential criteria for the formation and stabilization of radical species. For a radical to be effectively stabilized, a nodal plane must exist at the radical center. This condition is only met when the substituent is oriented orthogonally to the core. Achieving such an orientation depends on the nature of the substituent. Specifically, the substituent must be appropriately modified, they should bear sterically demanding groups at the *ortho* positions. These bulky groups prevent rotation around the molecular axis, thereby preventing linear alignment with the core. This restriction enforces the orthogonal arrangement necessary to establish a nodal plane, that prevents the interaction of the orbitals of the substituents with the core.

In principle, a similar effect could be achieved by modifying the core itself, through the introduction of methyl groups at specific positions to restrict or entirely prevent rotation of the attached substituents. However, such approaches were not made as it involves considerable synthetic effort and hence will not be discussed in the scope of this work. Overall, despite indications from the respective NMR spectrum, such as the absence of characteristic resonances, there is no clear evidence that a radical species was formed. However, neither structure was subjected to further investigation.

The group of *Yang et al.*[74] further expanded the scope of substituents by exploring the influence of polycyclic aromatic groups such as anthracene (An). In order to evaluate the effect of anthracene on both the heptacyclic structure and its radical character, a *Grignard* reagent was prepared from 9-bromoanthracene (**92**) and reacted with dialdehyde **48**. However, subsequent treatment with $BF_3{\cdot}OEt_2$ did not furnish the heptacyclic precursor (**Scheme 30**). It remains unclear, whether the failure occurred during the formation of the *Grignard* reagent or during the subsequent cyclization to the heptacyclic structure **94**, as

intermediate **93** was not isolated and subjected directly to a *Lewis* acid-induced *ortho* fusion. Since neither the ^{1}H NMR nor the mass spectra provided evidence of the desired precursor, the synthesis of **94** is considered as unsuccessful. No further investigations were conducted regarding this issue, and the focus was redirected toward exploring other promising substituents.

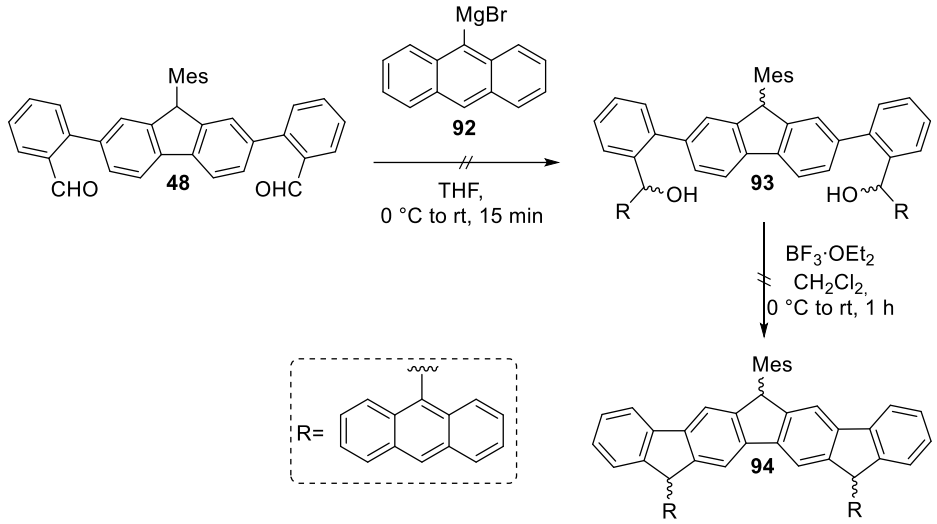

Scheme 30: Unsuccessful attempt to introduce anthracene to the heptacyclic system.

Alternatively, adamantyl (Ad) can be utilized as a promising substituent with sufficient bulkiness. Therefore, a *Grignard* reagent was prepared from 1-bromoadamantane (**95**) and reacted with dialdehyde **48**. Subsequently, the crude product **96** was treated with $BF_3{\cdot}OEt_2$ to induce the *ortho* fusion to the heptacyclic scaffold **97** (**Scheme 31**). Again, the desired precursor could not be detected neither in the ^{1}H NMR nor the mass spectra, suggesting the failure of the synthesis.

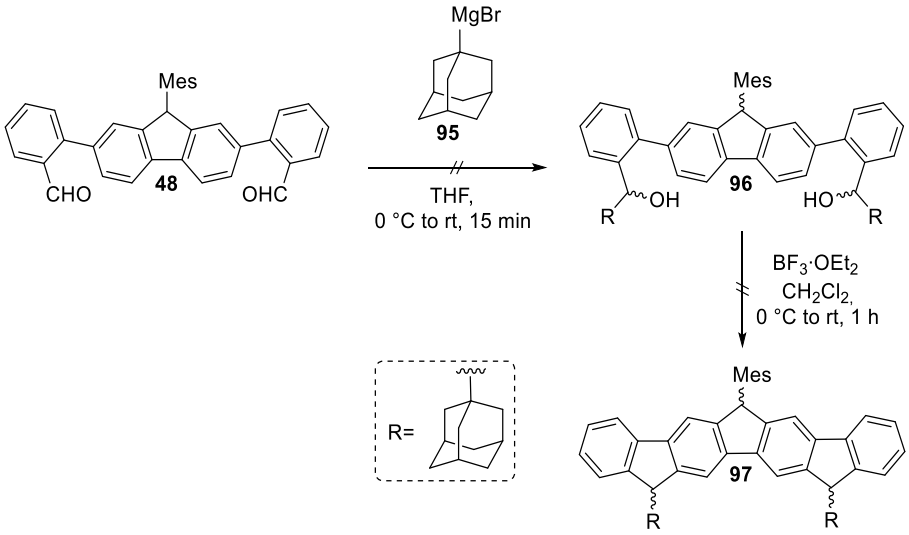

Scheme 31: Unsuccessful attempt to introduce adamantane to the heptacyclic system.

In this chapter, the influence of various substituents on the stability of heptacyclic radicals was systematically investigated. While mesityl groups enabled successful radical formation, phenyl and related substituents, *e.g.* C_6F_5 and $C_6H_3(CF_3)_2$, were unable to form stable radicals. The incorporation of substituents such as anthracenyl and adamantyl were unsuccessful. This instability can be attributed to the lack of steric hindrance, which allows unrestricted rotation and orbital overlap with the core, promoting subsequent reactions such as dimerization. The results highlight that effective radical stabilization requires bulky *ortho* substituents to maintain an orthogonal alignment and to preserve nodal planes at the radical center. Furthermore, the NOON values were evaluated for **83** and **79** and y_0 values of 0.25 and 0.26 were obtained. These results are in accordance with obtained y_0 values for previously described systems. Based on these observations, the focus shifts to extended systems with larger aromatic units to investigate the effects of the π-system extension on the properties of the radicals. This can be accomplished by applying the concept of *ortho* linking established in this project to other terphenyl precursors. By incorporating conjugated aromatic substructures (such as naphthalene units) into the teraryls, it is possible to generate radicals consisting of more rings. The following chapter will explore the synthesis of such systems in greater detail and highlight the differences compared to the previously discussed structures.

4.3 Synthesis of Nonacyclic Scaffolds

Given the limited number of CP-PAH radicals currently investigated, expanding the range of accessible substrates is of significant importance. While the previous chapter focused on the variation of substituents on the existing scaffold, this chapter aims to extend the π-system to gain insight into larger systems.

The most convenient approach to access these systems is by extending the π-system of the coupling reagents. Replacing benzene units with naphthalene building blocks increases the size of the scaffold from a heptacyclic to a nonacyclic system. Through targeted functionalization, the structure of the resulting polyaromatics can be precisely tuned, allowing for the formation of possible three symmetric regioisomers. To achieve a comparable system, the focus was set on the synthesis of nonacyclic structures incorporating rings A and B. Structure C should be similarly achievable but will not be discussed in the scope of this work. **(Figure 23**).

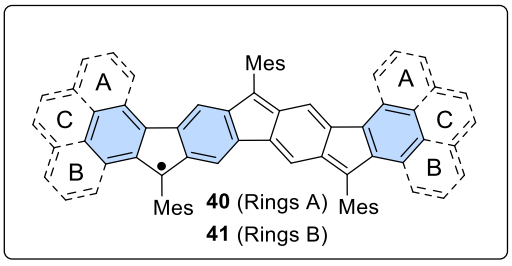

Figure 23: Possible three different regioisomers of a nonacyclic system.

The synthesis of the desired radicals was initiated by the preparation of the corresponding boronates **101** and **105** (**Scheme 32** and **33**).

Boronate **101** was synthesized in an overall yield of 58% over three consecutive steps (**Scheme 32**). Starting from commercially available 1-bromo-2-methylnaphthalene (**98**), bromination with *N*-bromo succinimide (NBS) afforded intermediate **99** in an excellent yield of 91%.[139] Subsequent hydrolysis of the resulting dibromomethyl derivative **99** generated the corresponding carbaldehyde **100** in an excellent yield of 93%.[139] Finally, a *Miyaura* borylation afforded boronate **101** in a fair yield of 68%.[140]

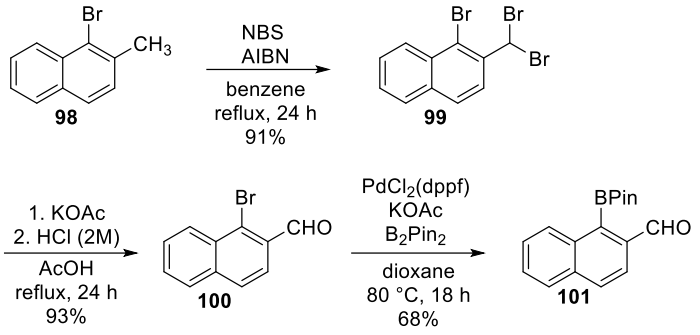

Scheme 32: Synthesis route towards boronate **101**.

Two different strategies were investigated for the synthesis of boronate **105**. In an initial attempt, following the procedure reported by *Li et al*.,[141-142] 3,4-dihydronaphthalen-2(1*H*)-one (**102**) was reacted with DMF and PBr_3, affording intermediate **103** in a good yield of 76%. Subsequent oxidation of **103** with 2,3-dichloro-5,6-dicyano-1,4-benzoquinone (DDQ) generated compound **104** in a good yield of 72% with small traces of impurities, which could not be separated from the product. In a final step, **104** was subjected to a *Miyaura* borylation, which resulted in the isolation of a defunctionalized naphthyl building block, as the ^{1}H NMR revealed (**Scheme 33**).

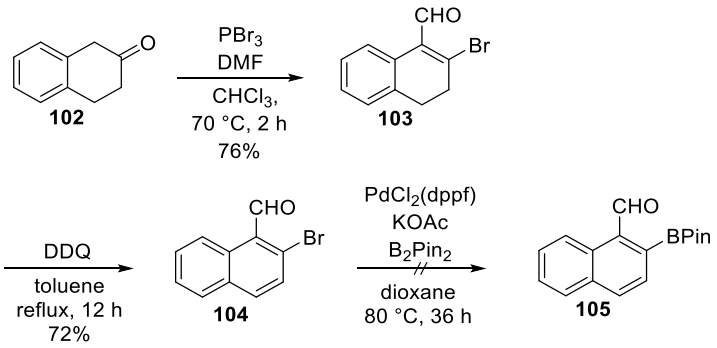

Scheme 33: Unsuccessful synthesis route towards boronate **105**.

In an alternative approach, commercially available 2-methoxynaphthalene **106** was formylated in a *Vilsmeier-Haack* reaction to yield the corresponding aldehyde **107** in an excellent yield of 94%.[143] Subsequent demethylation with $AlCl_3$ furnished 2-hydroxynaphthalene-1-carbaldehyde (**108**) in a good yield of 76%.[142, 144] As the final borylation reaction step requires the presence of either a halogen or a triflate, compound **108** was reacted with Tf_2O to generate intermediate **109** in a fair yield of 61%.[145] In a concluding step, **109** was borylated in a *Miyaura* reaction, affording boronate **105** in a quantitative yield. Overall, the targeted boronate **105** was obtained in a total yield of 44% over four consecutive reaction steps (**Scheme 34**).

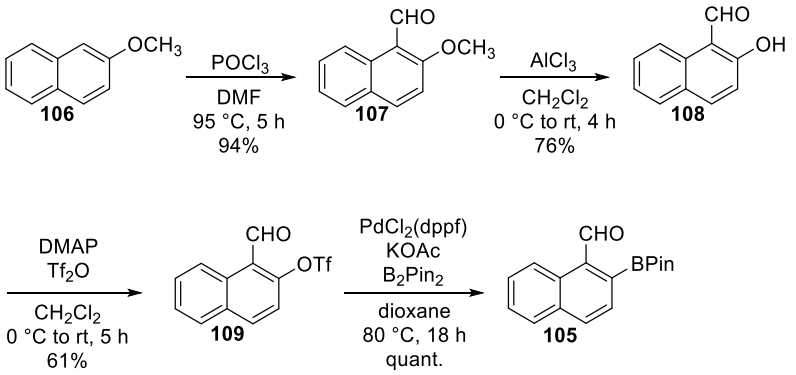

Scheme 34: Alternative synthesis route towards boronate **105**.

The conversion of commercially available 2,7-dibromo-fluoren-9-one (**45**) to the respective mesityl-substituted fluorene **46** was conducted according to the already described procedure. Double *Suzuki* coupling of boronates **101** and **105** with the fluorene building block **46**, respectively, afforded dicarbaldehydes **110** and **111** in yields of 67% and 44%, respectively. In a nucleophilic addition with MesMgBr, both dicarbaldehydes were subjected to the corresponding dialcohols **112** and **113** and subsequently transferred to the nonacyclic structures in a *Lewis* acid-promoted cyclization in good yields of 79% (**114**) and 78% (**115**), respectively (**Scheme 35**). Analysis by NMR spectroscopy provided evidence for the presence of three diastereoisomers for both precursors. It is assumed, that no regioisomers were formed during this reaction step, which is supported by the evidence of observed similar splitting patterns in the ^{1}H NMR spectra, which align with those of the previously described radical precursor **50**.

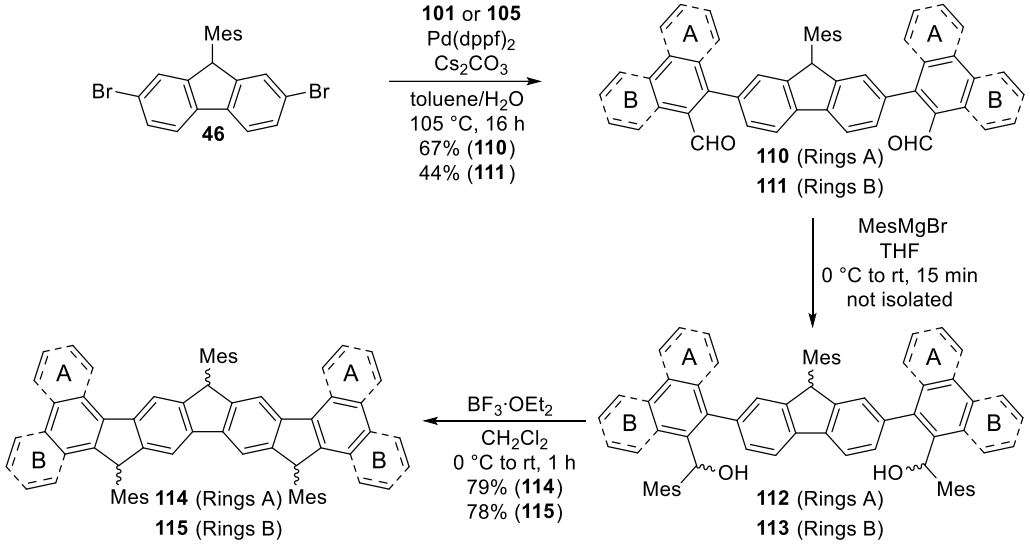

Scheme 35: Synthetic route of radical precursors **114** and **115**.

To finalize the synthesis route, precursors **114** and **115** were deprotonated with KO*t*Bu and immediately oxidized with *p*-chloranil furnishing a dark green solid (**40**) in an excellent yield of 96%. Radical **41** was obtained analogous to **40** in a quantitative yield as a dark blue solid (**Scheme 36**).

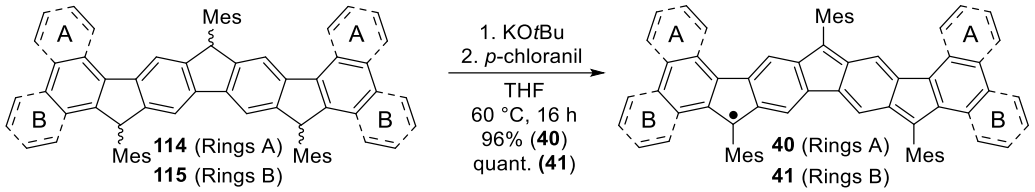

Scheme 36: Synthesis of radicals **40** and **41**.

Conventional analytical methods such as mass spectrometry provides a sufficient indication of the success of the reaction but cannot verify the structure of compounds **40** and **41**. Therefore, verification was intended by X-ray crystallographic analysis. Many attempts were made to obtain single crystals suitable for X-ray crystallographic analysis of **40** and **41**, but the tendency to form dendritic crystals or amorphous solid-state structures, like in case of radical **39**, prevented crystallographic structure elucidation. Fortunately, single crystals of their corresponding precursors **114** and **115** could be obtained by slow evaporation in toluene, yielding colorless crystals suitable for X-ray analysis (**Figure 24**). These crystallographic data not only confirmed the constitutional framework of the polycyclic cores, but also of the radicals, since the finalizing oxidation step to form the radicals is inactive in terms of skeletal modification of the polyarene, as previously demonstrated.[93] Therefore, the solid-state structures of precursors **114** and **115** can be considered as a strong evidence for the proposed linear anellation of the targeted compounds. While **114** crystallized in a triclinic crystal system, **115** crystallized in a monoclinic crystal system. This outcome supports the assumption that more than one diastereoisomer was formed during the respective cyclization.

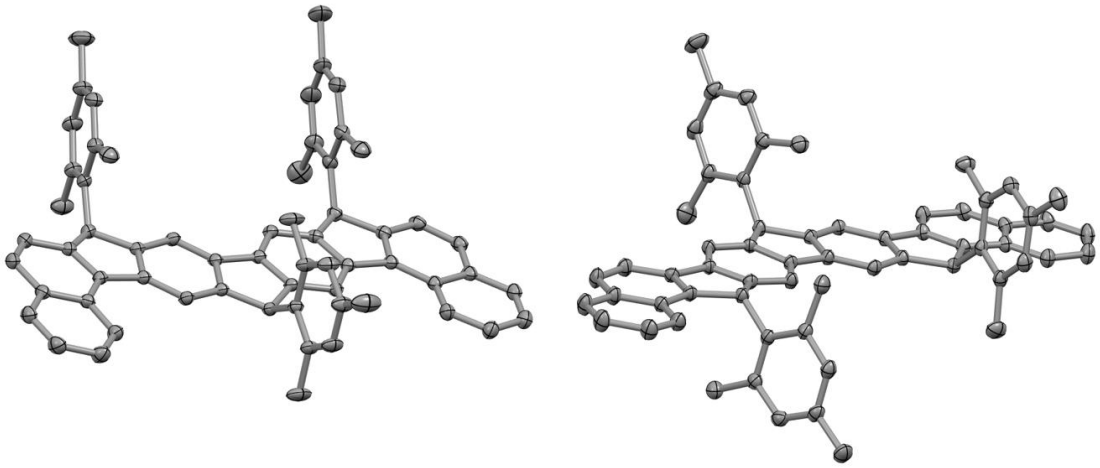

Figure 24: Molecular solid-state structures of all-*cis*-**114** (left) and *cis,trans*-**115** (right) obtained by single-crystal X-ray diffraction. Hydrogen atoms and co-crystallized toluene molecules are not shown for clarity. Thermal ellipsoids are drawn at the 30% probability level. Data was provided by Dr. *Jonas Wenzel*.[146]

A previously described compound **43** by *Herzog et al*.[93] represents the first helical and thus chiral CP-PAH stable carbon-centered radical (**Figure 12**). To further expand the scope of possible helical radical structures and to investigate whether a separation of both isomers, *P* and *M,* is possible by HPLC, since a separation by *Herzog et al*.[93] did not succeed for the heptacyclic system. Therefore, this helical scaffold **43** was employed as a template and its π-system targeted for extension by using suitable naphthyl moieties, as introduced for the linear systems. The possible three regioisomers are shown in **Figure 25**.

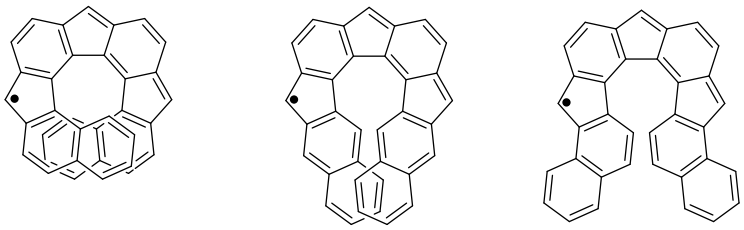

Figure 25: Possible three regioisomers of π-extended helical carbon-centered radicals.

The corresponding boronates **101** and **105** required for the preparation of structure **116-I** and **116-III** have already been described in this chapter. Since structure **116-I** could potentially cause synthetic difficulties due to its steric nature, the synthesis of the sterically least demanding structure **116-III** was pursued as proof of concept.

The preparation of the required fluorene **122** was carried out according to *Herzog et al*.[93] However, the reported one-pot synthesis of 2,2',6,6'-tetrabromo-1,1'-biphenyl (**118**) by *Perron et al*.[145] demonstrated several challenges including elaborate synthesis, moderate

yield and the use of hazardous reagents, which led to the consideration of an alternative synthesis route with milder reaction conditions.

Consequently, multiple efforts were made to initially synthesize 1,3-dibromo-2-iodobenzene (**119**), followed by its conversion to the corresponding biphenyl (**118**). Following a published method,[147] 1,3-dibromobenzene (**117**) was iodinated by generating lithium diisopropylamide (LDA) *in situ* through the reaction of *n*-BuLi and diisopropylamine (DIPA) at −78°C, followed by the addition of iodine, obtaining compound **119** in a yield of 40%. The reported yield of 93% could not be reproduced, possibly due to the absence of a syringe pump for the controlled addition of 1,3-dibromobenzene (**117**) to the *in situ* generated LDA, as used in the original procedure. As an alternative approach and to minimize the harsh reaction conditions, 2,6-dibromoaniline (**120**) can be utilized as a starting agent to initiate a *Sandmeyer*-type reaction (**Scheme 37**).

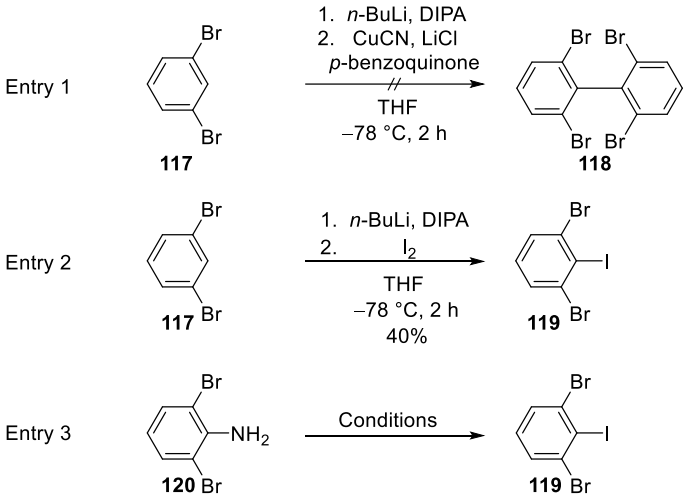

Scheme 37: One-pot synthesis of **118**. Alternative synthetic approaches to generate **119**.

Two similar approaches were conducted according to *Witten et al*.[148] and *Greulich et al*.[149] to generate 1,3-dibromo-2-iodobenzene (**119**) in yields of 41% and 92%, respectively (**Table 3**).

Table 2: Different reaction conditions to obtain 1,3-dibromo-2-iodobenzene **119**.

Entry	Conditions	Yield
1	Conc. HCl, $NaNO_2$, KI 0 °C, 5 h	41%
2	Conc. H_2SO_4, $NaNO_2$, KI 0 °C, 5 h	92%

Furthermore, *Greulich et al*.[149] exploited the conversion of **119** to the corresponding biphenyl **118** through a chemoselective iodine-lithium exchange with *n*-BuLi and a subsequent $CuBr_2$-mediated oxidative homocoupling (*Ullmann* coupling) to generate **118** in a poor yield of 25% (**Scheme 38**).

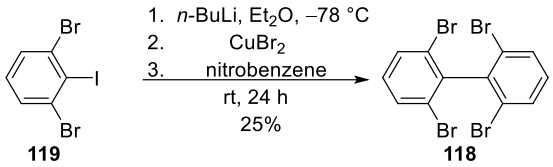

Scheme 38: Synthesis of biphenyl **118** through a $CuBr_2$-mediated oxidative homocoupling.

Leroux et al.[150] investigated the role of nitrobenzene in this reaction system. Their observations revealed that nitrobenzene remains unchanged, since no reduction products were isolated. Instead, it ensures higher reaction yields by acting as a co-solvent, facilitating higher solubility and reactivity of the copper species. This, in turn, enhances transmetalation and the subsequent reductive elimination. In contrast, increasing the amount of $CuBr_2$ did not result in an increased yield, which was also observed in the conducted experiments. Despite multiple attempts, only a yield of 25% was achieved. Possible reasons can be traced to the insolubility of the copper species in Et_2O and the insufficient solubility increase by the co-solvent. Since Nitrobenzene is highly toxic, no attempts were made to increase the amount used and the synthesis route continued with the obtained amount of product. In an alternative approach, the homocoupling can be facilitated by the use of freshly activated copper as reported by *Holzwarth et al*.[151] However, under these conditions, the desired biphenyl species **118** could only be obtained in traces. The reflux time of 3 h likely leads to unwanted functionalization on the bromine atoms, making this approach rather ineffective for the underlying system (**Scheme 39**).

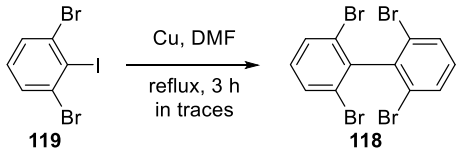

Scheme 39: Alternative homocoupling of **119** with freshly activated copper.

For this reason, no further approaches were pursued. Instead, the synthesized biphenyl **118** was subjected to a halogen-metal exchange reaction in the presence of methyl chlorocarbonate to obtain the corresponding fluorenone **121** in a yield of 65%. In a

subsequent reaction step, **121** was converted in a one-pot approach to its corresponding mesityl substituted fluorene **122** in a yield of 46% **(Scheme 40**).

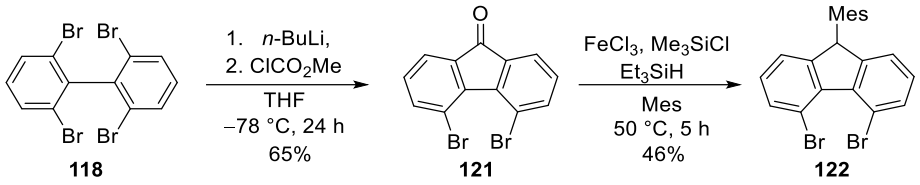

Scheme 40: Synthesis of biphenyl **118**, subsequent conversion to fluorenone **121** and its corresponding mesityl substituted fluorene **122**.

Next, fluorene **122** was subjected to a double *Suzuki* coupling with boronate **101**. The coupling of sterically demanding compounds can be facilitated by using SPhos as co-ligand. However, analysis by ^{1}H NMR spectroscopy revealed that only the mono-coupled species was generated without any traces of the bicoupled product **123** (**Scheme 41**). The unsuccessful outcome can likely be attributed to the steric hindrance imposed by the scaffold. It can be assumed that the coupling proceeds stepwise, with the first coupling unit occupying a considerable amount of space and thereby hindering the addition of the second unit.

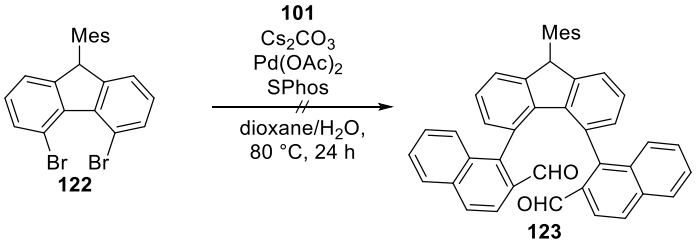

Scheme 41: Unsuccessful double *Suzuki* coupling of **122** with boronate **101** to obtain **123**.

Due to the labor-intensive synthesis of fluorene **122** and the limited amount available, no attempts were made to screen for reaction conditions.

4.3.1 Radical Character of the Nonacyclic Systems

The radical nature of **40** and **41** was initially confirmed by the absence of any resonances in conventional frequency ranges of their respective NMR spectra. Further evidence for their radical character was provided by their EPR activity. Measured X-band EPR spectra (**Figure 26**) for both radicals showed broad single lines centered around g = 2.0027 (**40**) and g = 2.0024 (**41**), respectively, without any discernible hyperfine couplings. Additionally, computationally calculated parameters allowed the simulation of both spectra, which showed overall good agreement with the experimentally obtained plot.

The broad singlet can again be explained by calculating the hyperfine coupling constants. These reveal that no strong coupling of individual protons is present, which would have resulted in a resolvable splitting pattern. Instead an equal participation of all protons is observed, leading to the broad signal.[94]

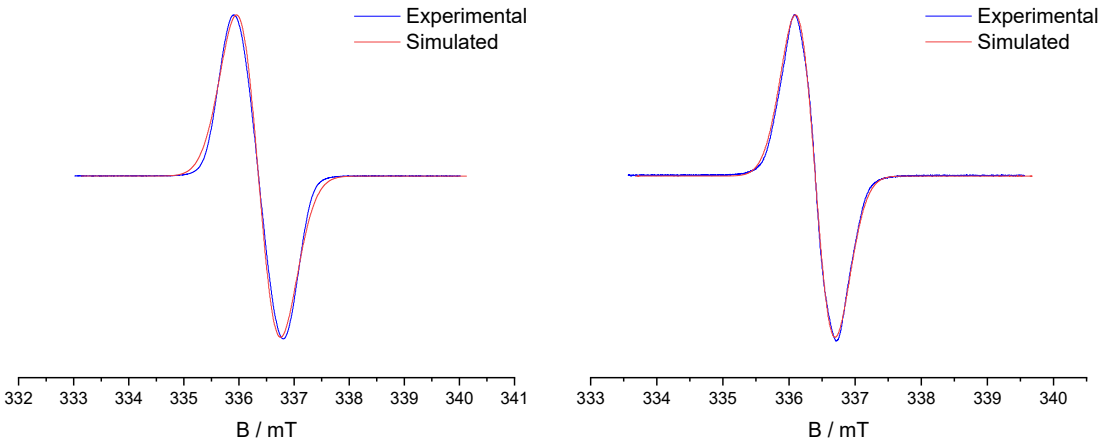

Figure 26: Measured cw X-band (9.4214 GHz) EPR spectra (blue) of **40** and **41** in toluene (0.1 mM) at ambient temperature showing a single resonance signal centered at *g* = 2.0027 (**40**) and *g* = 2.0024 (**41**). Simulated spectra (red) were obtained for **40** (S = ½, no hyperfine couplings, linewidth peak-to-peak (lwpp) = 0.95) and **41** (S = ½, no hyperfine couplings, lwpp = 0.6). Data provided by Dr. *Jonas Wenzel*.[146]

As already described for the heptacyclic system, again three distinct resonance formulas can be derived for **40** and **41** (**Scheme 42**). Within this ensemble, structures **40/41-I** and **40/41-III** are particularly noteworthy. Structures **40/41-I**, monoradical species, retain three intact benzene units. Structures **40/41-III**, triradical species, preserve the largest possible number of intact benzene rings making them the most relevant according to *Clar's* rule. In contrast, structure **40/41-II**, also monoradical species, display intact benzene units only on the terminal rings and are therefore the least significant members of the ensemble.

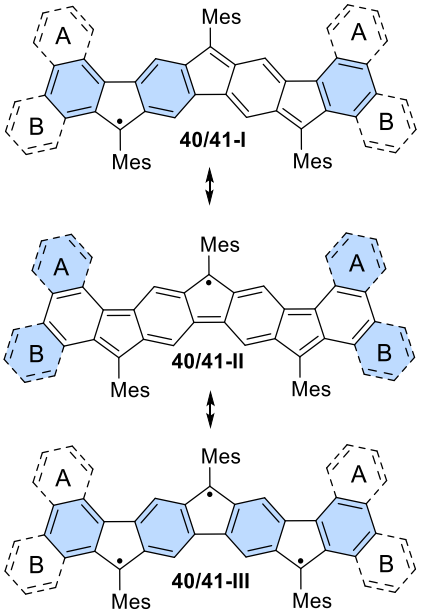

Scheme 42: Resonance formulas of radicals **40** and **41**; Structures **40/41-I** and **40/41-II** exhibit monoradical character, while **40/41-III** exhibit a triradical configuration. Fully intact benzene units are highlighted in blue.

As mentioned, structures **40/41-III** display a triradical character. However, calculation of the natural orbital occupation numbers (NOONs) and application of the *Yamaguchi* scheme led to y values of only 0.36 (**40**) and 0.39 (**41**), respectively, indicating a small contribution of their triradical character. These results support the assumption that, while structures **40/41-III** may be thermodynamically more stable, the resonance forms **40/41-I** are the favoured representations.

4.4 Synthesis of a Undecacyclic Radical System

The previous chapters explored various aspects, including the investigation of different substituents and their influence on radical systems, ultimately allowing for the derivation of criteria regarding radical formation and compound stabilization. In addition, efforts were made to expand the π-system by employing suitable building blocks, thereby broadening the range of possible structural motifs and enabling the identification of key characteristics.

The focus will now shift not only to expanding the π-system, as in the previous chapter, but also to increasing the number of potential radical centers within the framework. While this can be achieved using the synthetic strategies introduced in previous chapters, it requires a suitably modified building block. Given the considerable synthetic challenges associated with such a building block, the synthesis of a more accessible dimethyl

substituted building block **124** will first be pursued as a proof of concept. This compound will then serve as a coupling reagent for the previously described *Suzuki* coupling with the mesityl substituted fluorene **46**. Upon obtaining the corresponding radical, work will proceed with the synthesis of the mesityl substituted building block **125** (**Figure 27**).

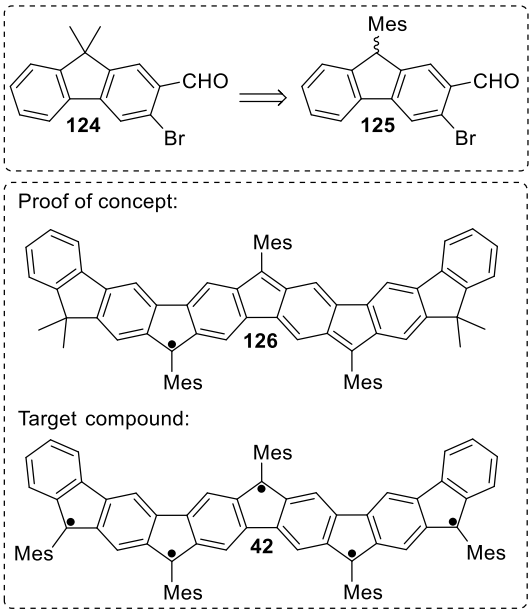

Figure 27: Illustrated are the patent reported building block **124** and the targeted building block **125**; compound **126** as proof of concept and the targeted structure **42**.

The synthesis towards radical **126** was initiated by the preparation of the corresponding building block **125**. Starting point of the synthesis was the bromination of the commercially available 9,9-dimethyl-9*H*-fluoren-2-amine (**127**) with NBS, obtaining 3-bromo-9,9-dimethyl-9*H*-fluoren-2-amine (**128**) in an excellent yield of 95%. In the following step, **128** was reacted in a *Sandmeyer*-type reaction, affording the halogenated species **129** in a fair yield of 61%. Treatment of **129** with ^{i}PrMgCl provided the *in situ* generated *Grignard* species, which was converted to the aldehyde **124** with DMF in a good yield of 70%. In a concluding step, **124** was reacted in a *Miyaura* borylation, affording the desired building block **130** in a fair yield of 59%. Overall, the targeted structure was obtained in a total yield of 24% over four consecutive reaction steps (**Scheme 43**).

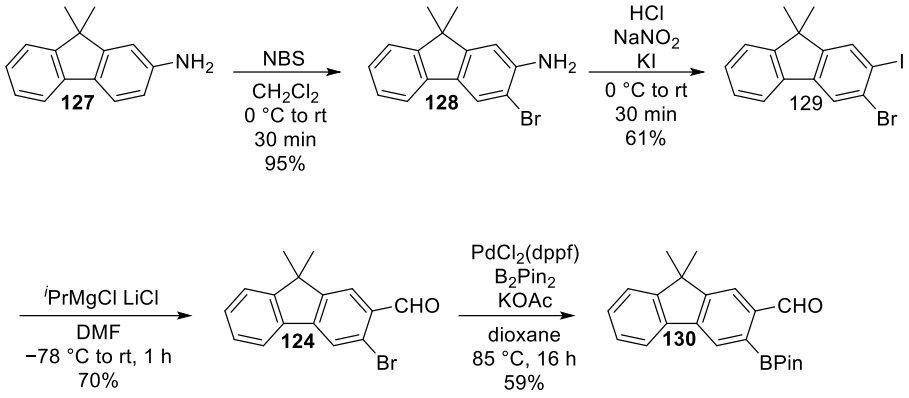

Scheme 43: Synthesis route towards building block **130**.

Subsequent double *Suzuki* coupling of **46** with boronate **130** generated **131** in a fair yield of 52%. Following nucleophilic addition with MesMgBr converted dicarbaldehyde **131** into the corresponding dialcohol **132** and treatment with $BF_3 \cdot OEt_2$ furnished precursor **133** in a good yield of 77% over two steps as a pink solid (**Scheme 44**). As already described for previous radical precursors, no formation of regioisomers should be possible due to the steric hindrance ensured by the bulky mesityl groups.

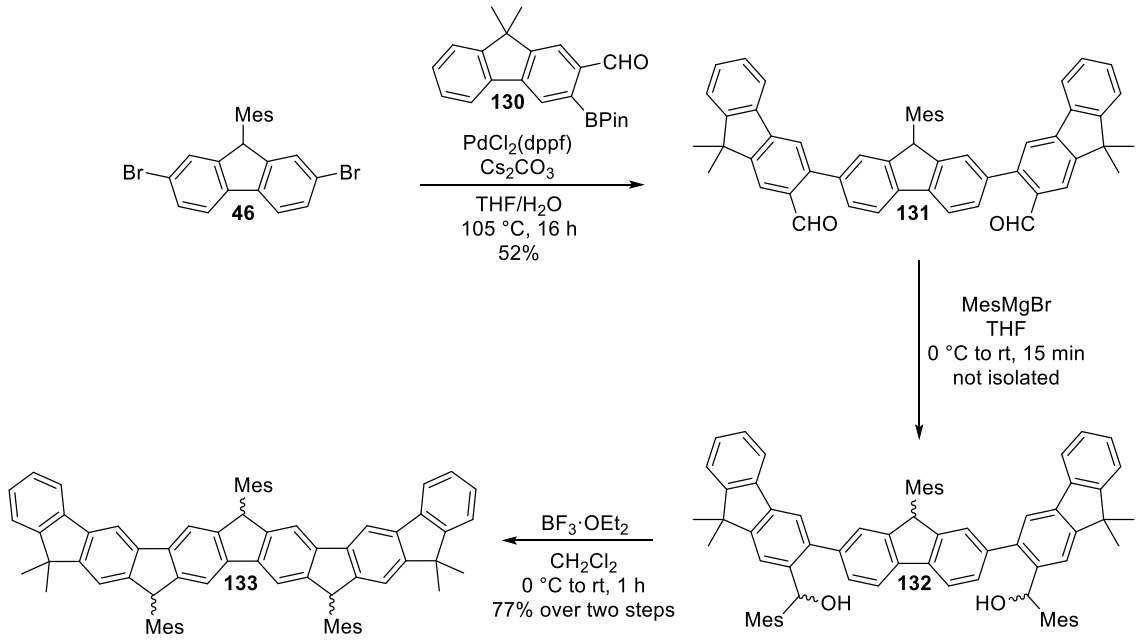

Scheme 44: Synthesis route towards precursor **133**.

In a concluding step, the mixture of isomers of **133** were deprotonated with KO*t*Bu and immediately oxidized with *p*-chloranil, furnishing radical **126** in a very good yield of 81% as a dark green solid (**Scheme 45**).

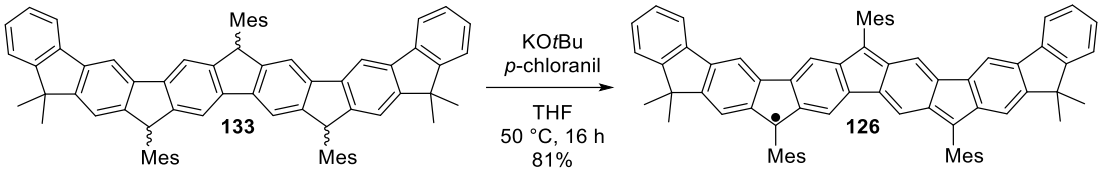

Scheme 45: Synthesis of radical **126**.

The synthesis of radical **126** provides a fundamental basis for further investigation of π-extended radical systems. It not only serves as proof of concept that larger structures with notable stability can be achieved, but also as a template for a particularly intriguing system. As illustrated in **Figure 27**, replacing both methyl groups on the five-membered rings with a mesitylene unit and a hydrogen atom, would yield an entirely novel structure, one that may potentially exhibit a pentaradical character. The synthesis and comprehensive analysis of this new radical will be discussed in detail in the following section and is initiated by the preparation of the required building block **125**, which is derived from the previously introduced structure **124** (**Figure 27**).

In this context, commercially available 9*H*-fluoren-2-amine (**134**) was utilized as a staring agent, enabling two potential synthetic pathways to access compound **137**. In the first approach, **134** can be subjected to a bromination using NBS, affording the corresponding brominated intermediate **135** in a good yield of 72%. Subsequent iodination of the amine moiety through a *Sandmeyer*-type reaction provided **136** in a poor yield of 31%. The poor yield can be attributed to the formation of an undesired side product with polarity similar to that of the product. This complicated the purification by column chromatography and required subsequent recrystallization. In a final step, **136** was treated with KOH under oxygen atmosphere, generating the oxidized product **137** in a poor yield of 42%. Overall, this synthetic sequence allowed to obtain building block **137** in a total yield of 9% over three consecutive reaction steps (**Scheme 46**).

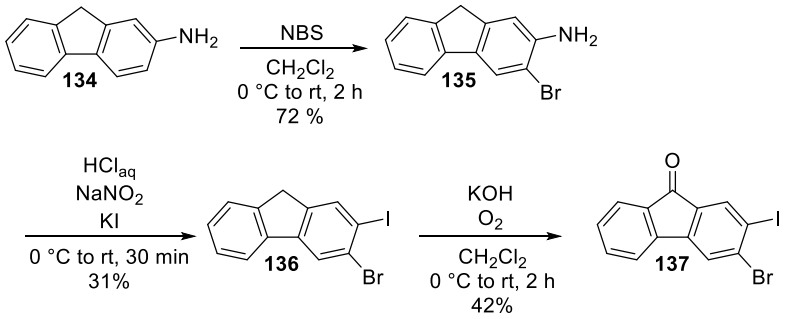

Scheme 46: First synthetic approach towards **137**.

In a second approach, 9*H*-fluoren-2-amine (**134**) was initially oxidized to the corresponding fluorenone derivative **138** in an excellent yield of 95%. Subsequent bromination with NBS resulted in intermediate **139** in a very good yield of 88%. In a finalizing step, iodine was introduced to **139** through a *Sandmeyer*-type reaction, obtaining **137** in a poor yield of 26%. As already discussed, the noticeable poor yield can be attributed to the formation of an unwanted species. Overall, **137** was obtained in an improved total yield of 22% over three consecutive reaction steps (**Scheme 47**).

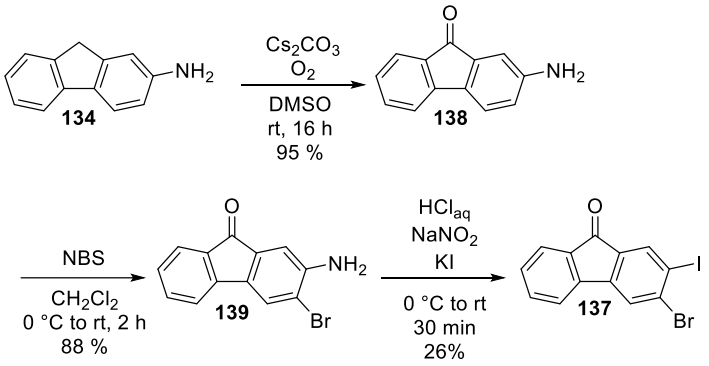

Scheme 47: Second synthetic approach towards **137**.

The comparison of both synthetic sequences highlights their advantages and limitations. In general, the bromination step provided similar yields in both approaches. The most significant difference in terms of yield is observed for the oxidation step. While the second sequence afforded the fluorenone derivative (**138**) in excellent yield of 95%, the first sequence resulted in a considerably lower yield of 42%. This lower yield can possibly be attributed to the shorter reaction time of 2 h, resulting in an incomplete conversion of the starting material, which was also confirmed by ^{1}H NMR spectroscopy. The iodination in both sequences through a *Sandmeyer*-type reaction generally resulted in low yields. Again, the formation of an unwanted species in competition to the desired compound was observed, which was separated from the product by recrystallization. Overall, it appears to be more advantageous to shift the iodation step, since this reaction step tends to limit the overall yield regardless of the sequence.

The obtained fluorenone **137** was converted to the corresponding mesityl-substituted fluorene **141**. Therefore, a two-step strategy was employed, by nucleophilic addition of the MesMgBr reagent and subsequent reduction to the corresponding alcohol **140** in a fair yield of 68%. Since previous attempts on different systems provided better yields for this method, an attempt was made to enhance the yield by utilizing the one-pot approach.

Applying this strategy allowed to obtain the corresponding mesityl substituted fluorene **141** in an excellent yield of 91% (**Scheme 48**).

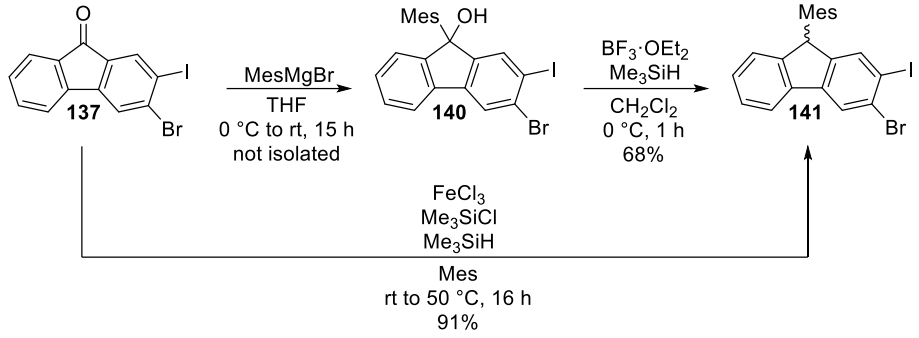

Scheme 48: Two different approaches towards **141**, including the two-step method and the one-pot strategy.

Subsequent treatment of **141** with ^{i}PrMgCl·LiCl formed the *in situ* generated *Grignard* species, which was then converted to the aldehyde **125** with DMF in a fair yield of 58%. In a concluding step, **125** was reacted in a *Miyaura* borylation, furnishing boronate **142** in a quantitative yield (**Scheme 49**).

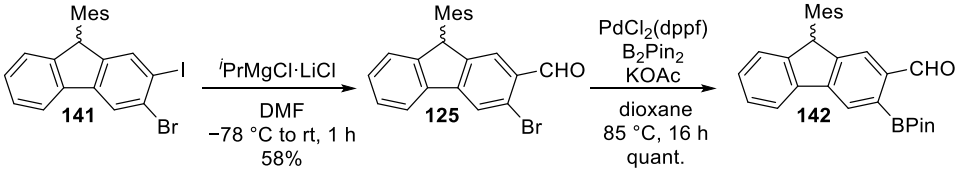

Scheme 49: Synthesis of boronate **142**.

Next, the obtained boronate **142** was subjected to a double *Suzuki* coupling with 2,7-dibromo-9-mesityl-9*H*-fluorene (**46**), obtaining the coupled product **143** in a poor yield of 4% (**Scheme 50**). Further investigation of this reaction step revealed that the desired product (**143**) is only generated unfavorably. Identified by products reveal the presence of the mono coupled species and further unfunctionalized starting materials probably caused by protodeboronation, which is described as the hydrolysis of a boronic acid to the parent arene and boric acid. Such behavior is especially observed for boronic acids, which do not withstand the harsh reaction conditions, making them prone to protodeboronation. Based on NMR spectroscopy it is assumed that the mono-coupled species shown in **Scheme 50** within the box was isolated, which would possibly enable the synthesis of another isomer of the heptacyclic system.

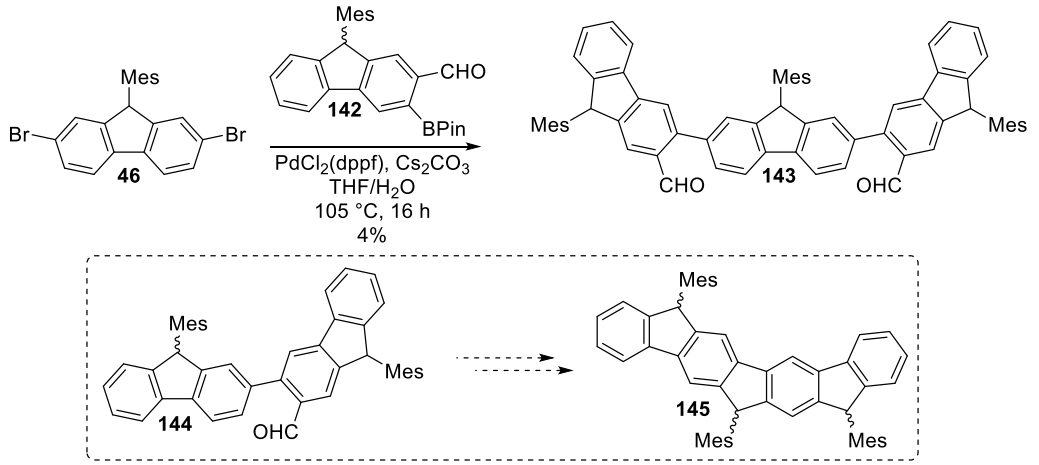

Scheme 50: *Suzuki* coupling of boronate **142** with building block **46**; isolation of the mono-coupled species **144**, further allowing the synthesis of another isomer (**145**) of the heptacyclic system.

In an alternative approach, instead of borylating compound **125**, the core building block **46** was subjected to a *Miyaura* borylation, generating the borylated intermediate **146** in a fair yield of 59%. This intermediate was then reacted in a double *Suzuki* coupling with **125** to obtain the bicoupled product **143** in a slightly improved yield of 15% (**Scheme 51**). An advantage of this reaction sequence was the simplified purification. However, no significant improvement in the overall yield could be achieved.

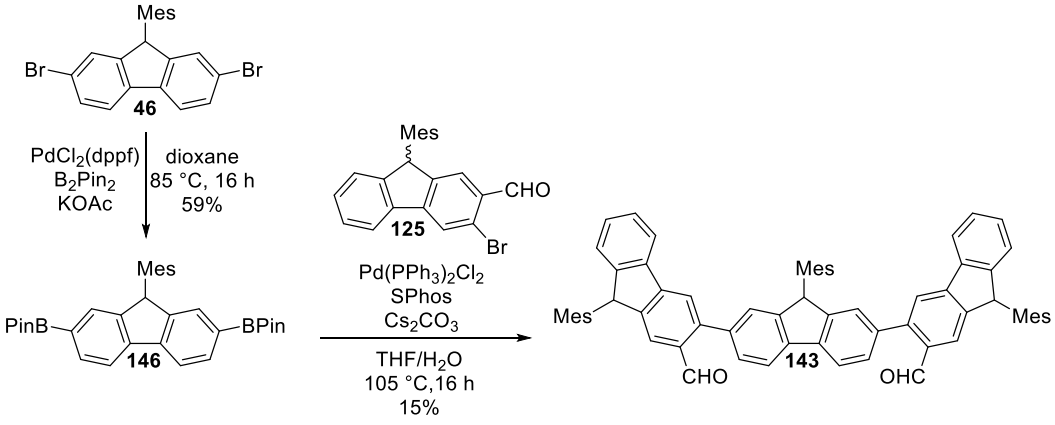

Scheme 51: Alternative sequence to synthesize **143**.

Intermediate **143** was next subjected to a nucleophilic addition using a mesityl *Grignard* reagent, followed by an intramolecular cyclization promoted by $BF_3 \cdot OEt_2$, furnishing the undecacyclic scaffold (**148**) composed of alternating five- and six-membered rings in a yield of 88%. The synthetic sequence was completed with the conversion of **148** to the corresponding radical species by deprotonating with KO*t*Bu and immediate oxidation with *p*-chloranil to yield the target product **42** in traces as a violet solid (**Scheme 52**).

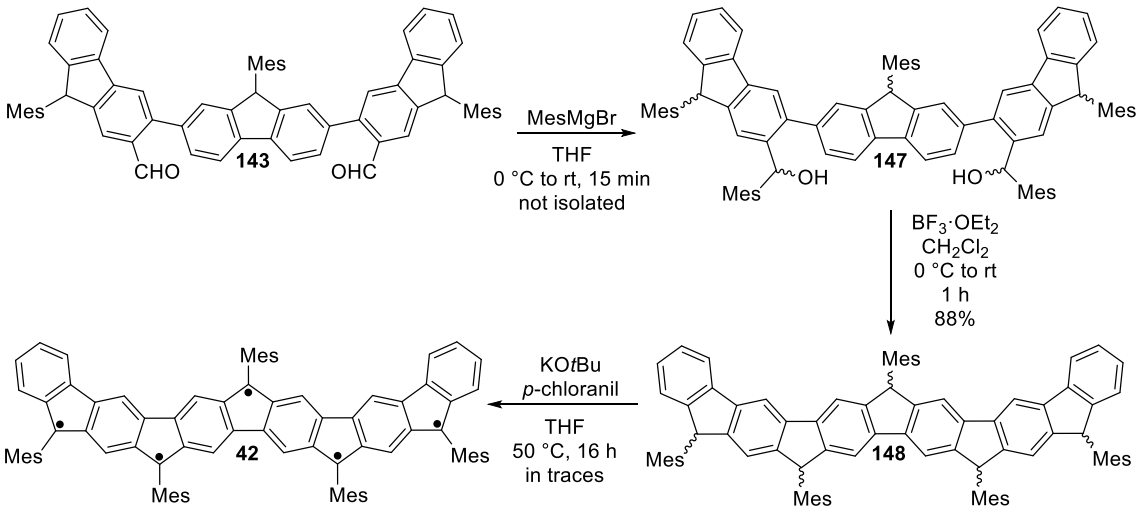

Scheme 52: Synthesis sequence to obtain radical **42**.

In the following section, the radical character of compounds **126** and **42** will be discussed utilizing both experimental and computational methods.

4.4.1 Radical Character of Undecacyclic Systems

The radical nature of **126** was initially confirmed by the absence of any resonances in conventional frequency ranges in its respective NMR spectra. Further evidence for the radical character was provided by its EPR activity. A measured X-band EPR-spectra (**Figure 28**) shows a broad single line centered around g = 2.0038 without any discernible hyperfine couplings.

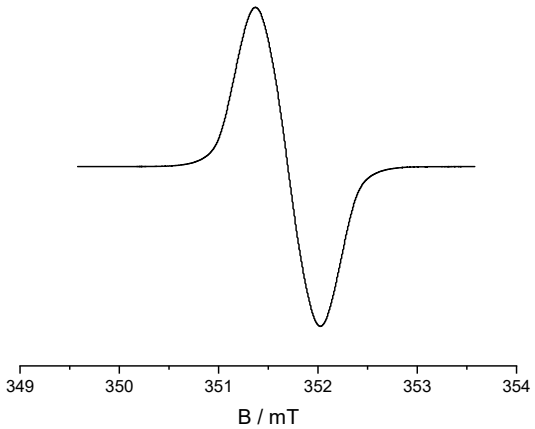

Figure 28: Cw X-band (9.4214 GHz) EPR spectrum of **126** in toluene (1 mM) at ambient temperature showing a single resonance signal centered at g = 2.0037. Data provided by M. Sc. *Johannes Werner.*

A detailed investigation of the possible resonance structures of **126** (**Scheme 53**) reveals correlations with prior described conclusions. Among these, structures **126-I** (monoradical species) and **126-III** (triradical species) are particularly outstanding,

preserving five and six intact benzene units, respectively. Structure **126-II** (monoradical species) retains no intact benzene units and is therefore the least significant member of the ensemble. The terminal benzene rings do not contribute to the electronic delocalization of the system, due to the interruption of conjugation by the dimethyl groups on the outer cyclopentadiene units. Under this assumption, the presented compound would be formally equivalent to the linear heptacyclic system **39**. In conclusion, the incorporation of building block **130** enabled the expansion of the molecular framework but had only a limited impact on the radical's intrinsic properties.

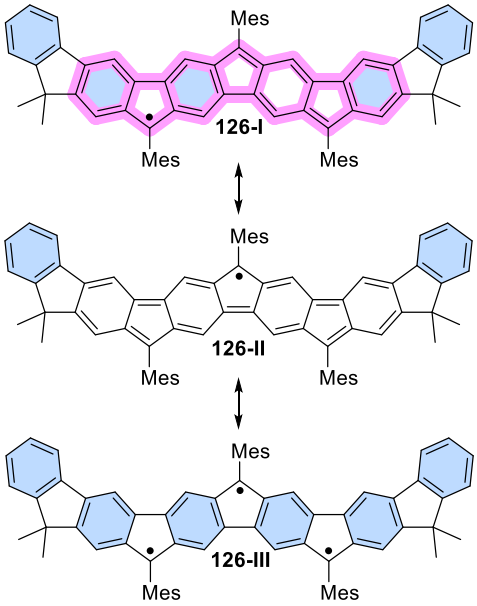

Scheme 53: Resonance formulas of radical **126**; Structure **126-III** exhibits triradical character, while **126-II** and **126-I** exhibit a monoradical configuration. Fully intact benzene units are highlighted in blue. Comparison to the linear heptacyclic radical system (**39**) is highlighted in purple.

In principle, the triradical contribution can be estimated by calculating the natural orbital occupation numbers (NOONs) and applying *Yamaguchi* scheme. However, no significant deviation of the triradical character compared to **39** is to be expected, due to the interruption of the conjugation. Analogous to **39**, the electronic structure remains effectively delocalized only within the highlighted heptacyclic subunit (**Scheme 53**). Consequently, the radical character of both systems is anticipated to be closely comparable.

In contrast, evaluation of the radical nature of **42** posed some difficulties. The comparison of the NMR spectra of radical **42** and its precursor **148** revealed the partial or complete disappearance of several distinct signals, generally supporting the paramagnetic behavior

of the compound. However, analysis by mass spectrometry could not provide the necessary evidence for the formation of the radical species. Therefore, the successful synthesis of **42** could not be confirmed with absolute certainty. Further evidence was provided by the EPR activity of **42** (**Figure 29**). A measured X-band EPR spectrum shows a broad single line centered around g = 2.0063 without any discernible hyperfine couplings. Due to the limited availability of the compound, a higher-quality spectrum could not be obtained. Nevertheless, computationally derived parameters enabled the simulation of the corresponding spectrum, which showed overall good agreement with the experimental data. This supports the conclusion that the compound exhibits a radical character.

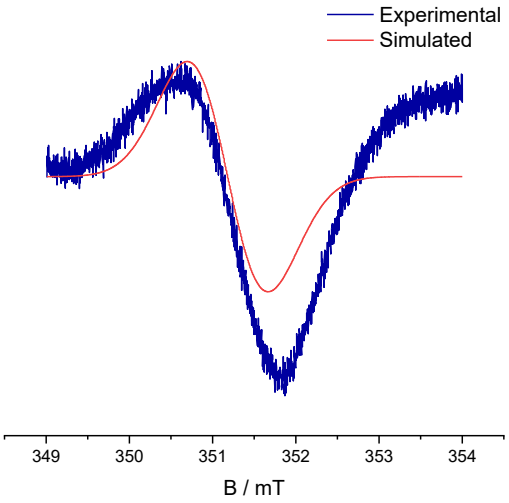

Figure 29: Cw X-band (9.4214 GHz) EPR spectrum of **42** in toluene (1 mM) at ambient temperature showing a single resonance signal centered at g = 2.0063. Data provided by M. Sc. *Johannes Werner.*

Selected possible resonance structures of compound **42** are shown in **Scheme 54**. Among these, structure **42-I** represents a particularly intriguing system, since it allows for a pentaradical configuration while preserving six fully intact benzene units, formally making it the most significant in the ensemble of possible resonance structures. However, the stabilization of this electron configuration might be impossible. In contrast, structure **42-II** features a triradical configuration with four intact benzene units, while structure **42-III** adopts a monoradical configuration with three intact benzene units. A rather interesting comparison can be made between structures **42-II** and **42-III**. While the previously described radicals displayed a dominant monoradical configuration, this system may result in a dominant triradical configuration.

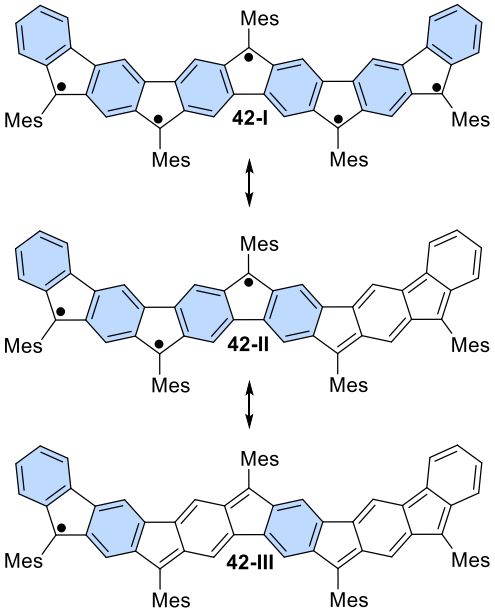

Scheme 54: Most relevant resonance structures of radical **42**. Structure **42-I** exhibits pentaradical character, while **42-II** exhibits triradical character and **42-I** a monoradical configuration. Fully intact benzene units are highlighted in blue.

The evaluation of the pentaradical character of **42** is highly complex and therefore not conducted in this work. However, the assessment of the triradical character is more accessible. While previous systems have consistently exhibited a monoradical configuration, in this case, a stable or even dominant triradical species may be present. This behavior can be examined in a similar manner to the systems described previously. However, it is anticipated that such an investigation presents additional challenges and complexities, requiring more comprehensive analysis. Therefore, it falls outside the scope of the present work and will not be examined further.

4.5 CP-PAH Exhibiting Potential Diradical Character

Through appropriate modification, a target structure can be achieved which theoretically exhibits a biradical character, as observed for the described IF. For this purpose, it appears reasonable to employ a previously by the group of *Majewski*[127] reported substructure as the core and to modify it accordingly through appropriate synthetic methods (**Figure 30**).

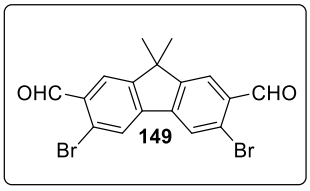

Figure 30: Building block **149** as a core unit.

The synthesis started with the bromination of **150** with NBS, obtaining **151** in a poor yield of 14%. This low yield can be attributed to the relatively short reaction time of 3 h. To address this issue, another batch was set up while increasing the reaction time to 18 h. Nevertheless, no significant improvement in the yield was observed. Further investigation by ^{1}H NMR spectroscopy revealed the presence of the three brominated species, which occurs as an unwanted side reaction, possibly explaining the resulting poor yield. Subsequently performed *Sandmeyer*-type reaction yielded the halogenated species **152** in a poor yield of 30%. Treatment of **152** with ^{i}PrMgCl LiCl formed the *in situ* generated *Grignard* species, which was then converted to the aldehyde **149** with DMF in a poor yield of 15%. A direct comparison with **124** (the mono-functionalized building block discussed in **Scheme 43**) shows a significant difference in the obtained yields (15% vs 70%) and confirms that double functionalization reactions generally result in lower yields, in contrast to the single equivalent reactions. Assuming, the addition of the formyl units proceeds step by step, extensions of the reaction time for the formation of the *Grignard* reagent and the subsequent nucleophilic addition could result in an improvement of the isolated yields. Furthermore, it is plausible that unwanted aryne formation occurs during the reaction. This highly reactive intermediate can participate in side reactions, leading to an overall reduced yield.[152] Nevertheless, the obtained building block **149** was subjected to a double *Suzuki* coupling with phenylboronic acid (**153**) to obtain intermediate **154** in a fair yield of 55% (**Scheme 57**). Since the amount of product obtained for the previous reaction step was not sufficient to continue the reaction sequence, the conversion to the diol, followed by the intramolecular cyclization to the heptacyclic core **155** and the conversion to the targeted radical species **156** could not be performed.

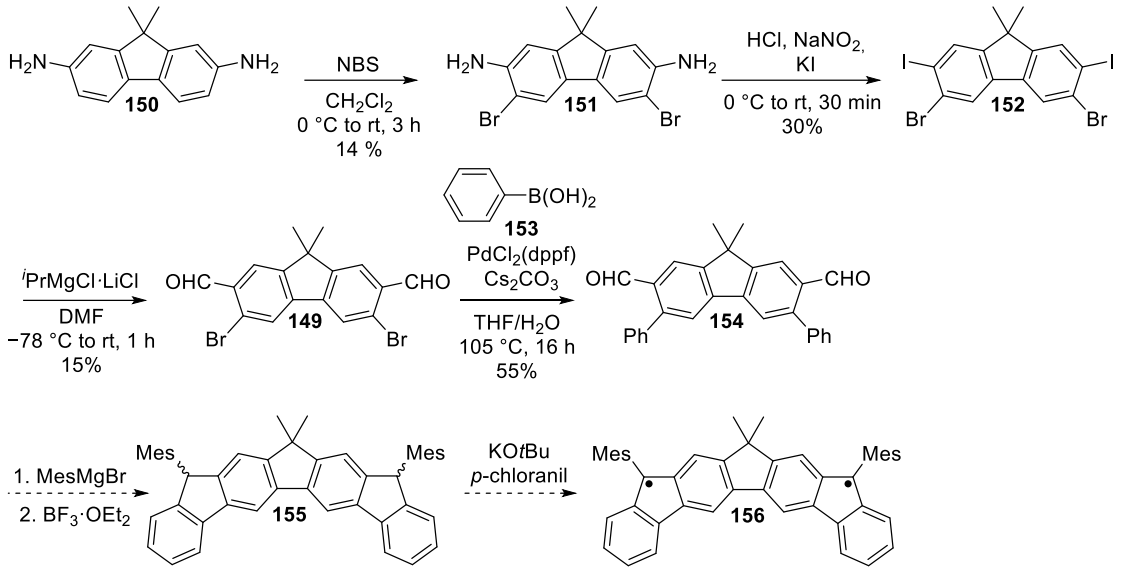

Scheme 55: Synthesis route towards diradical **156**.

Nevertheless, the structural features of **156** provide a foundation for in-depth analysis and critical discussion. In **Scheme 56** two resonance formulas are shown of **156**. While resonance structure **156-I** exists in its closed-shell form, structure **156-II** exhibits a potential diradical character. As already discussed in Chapter **2.1.2**, similar compounds based on IF exhibit only a biradical character but are primarily defined by their closed-shell configuration. The open-shell configuration arises from an increase in the number of intact benzene units, which according to *Clar's* rule represents the most stable configuration. A similar pattern is observed here. While the closed-shell configuration shows intact units only at the termini of the framework, the open-shell structure gains two additional intact benzene units.

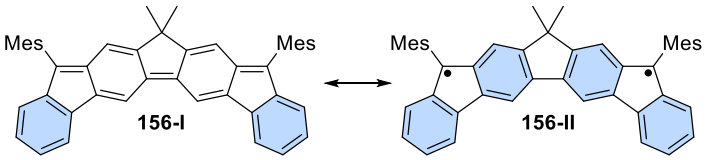

Scheme 56: Resonance structures of **156**. Structure **156-I** exists in its closed-shell form, while structure **156-II** exhibits potential diradical character. Fully intact benzene units are highlighted in blue.

4.6 Contributions to the Synthesis of Polycyclic Hydrocarbons Containing Seven-Membered Rings

The synthesis of polyaromatic hydrocarbons has predominantly focused on cyclopentadiene units, whereas cycloheptatriene units have only been studied in a few cases.[153-155] In order to investigate the potential for synthesizing polycyclic radicals

incorporating cycloheptatriene motifs, preliminary work has been carried out to investigate the required *ortho* fusion.

Pentacycle **165** (**Scheme 60**) can be described as a closed-shell compound and is clearly not a radical, due to its even number of seven-membered rings. Nevertheless, its preparation can serve as a valuable template for the construction of larger polycycles bearing unpaired electrons, *i.e*., radicals. Furthermore, these less studied structures can significantly influence the properties of the radicals and even display unexpected reactivity during their synthesis, or their applications for example in organic electronics, due to their observed low HOMO/LUMO gaps.[154] The synthesis of pentacycle **157** and its key intermediate, diketone **158**, has been reported several times (**Scheme 57**).[153, 155-156] However, preparation of **157** was achieved in this work in a significantly shortened and simplified sequence with a slightly improved overall yield of 21%.

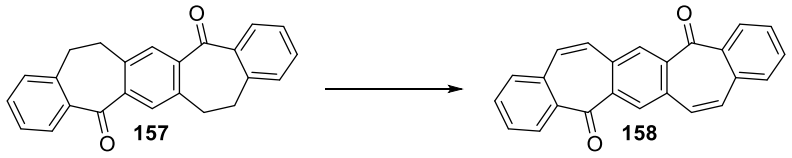

Scheme 57: Pentacycle **157** and the key intermediate diketone **158**.

In contrast to the described preparation of pentacycle **157**,[155] in this approach the synthesis was initiated by the esterification of 2,5-dibromoterephthalic acid (**159**) to obtain dimethyl 2,5-dibromoterephthalate (**160**) in an excellent yield of 96%. Subsequent transformation of **160** in a palladium-mediated *Heck* coupling with styrene resulted in the bicoupled species **161** in a fair yield of 66%. Although the formation of *E*/*Z* isomers is theoretically possible in this reaction step, analysis by NMR spectroscopy indicates that such isomers are not formed. This can be concluded from the absence of the corresponding resonances in the spectrum, likely due to the steric nature of the core. Subsequent reduction with H_2 gave **162** in a good yield of 79%. The sequence was finalized with the saponification of the ester function (**162**), giving **163** in an excellent yield of 94% (**Scheme 58**).

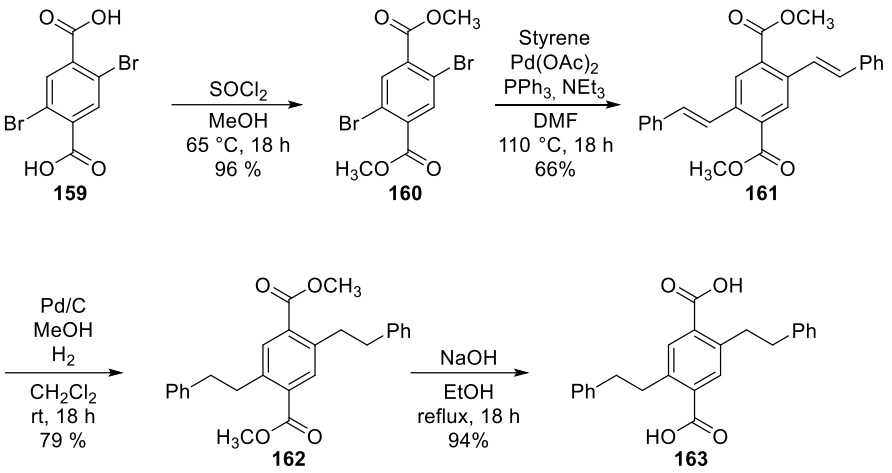

Scheme 58: Reaction sequence to synthesize **163**.

As previously described, the double intramolecular cyclization of **163** was described several times in literature and can be performed under various reaction conditions. In this context, *Yang et al*.[155] utilized polyphosphonic acid at 155 °C. However, this approach proved to be challenging in practice, due to the honey-like viscosity of the substance, which made handling and transfer very difficult. Furthermore, it was observed that no homogeneous mixture was formed, resulting in a significant portion of the starting material reacting only partially or not at all. This probably explains the reduced yield of 53% compared to the reported yield of 60%. In a later publication *Yang et al*.[154] reported on the synthesis of a similar pentacycle consisting of a cycloheptatriene unit and a cyclopentadiene unit, as well as on the corresponding cyclization using methanesulfonic acid. However, applying these conditions to this system did not yield the desired product. *Kobin et al*.[157] reported a more interesting approach by converting the carbonyl function into the more reactive acetyl chloride species, followed by condensation by using methanesulfonic acid. Following the reported procedure, $AlCl_3$ was employed to catalyze the cyclization similarly to *Friedel-Crafts* acylation, yielding diketone **157** in an excellent yield of 96%. In order to introduce the double bonds on the cycloheptatriene moiety, radical bromination was performed and immediately eliminated obtaining diketone **158** in a yield of 46% over two reaction steps (**Scheme 59**).

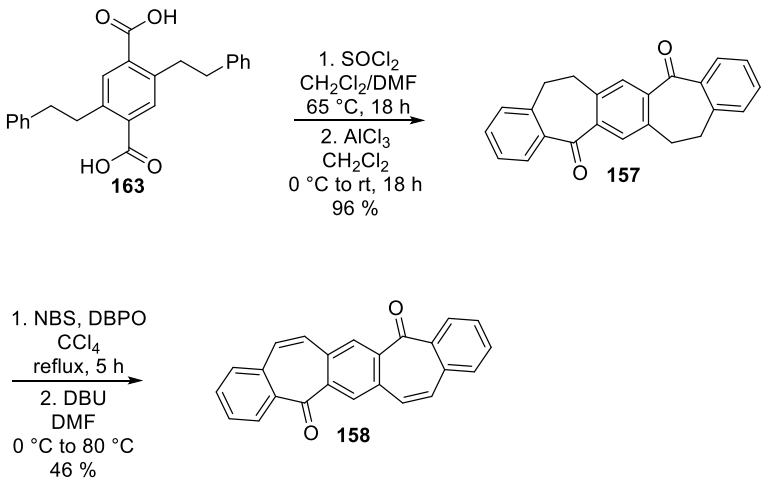

Scheme 59: Synthetic route towards diketone **158**.

Mesitylene was utilized several times in this work as a bulky residue on the polycyclic cores and was again used in this context to obtain diol **164** in a quantitative yield. Confirmation of the product could not be achieved by ^{1}H NMR spectroscopy due to the presence of diastereoisomers, which could not be separated by column chromatography due to their similar polarities, generally complicating structure elucidation. However, mass spectrometry confirmed the successful formation of **164**. Subsequent treatment with $SnCl_2$ under acidic conditions did not yield the reduced species **165** (**Scheme 60**). A possible reason for the failure of the reaction may lie in the inherent instability of both the dialcohol **164** and its corresponding reduced product **165**. Since the double bond on the heptacyclic unit does exhibit strong double-bond character, possible side reactions cannot be neglected, *e.g.*, activation with sunlight or polymerization in the purification process by column chromatography. The acidic nature of silica gel might be sufficient enough to initiate such polymerization. This high reactivity is further supported by the antiaromatic nature of the product. Similar behavior was also reported by *Yang et al.*,[154] who reported the required deactivation of the used silica gel prior to purification, which again did not allow to isolate the desired product, which is why no further efforts were attempted to isolate the reduced species.

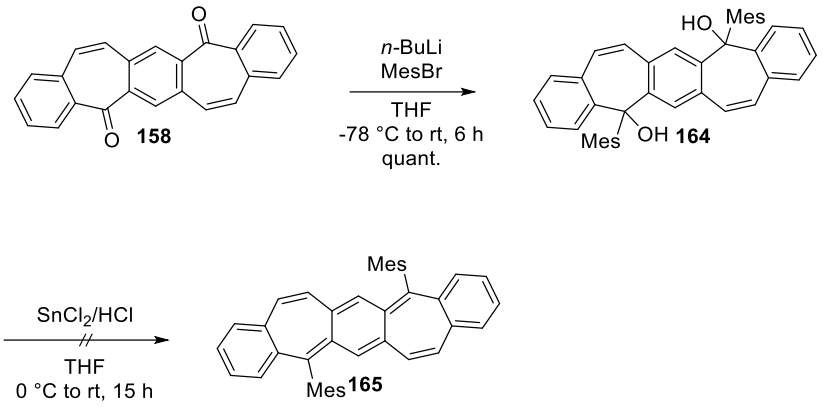

Scheme 60: Unsuccessful attempt to synthesize **165**.

Analogously, the corresponding isomer of **158** has not been reported in the literature. However, it should be easily accessible through variation of the starting material (**Scheme 61**). In this context, commercially available dimethyl 2-aminoterephthalate (**166**) was selectively brominated with NBS to afford intermediate **167** in a yield of 31%. The relatively low yield can be attributed to the formation of differently substituted species. A following S*andmeyer*-type reaction allowed to obtain the iodinated species **168** in a yield of 48%. Subsequent palladium-mediated *Heck* coupling with styrene did not result in the bicoupled species **169**. Analysis by ^{1}H NMR spectroscopy revealed the presence of the mono-coupled species, with a defunctionalization at the C−Br bond. A possible reason might be due to the different reactivities of iodine and bromine. Assuming the substitution proceeds stepwise, this would result in the formation of the mono-coupled species. This intermediate, in combination with the ester moiety, could sterically hinder the subsequent coupling. This interpretation would also confirm the observed mono-coupled species observed in the ^{1}H NMR spectrum. Alternatively, introducing bromine during the *Sandmeyer* reaction step could result in equal reactivity at both positions. However, this approach does not eliminate the possibility that stepwise substitution remains the limiting factor.

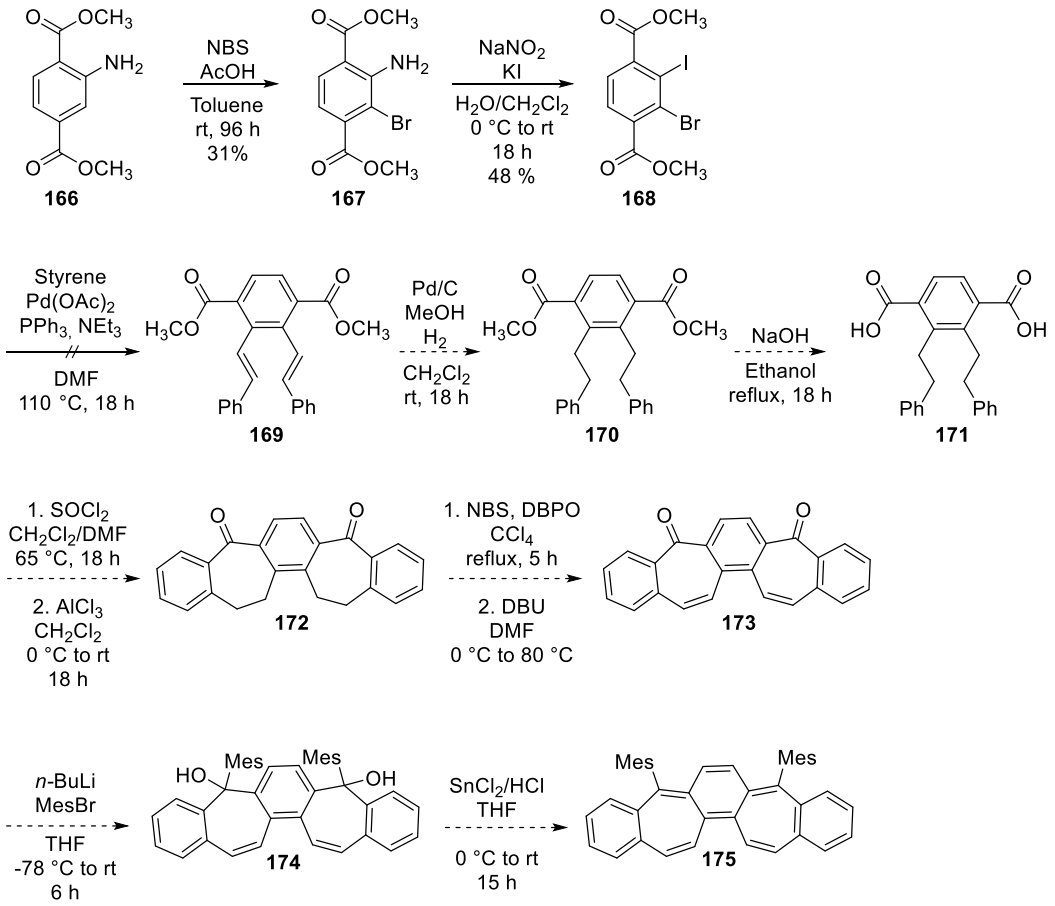

Scheme 61: Proposed synthetic route to obtain pentacycle **175**.

The preliminary work on the synthesis of cycloheptatriene-containing polyaromatic hydrocarbons has not only resulted in alternative and improved synthetic strategies but has also provided valuable insights into further potential target compounds featuring polycyclic radicals. While these target structures have not yet been explored, a brief outline of potential future directions is provided in the 'Outlook' section.

4.7 Investigation of the Properties of the Synthesized Radical Systems

4.7.1 Optical and Electrochemical Properties

In order to enable photophysical characterization of the synthesized radical systems, UV/Vis absorption spectra were initially recorded in CH_2Cl_2. These measurements provide insights into the electronic structure and absorption properties of the compounds and serve as a basis for further spectroscopic investigations.

4.7.1.1 Optical and Electrochemical Properties of the Heptacyclic Systems

The absorption spectrum of **39** (linear heptacyclic radical) displays a series of intense bands across a broad spectral range, extending from the ultraviolet into the visible region (**Figure 31**).

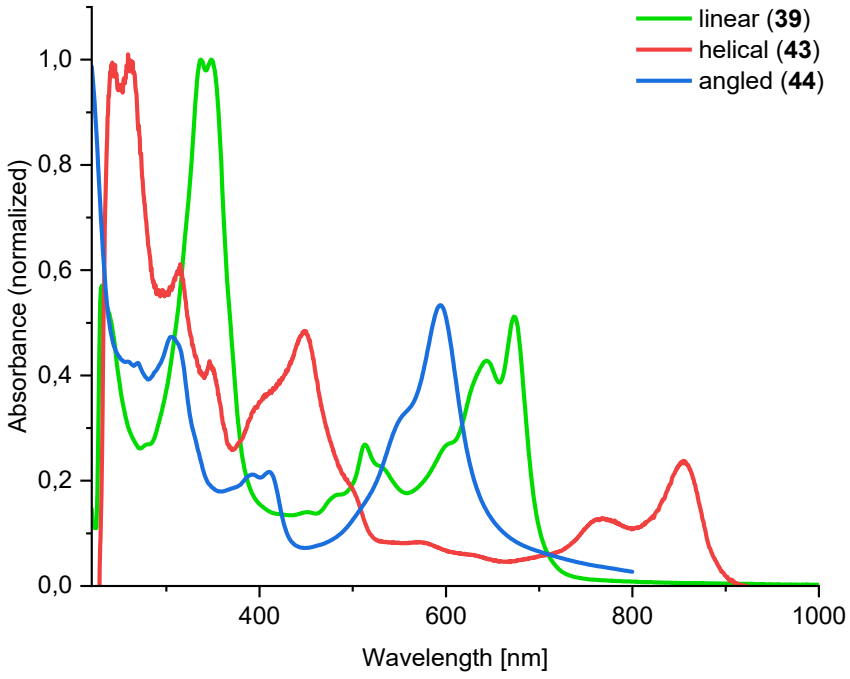

Figure 31 Comparison of UV/Vis Spectra of **39**, **43** and **44**.

The first absorptions appear at 230 nm, followed by two prominent bands of nearly identical intensity between 300–375 nm, with maxima at 337 nm and 348 nm. In the visible region, a weak absorption appears at 450 nm, followed by more substantial peaks at 479 nm and 514 nm. Between 563 nm and 700 nm, three significant absorption

features are noted. The first, at 602 nm, may be interpreted as a shoulder of the more dominant peak at 644 nm. The final well-defined peak appears at 675 nm.

In contrast, **44** (angled heptacyclic radical) exhibits a mirrored pattern of the absorption bands in the region between 218–350 nm, with a slight hypsochromic shift. This shift becomes particularly evident when comparing the absorption bands of **39** (linear system) at 515 nm with **44** (angled system) 393–411 nm, resulting in an overall shift of 113 nm. A similar shift is observed in the region between 640–675 nm (linear) and 545-600 nm (angled system). A direct comparison between **39** and **44** reveals minimal spectral similarity. In particular, the broad absorption band between 300–375 nm and the three significant bands in the region between 563–700 nm in the linear structure are absent in the helical isomer **43**. Instead, **43** displays several absorptions in the UV region and distinctive absorptions in the range between 750–900 nm, where the linear structure shows no activity. However, the spectra of **44** and **43** display more comparable patterns, particularly in the region between 215–500 nm, with the angled isomer again showing a slight hypsochromic shift. As with the comparison between linear and helical forms, absorption in the 500–650 nm region remains faint for the helical isomer, while the angled isomer lacks features in the 750–900 nm range. Considering an overall similarity in the absorption patterns between **39** (linear system), **44** (angled system), and **43** (helical system), the observed absorptions at different wavelengths can possibly be attributed to hypsochromic shift in the angled isomer or a bathochromic shift in the helical isomer. Despite the identical molecular composition of the three compounds, these variations are best explained by structural effects. This hypothesis is further supported by the work of *Tian et al*.,[158] who investigated three fluorenyl-based radical isomers and reported distinct absorption profiles for each compound.

Further investigations examined the impact of substituents (2,6-dichlorophenyl and Ph) on the photochemical properties of the linear heptacyclic system. **Figure 32** illustrates the corresponding absorption spectra of **39** (Mes), **79** (Ph) and **83** (2,6-dichlorophenyl) and enables a direct comparison of their respective absorption behavior.

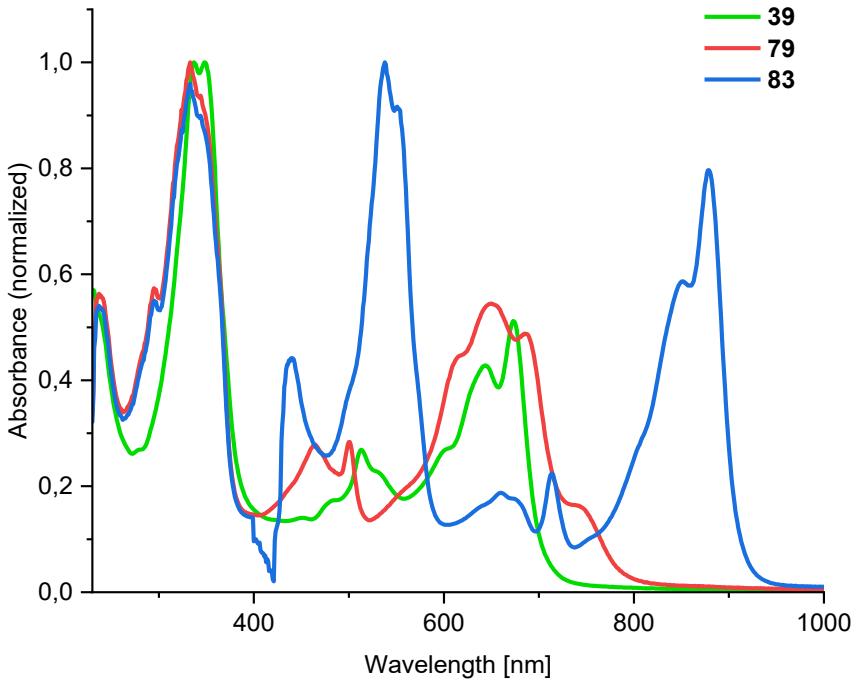

Figure 32: Comparison of UV-Vis Spectra of **39**, **79** and **83**.

The comparison between **39** (Mes) and **79** (Ph) reveals little to no changes in the electronic transition of the system. In contrast, the incorporation of 2,6-dichlorophenyl substituents (**83**) on the linear scaffold leads to significant changes, especially in the visible region. For instance, the bands between 425–600 nm are close to completely absent in both **39** and **79**, whereas the most prominent absorption is observed for **83** in this region. This trend is reversed between 600–725 nm, where a pronounced absorption is observed for **39** and **79** and a very weak absorption band for **83**. Another major difference is observed between 750–930 nm, where no absorption is observed for **39** and **79**, whereas **83** exhibits pronounced absorption in the region. Overall, these observations indicate that electron withdrawing groups on the substituents have significant influence on the absorption behavior.

Additionally, quantum chemical calculations can be utilized to simulate absorption spectra, allowing for direct comparison with experimentally obtained results. Therefore, the UV/Vis/NIR spectrum of **39** was computed using a time-dependent density functional theory (TD-DFT) calculation at the UPBE0/def2-TZVP/GD3BJ level, with a simulated solvent field of CH_2Cl_2. Overall, the calculated spectrum shows good agreement with the experimental data, as illustrated in **Figure 33**. This representation is intended primarily to demonstrate that quantum chemical calculations can produce spectra in good agreement

with experimentally obtained data. For this reason, no further comparison between experimental and calculated spectra will be made for the remaining compounds.

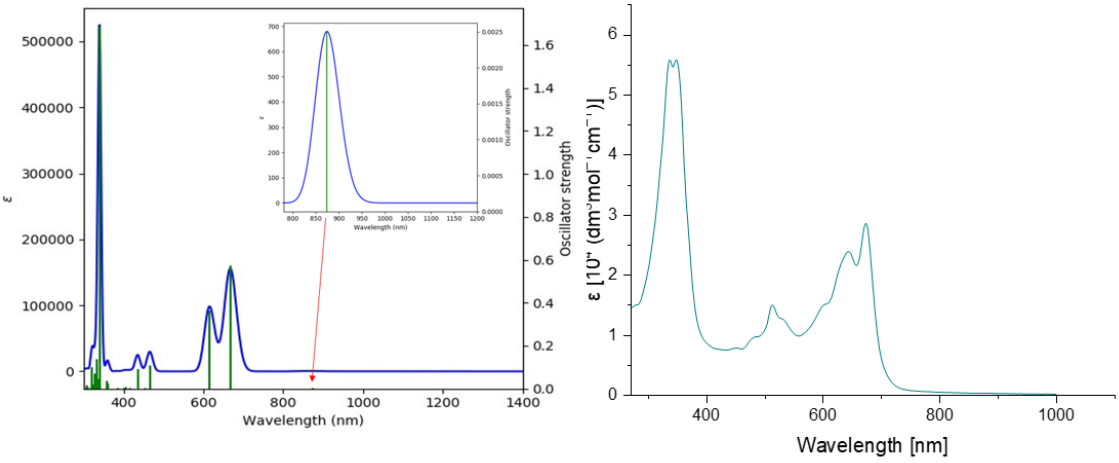

Figure 33: UV/Vis/NIR spectrum of **39**: calculated (left); measured in CH_2Cl_2 (right)

Another interesting absorption feature is provided by the simulated spectra, in which a very weak absorption band at 874 nm, characterized by a low oscillator strength (*f*=0.003) is observed (**Figure 33**). To verify whether this transition is also present in the measured spectrum, the measurement range was extended to 1000 nm. However, the results obtained indicate that no additional absorption bands were detected beyond the final observed peak at 675 nm.

Table 5 provides a summary of all other calculated transitions. In particular, the vanishingly small absorptions at 924 nm (1.34 eV, oscillator strength *f*=0.0000) and at 874 nm (1.42 eV, *f*=0.003) are noticeable, both of which are not visible in the experimental UV/Vis spectra. The former is characterized by the SOMO→LUMO transition of the *α*-spin (50%) and by HOMO−1→LUMO transition of the *β*-spin, whereas the latter is almost exclusively due to a SOMO→LUMO transition of the β-spin (93%). A pronounced transition at 667 nm (1.86 eV, *f*=0.57) can essentially be attributed to the SOMO→LUMO transition of the α-spin (37%) and the HOMO−1→LUMO transition of the β-spin (28%). Another distinctive absorption at 616 nm (2.01 eV, *f*=0.36) can be attributed to the HOMO−1→LUMO transition of the *α*-spin (38%) and HOMO−1→LUMO transition of the β-spin (38%). The most significant transmission in terms of oscillator strength can be assigned to the transmission at 339 nm (3.65 eV, *f*=1.7) with HOMO−1→LUMO+1 transition of the *α*-spin (37%) and SOMO→LUMO+2 transition of the β-spin (41%).

Table 3: Calculated absorptions of **39** and their corresponding transitions

Calculated transition				
Energy [eV]	**Wavelength [nm]**	**Oscillator strength, *f***	**Transition *α* spin**	**Transition β spin**
1.34	924	0.0000	SOMO → LUMO (50%)	H–1 → LUMO (47%)
1.42	874	0.0025	–	SOMO → LUMO (93%)
1.86	667	0.57	SOMO → LUMO (37%) H–1 → LUMO (19%)	SOMO → L+1 (10%) H–1 → LUMO (28%)
2.01	616	0.36	H–1 → LUMO (38%) SOMO → LUMO (10%)	H–1 → LUMO (22%) SOMO → L+1 (19%)
2.66	466	0.11	SOMO → L+1 (60%)	H–5 → LUMO (12%)
2.84	435	0.092	H–2 → LUMO (44%)	H–1 → L+1 (38%)
3.63	341	0.18	H–7 → LUMO (84%) H–1 → L+1 (4%)	SOMO → L+2 (4%)
3.65	339	1.7	H–1 → L+1 (37%)	SOMO → L+2 (41%)
3.86	321	0.10	H–2 → L+2 (10%)	H–1 → L+3 (15%)

Additionally, TD-DFT calculations allow for the visualization of the corresponding molecular orbitals. Selected orbitals are shown in **Figure 34**, enabling an evaluation of the HOMO/LUMO-, or more precisely, SOMO/LUMO gaps, which were addressed in the theoretical section of this work. The obtained SOMO/LUMO gap of 2.48 eV for **39** is slightly higher than the gap observed for its helical isomer **43** of 2.36 eV.

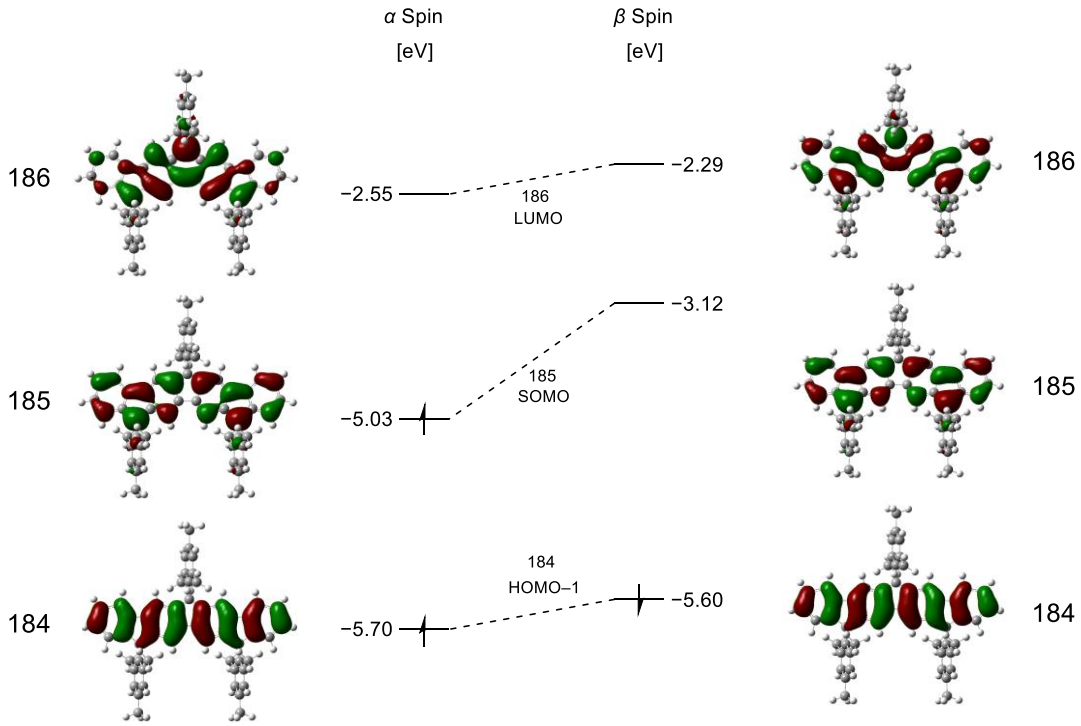

Figure 34: Selected molecular orbitals of **39**. Including LUMO, SOMO and HOMO–1 orbitals.

Furthermore, modification of the linear scaffold with selected substituents resulted in comparable SOMO/LUMO gaps: 2.47 eV for **83** and 2.33 eV for **79**. In contrast, a significant reduction in the gap was observed for the angled motif **44**, resulting in a SOMO/LUMO gap of 1.63 eV. This significant decrease indicates high reactivity and a pronounced antiaromatic character for **44**.

Previous optoelectronic studies on the IF scaffold have shown an absence of fluorescence emission.[159] In this context, *Rose et al*.[160] used femtosecond transient absorption spectroscopy to investigate the excited-state dynamics of this compound class. Their findings revealed exceptionally short S_1 lifetimes of approximately 10^{-11} s, in contrast to typical fluorescence lifetimes, which are usually greater than 10^{-9} s. As a result, the S_1-S_0 transition proceeds *via* non-radiative internal conversion, facilitated by a conical intersection between the potential energy surfaces of the S_1 and S_0 states. Consistent with these findings, the present investigation of radical **39** also confirmed this behavior, thereby preventing the acquisition of the respective fluorescence spectrum,[94] which is also in agreement with prior results.[93]

Beyond the optical characterization, the redox properties of **39** were examined by cyclovoltammetry (CV). The obtained voltammogram is shown in **Figure 35**, and the corresponding half-wave potentials are listed in **Table 6**.

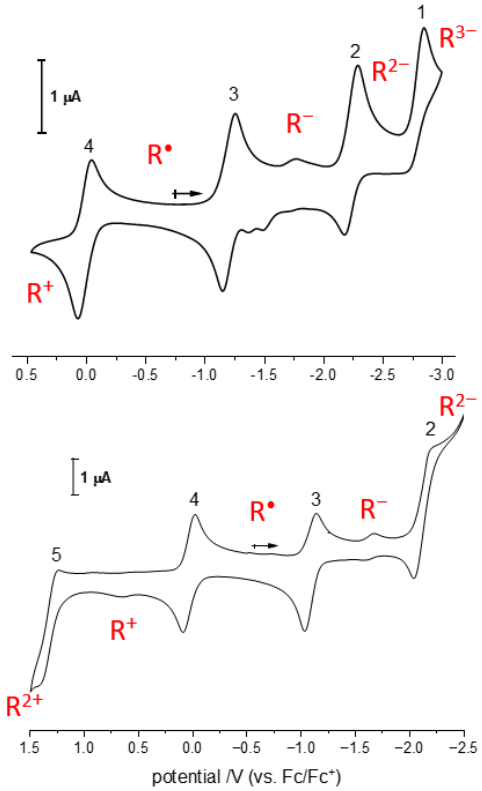

Figure 35: Cyclic voltammograms of **39** recorded in THF (top) and CH_2Cl_2 (bottom) at room temperature (vs. Fc/Fc+, *v* (THF, CH_2Cl_2)=100 mV s^{-1}; Pt/[nBu_4][$Al(OC_4F_9)_4$]/Ag). For clarity only the second of three measured cycles is depicted. Data provided by Dr. *Jonas Wenzel*.[94]

Half-wave potentials, peak potential differences and corresponding i_{pc}/i_{pa} values of **39** in THF and CH_2Cl_2 are summarized in **Table 6**. Identical redox processes in both solvents are indicated by the same numbers and colors.

Table 4: Half-wave potentials, peak potential differences and corresponding i_{pc}/i_{pa} values of **39** in THF and CH_2Cl_2.

Redox process	Solvent	$E^0_{½}$ / V	ΔE_p / mV	i_{pc}/i_{pa}
$E^0_{½}$ (1)	THF	–2.77	–	–
$E^0_{½}$ (2)		–2.23	112	~1.76
$E^0_{½}$ (3)		–1.18	105	~1.34
$E^0_{½}$ (4)		+0.01	115	~0.81
$E^0_{½}$ (2)	CH_2Cl_2	–2.13	169	–
$E^0_{½}$ (3)		–1.09	107	~0.64
$E^0_{½}$ (4)		+0.03	63	~1.00
$E^0_{½}$ (5)		+1.31	180	~0.06

CV enabled the electrochemical characterization of radical **39**, whereby the redox potentials were determined against the ferrocene/ferrocenium pair Fc/Fc^+. In tetrahydrofuran (THF), one irreversible and three quasi-reversible redox processes were observed at half-wave potentials ($E^0_{½}$ vs. Fc/Fc^+) of –2.77, –2.23, –1.18, and +0.01 V. The first three values correspond to successive reductions to the trianion, dianion, and monoanion, respectively. In CH_2Cl_2, four quasi-reversible redox processes were detected at $E^0_{½}$ values of –2.13, –1.09, +0.03, and +1.31 V (vs. Fc/Fc^+). The latter two steps are most likely associated with the formation of the monocation and dication, respectively. The assignment of these redox transitions to the species [**39**]$^{2+}$, [**39**]$^+$, [**39**], [**39**]$^-$, and [**39**]$^{2-}$ is supported by the observation that compound **39** is not reduced by decamethylferrocene ($FeCp_2$, $E^0_{½}$ = –0.59 V in CH_2Cl_2[161]), but readily reacts with decamethylcobaltocene ($CoCp^*_2$, $E^0_{½}$ = –1.94 V in CH_2Cl_2[161]). Additionally, the formation of **39** from its precursor **50** upon treatment with KO*t*Bu under ambient air suggests that intermediate species such as [**39**]$^{n-}$ may undergo oxidation during the process.

4.7.1.2 Optical and Electrochemical Properties of the Nonacyclic Systems

The optical properties of the radicals **40** and **41** were also examined. The spectra recorded in CH_2Cl_2 were once again compared with their corresponding calculated spectra **(Figure 36**). A good agreement between the experimental and calculated spectra is also observed in this case. However, as previously described for the heptacyclic compounds **39**, **43**, and **44**, the geometric orientation appears to exert a significant influence on the absorption bands. Compound **40** displays five distinct and characteristic absorption bands, whereas compound **41** exhibits only one distinct absorption band and a broad band covering a wide spectral range.

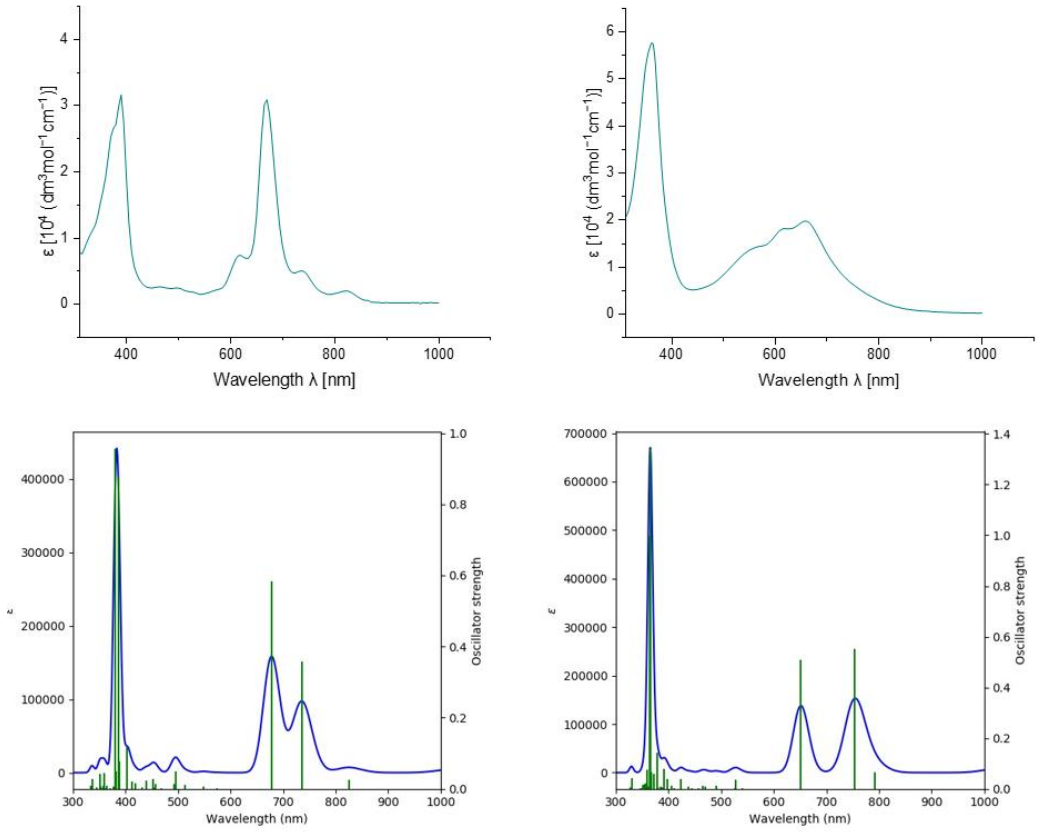

Figure 36: Comparison of measured UV/Vis/NIR spectra in CH_2Cl_2 (top) of **40** and **41** with their corresponding calculated spectra (bottom) in the same solvent system.

The absorption of **40** and **41** are summarized in **Table 7**. Both compounds exhibit a series of intense bands across a broad spectral range, extending from the ultraviolet into the visible region. For compound **40**, the earliest absorptions appear at 229 nm. A prominent band at 295 nm is in good agreement with the computed spectra. The area between

440 nm and 540 nm exhibits vanishingly small absorption bands, consistent with theoretical predictions. Absorption in the visible range is first noted at 620 nm, followed by a more substantial peak at 670 nm and a less pronounced absorption at 735 nm. The last observed peak at 825 nm, again shows good agreement with the computed spectra.

Interestingly, the first three absorptions at 229, 296 and 362 nm of compound **41** are in good correlation in terms of absorption wavelength and peak intensity with compound **40**. However, for the region between 440 and 800 nm, no distinct peaks are observed. Instead, a broad peak is visible, possibly covering three distinct absorptions at 575, 620 and 660 nm. Also, in comparison to **40**, the computed absorption at around 800 nm is not visible in the measured spectrum. A possible explanation might be that the rather small absorption band is fused with the more pronounced broad band, and therefore not visible.

Table 5: Absorptions of **40** and **41** in comparison.

Compound	λ_{abs} [nm]	Compound	λ_{abs} [nm]
40	229 295 375 390 495 620 670 735 825	**41**	229 296 362 575 620 660

No fluorescence activity was observed for radicals **40** and **41.** As already described for radical **39**, IFs show extremely short excitation lifetimes, possibly due to conical intersection.

Again, the calculated absorption can be attributed to their corresponding transitions. These transitions are summarized in the experimental section.

TD-DFT calculations enabled the visualization of the SOMO/LUMO orbitals of **40** and **41**, allowing for an evaluation of their corresponding SOMO/LUMO gaps and comparison with previously discussed values for heptacyclic systems. The calculated gaps of 2.37 eV (**40**) and 2.33 eV (**41**) are slightly lower than those observed in the linear (2.48 eV) and helical (2.36 eV) heptacyclic analogues.

No valid CV spectra could be recorded for radicals **40** and **41**. The data suggests the presence of an additional species that could not be separated by column chromatography. However, analysis by TLC showed no indication of impurities. To further investigate this, liquid chromatography-mass spectrometry (LC-MS) was employed to identify this unknown species. Despite analyzing various fractions of both radicals **40** and **41**, no conclusive results were obtained. Similarly, LC-MS measurements of radical **39** did not yield any significant results, preventing any definitive conclusions. An alternative analysis using high performance liquid chromatography (HPLC) was considered. However, the available system operates under conditions that are unsuitable for these compounds, making this method impractical. One hypothesis is that radicals **40** and **41**may exhibit lower stability compared to **39**, with the unidentified species potentially arising from decomposition. However, this possibility was ruled out, as measurements taken immediately after successful synthesis produced identical results. Therefore, no further investigations were conducted regarding this issue. The spectra are here included for the purpose of completeness but should be taken with caution to avoid misleading interpretations (**Figure 37**).

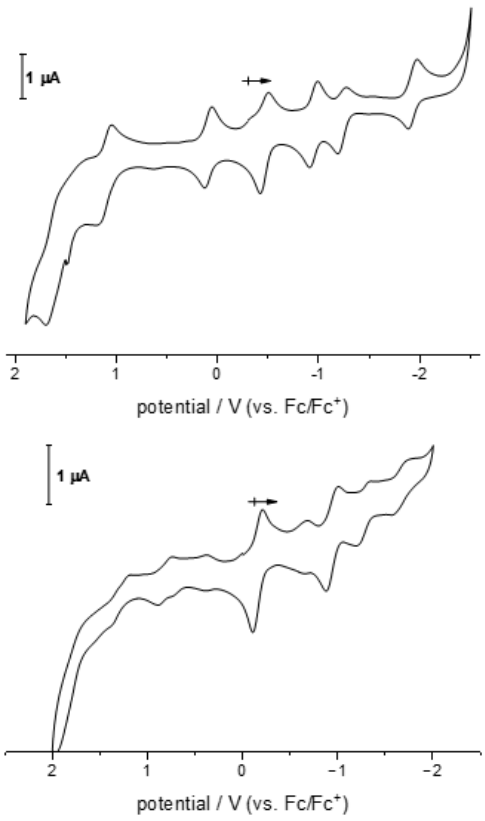

Figure 37: Cyclic voltammograms of **40** (top) and **41** (bottom) recorded in CH_2Cl_2 at room temperature (vs. Fc/Fc+, *v* (THF, CH_2Cl_2)=100 mV s^{-1}; Pt/[nBu_4][$Al(OC_4F_9)_4$]/Ag). For clarity only the second of three measured cycles is depicted. Data provided by Dr. *Jonas Wenzel*.[146]

4.7.1.3 Optical Properties of the Undecacyclic Systems

The optical properties of the undecacyclic compounds **126** and **42** were also examined and compared with each other (**Figure 38**).

The absorption spectrum of **126** displays a series of intense bands across a broad spectral range, extending from the ultraviolet into the visible region. The first absorptions appear at 230 nm, followed by a weak absorption at 280 nm and a prominent band of greater intensity between 320-410 nm, with its maximum at 367 nm. In the visible region, a weak absorption is present at 500 nm, followed by more substantial peak at 530 nm. Between 600 and 770 nm, three significant absorptions are noted. The first at 640 nm, followed by a peak at 680 nm and a substantial peak at 740 nm.

In contrast, **42** exhibits a similar pattern with absorptions at 220 nm, a weak absorption at 295 nm and an absorption band at 350 nm. The absorptions in the visible region at 515 nm and 550 nm are in comparison to **126** more pronounced. However, the major

difference is observed between 600 nm and 770 nm, since no activity at all is observed for **42**, whereas **126** displays a series of intense bands in this region.

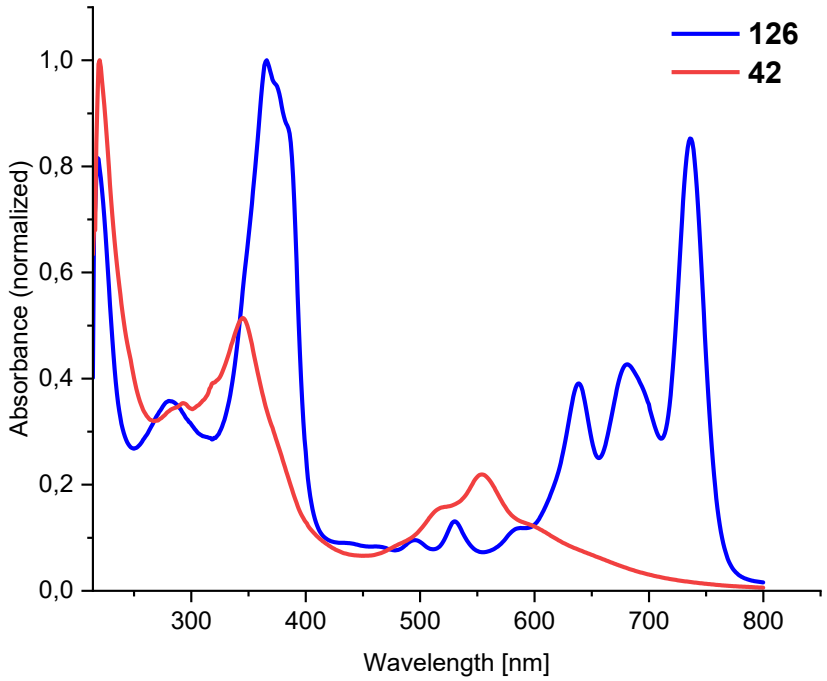

Figure 38: Comparison of UV-Vis Spectra of **126** and **42**.

4.7.2 Aromaticity of the Synthesized Compounds

4.7.2.1 Aromaticity of the Heptacyclic Systems

Aromaticity, or more precisely an aromatic or antiaromatic character, is an important feature of a fully conjugated cyclic or polycyclic system, as it correlates with its optoelectronic properties.[95] It is simply estimated by the rule of *Clar*,[162] which describes the tendency of polyaromatic systems to have a maximum number of fully intact benzene rings in their *Lewis* structure. This does not only allow to assess the relative thermodynamic stability of isomeric forms but also enables the identification of the most significant resonance structures within a given system. In this context, three distinct resonance structures with varying radical and aromatic character can be proposed for compound **39** (**Scheme 62**). Among these, structure **39-III**, featuring four fully aromatic benzene rings (highlighted in blue) and structure **39-I** with three fully aromatic rings, are considered the most significant in terms of stability according to *Clar's* rule. Further investigations established that structure **39-I** with a monoradical configuration, contributes most prominently among the possible resonance structures. Additionally, the presented system contains an indacene core (highlighted in red) along with its polycyclic

fused IF moiety. Indacene presents a particularly interesting system in the concept of aromaticity. Due to its twelve π-electrons [4*n*], it would be formally classified as an antiaromatic species and is consequently an unstable molecule with alternating bond lengths. However, *s*-indacenes substituted with bulky residues have been reported to exhibit considerable stability, which enabled their isolation and thorough characterization, challenging the conventional definitions of aromaticity and antiaromaticity.

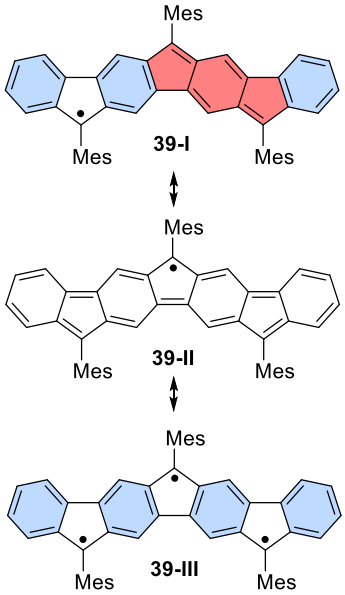

Scheme 62: Resonance formulas of radical **39**; Structure **39-III** exhibits triradical character, while **39-I** and **39-II** exhibit a monoradical configuration. Fully intact benzene units are highlighted in blue; the indacene core is highlighted in red.

Due to the paramagnetic nature of compound **39**, no resonances were detected within the conventional frequency range in the ^{1}H NMR spectrum, preventing direct insight into its shielding behavior. However, in recent years computational DFT methods became a powerful tool to elucidate and analyse the aromatic or antiaromatic character of such systems. Among possible approaches, the nucleus-independent chemical shift XY (NICS-XY) scan has proven particularly effective. This approach allows to predict and visualise the ring current in polycyclic systems by simulating a molecules magnetic response to an external magnetic field.[114]

Applying the NICS-XY scan to compound **39** an elucidation for its aromaticity can be made (**Figure 39**). The results suggest that rings D and D’ are fully aromatic, rings C, C’ and especially A are antiaromatic, while rings B and B’ are on the borderline between aromatic and antiaromatic. This rather unusual behavior observed for the inner six-membered rings

(six-membered rings, *i.e.* benzene units, usually show a pronounced aromatic character) can be explained by the fact that these are part of the antiaromatic indacene unit within the heptacyclic scaffold. Assuming that the six-membered rings are part of the indacene unit, they do not show untypical behavior but rather reflect the paratropic ring current defined for indacene.

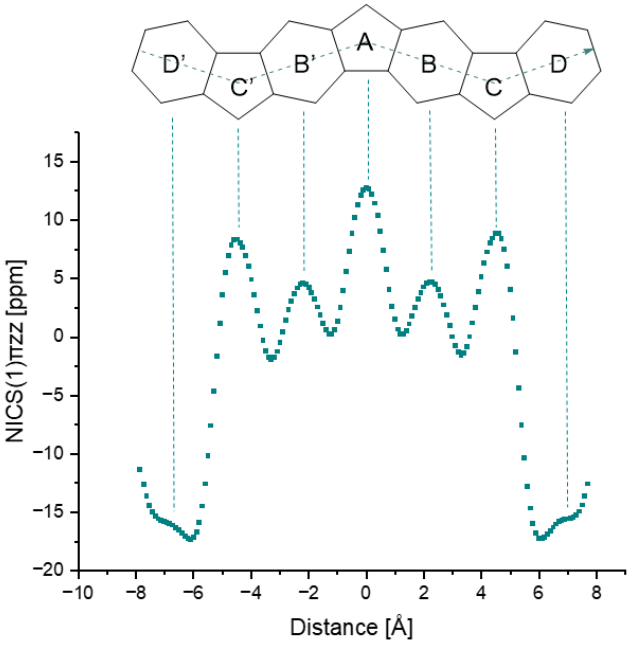

Figure 39: NICS(1)$_{\pi ZZ}$ scan of the heptacyclic scaffold.

As described in the introduction section, aromaticity can also be evaluated using structural criteria. In this context, HOMA values of 0.96, 0.38, 0.68, and 0.42 were obtained for the discussed system, showing good agreement with the data obtained from the NICS-XY scan. However, the structural parameters required for the HOMA calculations were obtained from the optimized structures, as no crystal structures of the radicals could be obtained. While this approach provides useful insights, it is important to note that the HOMA index is fundamentally an experimentally derived criterion. For more accurate conclusions, the evaluation should ideally be based on parameters derived from crystallographic data. This method is presented for demonstration purposes only and will not be discussed further in this work.

Aromaticity can also be quantified by examining the ring currents in the π-system. The anisotropy of the induced current density can be calculated and visualized using *Herges*' ACID method (**Figure 40**). The respective calculations were performed with the parent polycycles without mesityl groups to obviate their influence on the ring currents. The

obtained results suggest that rings D and D’ exhibit diatropic (clockwise) ring currents, which indicates an aromatic character and is fully consistent with the NICS-XY scan data. On the other hand, rings C, C’ and A show paratropic (counterclockwise) ring currents, indicating their antiaromatic character. The unusual behavior is again observed for rings B and B’; both paratropic and diatropic ring currents are present, which again in agreement with the NICS-XY scan.

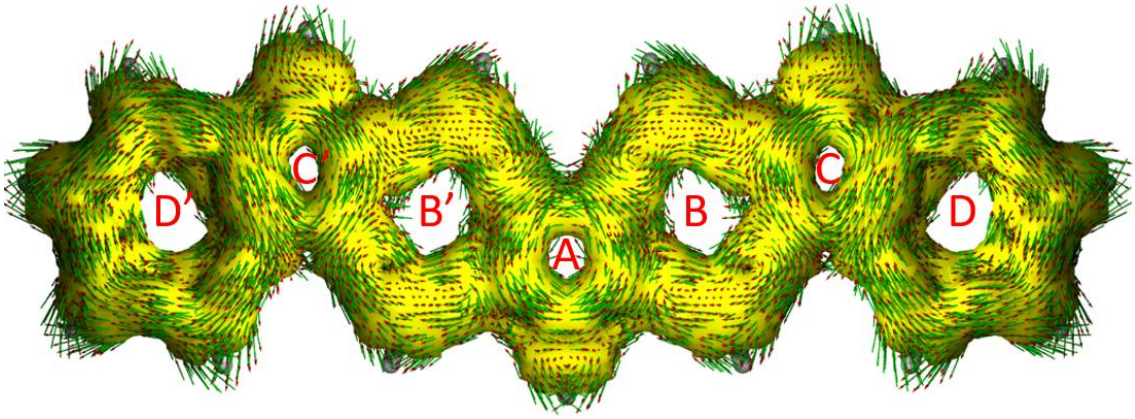

Figure 40: ACID plot of the heptacyclic scaffold. The ring current is visualized with vector arrows on the isosurface. The clockwise circulation (diatropic ring current) describes the aromatic system of benzene.

4.7.2.2 Aromaticity of the Nonacyclic Systems

As previously discussed, resonance structures **40/41-I** and **40/41-III** are the most significant contributors to the overall resonance ensemble in terms of stability. However, their negligible calculated triradical character suggests that structures **40/41-I**, each containing three fully aromatic benzene rings, are the most relevant among the possible resonance structures (**Scheme 63**).

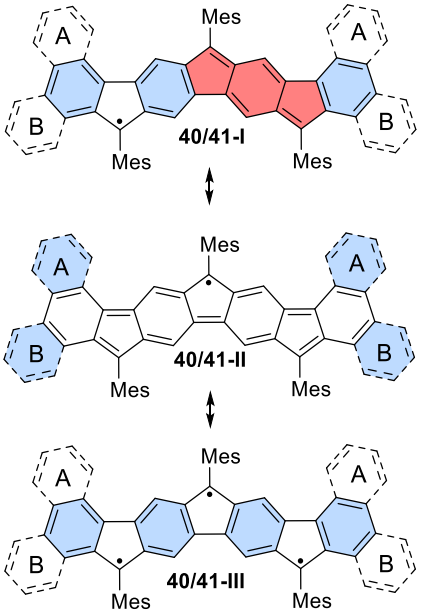

Scheme 63: Resonance formulas of radicals **40** and **41**; Structure **40/41-III** exhibits triradical character, while **40/41-I** and **40/41-II** exhibit a monoradical configuration. Fully intact benzene units are highlighted in blue; the indacene core is highlighted in red.

To further investigate the shielding behavior of compounds **40** and **41** and to assess their aromatic or antiaromatic character, the NICS-XY scan again was employed. The obtained results suggest that rings E, E', D, and D' exhibit aromaticity comparable to that of a benzene ring. In contrast C, C', and particularly A show clear signs of antiaromatic character. Rings B and B' demonstrate a borderline behavior, showing neither clear aromatic nor antiaromatic properties (**Figure 41**).

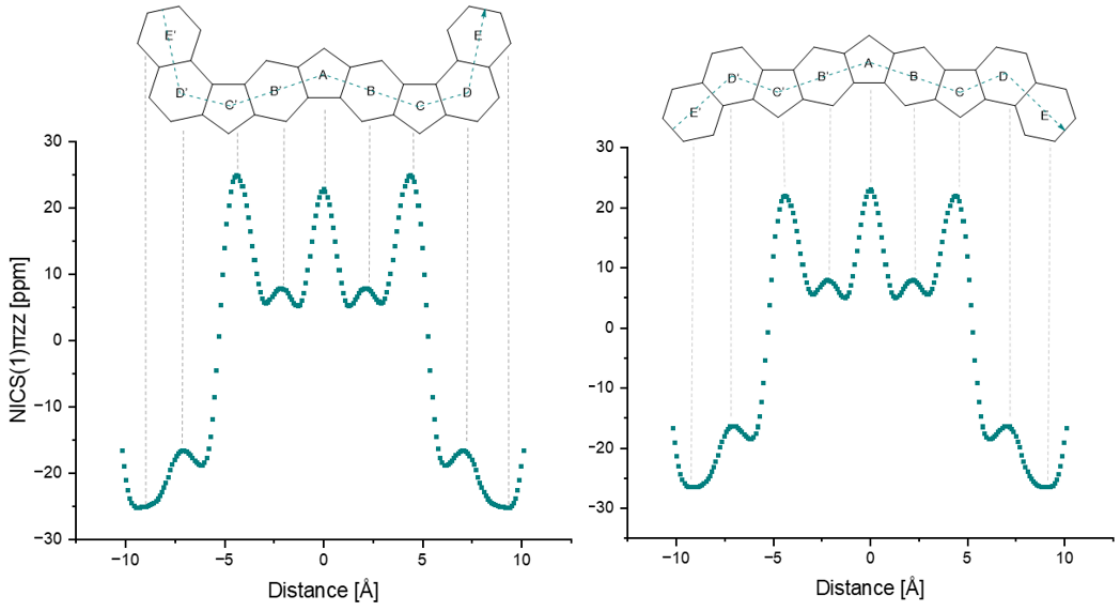

Figure 41: NICS(1)$_{\pi zz}$ scan of radicals **40** and **41**.

To further validate the NICS data and quantify the degree of aromaticity, the ACID method developed by *Herges* was also employed (**Figure 42**). As before, all calculations were carried out on the parent polycyclic frameworks without mesityl substituents, in order to avoid their potential influence on the ring currents. The resulting currents indicate that rings E, E', D, and D' exhibit diatropic (clockwise) ring currents, demonstrating their aromatic character. In contrast, rings C, C', and especially A display pronounced paratropic (anticlockwise) ring currents, confirming their antiaromatic nature. Rings B and B' however, show borderline behavior, with both diatropic and paratropic contributions, which was also confirmed by the NICS-XY scan. Overall, the results obtained from both methods are in good agreement and complement each other.

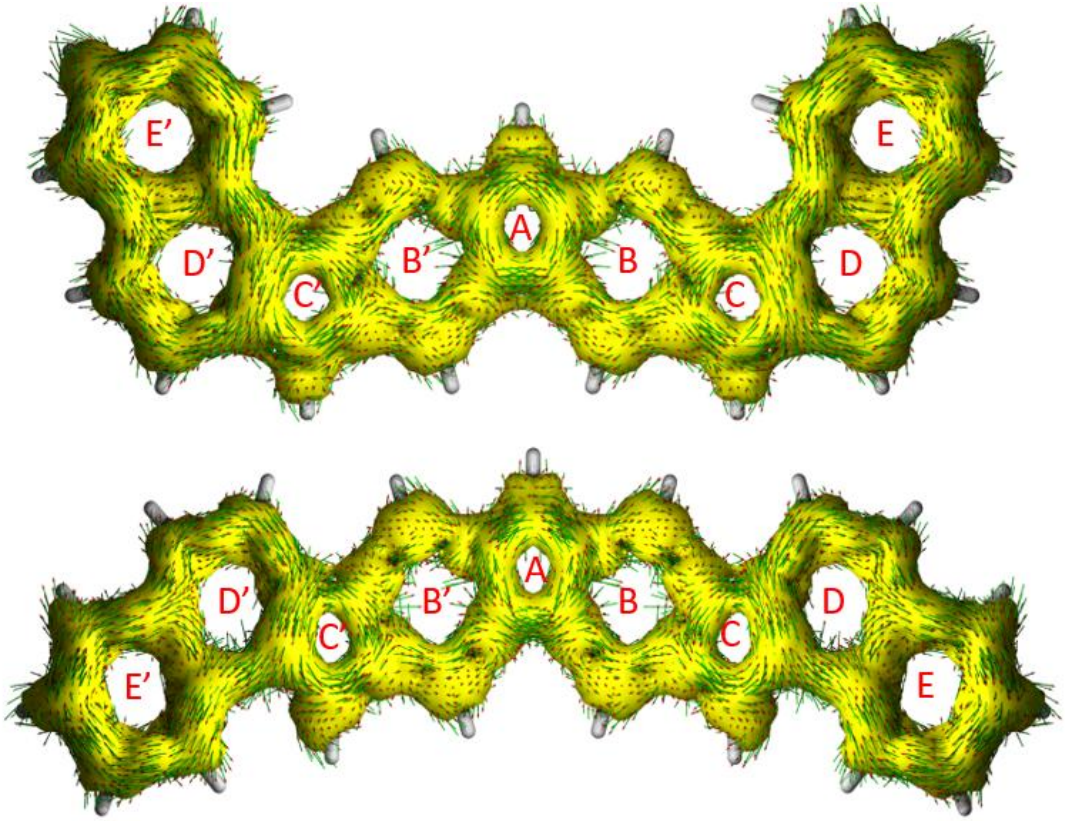

Figure 42: ACID plots of **40** and **41**. The ring current is visualized with vector arrows on the isosurface. The clockwise circulation (diatropic ring current) describes the aromatic system of benzene.

4.7.2.3 Aromaticity of undecacylic systems

Aromaticity was also evaluated for the undecacylic system employing the abovementioned methods. Again, the simplest estimation was made applying the rule of *Clar*. Since the conjugation of the compound is interrupted beyond the fifth ring, the system shows a strong resemblance to the previously discussed heptacyclic structure **39**

(**Scheme 63**). As a result, structure **126-I** with five intact benzene units is the most significant among the possible resonance structures (**Scheme 64**). In contrast, the structure of **42** allows for more possible resonance structures with each exhibiting distinct electronic configuration. A brief selection is demonstrated in **Scheme 64**. Among these structures **42-I** displays the most amount of intact benzene units as a pentaradical species, formally making it the most stable structure. Structure **42-II**, a triradical species, retains four intact benzene units and structure **42-III**, a monoradical species, retains three benzene units.

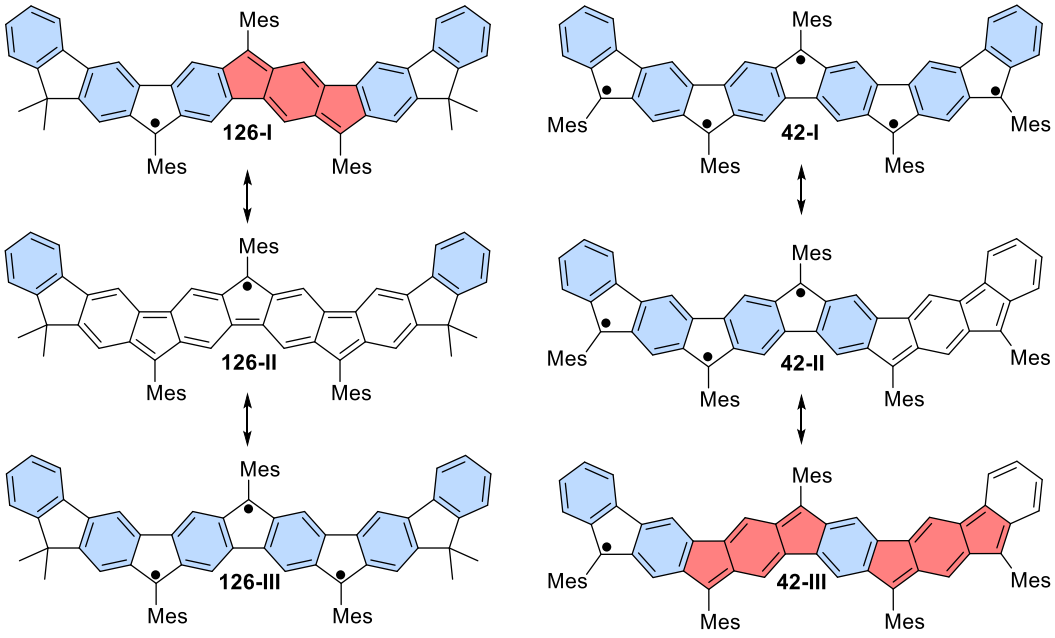

Scheme 64: Resonance formulas of radicals **126** and **42**; (left): Structure **126-III** exhibits triradical character, while **126-I** and **126-II** exhibit a monoradical configuration. (right): Structure **42-I** exhibits pentaradical character with six fully intact benzene units, while **42-II** exhibits triradical character with four intact benzene units and **42-III** displaying monoradical character with three intact benzene units. Fully intact benzene units are highlighted in blue; the indacene core is highlighted in red.

The shielding behavior of the undecacyclic systems was investigated by employing the NICS-XY scan (**Figure 43**). The results suggest that all five-membered rings display antiaromatic character, which is especially pronounced in rings E', C', C and E. The inner six-membered rings D', B', B and D display a borderline behavior, which is again due to the presence of indacene units within the framework, particularly between E', D' and C' and C', B' and A. In contrast, clear aromatic character is observed only in the outer six-membered rings, while the rest of the framework shows predominantly antiaromatic behavior.

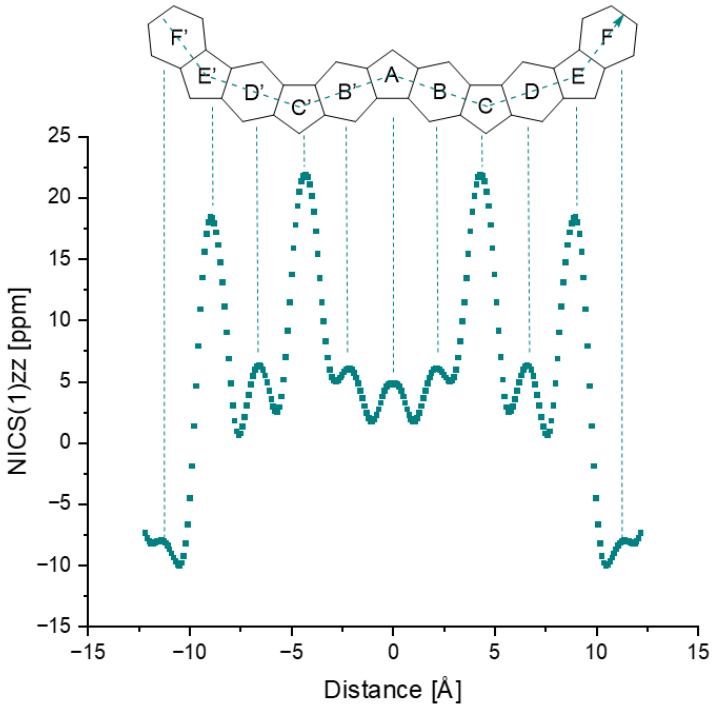

Figure 43: NICS scans of the undecacyclic system.

The aromaticity of **42** was further quantified by the ACID method (**Figure 44**). The results suggest antiaromatic behavior for the pentacyclic rings. For rings B', B, D' and D again a combination of aromatic and antiaromatic character is observed, which is in agreement with the corresponding NICS-XY scan. Aromaticity is only observed for the terminal rings F' and F.

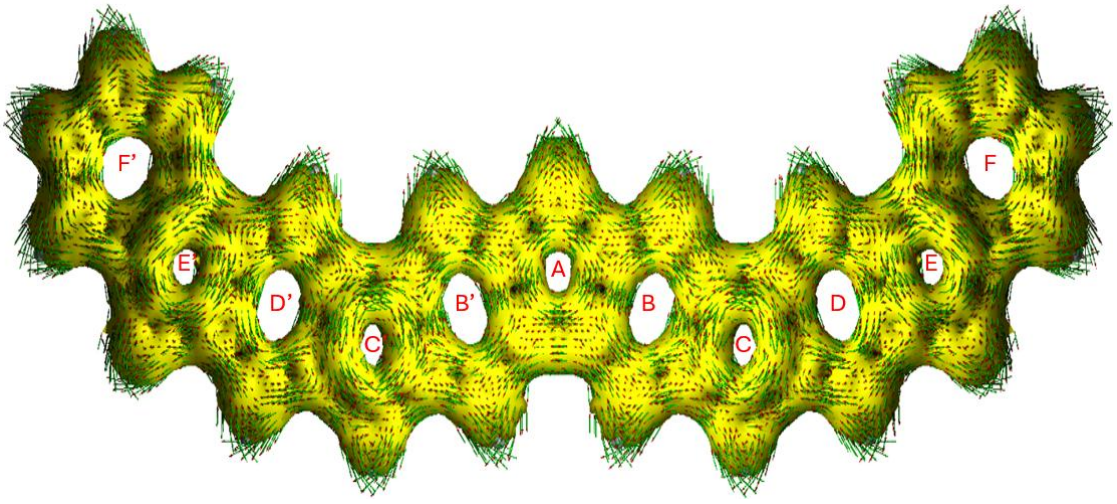

Figure 44: ACID plot of **42**. The ring current is visualized with vector arrows on the isosurface. The clockwise circulation (diatropic ring current) describes the aromatic system of benzene.

The comparison of the NICS-XY-scans (**Figure 37**) of selected radicals including **43**, **39**, **40**, **41**, and **42** reveals significant differences in aromatic character across the ring systems.

The scans for compounds **43** (violet) and **39** (green) show similar NICS values for the outer six-membered rings D and D', but significant differences in all other rings. A more pronounced antiaromatic behavior of **43** (violet) is not only observed in the outer five-membered rings C, C', and even more significant in the central ring A, but also in the inner six-membered rings B and B'. In compound **39** (green) the inner six-membered rings are closer to the borderline between aromatic and antiaromatic character.

A comparison of **40** (red) and **41** (orange) reveals no substantial differences. However, extending the outer π-system in these linearly aligned heptacyclic compounds significantly alters the NICS profiles, particularly in the five-membered rings, a trend which was also observed in IF derivatives.[163] Comparing scans of **39** (green) with **40** (red) shows a two-fold increase of the antiaromatic character for ring A (from 12.7 ppm for radical **39** (green) to 23.0 ppm for **40** (red)) and a three-fold increase for rings C and C' (from 8.3 ppm to 24.9 ppm). For six-membered rings B and B' only a small increase (4.5 ppm to 7.5 ppm) is observed, whereas virtually identical values are calculated for rings D and D'. However, rings E and E', which are only present in **40** (red) (25.0 ppm) and **41** (orange) (26.5 ppm), exhibit strong aromatic behavior.

When comparing the undecacyclic system to the nona- and heptacyclic systems, only minor similarities and significant differences are observed across most of the framework. While ring A consistently shows enhanced antiaromatic behavior in all systems, ring A of **42** (blue) exhibits the least degree of antiaromatic character. A notable contrast is also seen in rings D' and D. While all systems display antiaromatic behavior in these regions, the scan of **42** (blue) displays a particularly pronounced antiaromatic character, likely due to the presence of an indacene unit within the framework. Furthermore, in the NICS-XY scan of **42** (blue), aromatic character is confined to the outer six-membered rings, which in contrast is less pronounced than in the other systems.

The obtained data from the NICS-XY-scans thus indicate strong antiaromatic behavior for the majority of the scaffold. This is further supported by calculated low SOMO/LUMO gaps: **43** (violet): 2.36 eV; **39** (green): 2.48 eV; **40** (red): 2.37 eV; **41** (orange): 2.33 eV; **42** (blue): 1.83 eV, which is typical for antiaromatic compounds.[164] Despite their strong antiaromatic character, all compounds indicate high stability, ultimately challenging the conventional definitions of aromaticity and antiaromaticity.[165-167]

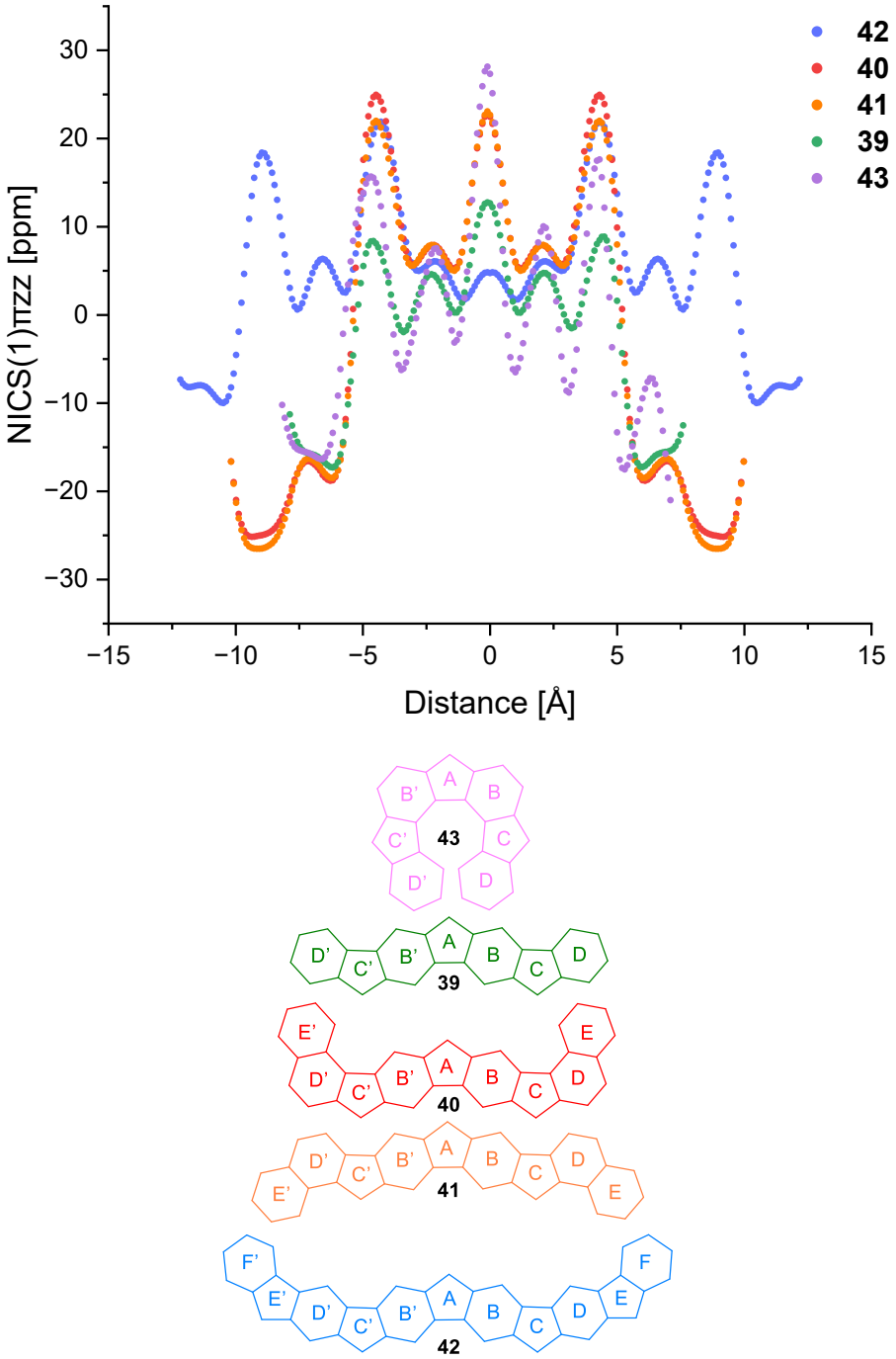

Figure 45: Comparison of selected NICS-XY scans including compounds **43**, **39**, **40**, **41**, and **42**.

5 Summary and Outlook

In the scope of this work, a variety of novel, stable carbon-centered radicals were synthesized, and a general synthetic strategy was developed. The accessibility of these compounds enabled a thorough investigation of different radical systems. Previously, radical stabilization was primarily achieved by utilizing mesitylene as a bulky substituent. In this work, a range of substituents was introduced onto the heptacyclic scaffold, aiming not only for molecular novelty but also to establish criteria for radical formation and stabilization. While phenyl and 2,6-dichlorophenyl groups afforded stable radicals, the incorporation of C_6F_5 and $Ph(CF_3)_2$ groups did not result in stable systems (**Scheme 65**).

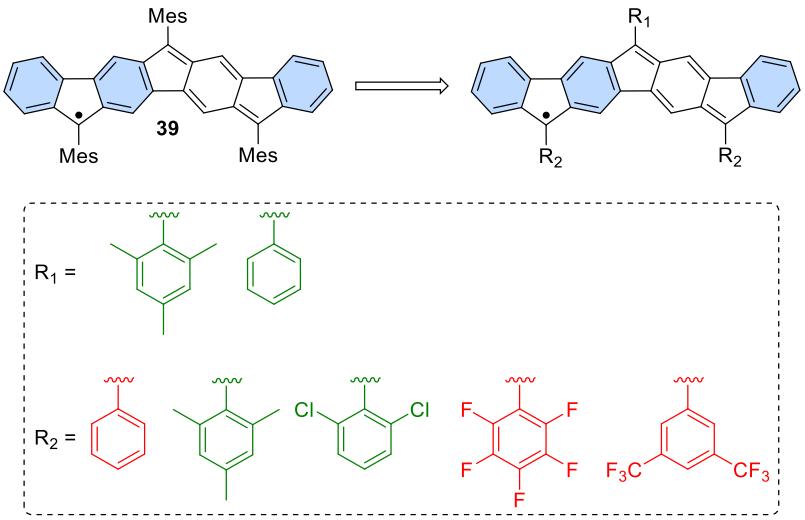

Scheme 65: Substitution of the mesityl units by different substituents. Successful attempts are highlighted in green, unsuccessful attempts are highlighted in red.

The extension of the π-system through the synthesis of nonacyclic systems enabled the investigation of decreased HOMO/LUMO gaps. While most reported compounds are based on mono- or triradical systems, further focus was not only set on expanding the π-system of the nonacycles but also on increasing the number of potential radical sites. This allowed the successful synthesis and investigation of an undecacyclic system with potential pentaradical character (**Scheme 66**). EPR spectroscopy revealed the radical nature of **42**. Although no investigations regarding the pentaradical character could be conducted, calculations revealed a significant contribution of the triradical configuration.

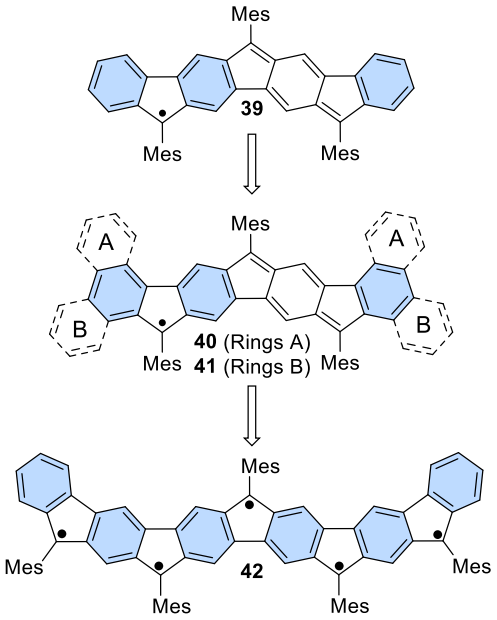

Scheme 66: Heptacyclic-, nonacyclic-, and undecacyclic radical systems

Initial evaluation for the radical character was provided by the absence of resonances in conventional frequency ranges in the recorded ^{1}H NMR spectra and by the compounds EPR activity. Additional confirmation was provided by mass spectrometry.

A comprehensive investigation of their physical and spectroscopic properties was conducted using a combination of experimental techniques, including UV/Vis spectroscopy, EPR spectroscopy, and cyclic voltammetry, as well as quantum chemical calculations. This not only enabled the comparison between the experimentally obtained data with calculated spectra, but also allowed further insights into the compound's properties, such as spin densities, aromaticity, and orbital energies.

The mono-radicals are best described with the unpaired electron located in the outer five-membered rings; these resonance formulas show the largest number of fully intact benzene rings. This observation was further supported by computing their corresponding triradical character, which turned out to be negligibly small.

The concept of aromaticity displays a key feature of these polycyclic compounds. An aromatic character can generally be derived from experimentally obtained data, especially from ^{1}H NMR. However, since the targeted compounds are inactive for NMR spectroscopy, their aromatic or antiaromatic behavior was derived from DFT calculations. Among further methods, calculations of NICS were used to quantify the compound's aromatic character. A different method to quantify aromaticity is based on calculated

induced ring currents. The anisotropy of induced current densities was calculated and visualized using *Herges'* ACID method. Both applied methods yielded similar results, ultimately complementing each other.

Additionally, an attempt was made to synthesize a heptacyclic compound with potential diradical character. However, since the amount of product obtained was not sufficient to continue the reaction sequence, the conversion to the possibly radical species could not be performed. Nonetheless, the structural features of **156** offer a solid basis for analysis and discussion. As shown in **Scheme 67**, two resonance structures can be proposed. While resonance structure **156-I** exists in its closed-shell form, structure **156-II** exhibits a potential diradical character. As already discussed in Chapter **2.1.2**, similar compounds based on IF exhibit only a biradical character but are primarily defined by their closed-shell configuration. The open-shell configuration arises from an increase in the number of intact benzene units, which according to *Clar's* rule represents the most stable configuration. A similar pattern is observed here. While the closed-shell configuration shows intact units only at the termini of the framework, the open-shell structure gains two additional intact benzene units.

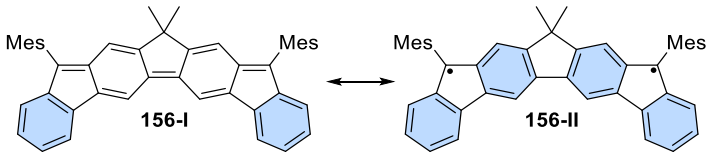

Scheme 67: Resonance structures of **156**. Fully intact benzene units are highlighted in blue.

As a complementary side project, the cyclopentadiene units in the heptacycles were replaced with cycloheptatriene units. However, the finalizing step could not be carried out due to the general instability of the target structure. However, this reaction sequence allows to be utilized as a template for the potential synthesis of larger polycycles with unpaired electrons, *i.e.*, radicals. **176** can be generated by a commercially available fluorene derivative and subjected with **178** to a *Sonogashira* coupling with **177**. Subsequent cyclization to **179**, followed by bromination/elimination and nucleophilic addition affords diol **180**. The sequence can be finalized by the reduction of the diol **180** and subsequent conversion to the desired radical **181** (**Scheme 68**). By appropriately modifying the starting materials, additional regioisomers of this rare compound class can be accessed.

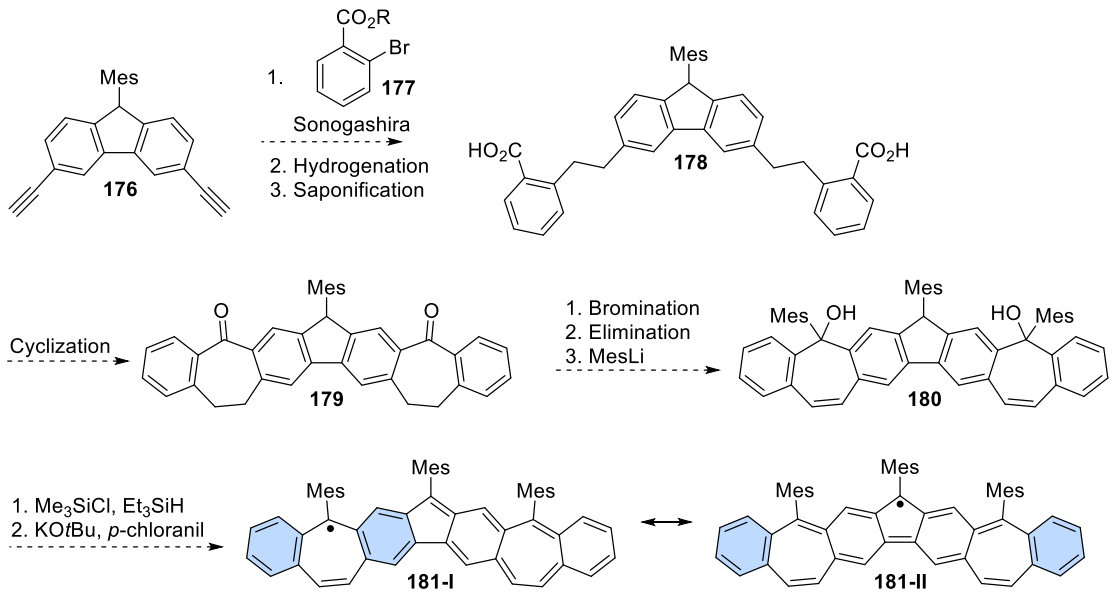

Scheme 68: Synthetic route toward cycloheptatriene-based radical systems.

Future investigations will focus on the comprehensive characterization of these novel systems using both experimental methods and quantum chemical calculations. Given their redox activity, these systems offer promising potential for further electrochemical studies, with CV providing insights into their oxidation and reduction behavior. Additionally, UV/Vis/NIR spectroscopy will be employed to gain a better understanding of their electronic transitions. These experimental approaches will be supported by quantum chemical calculations, which will not only provide orbital energies but also simulate spectroscopic spectra.

6 Experimental Part

6.1 General Procedure

6.1.1 Preparative Work

The experimental work was conducted using standard laboratory techniques. Air- and moisture-sensitive substances were handled under an inert atmosphere using the *Schlenk* technique with argon. Fine powders and granular solids were introduced under an argon counterflow, while liquids were added through rubber septa using plastic syringes or stainless-steel cannulas.

The desired temperatures for each reaction were controlled using a heating stirrer equipped with a temperature sensor. For cooling and conducting low-temperature reactions, the following refrigerant mixtures were employed:

1. Ice/water, 0 °C
2. Ice/Brine, −15 °C
3. Dry ice/^{i}PrOH, −78 °C

Solvents were removed using rotary evaporators under reduced pressure in the temperature range between 25 and 60 °C.

Purification was generally performed by column chromatography using the 'flash chromatography' technique described by *Still et al*..[168-169] Silica gel 60 (0.063×0.200 mm, 70–230 mesh ASTM) (*Merck*), Geduran® Silica gel 60 (0.040×0.063 mm, 230–400 mesh ASTM) (*Merck*) or Celite® (*Fluka*) and sea sand (calcined, purified with hydrochloric acid, *Riedel–de Haën*) were used as stationary phase. Technical solvents were pre-distilled before use.

6.1.2 Solvents and Reagents

Solvents of technical quality were distilled prior to use. Solvents of p.a. (per analysis) quality were commercially purchased (*Acros Organics*, *Fisher Scientific*, *Sigma Aldrich*) and used without further purification.

Reagents were commercially purchased from industry companies (*Abcr*, *Acros*, *Alfa Aesar*, *Fluka*, *Iris*, *Maybridge*, *Merck*, *Riedel–de Haën*, and *Sigma Aldrich*) and used without further purification if not stated otherwise.

Absolute solvents were purchased either directly, such as pyridine, toluene and DMF, or prepared from analytical-grade solvents by drying. 1,4-dioxane, THF and diethyl ether were dried using the ketyl method, involving sodium as the drying agent followed by distillation. CH_2Cl_2 was dried over CaH_2 and then distilled. Small quantities of chloroform and methanol were dried over molecular sieve with a pore size of 4.00 Å and subsequently distilled.

6.1.3 Analytics and Devices

6.1.3.1 Analytical Balance

For weighing, a *Mettler AE 200* precision balance was used for small quantities, while larger amounts were measured with a *Sartorius Acculab ALC coarse* balance. Stock solutions for quantitative UV/Vis-NIR spectroscopy were prepared using a *Precisa Gravimetrics AG ES 225 SM-DR* analytical balance.

6.1.3.2 Reaction Control

Analytical thin layer chromatography was carried out using silica coated aluminum plates (silica 60, F_{254}, layer thickness: 0.25 mm) with fluorescence indicator by *Merck*. The spots were detected by fluorescence quenching of UV/light at λ = 254 nm or λ = 366 nm and subsequent staining with phosphomolybdic acid solution (5% phosphomolybdic acid in ethanol, dip solution); potassium permanganate solution (1.00 g potassium permanganate, 2.00 g AcOH, 5.00 g sodium bicarbonate in 100 mL water, dip solution); Mostain solution (5% $(NH_4)6Mo_7O_{24}$ in 10% sulfuric acid with 0.03% $Ce(SO_4)$-2) or β-naphthol solution (10% β-naphthol, 10% AcOH and 80% ethanol, dip solution) followed by heating in a hot air stream. For amino acids the Seebach reagent (2.5% phosphomolybdic acid, 1.0% cerium(IV) sulfate tetrahydrate, 6.0% conc. sulfuric acid, 90.5% water; dipping solution) was used with subsequently heating in a hot-air flow. Amines were detected by dipping the TLC-plate in ninhydrin solution (0.2% ninhydrin in 0.1% AcOH in EtOH, dip solution) and subsequently heating in a hot-air stream. Alcohols were detected by dipping the TLC-plate in $KMnO_4$-solution (1.5 g of $KMnO_4$, 10 g K_2CO_3 and 10 mL 10% NaOH in 200 mL of water) and subsequently heating in hot air stream.[170]

6.1.3.3 Nuclear Magnetic Resonance Spectroscopy (NMR)

NMR spectra were recorded using the following device: ^{1}H-NMR: *Bruker* Avance 400 (400 MHz), *Bruker* Avance 500 DRX 500 (500 MHz), ^{13}C-NMR: *Bruker* AM 400 (100 MHz), *Bruker* Avance 500 DRX 500 (125 MHz), ^{19}F-NMR: *Bruker* Avance 400 (376 MHz). All measurements were carried out at room temperature. The chemical shift of ^{19}F-NMR-spectra is calculated by the device without reference. The following solvents from *Eurisotop* were used: chloroform-d_1. Chemical shifts δ were expressed in parts per million (ppm) and referenced to chloroform-d_1 (^{1}H: δ =7.26 ppm, ^{13}C: δ =77.0 ppm),[171] The signal structure is described as follows: s=singlet, d=doublet, t=triplet, q=quartet, quin=quintet, b=broad singlet, m=multiplet, kb=complex area, dt=doublet of triplets. The spectra were analyzed according to the first order. All coupling constants are absolute values and expressed in Hertz (Hz). The following abbreviations were used for the assignment of the signals: Ar-H=aromatic, C-Ar=aromatic.

6.1.3.4 EPR Spectroscopy

CW-EPR spectra were recorded on a *Bruker* 'EMXplus' X-band spectrometer (microwave frequency: 9.43 GHz). Measurements were carried out on sample solutions in benzene or on solid samples embedded in a KCl matrix.

6.1.3.5 Mass Spectrometry (EI-MS, FAB-MS and ESI)

Mass spectra were recorded on a *Finnigan* MAT 95 mass spectrometer using electron ionization-mass spectrometry (EI-MS) or fast atom bombardment-mass spectrometry (FAB-MS). For FAB measurements *m*-nitrobenzyl alcohol (3-NBA) was used as the matrix. The software of FAB and EI adds the mass of one electron. The molecular ion is abbreviated $[M]^{+}$ for EI-MS, the protonated molecular ion is abbreviated [*M*+H] for FAB-MS. Electrospray ionization-mass spectrometry (ESI-MS) spectra were recorded on a *Thermo Fisher Scientific Q Exactive* mass spectrometer. Calibration was carried out using premixed calibration solutions (*Thermo Fisher Scientific*). The molecular fragments are stated as ratio of mass per charge *m/z*.

6.1.3.6 Infrared Spectroscopy (IR)

IR spectra were recorded on a BRUKER IFS 88 using ATR (Attenuated Total Reflection) for solids. The absolute intensities of the peaks are given as follows: vs=very strong 0-9% T, s=strong 10-39% T, m=medium 40-69% T, w=weak 70-89% T, vw=very weak 90-100% T.

6.1.3.7 UV-Vis-NIR-Absorption Spectroscopy

UV/Vis absorption spectra (200–750 nm) were recorded using the '*Cary 60*' photometer, while UV-Vis-NIR spectra (200–1500 nm) were measured with the '*Cary 5000*' spectrophotometer from *Agilent*. All measurements were performed in 1.00 cm quartz glass cuvettes (*Hellma*), temperature-controlled at 20 °C. For quantitative analysis, the linearity of the results was verified in accordance with the *Lambert-Beer law*.

6.1.3.8 Fluorescence Spectroscopy

Fluorescence was measured in the ultraviolet and visible spectral range using the '*Fluoromax-4*' device from *HORIBA*. Sample solutions, with a concentration of 50 µmol L^{-1} were tempered to 20 °C in quartz glass cuvettes. Instrument calibration was performed using the Raman scattering signal of water.

6.1.3.9 X-Ray diffractometry

Diffraction data were measured using a Stoe *STADIVARI* diffractometer and Ga-Kα (1.34134 Å) radiation. Absorption corrections were carried out using the *STOE LANA* software package.[172] Structure solution was carried out using *OLEX2* 1.5[173] by dual-space direct methods with *SHELXT*,[174] by full-matrix least-squares refinement using *SHELXL-2014/7*.[174] All non-hydrogen atoms were refined anisotropically. The contribution of the hydrogen atoms, in their calculated positions, was included in the refinement using a riding model. A full listing of atomic coordinates, bond lengths, angles and displacement parameters for all the structures have been deposited at the Cambridge Crystallographic Data Centre.[175-178]

6.1.3.10 Cyclovoltammetry

Cyclic voltammograms were measured with a suitable potentiostat and an electrochemical cell within a glovebox. A freshly polished Pt disk as working electrode, a Pt wire as a counter electrode and an Ag wire as (pseudo)reference electrode were used in 0.01 mM $[NBu_4][Al(OC_4F_9)_4]$ solution as electrolyte). Potentials were calibrated against the Fc/Fc^+ couple (internal standard; Fc* = decamethyl ferrocene).

6.2 Quantum Chemical Calculations

The structural optimization, frequency and IRC analyses, simulations of UV/Vis and EPR spectra as well as the calculation of NMR data for the ACID calculations were carried out as (u)(TD-)DFT calculations with the program package '*Gaussian16*' on the '*JUSTUS2*'

cluster of the state of Baden-Württemberg.[179] The *GD3BJ* dispersion-corrected *PBE0* or *PBE1PBE* functional and the *Def2-TZVP* basis set were used in all instances.[179-182] '*GaussView*' versions 3.0.9 and 6.1.1 were used as the graphical user interface, which was also used to generate the images of molecules and orbitals shown.[183] When calculating the UV/Vis, 50 states were taken into account and the solvent was simulated using the CPCM method (Conductor-like Polarizable Continuum Model).[184-185] The evaluation of the time-dependent calculations was carried out using the '*GaussSum*' program. The ACID calculations were carried out with the program packages of the same name.[117-118, 186-187] The NICS-XY scans were generated with the program 'Aroma' and the older 'Gaussian09' at the *B3LYP/6-311+G** level.[115-116, 188-192] The NBO occupation numbers required to determine the radical character according to *Yamaguchi* were determined at the *uHF/Def2-TZVP* level with '*Gaussian16*'.[72, 181-182, 193]

6.3 Synthetic Procedure

2,7-Dibromo-9-mesityl-9*H*-fluorene (46)

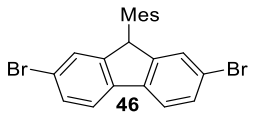

Following a published method,[125] Me_3SiCl (1.06 g, 1.24 mL, 9.76 mmol, 1.10 eq.) and Et_3SiH (1.09 g, 1.50 ml, 9.37 mmol, 1.06 eq.) were added under an argon atmosphere to a solution of 2,7-dibromofluoren-9-one (**45**; 3.00 g, 8.88 mmol, 1.00 eq.) and anhydrous $FeCl_3$ (72.0 mg, 444 µmol, 0.05 eq.) in mesitylene (8 mL). The mixture was stirred for 2 h at rt, heated for 18 h to 50 °C, cooled to rt, quenched with H_2O (20 mL) and extracted with CH_2Cl_2 (3×100 mL). The combined organic layers were washed with H_2O (3×100 mL), dried (Na_2SO_4), concentrated at reduced pressure, and purified by column chromatography (silica gel, *n*-hexane) to yield **46** (2.89 g, 6.54 mmol, 74%) as pale orange crystals.

R_f = 0.38 (*n*-hexane).

^{1}H NMR (400 MHz, $CDCl_3$): δ (ppm) 7.65 (d, 2H; Ar-H), 7.55–7.48 (m, 2H; Ar-H), 7.33 (t, *J* = 1.5 Hz, 2H; Ar-H), 7.03–7.01 (m, 1H; Ar-H), 6.72–6.65 (m, 1H; Ar-H), 5.44 (s, 1H; Ar-H), 2.64 (s, 3H; CH_3), 2.30 (s, 3H; CH_3), 1.13 (s, 3H, CH_3).

^{13}C NMR (100 MHz, $CDCl_3$, ppm): δ 149.1 (C), 138.9 (C), 137.8 (C), 137.8 (C), 137.1 (C), 132.3 (C), 130.9 (CH), 130.4 (CH), 129.2 (CH), 127.5 (CH), 121.7 (C), 121.5 (CH), 49.7 (CH), 21.8 (CH_3), 21.0 (CH_3), 18.9 (CH_3).

IR (ATR, cm^{-1}): $\tilde{\nu}$ = 2949 (w), 2918 (w), 2860 (w), 1881 (vw), 1734 (vw), 1596 (w), 1568 (w), 1482 (w), 1455 (s), 1443 (m), 1411 (m), 1401 (m), 1394 (m), 1377 (w), 1258 (w), 1235 (w), 1162 (w), 1058 (s), 1031 (w), 1004 (m), 898 (m), 878 (m), 868 (w), 853 (m), 830 (w), 810 (vs), 796 (vs), 768 (w), 756 (w), 663 (m), 616 (m), 465 (s), 414 (m).

MS (FAB): *m/z* (%): 443.9 (10) $[M]^+$, 442.9 (6) $[M]^+$, 440.9 (5) $[M]^+$, 363.0 (7) $[M-Br]^+$, 361.0 (7) $[M-Br]^+$, 324.8 (4) $[M-Mes]^+$, 322.8 (8) $[M-Mes]^+$, 320.8 (4) $[M-Mes]^+$; HRMS (FAB): *m/z* calcd for $C_{22}H_{18}{}^{79}Br^{81}Br$: 441.9749 $[M]^+$; found: 441.9751.

2,2'-(9-Mesityl-9*H*-fluorene-2,7-diyl)dibenzaldehyde (48)

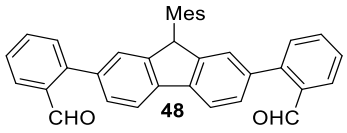

$PdCl_2$(dppf) (248 mg, 339 µmol, 0.15 eq.) was added under an argon atmosphere to a degassed (10 min) mixture of fluorene **46** (1.00 g, 2.26 mmol, 1.00 eq.), (2-formylphenyl)boronic acid (**47**; 848 mg, 5.66 mmol, 2.50 eq.), and Cs_2CO_3 (3.68 g, 11.3 mmol, 5.00 eq.) in toluene/H_2O (1:1; 20 mL). The mixture was heated to 105 °C for 18 h, cooled to rt, and the aqueous layer was extracted with CH_2Cl_2 (3×100 mL). The combined organic layers were dried (Na_2SO_4), concentrated at reduced pressure, and purified by column chromatography (silica gel, *n*-hexane/EtOAc 9:1) to yield **48** (804 mg, 1.63 mmol, 72%) as a beige solid.

R_f = 0.22 (*n*-hexane/EtOAc 9:1).

^{1}H NMR (400 MHz, $CDCl_3$): δ (ppm) 9.99 (s, 2H; CHO), 8.04–7.93 (m, 4H; Ar-H), 7.61 (m, 2H; Ar-H), 7.53–7.40 (m, 6H; Ar-H), 7.33–7.21 (m, 2H; Ar-H), 7.02–6.93 (m, 1H; Ar-H), 6.76–6.62 (m, 1H; Ar-H), 5.64 (s, 1H; Ar-H), 2.67 (s, 3H; CH_3), 2.24 (s, 3H; CH_3), 1.20 (s, 3H; CH_3).

^{13}C NMR (100 MHz, $CDCl_3$, ppm): δ 192.5 (CHO), 148.1 (C), 146.1 (C), 140.3 (C), 137.8 (C), 137.6 (C), 137.4 (C), 136.9 (C), 133.9 (C), 133.6 (CH), 133.0 (C), 131.0 (CH), 130.9 (CH), 129.6 (CH), 129.2 (CH), 127.9 (CH), 127.8 (CH), 125.8 (CH), 120.3 (CH), 50.0 (CH), 22.0 (CH_3), 21.0 (CH_3), 19.0 (CH_3).

IR (ATR, cm^{-1}): $\tilde{\nu}$ = 2961 (w), 2919 (w), 2894 (w), 2868 (w), 2843 (w), 2749 (w), 1737 (vw), 1686 (vs), 1650 (w), 1595 (m), 1568 (w), 1482 (w), 1460 (m), 1445 (m), 1411 (w), 1391 (m), 1375 (w), 1252 (m), 1244 (m), 1191 (s), 1157 (w), 1096 (w), 1026 (w), 1014 (w), 1003 (w), 907 (w), 897 (w), 850 (m), 832 (vs), 805 (m), 790 (w), 761 (vs), 734 (m), 721 (m), 714 (w), 671 (w), 652 (w), 637 (m), 611 (w), 592 (w), 554 (w), 537 (w), 524 (w), 499 (w), 458 (w), 441 (m), 424 (w).

MS (FAB): *m/z* (%): 494.2 (6) $[M+2]^+$, 493.2 (22) $[M+1]^+$, 492.2 (42) $[M]^+$, 374.1 (10) $[M+1-Mes]^+$, 373.1 (30) $[M-Mes]^+$; HRMS (FAB): *m/z* calcd for $C_{36}H_{28}O_2$: 492.2084 $[M]^+$; found: 492.2086.

((9-Mesityl-9*H*-fluorene-2,7-diyl)bis(2,1-phenylene))bis(mesitylmethanol) (49)

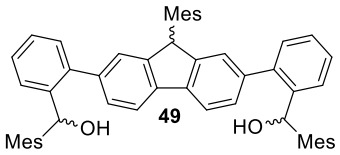

Following a published method,[126] MesMgBr (1.00 M in THF; 1.21 g, 5.45 mL, 5.45 mmol, 5.00 eq.) was added dropwise under an argon atmosphere to a cooled (0 °C) solution of fluorene **48** (535 mg, 1.09 mmol, 1.00 eq.) in anhydrous THF (20 mL). After addition was completed, the cooling bath was removed and the mixture stirred for 15 min at rt. Saturated aqueous NH_4Cl solution (30 mL) was added, stirring was continued for 10 min, and the mixture was extracted with CH_2Cl_2 (3×100 mL). The combined organic layers were dried (Na_2SO_4) and concentrated at reduced pressure.

6,12,15-Trimesityl-12,15-dihydro-6*H*-cyclopenta[2,1-*b*:3,4-*b*']difluorene (50)

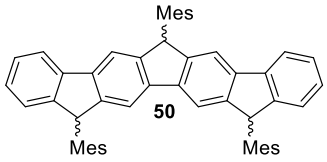

The remnant (**49**) was dissolved in anhydrous CH_2Cl_2 (40 mL) and the solution was cooled to 0 °C. $BF_3{\cdot}OEt_2$ (968 mg, 864 µL, 6.82 mmol, 5.00 eq.) was added under an argon atmosphere and the mixture was stirred for 1 h at rt. Saturated aqueous NH_4Cl solution (30 mL) was added, stirring was continued for 10 min, and the mixture was extracted with CH_2Cl_2 (3×100 mL) The combined organic layers were dried (Na_2SO_4), concentrated at reduced pressure, and purified by column chromatography (silica gel, *n*-pentane/CH_2Cl_2 4:1) to yield **50** (705 mg, 1.01 mmol, 93%) as a pale orange solid. The product was obtained as a mixture of isomers, thus resulting in additional hardly discriminable signals in the spectra. Only the most pronounced signals are given.

R_f = 0.37 (*n*-pentane/CH_2Cl_2 4:1).

^{1}H NMR (400 MHz, $CDCl_3$): δ (ppm) 7.71 (m, 2H; Ar-H), 7.62 (m, 2H; Ar-H), 7.51 (m, 2H; Ar-H), 7.36–7.29 (m, 2H; Ar-H), 7.22–7.12 (m, 5H; Ar-H), 7.04 (d, 2H; Ar-H), 6.73–6.61 (m, 3H; Ar-H), 5.60 (d, 3H; Ar-H), 2.79 (d, 9H; CH_3), 2.31 (d, 9H; CH_3), 1.07 (d, 9H; CH_3).

^{13}C NMR (100 MHz, $CDCl_3$, ppm): δ 147.7 (C), 147.0 (C), 146.9 (C), 146.7 (C), 146.6 (C), 141.1 (C), 140.8 (C), 140.7 (C), 140.5 (C), 138.3 (C), 138.2 (C), 138.1 (C), 138.0 (C), 137.8 (C), 136.5 (C), 136.4 (C), 136.3 (C), 134.8 (C), 134.4 (C), 130.8 (CH), 130.6 (CH), 129.1 (CH), 129.0 (CH), 127.0 (CH), 126.9 (CH), 124.2 (CH), 120.2 (CH), 116.0 (CH), 115.9 (CH), 49.6 (CH), 49.6 (CH), 49.4 (CH), 22.2 (CH_3), 22.0 (CH_3), 22.0 (CH_3), 21.1 (CH_3), 21.0 (CH_3), 21.0 (CH_3), 18.9 (CH_3), 18.8 (CH_3), 18.6 (CH_3).

IR (ATR, cm^{-1}): $\tilde{\nu}$ = 3061 (w), 3009 (w), 2962 (w), 2918 (m), 2856 (w), 2734 (w), 2228 (w), 2167 (w), 2061 (w), 2014 (vw), 1962 (w), 1731 (w), 1612 (w), 1579 (w), 1480 (s), 1448 (s), 1425 (s), 1378 (m), 1299 (m), 1282 (s), 1244 (w), 1180 (w), 1156 (w), 1024 (m), 1013 (m), 936 (w), 890 (m), 856 (m), 844 (vs), 800 (m), 768 (vs), 739 (vs), 727 (vs), 589 (w), 564 (m), 414 (s).

MS (FAB): *m/z* (%): 699.3 (6) $[M+3]^+$, 698.3 (24) $[M+2]^+$, 697.3 (67) $[M+1]^+$, 696.3 (100) $[M]^+$, 695.3 (13) $[M-1]^+$, 578.2 (12) $[M+1-\text{Mes}]^+$, 577.2 (23) $[M-\text{Mes}]^+$, 576.2 (9)

[*M*−1−Mes]$^+$, 457.1 (9) [*M*−2Mes]$^+$; HRMS (FAB): *m/z* calcd for $C_{54}H_{48}$: 696.3749 [*M*]$^+$; found: 696.3751.

6,12,15-Trimesitylcyclopenta[2,1-*b*:3,4-*b*']difluorenyl Radical (39)

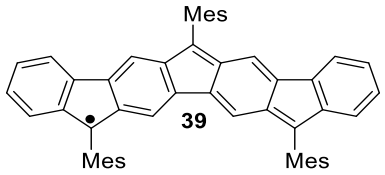

Following a published method,[74] precursor **50** (590 mg, 847 µmol, 1.00 eq.) and KO*t*Bu (1.33 g, 11.9 mmol, 14.0 eq.) were dissolved in anhydrous THF (60 mL) under an argon atmosphere and heated for 16 h to 60 °C. The mixture was allowed to cool to rt and *p*-chloranil (937 mg, 3.81 mmol, 4.50 eq.) was added. After stirring for 10 min, the mixture was concentrated at reduced pressure. The obtained remnant was purified by column chromatography (silica gel, *n*-pentane/CH_2Cl_2 4:1) to yield **39** (403 mg, 581 µmol, 69%) as a dark green solid.

R_f = 0.33 (*n*-pentane/CH_2Cl_2 4:1).

m.p. 356 °C.

IR (ATR, cm^{-1}): $\tilde{\nu}$ = 3388 (w), 3051 (w), 2953 (s), 2918 (vs), 2850 (vs), 2752 (m), 2734 (m), 2689 (w), 2670 (w), 1948 (w), 1912 (w), 1878 (w), 1805 (w), 1734 (w), 1609 (s), 1565 (w), 1538 (w), 1513 (s), 1463 (vs), 1434 (vs), 1374 (vs), 1336 (vs), 1320 (s), 1288 (m), 1259 (m), 1225 (m), 1214 (m), 1181 (vs), 1149 (m), 1128 (vs), 1094 (m), 1057 (m), 1033 (m), 1014 (s), 996 (m), 972 (m), 938 (m), 898 (vs), 880 (s), 849 (vs), 807 (m), 776 (s), 755 (vs), 735 (m), 715 (vs), 677 (s), 653 (w), 578 (m), 560 (m), 510 (w), 441 (w), 402 (s).

UV/Vis (CH_2Cl_2, nm ($mol^{-1}dm^3cm^{-1}$)): λ_{max} (ε) = 337 (58,000), 349 (59,000), 479 (8,000), 513 (14,000), 604 (19,000), 644 (34,000), 672 (42,000).

MS (ESI): *m/z* (%): 696.3 (3) $[M+3]^+$, 695.3 (16) $[M+2]^+$, 694.3 (58) $[M+1]^+$, 693.3 (100) $[M]^+$; HRMS (ESI): *m/z* calcd for $C_{54}H_{45}$: 693.3516 $[M]^+$; found: 693.3502.

2,7-Dinitro-9*H*-fluoren-9-one (54)

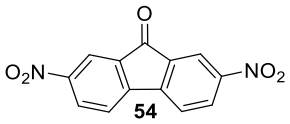

54

Variant A:

Following a published protocol,[194] fluoren-9-one (**53**, 5.00 g, 27.7 mmol, 1.00 eq.) was added to a stirring mixture of fuming nitric acid (50 mL) and acetic acid (25 mL) and stirred at rt for 1 h. Subsequently, stirring was stopped and the mixture left to crystallize as long yellow needles. Filtration, washing with small portions of cold acetic acid and water and drying allowed to obtain **54** as yellow crystals (4.00 g, 14.8 mmol, 53%). The obtained data is agreement with published data.[194]

Variant B:

Following a published protocol,[195] 2,7-dinitro-9*H*-fluorene (**57**; 1.00 g, 3.90 mmol, 1.00 eq.) and KOH (219 mg, 3.90 mmol, 1.00 eq.) were suspended in 15 mL THF and stirred at rt for 8 h. Next, the mixture was filtered to remove excess KOH and the filtrate concentrated. The crude product was washed with water, dried and purified by recrystallization from ethanol to obtain **54** (493 mg, 1.83 mmol, 47%) as yellow crystals. The obtained data is agreement with published data.[195]

^{1}H NMR (400 MHz, $CDCl_3$): δ (ppm) 8.6 (d, J = 2.1 Hz, 2H), 8.5 (dd, J = 8.2, 2.1 Hz, 2H), 7.9 (d, J = 8.3 Hz, 2H).

2,7-Diamino-9*H*-fluoren-9-one (55)

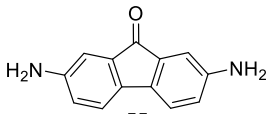

55

Variant A:

Following a published protocol,[196] $SnCl_2$ $2H_2O$ (8.35 g, 37.0 mmol, 10.0 eq.) was added to a solution of 2,7-dinitrofluoren-9-one (**54**, 1.00 g, 3.70 mmol, 1.00 eq.) in 50 mL EtOAc under an argon atmosphere and the resulting mixture stirred for 24h under reflux. The mixture was allowed to cool to rt, poured onto ice and quenched by a sat. $NaHCO_3$ solution. After filtration, the filtrate was extracted with EtOAc and the combined organic layers dried over Na_2SO_4, filtered and the solvent evaporated under reduced pressure. The obtained crude product was purified by column chromatography (silica gel, *n*-hexane/EtOAc 2:1) to yield **55** (78.0 mg, 371 µmol, 10%) as a red solid. The obtained data is in agreement with published data.[196]

Variant B:

Following a published protocol,[197] Cs_2CO_3 (498 mg, 1.53 mmol, 3.00 eq.) was added to a mixture of 9*H*-fluorene-2,7-diamine (**58**, 100 mg, 510 µmol, 1.00 eq.) in DMSO (3 mL) and stirred at rt for 16 h. Water was added to the mixture and the formed precipitate filtered, washed with water and dried under vacuum to obtain **55** (74.0 mg, 352 µmol, 69%) as a red solid.

^{1}H NMR (400 MHz, DMSO): δ (ppm) 7.1 (d, J = 7.9 Hz, 2H, Ar-H), 6.7 (d, J = 2.1 Hz, 2H, Ar-H), 6.6 (dd, J = 7.9, 2.2 Hz, 2H, H-Ar), 5.3 (s, 4H, NH_2).

9*H*-Fluorene-2,7-diamine (58)

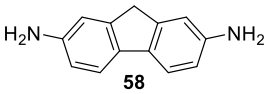

58

Following a published protocol,[198] Pd/C (62.3 mg, 585 µmol, 0.05 eq.) was added to a mixture of 2,7-dinitro-9*H*-fluorene (**57**; 3.00 g, 11.7 mmol, 1.00 eq.) in methanol (100 mL) and stirred at rt for 24 h under H_2 atmosphere. Next, the reaction mixture was filtered over a pad of Celite and washed with EtOAc and the filtrate concentrated under reduced pressure to obtain **58** (2.29 g, 11.7 mmol, quant.) as a red solid. The obtained data is in agreement with published data.[198]

^{1}H NMR (400 MHz, $CDCl_3$): δ (ppm) 7.4 (d, J = 8.1 Hz, 2H, H-Ar), 6.8 (d, J = 2.1 Hz, 2H, H-Ar), 6.7 (dd, J = 8.0, 2.2 Hz, 2H, H-Ar), 3.7 (s, 2H, CH_2), 3.6 (s, 4H, NH_2).

N,N'-(9*H*-fluorene-2,7-diyl)diacetamide (59)

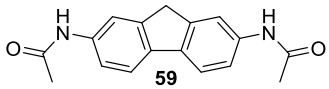

59

Following a published protocol,[199] 9*H*-fluorene-2,7-diamine (**58**; 100 mg, 510 µmol, 1.00 eq.) was dissolved in dry THF (10 mL) and purged with argon. Acetyl acetate (130 mg, 120 µL, 1.27 mmol, 2.50 eq.) and triethylamine (129 mg, 177 µL, 1.27 mmol, 2.50 eq.) were added under an argon atmosphere. The final mixture was stirred at rt overnight. After the completion of the reaction, the solution was poured on ice water, the precipitate was filtered and dried to obtain **59** (129 mg, 460 µmol, 90%) as a red solid. The obtained data is in agreement with published data.[199]

^{1}H NMR (400 MHz, DMSO): δ (ppm) 10.0 (s, 2H, NHAc), 7.9 (d, J = 1.9 Hz, 2H, H-Ar), 7.7 (d, J = 8.2 Hz, 2H, H-Ar), 7.5 (dd, J = 8.3, 1.9 Hz, 2H, H-Ar), 3.9 (s, 2H, CH_2), 2.1 (s, 6H, $COCH_3$).

N,N'-(9-oxo-9*H*-fluorene-2,7-diyl)diacetamide (60)

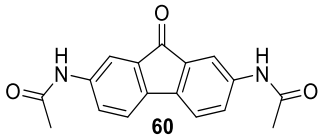

60

Variant A:

Following a published protocol,[199] 2,7-diaminofluoren-9-one (**55**; 80.0 mg, 381 µmol, 1.00 eq.) was dissolved in dry THF (10 mL) and purged with argon. Acetyl acetate (97.1 mg, 89.9 µL, 951 µmol, 2.50 eq.) and triethylamine (96.3 mg, 132 µL, 951 µmol, 2.50 eq.) were added under an argon atmosphere. The final mixture was stirred at rt overnight. After the completion of the reaction, the solution was poured on ice water, the precipitate was filtered and dried to obtain **60** (48 mg, 163 µmol, 43%) as a red solid. The obtained data is in agreement with published data.[199]

Variant B:

In variation to a published protocol,[197] Cs_2CO_3 (349 mg, 1.07 mmol, 3.00 eq.) was added to a mixture of 9*H*-fluorene-2,7-diamine (**58**; 100 mg, 357 µmol, 1.00 eq.) in DMSO (6 mL) and stirred at rt for 16 h. Water was added to the mixture and the formed precipitate filtered, washed with water and dried under vacuum to obtain **60** (74.0 mg, 248 µmol, 70%) as a red solid. The obtained data is in agreement with published data.[199]

^{1}H NMR (400 MHz, DMSO): δ (ppm) 10.2 (s, 2H, NHAc), 7.9 (d, J = 2.0 Hz, 2H, H-Ar), 7.7 (dd, J = 8.1, 2.0 Hz, 2H, H-Ar), 7.6 (s, 2H, H-Ar), 2.1 (s, 6H, $COCH_3$).

3,6-Dibromo-9*H*-fluoren-9-one (64)

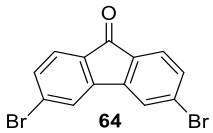

64

In slight variation to a published protocol,[200] KOH (831 mg, 14.8 mmol, 20.0 eq.) and 3,6-dibromophenanthrene-9,10-dione (**63**; 271 mg, 0.74 mmol, 1.00 eq.) in 20 mL water were heated to 130 °C for 4 h. $KMnO_4$ (585 mg, 3.70 mmol, 5.00 eq.) was added to this mixture portion wise and stirring continued while heating at 130 °C for 14 h. After cooling to rt, the mixture was neutralized with conc. H_2SO_4, and sodium disulfite was added carefully to the slightly acidic mixture until it turned light yellow. The precipitate was filtered off and washed with water. Subsequent purification by column chromatography (silica gel, CH_2Cl_2) to yield **64** (222 mg, 0.66 mmol, 89%) as a yellow solid. The NMR data are in agreement with published data.[200]

^{1}H NMR (400 MHz, $CDCl_3$): δ (ppm) 7.67 (dd, J = 1.57, 0.56 Hz, 2H, Ar-H), 7.54 (d, J = 0.58 Hz, 2H, Ar-H), 7.50 (d, J = 1.56 Hz, 2H, Ar-H).

3,6-Dibromo-9-mesityl-9*H*-fluoren-9-ol (66)

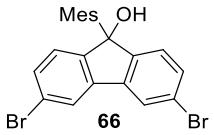

66

Following a published protocol,[201] MesMgBr (1M in THF; 496 mg, 2.22 mL, 2.22 mmol, 1.50 eq.) was added under an argon atmosphere to a cooled solution (0 °C) of 3,6-dibromofluoren-9-one (500 mg, 1.48 mmol, 1.00 eq.) in 20 mL dry THF. After fully addition, the cooling bath was removed and the final mixture stirred at rt for 15 h. NH_4Cl was added, stirring continued for 10 min and the phases separated. The aqueous phase was extracted with CH_2Cl_2 and the combined organic layers were dried over Na_2SO_4, filtered and concentrated under reduced pressure.

3,6-Dibromo-9-mesityl-9*H*-fluorene (65)

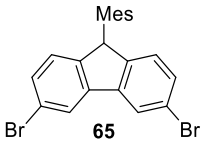

65

Variant A:

Following a published protocol,[201] BF_3 OEt_2 (310 mg, 277 µL, 2.18 mmol, 2.00 eq.) was added slowly under an argon atmosphere to a cooled (0 °C) solution of remnant **66** (500 mg, 1.09 mmol, 1.00 eq.) and triethylsilane (254 mg, 349 µL, 2.18 mmol, 2.00 eq.) in 20 mL dry CH_2Cl_2 and stirred for 1 h at 0 °C. Saturated aqueous $NaHCO_3$ solution and brine were added, stirring continued for 10 min and the phases separated. The aqueous layer was extracted with CH_2Cl_2 and the combined organic layers dried over Na_2SO_4, filtered and the solvent removed under reduced pressure. The obtained residue was purified by column chromatography (silica gel, *n*-hexane) to yield **65** (657 mg, 1.49 mmol, quant.) as a beige solid.

Variant B:

Following a published method,[125] Me_3SiCl (113 mg, 123 µL, 1.04 mmol, 1.10 eq.) and Et_3SiH (117 mg, 160 µl, 9.37 mmol, 1.06 eq.) were added under an argon atmosphere to a solution of 3,6-dibromo-9*H*-fluoren-9-one (**64**; 320 mg, 947 µmol, 1.00 eq.) and anhydrous $FeCl_3$ (7.68 mg, 47.3 µmol, 0.05 eq.) in mesitylene (7 mL). The mixture was stirred for 2 h at rt, heated for 18 h to 50 °C, cooled to rt, quenched with H_2O (20 mL) and extracted with CH_2Cl_2 (3×100 mL). The combined organic layers were washed with H_2O (3×100 mL), dried (Na_2SO_4), concentrated at reduced pressure, and purified by column chromatography (silica gel, *n*-hexane) to yield **65** (162 mg, 366 µmol, 39%) as pale orange crystals.

R_f = 0.8 (*n*-hexane/CH_2Cl_2 1:1).

^{1}H NMR (400 MHz, $CDCl_3$): δ (ppm) 7.91 (d, *J* = 1.8 Hz, 2H, H-Ar), 7.39 (dd, *J* = 8.1, 1.8 Hz, 2H, H-Ar), 7.08 (dd, *J* = 8.0, 1.1 Hz, 2H, H-Ar), 7.03 – 6.98 (m, 1H, H-Ar), 6.68 – 6.61 (m, 1H, H-Ar), 5.35 (s, 1H, CH), 2.64 (s, 3H, CH_3), 2.28 (d, *J* = 2.7 Hz, 3H, CH_3), 1.09 (s, 3H, CH_3).

^{13}C NMR (100 MHz, $CDCl_3$): δ (ppm) 146.5 (C), 141.8 (C), 137.8 (C), 136.9 (C), 132.5 (C), 130.8 (CH), 130.8 (CH), 129.2 (CH), 125.9 (CH), 123.7 (CH), 121.1 (C), 49.3 (CH), 21.9 (CH_3), 21.0 (CH_3), 18.9 (CH_3).

IR (ATR) $\tilde{\nu}$ (cm^{-1}) = 2961 (w), 2914 (w), 2856 (w), 1594 (w), 1565 (w), 1469 (m), 1456 (m), 1415 (s), 1392 (w), 1377 (w), 1262 (w), 1122 (w), 1103 (w), 1057 (m), 1024 (s), 885 (m), 866 (m), 837 (vs), 806 (m), 781 (vs), 752 (m), 730 (m), 703 (w), 688 (w), 670 (s), 652 (m), 635 (m), 572 (m), 557 (w), 540 (m), 507 (w), 470 (w), 416 (m), 390 (w), 381 (w).

MS (ESI): *m/z* (%): 441.9 (100) $[M+2]^+$, 440.9 (11) $[M+1]^+$, 439.9 (52) $[M]^+$, HRMS (ESI): *m/z* calcd for $C_{22}H_{18}Br_2$: 439.9775 $[M]^+$; found: 439.9777.

2,2'-(9-Mesityl-9*H*-fluorene-3,6-diyl)dibenzaldehyde (67)

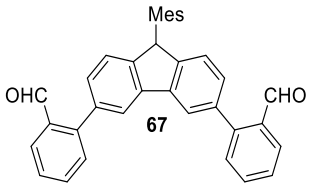

$PdCl_2$(dppf) (124 mg, 170 µmol, 0.150 eq.) was added under an argon atmosphere to a degassed (10 min) mixture of fluorene **65** (500 mg, 1.13 mmol, 1.00 eq.), (2-formylphenyl)boronic acid (373 mg, 2.49 mmol, 2.20 eq.), and Cs_2CO_3 (1.84 g, 5.65 mmol, 5.00 equiv) in toluene/H_2O (1:1; 15 mL). The mixture was heated to 105 °C for 18 h, cooled to rt, and the aqueous layer was extracted with CH_2Cl_2 (3×100 mL). The combined organic layers were dried (Na_2SO_4), concentrated at reduced pressure, and purified by column chromatography (silica gel, *n*-hexane/EtOAc 9:1) to yield **67** (463 mg, 940 µmol, 83%) as a beige solid.

R_f = 0.37 (*n*-hexane/EtOAc 9:1).

^{1}H NMR (400 MHz, $CDCl_3$): δ (ppm) 10.05 (d, *J* = 0.9 Hz, 2H, CHO), 8.05 (dd, *J* = 7.8, 1.5 Hz, 2H, Ar-H), 7.85 (d, *J* = 1.7 Hz, 2H, Ar-H), 7.67 (td, *J* = 7.5, 1.5 Hz, 2H, Ar-H), 7.59 – 7.48 (m, 4H, Ar-H), 7.36 (dt, *J* = 7.7, 0.9 Hz, 2H, Ar-H), 7.30 (dd, *J* = 7.7, 1.7 Hz, 2H, Ar-H), 7.07 (s, 1H, Ar-H), 6.72 (d, *J* = 2.0 Hz, 1H, Ar-H), 5.64 (s, 1H, CH), 2.74 (s, 3H, CH_3), 2.31 (s, 3H, CH_3), 1.20 (s, 3H, CH_3).

^{13}C NMR (100 MHz, $CDCl_3$): δ (ppm) 192.5 (CHO), 147.8 (C), 146.2 (C), 140.7 (C), 137.9 (C), 137.8 (C), 136.9 (C), 136.9 (C), 134.0 (CH), 133.7 (CH), 133.1 (C), 131.1 (CH), 130.8 (CH), 129.9 (CH), 129.2 (CH), 128.0 (CH), 127.8 (CH), 124.3 (CH), 121.9 (CH), 49.7 (CH), 21.9 (CH_3), 21.0 (CH_3), 19.1 (CH_3).

IR (ATR) $\tilde{\nu}$ (cm^{-1}) = 2968 (w), 2915 (w), 2840 (w), 2742 (w), 1687 (vs), 1595 (s), 1575 (w), 1561 (w), 1469 (w), 1448 (w), 1432 (w), 1390 (m), 1249 (m), 1193 (s), 1159 (w), 1096 (w), 1028 (w), 1010 (w), 897 (w), 847 (s), 819 (m), 798 (m), 761 (vs), 737 (m), 721 (w), 701 (m), 663 (w), 642 (m), 633 (m), 613 (w), 575 (w), 555 (w), 548 (w), 441 (w), 422 (w).

MS (ESI): *m/z* (%):495.2 (8) $[M+3]^+$, 494.2 (39) $[M+2]^+$, 493.2 (100) $[M+1]^+$, HRMS (ESI): *m/z* calcd for $C_{36}H_{28}O_2$: 492.2089 $[M]^+$; found: 493.2170 $[M+1]^+$.

((9-Mesityl-9*H*-fluorene-3,6-diyl)bis(2,1-phenylene))bis(mesitylmethanol) (68)

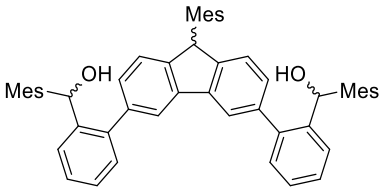

Following a published method,[126] MesMgBr (1.00 M in THF; 453 mg, 2.03 mL, 2.03 mmol, 5.00 eq.) was added dropwise under an argon atmosphere to a cooled (0 °C) solution of fluorene **67** (200 mg, 406 µmol, 1.00 eq.) in anhydrous THF (15 mL). After addition was completed, the cooling bath was removed and the mixture stirred for 15 min at rt. Saturated aqueous NH_4Cl solution (30 mL) was added, stirring was continued for 10 min, and the mixture was extracted with CH_2Cl_2 (3×100 mL). The combined organic layers were dried (Na_2SO_4) and concentrated at reduced pressure.

11,13,15-Trimesityl-13,15-dihydro-11H-cyclopenta[1,2-b:4,3-b']difluorene (69)

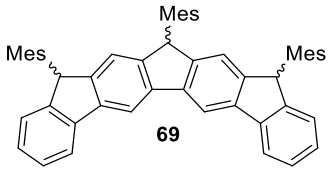

69

The remnant (**68**) was dissolved in anhydrous CH_2Cl_2 (20 mL) and the solution was cooled to 0 °C. $BF_3{\cdot}OEt_2$ (194 mg, 173 µL, 1.36 mmol, 5.00 eq.) was added under an argon atmosphere and the mixture was stirred for 1 h at rt. Saturated aqueous NH_4Cl solution (30 mL) was added, stirring was continued for 10 min, and the mixture was extracted with CH_2Cl_2 (3×100 mL) The combined organic layers were dried (Na_2SO_4), concentrated at reduced pressure, and purified by column chromatography (silica gel, *n*-pentane/CH_2Cl_2 4:1) to yield **69** (283 mg, 406 µmol, quant.) as a pale orange solid. The product was obtained as a mixture of isomers, thus resulting in additional hardly discriminable signals in the spectra. Only the most pronounced signals are given.

R_f = 0.37 (*n*-pentane/CH_2Cl_2 4:1).

^{1}H NMR (400 MHz, $CDCl_3$): δ (ppm) 8.45 – 8.37 (m, 1H, Ar-H), 8.03 – 7.71 (m, 2H, Ar-H), 7.61 – 7.34 (m, 4H, Ar-H), 7.32 – 7.27 (m, 1H, Ar-H), 7.25 – 7.11 (m, 3H, Ar-H), 7.07 (d, *J* = 5.8 Hz, 1H, Ar-H), 7.06 – 6.95 (m, 2H, Ar-H), 6.95 (m, 1H, Ar-H), 6.67 – 6.50 (m, 3H, Ar-H), 5.96 – 5.37 (m, 3H, CH), 3.19 – 2.97 (m, 2H, CH_3), 2.72 – 2.51 (m, 7H, CH_3), 2.40 – 2.15 (m, 9H, CH_3), 1.36 – 1.04 (m, 9H, CH_3).

^{13}C NMR (100 MHz, $CDCl_3$): δ (ppm) 147.8 (C), 147.4 (C), 147.3 (C), 147.2 (C), 146.9 (C), 146.5 (C), 146.0 (C), 141.0 (C), 140.8 (C), 140.2 (C), 139.8 (C), 138.1 (C), 138.0 (C), 137.0 (C), 136.8 (C), 136.2 (C), 134.5 (C), 134.3 (C), 134.0 (C), 133.9 (C), 130.9 (CH), 130.7 (CH), 130.6 (CH), 130.6 (CH), 129.8 (CH), 129.7 (CH), 129.0 (CH), 128.9 (CH), 128.9 (CH), 127.2 (CH), 127.0 (CH), 127.0 (CH), 126.8 (CH), 126.7 (CH), 124.4 (CH), 124.2 (CH), 123.9 (CH), 122.8 (CH), 120.1 (CH), 119.8 (CH), 119.6 (CH), 119.5 (CH), 119.1 (CH), 115.6 (CH), 115.3 (CH), 111.4 (CH), 50.1 (CH), 50.0 (CH), 49.8 (CH), 49.7 (CH), 21.9 (CH3), 21.9 (CH3), 21.8 (CH3), 21.1 (CH3), 20.9 (CH3), 19.1 (CH3), 19.0 (CH3), 18.8 (CH3), 18.7 (CH3).

IR (ATR) $\tilde{\nu}$ (cm^{-1}) = 3003 (w), 2959 (m), 2915 (s), 2856 (m), 2162 (w), 1691 (w), 1615 (w), 1579 (w), 1477 (s), 1445 (vs), 1411 (m), 1375 (m), 1320 (w), 1288 (m), 1249 (w), 1170 (w),

1130 (w), 1013 (m), 938 (w), 890 (w), 849 (vs), 834 (m), 800 (w), 764 (vs), 754 (vs), 742 (vs), 725 (vs), 686 (w), 613 (w), 601 (w), 554 (w), 540 (w), 490 (w), 416 (w).

MS (ESI): *m/z* (%): 698.4 (1) $[M+2]^+$, 697.4 (1) $[M+1]^+$, 696.4 (6) $[M]^+$, HRMS (ESI): *m/z* calcd for $C_{54}H_{48}$: 696.3756 $[M]^+$; found: 696.4368.

2,7-Dibromo-9-phenyl-9*H*-fluorene (71)

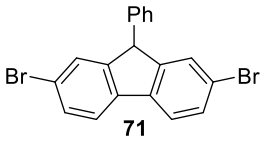

71

Following a published method,[125] Me_3SiCl (354 mg, 414 µL, 3.25 mmol, 1.10 eq.) and Et_3SiH (365 mg, 501 µL, 3.14 mmol, 1.06 eq.) were added under an argon atmosphere to a solution of 2,7-dibromofluoren-9-one (**45**; 1.00 g, 2.96 mmol, 1.00 eq.) and anhydrous $FeCl_3$ (240 mg, 1.48 mmol, 0.50 eq.) in benzene (10 mL). The mixture was stirred for 2 h at rt, heated for 18 h to 50 °C, cooled to rt, quenched with H_2O (20 mL) and extracted with CH_2Cl_2 (3×100 mL). The combined organic layers were washed with H_2O (3×100 mL), dried (Na_2SO_4), concentrated at reduced pressure, and purified by column chromatography (silica gel, *n*-hexane) to yield **71** (1.05 g, 2.62 mmol, 89%) as a pale orange powder.

R_f = 0.41 (*n*-hexane).

^{1}H NMR (400 MHz, $CDCl_3$): δ (ppm) 7.62 (d, *J* = 8.1 Hz, 2H, Ar-H), 7.51 (ddd, *J* = 8.1, 1.9, 0.7 Hz, 2H, Ar-H), 7.42 (t, *J* = 1.4 Hz, 2H, Ar-H), 7.30 (d, *J* = 7.8 Hz, 3H, Ar-H), 7.05 (dd, *J* = 7.7, 1.8 Hz, 2H, Ar-H), 5.01 (s, 1H, CH).

^{13}C NMR (100 MHz, $CDCl_3$): δ (ppm) 149.7 (C), 139.9 (C), 139.1 (C), 130.9 (CH), 129.2 (CH), 128.8 (CH), 128.4 (CH), 127.6 (CH), 121.7 (CH), 121.4 (CH), 54.4 (CH).

IR (ATR) $\tilde{\nu}$ (cm^{-1}) = 3081 (w), 3050 (w), 3020 (w), 3002 (w), 2955 (w), 2924 (w), 2877 (w), 2853 (w), 1595 (w), 1568 (w), 1489 (w), 1449 (s), 1412 (w), 1400 (w), 1259 (w), 1186 (w), 1156 (w), 1116 (w), 1102 (w), 1067 (w), 1052 (s), 1028 (w), 1004 (m), 921 (w), 885 (m), 870 (w), 841 (w), 824 (m), 805 (vs), 768 (w), 745 (vs), 718 (m), 698 (vs), 681 (m), 664 (m), 625 (w), 608 (s), 565 (w), 537 (w), 493 (vs), 476 (m), 441 (w), 426 (vs), 404 (w), 382 (w).

MS (ESI): *m/z* (%):401.9 (2) $[M+4]^+$, 400.9 (1) $[M+3]^+$, 399.9 (4) $[M+2]^+$, 398.9 (1) $[M+1]^+$, 397.9 (2) $[M]^+$, HRMS (ESI): *m/z* calcd for $C_{19}H_{12}Br_2$: 397.9306 $[M]^+$; found: 397.9410.

2,2'-(9-Phenyl-9*H*-fluorene-2,7-diyl)dibenzaldehyde (72)

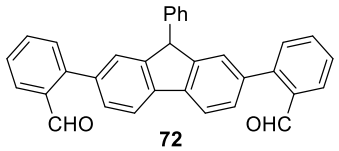

72

$PdCl_2$(dppf) (244 mg, 334 µmol, 0.15 eq.) was added under an argon atmosphere to a degassed (10 min) mixture of fluorene **71** (890 mg, 2.22 mmol, 1.00 eq.), (2-formylphenyl)boronic acid (734 mg, 4.89 mmol, 2.20 eq.), and Cs_2CO_3 (3.62 g, 11.1 mmol, 5.00 eq.) in toluene/H_2O (1:1; 20 mL). The mixture was heated to 105 °C for 18 h, cooled to rt, and the aqueous layer was extracted with CH_2Cl_2 (3×100 mL). The combined organic layers were dried (Na_2SO_4), concentrated at reduced pressure, and purified by column chromatography (silica gel, *n*-hexane/EtOAc 9:1) to yield **72** (932 mg, 2.07 mmol, 93%) as a beige solid.

R_f = 0.15 (*n*-hexane/EtOAc 9:1).

^{1}H NMR (400 MHz, $CDCl_3$): δ (ppm) 10.00 (d, *J* = 0.8 Hz, 2H, CHO), 8.01 (dd, *J* = 7.8, 1.5 Hz, 2H, Ar-H), 7.95 (d, *J* = 7.7 Hz, 2H, Ar-H), 7.61 (dd, *J* = 7.5, 1.5 Hz, 2H, Ar-H), 7.52 – 7.42 (m, 6H, Ar-H), 7.39 – 7.35 (m, 2H, Ar-H), 7.31 – 7.27 (m, 1H, Ar-H), 7.25 – 7.22 (m, 1H, Ar-H), 7.18 – 7.09 (m, 2H, Ar-H), 5.20 (s, 1H, CH).

^{13}C NMR (100 MHz, $CDCl_3$): δ (ppm) 192.5 (H-CO), 148.7 (C), 146.0 (C), 140.6 (C), 140.5 (C), 137.4 (C), 133.9 (CH), 133.7 (CH), 131.0 (CH), 130.0 (CH), 129.1 (CH), 128.4 (CH), 127.9 (CH), 127.8 (CH), 127.4 (CH), 127.2 (CH), 120.2 (CH), 54.7 (CH).

IR (ATR) $\tilde{\nu}$ (cm^{-1}) = 3057 (w), 3043 (w), 3026 (w), 3004 (w), 2955 (w), 2924 (w), 2847 (w), 2748 (w), 1686 (vs), 1594 (vs), 1493 (w), 1462 (m), 1448 (m), 1412 (w), 1390 (s), 1337 (w), 1295 (w), 1247 (m), 1193 (s), 1157 (w), 1132 (w), 1113 (w), 1096 (w), 1074 (w), 1044 (w), 1027 (w), 1003 (w), 958 (w), 924 (w), 911 (w), 824 (vs), 792 (w), 764 (vs), 741 (s), 727 (m), 718 (m), 698 (vs), 677 (m), 642 (s), 632 (s), 599 (m), 569 (w), 557 (w), 540 (m), 510 (w), 489 (w), 472 (w), 462 (w), 443 (m), 425 (m), 394 (w), 388 (w).

MS (ESI): *m/z* (%): 452.1 (8) $[M+2]^+$, 451.1 (23) $[M+1]^+$, 450.1 (29) $[M]^+$, 449.1 (4) $[M-1]^+$, HRMS (ESI): *m/z* calcd for $C_{33}H_{22}O_2$: 450.1620 $[M]^+$; found: 450.1614.

((9-Phenyl-9*H*-fluorene-2,7-diyl)bis(2,1-phenylene))bis(phenylmethanol) (73)

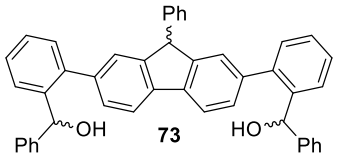

Following a published method,[126] PhMgBr (1.00 M in THF; 1.01 g, 5.55 mL, 5.55 mmol, 5.00 eq.) was added dropwise under an argon atmosphere to a cooled (0 °C) solution of fluorene **72** (500 mg, 1.11 mmol, 1.00 eq.) in anhydrous THF (15 mL). After addition was completed, the cooling bath was removed and the mixture stirred for 15 min at rt. Saturated aqueous NH_4Cl solution (30 mL) was added, stirring was continued for 10 min, and the mixture was extracted with CH_2Cl_2 (3×100 mL). The combined organic layers were dried (Na_2SO_4) and concentrated at reduced pressure.

6,12,15-Triphenyl-12,15-dihydro-6H-cyclopenta[2,1-b:3,4-b']difluorene (74)

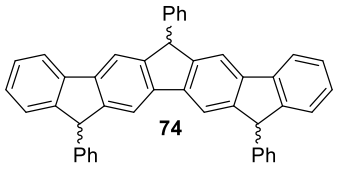

The remnant (**73**) was dissolved in anhydrous CH_2Cl_2 (40 mL) and the solution was cooled to 0 °C. $BF_3{\cdot}OEt_2$ (350 mg, 313 µL, 2.47 mmol, 5.00 eq.) was added under an argon atmosphere and the mixture was stirred for 1 h at rt. Saturated aqueous NH_4Cl solution (30 mL) was added, stirring was continued for 10 min, and the mixture was extracted with CH_2Cl_2 (3×100 mL) The combined organic layers were dried (Na_2SO_4), concentrated at reduced pressure, and purified by column chromatography (silica gel, *n*-pentane/CH_2Cl_2 4:1) to yield **74** (158 mg, 0.27 mmol, 56%) as a pale orange solid. The product was obtained in a mixture of isomers, resulting in additional hardly discriminable signals in the spectra. Thus, no reasonable spectra could be measured.

R_f = 0.37 (*n*-pentane/CH_2Cl_2 4:1).

IR (ATR) $\tilde{\nu}$ (cm^{-1}) = 3055 (w), 3026 (w), 2962 (vw), 2921 (vw), 2847 (vw), 1596 (w), 1582 (vw), 1492 (w), 1451 (w), 1421 (w), 1326 (vw), 1285 (w), 1261 (w), 1150 (w), 1072 (w), 1028 (w), 1018 (w), 892 (w), 817 (w), 768 (m), 749 (s), 734 (vs), 694 (vs), 666 (m), 647 (w), 625 (w), 615 (w), 605 (w), 596 (w), 577 (w), 561 (w), 528 (m), 480 (w), 412 (m), 398 (w), 385 (w).

MS (ESI): *m/z* (%): 572.2 (11) $[M+2]^+$, 571.2 (36) $[M+1]^+$, 570.2 (59) $[M]^+$, 569.2 (7) $[M-1]^+$, HRMS (ESI): *m/z* calcd for $C_{45}H_{30}$: 570.2348 $[M]^+$; found: 570.2390.

((9-Phenyl-9*H*-fluorene-2,7-diyl)bis(2,1-phenylene))bis(mesitylmethanol) (77)

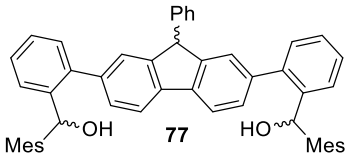

Following a published method,[126] MesMgBr (1.00 M in THF; 0.99 g, 4.44 mL, 4.44 mmol, 5.00 eq.) was added dropwise under an argon atmosphere to a cooled (0 °C) solution of fluorene **72** (400 mg, 0.88 mmol, 1.00 eq.) in anhydrous THF (15 mL). After addition was completed, the cooling bath was removed and the mixture stirred for 15 min at rt. Saturated aqueous NH_4Cl solution (30 mL) was added, stirring was continued for 10 min, and the mixture was extracted with CH_2Cl_2 (3×100 mL). The combined organic layers were dried (Na_2SO_4) and concentrated at reduced pressure.

12,15-Dimesityl-6-phenyl-12,15-dihydro-6H-cyclopenta[2,1-b:3,4-b']difluorene (78)

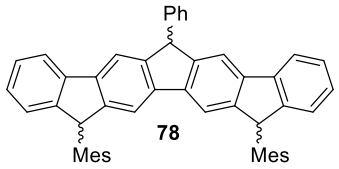

The remnant (**77**) was dissolved in anhydrous CH_2Cl_2 (20 mL) and the solution was cooled to 0 °C. $BF_3{\cdot}OEt_2$ (468 mg, 418 µL, 3.30 mmol, 5.00 eq.) was added under an argon atmosphere and the mixture was stirred for 1 h at rt. Saturated aqueous NH_4Cl solution (30 mL) was added, stirring was continued for 10 min, and the mixture was extracted with CH_2Cl_2 (3×100 mL) The combined organic layers were dried (Na_2SO_4), concentrated at reduced pressure, and purified by column chromatography (silica gel, *n*-pentane/CH_2Cl_2 4:1) to yield **78** (491 mg, 0.75 mmol, 84%) as a pale orange solid. The product was obtained as a mixture of isomers, thus resulting in additional hardly discriminable signals in the spectra. Only the most pronounced signals are given.

R_f = 0.1 (*n*-pentane/CH_2Cl_2 4:1).

^{1}H NMR (400 MHz, $CDCl_3$): δ (ppm) 7.74 – 7.69 (m, 4H, Ar-H), 7.54 – 7.45 (m, 2H, Ar-H), 7.38 – 7.29 (m, 5H, Ar-H), 7.21 (dtt, *J* = 13.8, 4.5, 1.5 Hz, 6H, Ar-H), 7.05 (s, 2H, Ar-H), 6.66 (d, *J* = 10.6 Hz, 2H, Ar-H), 5.50 (d, *J* = 6.6 Hz, 2H, CH), 5.20 (s, 1H, CH), 2.75 – 2.60 (m, 6H, CH_3), 2.29 (d, *J* = 8.7 Hz, 6H, CH_3), 1.12 (dd, *J* = 14.5, 9.3 Hz, 6H, CH_3).

^{13}C NMR (100 MHz, $CDCl_3$): δ (ppm) 147.9 (C), 147.8 (C), 147.7 (C), 147.6 (C), 147.2 (C), 147.1 (C), 142.5 (C), 142.4 (C), 141.1 (C), 141.0 (C), 140.8 (C), 140.5 (C), 138.1 (C), 138.0 (C), 137.9 (C), 137.8 (C), 136.4 (C), 134.2 (C), 134.1 (C), 130.7 (CH), 130.6 (CH), 129.0 (CH), 128.7 (CH), 127.0 (CH), 126.9 (CH), 124.2 (CH), 120.0 (CH), 117.0 (CH), 115.7 (CH), 115.6 (CH), 54.3 (CH), 49.6 (CH), 22.0 (CH_3), 22.0 (CH_3), 22.0 (CH_3), 21.0 (CH_3), 21.0 (CH_3), 18.9 (CH_3), 18.9 (CH_3), 18.9 (CH_3), 18.9 (CH_3).

IR (ATR) $\tilde{\nu}$ (cm^{-1}) = 3009 (w), 2953 (w), 2914 (m), 2853 (w), 1604 (w), 1477 (m), 1452 (m), 1431 (m), 1421 (m), 1375 (w), 1299 (w), 1285 (s), 1177 (w), 1153 (w), 1028 (w), 1014 (w), 882 (w), 843 (m), 806 (w), 766 (vs), 741 (vs), 727 (vs), 698 (vs), 586 (w), 554 (w), 544 (m), 507 (w), 460 (w), 415 (s).

MS (ESI): *m/z* (%): 657.3 (2) $[M+3]^+$, 656.3 (15) $[M+2]^+$, 655.3 (55) $[M+1]^+$, 654.3 (100) $[M]^+$,
HRMS (ESI): *m/z* calcd for $C_{51}H_{42}$: 654.3287 $[M]^+$; found: 654.3289.

12,15-Dimesityl-6-phenyl-radical (79)

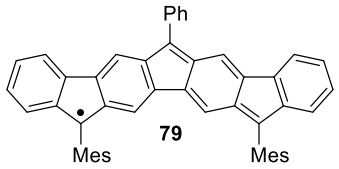

79

Following a published method,[74] precursor **78** (100 mg, 153 µmol, 1.00 eq.) and KO*t*Bu (234 mg, 2.14 mmol, 14.0 eq.) were dissolved in anhydrous THF (10 mL) under an argon atmosphere and heated for 30 min to 50 °C. The mixture was allowed to cool to rt and *p*-chloranil (113 mg, 458 µmol, 4.50 eq.) was added. After stirring for 10 min, the mixture was concentrated at reduced pressure. The obtained remnant was purified by column chromatography (silica gel, *n*-pentane/CH_2Cl_2 4:1) to yield **79** (81.0 mg, 124 µmol, 81%) as a dark green solid.

R_f = 0.3 (*n*-pentane/CH_2Cl_2 4:1).

IR (ATR, cm^{-1}): $\tilde{\nu}$ = 2952 (m), 2922 (vs), 2851 (s), 1509 (w), 1462 (m), 1434 (m), 1375 (w), 1336 (w), 1319 (w), 1262 (w), 1227 (w), 1177 (w), 1137 (w), 1120 (w), 1099 (w), 1072 (w), 1037 (w), 1027 (w), 1016 (w), 999 (w), 987 (w), 935 (w), 929 (w), 907 (w), 890 (m), 850 (m), 816 (w), 806 (w), 768 (m), 761 (m), 747 (m), 735 (vs), 701 (vs), 679 (m), 662 (m), 645 (w), 629 (w), 615 (w), 596 (w), 572 (w), 557 (w), 511 (w), 499 (w), 476 (w), 466 (w), 460 (w), 452 (w), 439 (w), 429 (w), 401 (m).

MS (ESI): *m/z* (%): 653.3 (15) $[M+2]^+$, 652.3 (55) $[M+1]^+$, 651.3 (100) $[M]^+$, HRMS (ESI): *m/z* calcd for $C_{51}H_{39}$: 651.3052 $[M]^+$; found: 651.3036.

((9-Mesityl-9*H*-fluorene-2,7-diyl)bis(2,1-phenylene))bis((2,6-dichlorophenyl)methanol) (81)

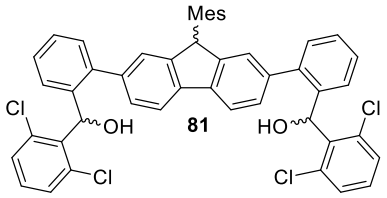

In slight variation to a published method,[137] ^{i}PrMgCl (2M in THF; 299 mg, 1.45 mL, 2.90 mmol, 14.3 eq.) was added dropwise under an argon atmosphere to a cooled (0°C) solution of 2-bromo-1,3-dichlorobenzene (**80**; 688 mg, 3.05 mmol, 15.0 eq.) in 30 mL anhydrous THF and stirred for 2 h. **48** (100 mg, 203 µmol, 1.00 eq.) in 10 mL anhydrous THF was added to this mixture dropwise and stirring continued for 15 h, while allowing the mixture to warm to rt. Saturated NH_4Cl solution was added, the phases separated and the organic phase washed with water and brine, dried over Na_2SO_4 and concentrated under reduced pressure.

12,15-bis(2,6-Dichlorophenyl)-6-mesityl-12,15-dihydro-6H-cyclopenta[2,1-b:3,4-b']difluorene (82)

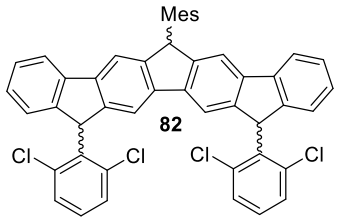

In slight variation to a published method,[137] $BF_3 \cdot OEt_2$ (144 mg, 129 µL, 1.02 mmol, 5.00 eq.) was added under an argon atmosphere to a solution of remnant **81** in CH_2Cl_2 and stirred for 30 min. Methanol was added to quench the reaction and the solvent removed under reduced pressure. The obtained crude was purified (silica gel, *n*-pentane:CH_2Cl_2 3:1) to yield **82** (99.7 mg, 133 µmol, 65%) as a brown solid. The product was obtained in a mixture of isomers, resulting in additional hardly discriminable signals in the spectra. Thus, no reasonable spectra could be measured.

*R*f = 0.52 (*n*-pentane:CH_2Cl_2 3:1)

IR (ATR, cm^{-1}): $\tilde{\nu}$ = 3051 (w), 3006 (w), 2955 (w), 2915 (w), 2850 (w), 1609 (vw), 1577 (w), 1560 (w), 1477 (w), 1432 (vs), 1378 (w), 1288 (w), 1179 (w), 1147 (w), 1086 (w), 1016 (w), 907 (w), 890 (w), 849 (w), 830 (m), 761 (vs), 735 (vs), 718 (vs), 691 (m), 679 (m), 653 (m), 630 (m), 620 (w), 609 (w), 579 (w), 561 (m), 465 (w), 424 (s), 405 (w), 390 (m), 384 (w).

MS (ESI): *m/z* (%): 753.1 (9) $[M+5]^+$, 752.1 (11) $[M+4]^+$, 751.1 (24) $[M+3]^+$, 750.1 (7) $[M+2]^+$; 749.1 (18) $[M+1]^+$; 748.1 (3) $[M+2]^+$; HRMS (ESI): *m/z* calcd for $C_{48}H_{32}Cl_4$: 748.1258 $[M]^+$; found: 748.1249.

Radical 83

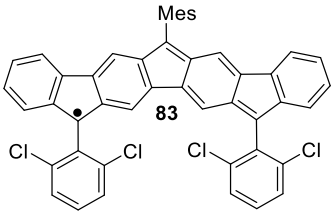

Following a published method,[74] precursor **82** (100 mg, 133 µmol, 1.00 eq.) and KO*t*Bu (209 mg, 1.87 mmol, 14.0 eq.) were dissolved in anhydrous THF (60 mL) under an argon atmosphere and heated for 16 h to 60 °C. The mixture was allowed to cool to rt and *p*-chloranil (147 mg, 600 µmol, 4.50 eq.) was added. After stirring for 10 min, the mixture was concentrated at reduced pressure. The obtained remnant was purified by column chromatography (silica gel, *n*-pentane/CH_2Cl_2 4:1) to yield **83** (51.5 mg, 68.7 µmol, 52%) as a dark green solid.

*R*f = 0.61 (*n*-pentane:CH_2Cl_2 4:1)

IR (ATR, cm^{-1}): $\tilde{\nu}$ = 2953 (w), 2919 (s), 2871 (w), 2850 (m), 1691 (w), 1679 (w), 1553 (m), 1538 (w), 1511 (w), 1455 (m), 1425 (vs), 1375 (w), 1336 (m), 1316 (w), 1258 (w), 1228 (w), 1191 (w), 1179 (w), 1149 (m), 1099 (m), 1086 (m), 1068 (m), 1017 (m), 966 (w), 952 (w), 936 (w), 898 (m), 870 (w), 844 (w), 786 (vs), 773 (vs), 751 (vs), 721 (vs), 707 (vs), 677 (vs), 649 (m), 630 (w), 622 (w), 613 (w), 586 (w), 567 (w), 521 (w), 510 (w), 506 (w), 493 (w), 484 (w), 473 (w), 449 (m), 426 (vs), 414 (w), 405 (w), 394 (w).

MS (ESI): *m/z* (%): 751.1 (7) $[M+6]^+$, 750.1 (23) $[M+5]^+$, 749.1 (52) $[M+4]^+$, 748.1 (48) $[M+3]^+$; 747.1 (100) $[M+2]^+$; 746.1 (38) $[M+1]^+$; 745.1 (72) $[M]^+$; HRMS (ESI): *m/z* calcd for $C_{48}H_{29}Cl_4$: 745.1023 $[M]^+$; found: 745.1033.

((9-Mesityl-9*H*-fluorene-2,7-diyl)bis(2,1-phenylene))bis((3,5-bis(trifluoromethyl)phenyl)methanol) (84)

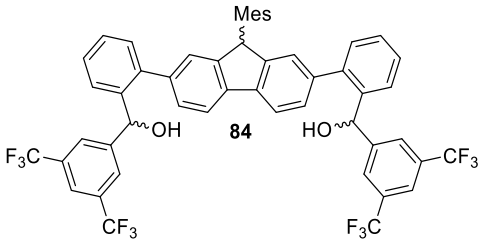

Variant A:

In slight variation to a published method,[137] ^{i}PrMgCl (2M in THF; 299 mg, 1.45 mL, 2.90 mmol, 14.3 eq.) was added dropwise under an argon atmosphere to a cooled (0 °C) solution of 1-bromo-3,5-bis(trifluoromethyl)benzene (**88**; 892 mg, 525 µL, 3.05 mmol, 15.0 eq.) in 30 mL anhydrous THF and stirred for 2 h. Fluorene **48** (100 mg, 203 µmol, 1.00 eq.) in 10 mL anhydrous THF was added to this mixture dropwise and stirring continued for 15 h, while allowing the mixture to warm to rt. Saturated NH_4Cl solution was added, the phases separated and the organic phase washed with water and brine, dried over Na_2SO_4 and concentrated under reduced pressure to yield **84**.

Variant B:

Preparation of the *Grignard* reagent: A solution of bromide (121 mmol) in THF (100 mL) was added to a solution of magnesium turnings (130 mmol) in 10 mL THF and activated with a single iodine crystal. The mixture was heated to 40 °C. After fully addition, the mixture was stirred for 1 h at 40 °C. The concentration of the reagent was not determined and a complete conversion was assumed.

Following a published method,[126] (3,5-bis(trifluoromethyl)phenyl)magnesium bromide (**88**; 966 mg, 3.05 mmol, 15.0 eq.) was added dropwise under an argon atmosphere to a cooled (0 °C) solution of fluorene **48** (100 mg, 203 µmol, 1.00 eq.) in 10 mL anhydrous THF. After fully addition, the cooling bath was removed and the mixture stirred for 15 min at rt. Saturated aqueous NH_4Cl solution (30 mL) was added, stirring continued for 10 min, and the mixture was extracted with CH_2Cl_2 (3×100 mL). The combined organic layers were dried (Na_2SO_4) and concentrated at reduced pressure to yield **84**.

12,15-bis(3,5-bis(Trifluoromethyl)phenyl)-6-mesityl-12,15-dihydro-6H-cyclopenta[2,1-b:3,4-b']difluorene (86)

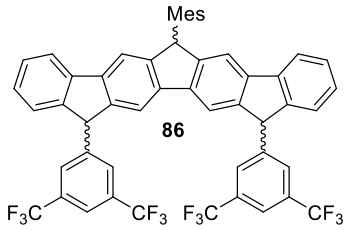

Variant A:

In slight variation to a published method,[137] $BF_3 \cdot OEt_2$ (144 mg, 129 µL, 1.02 mmol, 5.00 eq.) was added under an argon atmosphere to a solution of remnant **84** in CH_2Cl_2 and stirred for 30 min. Methanol was added to quench the reaction and the solvent removed under reduced pressure. The obtained crude was purified by column chromatography (silica gel, *n*-pentane:CH_2Cl_2 3:1) to yield **86** (59.0 mg, 66.7 µmol, 33%) as a beige solid. The product was obtained in a mixture of isomers, resulting in additional hardly discriminable signals in the spectra. Thus, no reasonable spectra could be measured.

Variant B:

In slight variation to a published method,[137] $BF_3 \cdot OEt_2$ (144 mg, 129 µL, 1.02 mmol, 5.00 eq.) was added under an argon atmosphere to a solution of remnant **84** in 25 mL CH_2Cl_2 and stirred for 1 h at rt. Saturated NH_4Cl solution was added, the phases separated and the aqueous phase extracted with CH_2Cl_2. The combined organic layers were dried over Na_2SO_4 and the solvent removed under reduced pressure. The obtained crude was purified by column chromatography (silica gel, *n*-pentane:CH_2Cl_2 3:1) to yield **86** (54.0 mg, 61.0 µmol, 30%) as a pink solid. The product was obtained in a mixture of isomers, resulting in additional hardly discriminable signals in the spectra. Thus, no reasonable spectra could be measured.

*R*f = 0.43 (*n*-pentane:CH_2Cl_2 3:1)

IR (ATR, cm^{-1}): $\tilde{\nu}$ = 2959 (vw), 2927 (w), 2856 (vw), 1618 (vw), 1469 (vw), 1463 (w), 1425 (w), 1373 (s), 1299 (w), 1275 (vs), 1169 (vs), 1125 (vs), 1108 (vs), 1030 (w), 1017 (w), 1003 (w), 976 (w), 938 (w), 898 (m), 868 (w), 851 (w), 840 (w), 832 (w), 803 (w), 768 (m), 756

(w), 737 (s), 715 (w), 704 (s), 681 (s), 664 (w), 645 (w), 630 (w), 595 (w), 551 (w), 418 (m), 408 (w), 402 (w).

MS (ESI): *m/z* (%): 886.2 (2) $[M+2]^+$; 885.2 (14) $[M+1]^+$; 884.2 (56) $[M]^+$; 883.2 (100) $[M-1]^+$
HRMS (ESI): *m/z* calcd for $C_{52}H_{32}F_{12}$: 884.2312 $[M]^+$; found: 884.2279.

((9-Mesityl-9*H*-fluorene-2,7-diyl)bis(2,1-phenylene))bis((perfluorophenyl)methanol) (85)

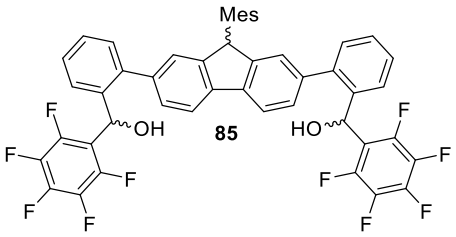

Variant A:

In slight variation to a published method,[137] ^{i}PrMgCl (2M in THF; 299 mg, 1.45 mL, 2.90 mmol, 14.3 eq.) was added dropwise under an argon atmosphere to a cooled (0°C) solution of 1-bromo-2,3,4,5,6-pentafluorobenzene (**89**; 966 mg, 3.05 mmol, 15.0 eq.) in 20 mL anhydrous THF and stirred for 2 h. Fluorene **48** (100 mg, 203 µmol, 1.00 eq.) in 10 mL anhydrous THF was added to this mixture dropwise and stirring continued for 15 h, while allowing the mixture to warm to rt. Sat. NH_4Cl solution was added, the phases separated and the organic phase washed with water and brine, dried over Na_2SO_4 and concentrated under reduced pressure to yield **85**.

Variant B:

Preparation of the *Grignard* reagent: A solution of bromide (121 mmol) in THF (100 mL) was added to a solution of magnesium turnings (130 mmol) in 10 mL THF and activated with a single iodine crystal. The mixture was heated to 40 °C. After fully addition, the mixture was stirred for 1 h at 40 °C. The concentration of the reagent was not determined and a complete conversion was assumed.

Following a published method,[126] (perfluorophenyl)magnesium bromide (**89**; 966 mg, 3.05 mmol, 15.0 eq.) was added dropwise under an argon atmosphere to a cooled (0 °C) solution of fluorene **48** (100 mg, 203 µmol, 1.00 eq.) in 10 mL anhydrous THF. After fully addition, the cooling bath was removed and the mixture stirred for 15 min at rt. Saturated aqueous NH_4Cl solution (30 mL) was added, stirring continued for 10 min, and the mixture was extracted with CH_2Cl_2 (3×100 mL). The combined organic layers were dried (Na_2SO_4) and concentrated at reduced pressure.

6-Mesityl-12,15-bis(perfluorophenyl)-12,15-dihydro-6H-cyclopenta[2,1-b:3,4-b']difluorene (87)

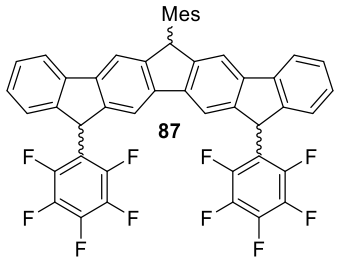

Variant A:

In slight variation to a published method,[137] $BF_3{\cdot}OEt_2$ (144 mg, 129 µL, 1.02 mmol, 5.00 eq.) was added under an argon atmosphere to a solution of remnant **85** in CH_2Cl_2 and stirred for 30 min. Methanol was added to quench the reaction and the solvent removed under reduced pressure. The obtained crude was purified by column chromatography (silica gel, *n*-pentane/CH_2Cl_2 3:1) to yield **87** (30.4 mg, 38.3 µmol, 19%) as a pink solid. The product was obtained in a mixture of isomers, resulting in additional hardly discriminable signals in the spectra. Thus, no reasonable spectra could be measured.

Variant B:

In slight variation to a published method,[137] $BF_3{\cdot}OEt_2$ (144 mg, 129 µL, 1.02 mmol, 5.00 eq.) was added under an argon atmosphere to a solution of remnant **85** in 25 mL CH_2Cl_2 and stirred for 1 h at rt. Saturated NH_4Cl solution was added, the phases separated and the aqueous phase extracted with CH_2Cl_2. The combined organic layers were dried over Na_2SO_4 and the solvent removed under reduced pressure. The obtained crude was purified by column chromatography (silica gel, *n*-pentane/CH_2Cl_2 3:1) to yield **87** (69.6 mg, 87.8 µmol, 43%) as a pink solid. The product was obtained in a mixture of isomers, resulting in additional hardly discriminable signals in the spectra. Thus, no reasonable spectra could be measured.

*R*f = 0.43 (*n*-pentane:CH_2Cl_2 3:1)

IR (ATR, cm^{-1}): $\tilde{\nu}$ = 2924 (w), 2859 (vw), 1653 (vw), 1604 (vw), 1520 (vs), 1499 (vs), 1466 (w), 1451 (w), 1424 (w), 1378 (w), 1317 (w), 1288 (w), 1120 (w), 1030 (w), 994 (vs), 983 (s), 972 (s), 950 (w), 847 (w), 829 (w), 806 (w), 768 (m), 745 (w), 724 (s), 708 (w), 650 (w), 455 (w), 411 (w).

MS (ESI): *m/z* (%): 794.1 (2) $[M+2]^+$; 793.1 (13) $[M+1]^+$; 792.1 (52) $[M]^+$; 791.1 (100) $[M-1]^+$

HRMS (ESI): *m/z* calcd for $C_{48}H_{26}F_{10}$: 792.1875 $[M]^+$; found: 792.1843.

1-Bromo-2-(dibromomethyl)naphthalene (99)

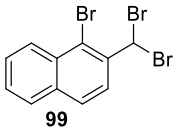

99

In slight variation of a published synthesis,[139] a solution of 1-bromo-2-methylnaphthalene (**98**; 2.21 g, 10.0 mmol, 1.00 equiv.), NBS (4.45 g, 25.0 mmol, 2.50 equiv.), and benzoyl peroxide (0.484 g, 2.00 mmol, 0.20 equiv.) in anhydrous benzene (40 mL) was heated to reflux for 24 h. The mixture was cooled to rt, filtered through Celite, washed with an aqueous sodium disulfite solution (3×100 mL) and extracted with CH_2Cl_2 (3×100 mL). The combined organic layers were concentrated at reduced pressure and purified by column chromatography (silica gel, *n*-hexane/EtOAc 9:1) to yield **99** (3.45 g, 9.10 mmol, 91%) as an orange solid. The NMR data are in agreement with published data.[139]

^{1}H NMR (400 MHz, $CDCl_3$): δ (ppm) 8.31 (dd, J = 8.6 Hz, J = 1.1 Hz, 1 H, Ar-H), 8.1 (d, J = 8.7 Hz, 1 H, Ar-H), 7.90 (d, J = 8.7 Hz, 1 H, Ar-H), 7.86–7.81 (m, 1 H, Ar-H), 7.64 (ddd, J = 8.4 Hz, J = 6.9 Hz, J = 1.4 Hz, 1 H, Ar-H), 7.61–7.53 (m, 1 H, Ar-H), 7.50 (s, 1 H, $CHBr_2$).

1-Bromo-2-naphthaldehyde (100)

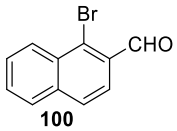

100

Following a published synthesis,[139] 1-bromo-2-(dibromomethyl)naphthalene (**99**; 10.0 g, 26.4 mmol, 1.00 equiv.) was added to a solution of KOAc (9.81 g, 100 mmol, 3.80 equiv.) in HOAc (130 mL) and the mixture was heated to reflux for 24 h. Aq. HCl solution (2M; 40 mL) was added and the mixture was heated to reflux for further 4 h, cooled to rt, and extracted with EtOAc (3×200 mL). The combined organic layers were washed with H_2O (3×200 mL), saturated aqueous $NaHCO_3$ solution (3×200 mL), and brine (3×200 mL), and concentrated at reduced pressure to yield **100** (9.79 g, 24.6 mmol, 93%) as a beige solid. The NMR data of the product are in agreement with published data.[139]

^{1}H NMR (400 MHz, $CDCl_3$): δ (ppm) 10.66 (d, J = 0.9 Hz, 1 H, CHO), 8.55–8.45 (m, 1 H, Ar-H), 7.93 (d, J = 8.5 Hz, 1 H, Ar-H), 7.89–7.82 (m, 2 H, Ar-H), 7.74–7.62 (m, 2 H, Ar-H).

1-(4,4,5,5-Tetramethyl-1,3,2-dioxaborolan-2-yl)-2-naphthaldehyde (101)

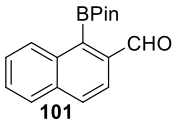

101

$PdCl_2$(dppf) (311 mg, 425 µmol, 0.100 equiv.) was added under an argon atmosphere to a degassed (ultrasonication, 10 min) solution of naphthaldehyde **100** (1.00 g, 4.25 mmol, 1.00 equiv.), KOAc (1.25 g, 12.8 mmol, 3.00 equiv.), and B_2Pin_2 (1.40 g, 5.53 mmol, 1.30 equiv.) in 1,4-dioxane (25 mL) and the solution was heated to 80 °C for 48 h. The mixture was cooled to rt and concentrated at reduced pressure. EtOAc (50 mL) was added and the solution was filtered (Celite), concentrated at reduced pressure, and purified by column chromatography (silica gel, *n*-hexane/EtOAc 9:1) to yield **101** (818 mg, 2.90 mmol, 68%) as a pale-yellow solid. The NMR data of the product are in agreement with published data.[140]

^{1}H NMR (400 MHz, $CDCl_3$): δ (ppm) 10.28 (s, 1 H, CHO), 8.25–8.13 (m, 1 H, Ar-H), 8.00–7.85 (m, 3 H, Ar-H), 7.59 (ddd, J = 8.6 Hz, J = 6.1 Hz, J = 1.6 Hz, 2 H, Ar-H), 1.55 (s, 12 H, 4×CH_3).

2-Bromo-1-naphthaldehyde (104)

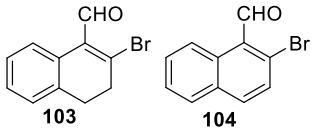

103 104

Following a published protocol,[141] DMF (1.50 g, 1.58 mL, 20.5 mmol, 3.00 eq.) was added dropwise under an argon atmosphere to a cooled (0 °C) solution of PBr_3 (4.63 g, 1.62 mL, 17.1 mmol, 2.50 eq.) in 25 mL dry CH_2Cl_2 and stirred for 1 h at 0 °C. A solution of 3,4-dihydro-1H-naphthalen-2-one (**102**; 1.00 g, 904 µL, 6.84 mmol, 1.00 eq.) in 25 mL dry CH_2Cl_2 was added to the suspension and the mixture refluxed for 1 h. After cooling to 0 °C aqueous $NaHCO_3$ solution was added, the phases separated, and the aqueous phase extracted with CH_2Cl_2. The combined organic layers were dried over Na_2SO_4, filtered and concentrated under reduced pressure. The obtained residue was purified by column chromatography (silica gel, EtOAc/*n*-hexane 1:3) to yield **103** (1.24 g, 5.23 mmol, 76%). **103** and DDQ (1.19 g, 5.23 mmol, 1.00 eq.) were refluxed in Toluene for 12 h. After cooling to rt, the mixture was filtered through a pad of Celite, and the filtrate concentrate under reduced pressure. The obtained residue was purified by column chromatography (silica gel, EtOAc/*n*-hexane 1:20) to yield **104** (718 mg, 3.05 mmol, 72%) as beige solid. The NMR data of the product are in agreement with published data.[141]

^{1}H NMR (400 MHz, $CDCl_3$): δ (ppm) 10.77 (s, 1H, CHO), 9.10 (dq, *J* = 8.7, 0.9 Hz, 1H, H-Ar), 7.88 (d, *J* = 8.8 Hz, 1H, H-Ar), 7.86 – 7.83 (m, 1H, H-Ar), 7.71 (s, 2H, H-Ar), 7.58 (m, *J* = 8.1, 6.9, 1.2 Hz, 1H, H-Ar).

2-Methoxy-1-naphthaldehyde (107)

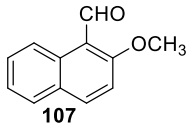

107

Following a published synthesis,[143] $POCl_3$ (16.5 g, 9.81 mL, 107 mmol, 3.40 equiv.) was added dropwise to a cooled solution (0 °C) of 2-methoxynaphthalene (**106**; 5.00 g, 31.6 mmol, 1.00 equiv.) in anhydrous DMF (25 mL) and the solution was stirred for 1 h at 0 °C and heated to 95 °C for 4 h. After cooling to rt, the mixture was quenched by pouring on water ice. The precipitate was filtered and the residue washed with small amounts of water and dried to yield **107** (5.52 g, 29.6 mmol, 94%) as a beige solid. The compound could be used without further purification in the next step. The NMR data of the product are in agreement with published data.[143]

^{1}H NMR (400 MHz, $CDCl_3$): δ (ppm) 10.90 (s, 1 H, CHO), 9.28 (dd, *J* = 8.7 Hz, *J* = 1.0 Hz, 1 H, Ar-H), 8.07 (d, *J* = 9.2 Hz, 1 H, Ar-H), 7.83–7.75 (m, 1 H, Ar-H), 7.62 (ddd, *J* = 8.6 Hz, *J* = 6.9 Hz, *J* = 1.5 Hz, 1 H, Ar-H), 7.42 (ddd, *J* = 8.1 Hz, *J* = 6.8 Hz, *J* = 1.2 Hz, 1 H, Ar-H), 7.31 (d, *J* = 9.1 Hz, 1 H, Ar-H), 4.06 (s, 3 H, CH_3).

2-Hydroxy-1-naphthaldehyde (108)

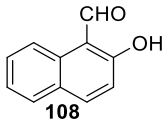

108

Following a published procedure,[142, 144] $AlCl_3$ (4.14 g, 31.0 mmol, 1.50 equiv.) was added in one batch to a cooled (−5 °C) solution of 2-Methoxy-1-naphthaldehyde (**107**; 3.85 g, 20.7 mmol, 1.00 equiv.) in CH_2Cl_2 (100 mL). The mixture was stirred for 5 min, was allowed to warm to rt, and stirred for further 4 h. The reaction was quenched by pouring the mixture on water ice. The mixture was extracted with CH_2Cl_2 (3×150 mL) and the combined organic layers were washed with $NaHCO_3$ (3×100 mL) and brine (3×100 mL), dried (Na_2SO_4), concentrated at reduced pressure, and purified by column chromatography (silica gel, *n*-hexane/EtOAc 9:1) to yield **108** (2.71 g, 15.7 mmol, 76%) as a pale yellow solid. The NMR data of the product are in agreement with published data.[142, 144]

^{1}H NMR (400 MHz, $CDCl_3$, ppm) δ (ppm) 13.16 (s, 1 H, OH), 10.82 (s, 1 H, CHO), 8.35 (d, *J* = 8.6 Hz, 1 H, Ar-H), 7.98 (d, *J* = 9.1 Hz, 1 H, Ar-H), 7.88–7.78 (m, 1 H, Ar-H), 7.62 (ddd, *J* = 8.5 Hz, *J* = 7.0 Hz, *J* = 1.4 Hz, 1 H, Ar-H), 7.44 (ddd, *J* = 8.1 Hz, *J* = 6.9 Hz, *J* = 1.1 Hz, 1 H, Ar-H), 7.15 (d, *J* = 9.0 Hz, 1 H, Ar-H).

1-Formylnaphthalen-2-yl Trifluoromethanesulfonate (109)

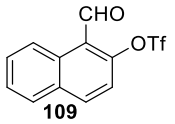

109

Following a published procedure,[202] trifluoromethanesulfonic anhydride (7.50 g, 4.47 mL, 26.6 mmol, 1.20 equiv.) was added under an argon atmosphere to a cooled (0 °C) solution of naphthol **108** (3.81 g, 22.2 mmol, 1.00 equiv.) and 4-(dimethylamino)pyridine (DMAP; 5.41 g, 44.3 mmol, 2.00 equiv.) in CH_2Cl_2 (60 mL), stirred for 30 min at 0 °C, allowed to warm to rt, and stirred for further 4 h. The reaction was quenched with water (50 mL) at 0 °C and extracted with CH_2Cl_2 (3×100 mL). The combined organic layers were washed with aqueous HCl (1M; 3×50 mL) and brine (3×100 mL), dried (Na_2SO_4), concentrated at reduced pressure and purified by column chromatography (silica gel, *n*-hexane/EtOAc 9:1) to yield **109** (4.11 g, 13.5 mmol, 61%) as a beige solid. The NMR data of the product are in agreement with published data.[202]

^{1}H NMR (400 MHz, $CDCl_3$): δ (ppm) 10.80 (s, 1 H, CHO), 9.18 (dd, *J* = 8.8 Hz, *J* = 1.0 Hz, 1 H, Ar-H), 8.19 (d, *J* = 9.0 Hz, 1 H, Ar-H), 7.94 (dt, *J* = 8.3 Hz, *J* = 1.0 Hz, 1 H, Ar-H), 7.77 (ddd, *J* = 8.6 Hz, *J* = 6.9 Hz, *J* = 1.5 Hz, 1 H, Ar-H), 7.66 (ddd, *J* = 8.2 Hz, *J* = 6.9 Hz, *J* = 1.2 Hz, 1 H, Ar-H), 7.49 (d, *J* = 9.0 Hz, 1 H, Ar-H).

2-(4,4,5,5-Tetramethyl-1,3,2-dioxaborolan-2-yl)-1-naphthaldehyde (105)

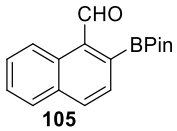

105

PdCl2(dppf) (265 mg, 362 µmol, 0.100 equiv.) was added under an argon atmosphere to a degassed (ultrasonication, 10 min) solution of tosylate **109** (1.10 g, 3.62 mmol, 1.00 equiv.), KOAc (1.07 g, 10.9 mmol, 3.00 equiv.), and B_2Pin_2 (1.19 g, 4.70 mmol, 1.30 equiv.) in 1,4-dioxane (25 mL). The mixture was heated to 80 °C for 48 h. After cooling to rt, the solvent was removed at reduced pressure. EtOAc (50 mL) was added and the solution was filtered (Celite), concentrated at reduced pressure, and purified by column chromatography (silica gel, *n*-hexane/EtOAc 9:1) to yield **105** (1.05 g, 3.72 mmol, quant.) as a pale-yellow solid.

R_f = 0.22 (*n*-hexane/EtOAc 9:1).

^{1}H NMR (400 MHz, $CDCl_3$): δ (ppm) 10.97 (s, 1 H, CHO), 9.00 (dd, *J* = 8.6 Hz, *J* = 1.1 Hz, 1 H, Ar-H), 8.05 (d, *J* = 8.1 Hz, 1 H, Ar-H), 7.93–7.86 (m, 1 H, Ar-H), 7.81 (d, *J* = 8.1 Hz, 1 H, Ar-H), 7.65 (ddd, *J* = 8.5 Hz, *J* = 6.8 Hz, *J* = 1.5 Hz, 1 H, Ar-H), 7.58 (ddd, *J* = 8.1 Hz, *J* = 6.8 Hz, *J* = 1.2 Hz, 1 H, Ar-H), 1.45 (s, 12 H, 4×CH_3)

^{13}C NMR (100 MHz, $CDCl_3$): δ (ppm) 194.8 (CHO), 137.0 (C), 134.7 (C), 133.5 (CH), 131.0 (CH), 129.9 (CH), 128.7 (CH), 128.6 (CH), 127.3 (CH), 124.6 (CH), 84.7 (C-4', C-5'), 25.03 (4×CH_3), one signal (C-2) was not observed due to the quadrupole moment of borane

IR (ATR): $\tilde{\nu}$ (cm^{-1}) = 3471 (w), 3455 (w), 3437 (w), 3422 (w), 3415 (w), 3407 (w), 3397 (w), 3383 (w), 3295 (w), 2979 (m), 2944 (w), 1681 (w), 1469 (m), 1370 (vs), 1349 (s), 1326 (s), 1275 (w), 1259 (w), 1213 (w), 1143 (vs), 1115 (vs), 1061 (w), 1048 (w), 1006 (w), 983 (w), 949 (vs), 884 (m), 864 (w), 850 (m), 827 (m), 781 (w), 775 (w), 751 (m), 711 (w), 697 (w), 671 (m), 649 (m), 639 (m), 618 (m), 609 (m), 596 (m), 578 (m), 552 (s), 521 (s), 510 (s), 496 (s), 479 (m), 465 (m), 458 (m), 449 (s), 442 (m), 428 (s), 407 (m), 398 (m), 381 (m)

MS (ESI): *m/z* (%): 284.1 (4) $[M+2]^+$, 283.1 (23) $[M+1]^+$, 282.1 (6) $[M]^+$, 592.2 (3) $[M]^+$; HRMS (ESI): *m/z* calcd for $C_{17}H_{19}BO_3$: 282.1427 $[M]^+$; found: 282.1535.

1,1'-(9-Mesityl-9*H*-fluorene-2,7-diyl)bis(2-naphthaldehyde) (110)

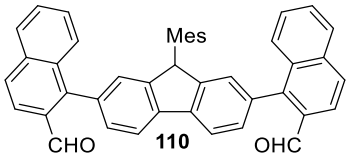

110

$PdCl_2$(dppf) (12.4 mg, 17.0 µmol, 0.15 equiv.) was added under an argon atmosphere to a degassed (ultrasonication, 10 min) mixture of dibromofluorene **46** (50 mg, 113 µmol, 1.00 equiv.), boronate **101** (80.0 mg, 283 µmol, 2.50 equiv.), and Cs_2CO_3 (184 mg, 565 µmol, 5.00 equiv.) in toluene/H_2O (1:1; 10 mL). The mixture was heated to 105 °C for 18 h, cooled to rt, and the aqueous layer was extracted with CH_2Cl_2 (3×100 mL). The combined organic layers were dried (Na_2SO_4), concentrated at reduced pressure, and purified by column chromatography (silica gel, *n*-hexane/EtOAc 9:1) to yield **110** (45.0 mg, 76.0 µmol, 67%) as a beige solid. The product was obtained as a mixture of isomers, thus resulting in additional hardly discriminable signals in the spectra.

R_f = 0.50 (*n*-hexane/EtOAc 9:1).

^{1}H NMR (400 MHz, $CDCl_3$): δ (ppm) 10.07 (s, 1 H, CHO), 9.87 (s, 1 H, CHO), 8.16–7.99 (m, 4 H, Ar-H), 7.92 (m, *J* = 8.8 Hz, *J* = 5.4 Hz, 4 H, Ar-H), 7.78 (m, *J* = 8.0 Hz, 1 H, Ar-H), 7.67–7.56 (m, 3 H, Ar-H), 7.55–7.47 (m, 3 H, Ar-H), 7.46–7.39 (m, 1 H, Ar-H), 7.31 (m, *J* = 8.4 Hz, 2 H, Ar-H), 6.85 (s, 1 H, Ar-H), 6.66 (d, *J* = 6.0 Hz, 1 H, Ar-H), 5.73 (m, *J* = 10.4 Hz, 1 H, Ar-H), 2.58 (m, *J* = 4.0 Hz, 3 H, CH_3), 2.16 (m, *J* = 5.8 Hz, 3 H, CH_3), 1.48–1.28 (m, 3 H, CH_3).

^{13}C NMR (100 MHz, $CDCl_3$): δ (ppm) 193.0 (CHO), 192.6 (CHO), 148.0 (C), 146.8 (C), 140.6 (C), 140.5 (C), 136.2 (C), 134.8 (C), 132.8 (C), 131.5 (C), 131.3 (C), 130.9 (C), 130.4 (CH), 130.2 (CH), 129.1 (CH), 129.0 (CH), 128.9 (CH), 128.8 (CH), 128.5 (CH), 128.4 (CH), 127.9 (CH), 127.8 (CH), 127.6 (CH), 127.1 (CH), 127.1 (CH), 127.0 (CH), 126.8 (CH), 122.3 (CH), 122.2 (CH), 120.3 (CH), 50.1 (CH), 21.9 (CH_3), 20.9 (CH_3), 18.9 (CH_3).

IR (ATR): $\tilde{\nu}$ (cm^{-1}) = 3058 (vw), 2956 (w), 2918 (w), 2850 (w), 2731 (w), 2322 (w), 2245 (vw), 2167 (vw), 1983 (vw), 1939 (vw), 1680 (vs), 1612 (w), 1594 (w), 1571 (w), 1460 (m), 1428 (m), 1411 (w), 1378 (s), 1332 (m), 1261 (m), 1232 (s), 1211 (m), 1188 (m), 1150 (m), 1086 (s), 1062 (s), 1028 (vs), 1018 (s), 1013 (s), 919 (s), 870 (s), 850 (s), 819 (vs), 800 (vs), 790 (vs), 771 (vs), 747 (vs), 727 (vs), 688 (s), 616 (s), 578 (m), 540 (m), 523 (s), 513 (s), 486 (vs), 470 (vs), 459 (vs), 450 (vs), 441 (vs), 433 (vs), 428 (vs), 414 (vs), 388 (vs).

MS (ESI): *m/z* (%): 595.2 (7) $[M+3]^+$, 594.2 (33) $[M+2]^+$, 593.2 (71) $[M+1]^+$, 592.2 (3) $[M]^+$, 565.4 (19) $[M+2–CHO]^+$, 564.4 (75) $[M+1–CHO]^+$, 563.5 (77) $[M–CHO]^+$; HRMS (ESI): *m/z* calcd for $C_{44}H_{32}O_2$: 592.2402 $[M]^+$; found: 592.2412.

2,2'-(9-Mesityl-9*H*-fluorene-2,7-diyl)bis(1-naphthaldehyde) (111)

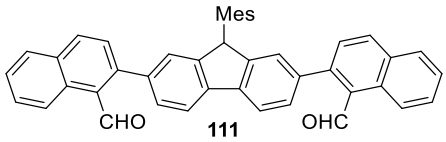

111

$PdCl_2$(dppf) (112 mg, 153 µmol, 0.15 equiv.) was added under an argon atmosphere to a degassed (ultrasonication, 10 min) mixture of dibromofluorene **46** (450 mg, 1.02 mmol, 1.00 equiv.), boronate **105** (718 mg, 2.54 mmol, 2.50 equiv.), and Cs_2CO_3 (1.66 g, 5.09 mmol, 5.00 equiv.) in toluene/H_2O (1:1; 20 mL). The mixture was heated to 105 °C for 18 h, cooled to rt, and the aqueous layer was extracted with CH_2Cl_2 (3×100 mL). The combined organic layers were dried (Na_2SO_4), concentrated at reduced pressure, and purified by column chromatography (silica gel, *n*-hexane/EtOAc 9:1) to yield **111** (266 mg, 0.450 mmol, 44%) as a beige solid.

R_f = 0.33 (*n*-hexane/EtOAc 9:1).

^{1}H NMR (400 MHz, $CDCl_3$): δ (ppm) 10.22 (s, 2 H, CHO), 9.29–9.19 (m, 2 H, Ar-H), 8.03 (m, *J* = 17.1 Hz, *J* = 8.1 Hz, 4 H, Ar-H), 7.90 (m, *J* = 8.3 Hz, *J* = 1.4 Hz, 2 H, Ar-H), 7.73–7.66 (m, 2 H, Ar-H), 7.58 (m, *J* = 8.1 Hz, *J* = 6.9 Hz, *J* = 1.2 Hz, 2 H, Ar-H), 7.54 (m, *J* = 8.4 Hz, 2 H, Ar-H), 7.51 (m, *J* = 7.0 Hz, *J* = 1.3 Hz, 2 H, Ar-H), 7.36 (m, 2 H, Ar-H), 6.97 (s, *J* = 1.9 Hz, 1 H, Ar-H), 6.69 (s, *J* = 1.9 Hz, 1 H, Ar-H), 5.69 (s, 1 H, Ar-H), 2.68 (s, 3 H, CH_3), 2.23 (s, 3 H, CH_3), 1.25 (s, 3 H, CH_3).

^{13}C NMR (100 MHz, $CDCl_3$): δ (ppm) 194.6 (H-CO), 148.2 (C), 148.1 (C), 140.5, (C) 138.4 (C), 137.9 (C), 137.6 (C), 136.9 (C), 134.0 (CH), 133.1 (C), 132.9 (C), 130.9 (CH), 130.5 (C), 130.3 (CH), 129.4 (CH), 129.2 (CH), 129.0 (C), 128.5 (CH), 128.4 (CH), 126.9 (CH), 126.2 (CH), 125.8 (CH), 120.3 (CH), 50.1 (CH), 22.0 (CH_3), 21.0 (CH_3), 19.1 (CH_3).

IR (ATR): $\tilde{\nu}$ (cm^{-1}) = 3050 (w), 3033 (w), 3012 (w), 3003 (w), 2946 (w), 2917 (w), 2851 (w), 2798 (w), 2755 (w), 1679 (vs), 1615 (w), 1589 (m), 1557 (w), 1504 (m), 1475 (m), 1455 (m), 1429 (m), 1408 (m), 1375 (w), 1353 (w), 1346 (w), 1310 (w), 1298 (w), 1264 (w), 1241 (w), 1213 (w), 1174 (m), 1146 (m), 1109 (w), 1055 (s), 1026 (w), 1016 (w), 1004 (w), 953 (w), 899 (w), 881 (w), 850 (w), 819 (vs), 800 (vs), 782 (m), 751 (vs), 735 (vs), 710 (s), 698 (s), 679 (w), 640 (m), 609 (m), 575 (w), 550 (m), 509 (s), 467 (m), 460 (m), 422 (m), 411 (m), 394 (w), 384 (w).

MS (ESI): *m/z* (%): 595.3 (1) $[M+3]^+$, 594.3 (9) $[M+2]^+$, 593.2 (19) $[M+1]^+$, 592.2 (1) $[M]^+$, 565.5 (7) $[M+2–CHO]^+$, 564.5 (39) $[M+1–CHO]^+$, 563.5 (100) $[M–CHO]^+$; HRMS (ESI): *m/z* calcd for $C_{44}H_{32}O_2$: 592.2402 $[M]^+$; found: 592.2347.

((9-Mesityl-9*H*-fluorene-2,7-diyl)bis(naphthalene-1,2-diyl))bis(mesitylmethanol) (112)

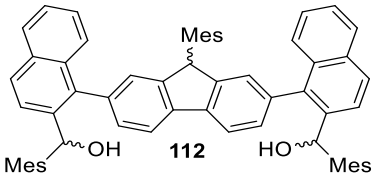

In accordance to a published method,[203] MesMgBr (1.00M in THF; 84.0 mg, 0.38 mL, 380 µmol, 5.00 equiv.) was added dropwise under an argon atmosphere to a cooled (0 °C) solution of biscarbaldehye **110** (45.0 mg, 76.0 µmol, 1.00 equiv.) in anhydrous THF (10 mL). After addition was completed, the cooling bath was removed and the mixture was stirred for 15 min at rt. Saturated aqueous NH_4Cl solution (20 mL) was added, stirring was continued for 10 min, and the mixture was extracted with CH_2Cl_2 (3×100 mL). The combined organic layers were dried (Na_2SO_4) and concentrated at reduced pressure.

10,18-Dihydro-7,10,18-trimesityl-7H-bisbenz[6,7]indeno[1,2-b:2',1'-h]fluorene (114)

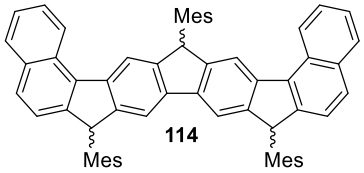

114

The remnant (**112**) was dissolved in anhydrous CH_2Cl_2 (10 mL) and the solution was cooled to 0 °C. $BF_3{\cdot}OEt_2$ (74.1 mg, 66 µL, 522 µmol, 5.00 equiv.) was added under an argon atmosphere and the mixture was stirred for 1 h at rt. Saturated aqueous NH_4Cl solution (20 mL) was added, stirring was continued for 10 min, and the mixture was extracted with CH_2Cl_2 (3×100 mL). The combined organic layers were dried (Na_2SO_4), concentrated at reduced pressure, and purified by column chromatography (silica gel, n-pentane/CH_2Cl_2 4:1) to yield **114** (66.0 mg, 83.0 µmol, 79%) as a pale orange solid. The product was obtained as a mixture of isomers, thus resulting in additional hardly discriminable signals in the spectra. Only the most pronounced signals are given.

R_f = 0.43 (*n*-pentane/CH_2Cl_2 4:1).

^{1}H NMR (400 MHz, $CDCl_3$): δ (ppm) 8.63 (m, *J* = 8.0 Hz, 2 H), 8.26–8.12 (m, 2 H), 7.92 (m, *J* = 8.4 Hz, *J* = 3.9 Hz, 2 H), 7.72 (m, *J* = 8.3 Hz, *J* = 4.3 Hz, 2 H), 7.67–7.57 (m, 4 H), 7.50 (m, *J* = 7.8 Hz, *J* = 3.3 Hz, 2 H), 7.33 (m, *J* = 8.2 Hz, *J* = 6.1 Hz, 2 H), 7.25–7.20 (m, 1 H), 7.12–7.06 (m, 2 H), 6.72–6.60 (m, 3 H), 5.84 (m, 1 H), 5.60 (m, *J* = 5.8 Hz, 2 H), 2.99 (m, *J* = 7.0 Hz, 3 H), 2.78 (m, *J* = 4.3 Hz, 6 H), 2.40–2.20 (m, 9 H), 1.14–1.00 (m, 9 H).

^{13}C NMR (100 MHz, $CDCl_3$): δ (ppm) 147.5 (C), 147.1 (C), 146.6 (C), 141.4 (C), 139.6 (C), 138.2 (C), 138.0 (C), 136.4 (C), 135.4 (C), 133.8 (C), 133.6 (C), 130.7 (CH), 130.5 (CH), 129.4 (CH), 129.2 (CH), 129.0 (CH), 127.9 (CH), 126.6 (CH), 125.0 (CH), 124.1 (CH), 122.3 (CH), 118.7 (CH), 115.8 (CH), 50.0 (CH), 22.0 (CH_3), 20.9 (CH_3), 18.4 (CH_3).

IR (ATR) $\tilde{\nu}$ (cm^{-1}) = 3048 (m), 3012 (s), 2956 (vs), 2918 (vs), 2853 (vs), 2819 (m), 2555 (m), 2517 (m), 2448 (m), 2360 (m), 2252 (m), 2170 (m), 2027 (m), 1890 (w), 1728 (w), 1612 (m), 1562 (m), 1516 (m), 1477 (s), 1453 (vs), 1378 (s), 1361 (vs), 1307 (vs), 1220 (m), 1142 (m), 1033 (m), 1013 (m), 1001 (m), 933 (m), 878 (m), 844 (s), 823 (s), 798 (s), 785 (vs), 773 (vs), 765 (vs), 732 (vs), 710 (w), 656 (w), 613 (w), 578 (m), 557 (w), 543 (m), 504 (w), 463 (w), 429 (w), 411 (m), 397 (m).

MS (ESI): *m/z* (%): 799.3 (2) $[M+3]^+$, 798.3 (4) $[M+2]^+$, 797.3 (8) $[M+1]^+$, 796.3 (5) $[M]^+$, 795.3 (9) $[M-1]^+$; HRMS (ESI): *m/z* calcd for $C_{62}H_{52}$: 796.4069 $[M]^+$; found: 796.3495.

((9-Mesityl-9*H*-fluorene-2,7-diyl)bis(naphthalene-2,1-diyl))bis(mesitylmethanol) (113)

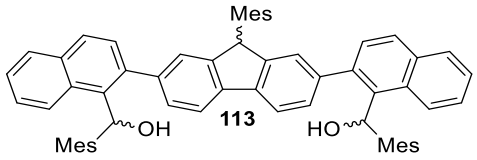

In accordance to a published method,[203] MesMgBr (1.00M in THF; 678 mg, 3.0 mL, 3.04 mmol, 5.00 equiv.) was added dropwise under an argon atmosphere to a cooled (0 °C) solution of biscarbaldehyde **111** (360 mg, 0.61 mmol, 1.00 equiv.) in anhydrous THF (10 mL). After addition was completed, the cooling bath was removed and the mixture stirred for 15 min at rt. Saturated aqueous NH_4Cl solution (20 mL) was added, stirring was continued for 10 min, and the mixture was extracted with CH_2Cl_2 (3×100 mL). The combined organic layers were dried (Na_2SO_4) and concentrated at reduced pressure.

16,19-Dihydro-8,16,19-trimesityl-8H-bisbenz[4,5]indeno[1,2-b:2',1'-h]fluorene (115)

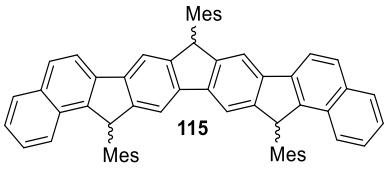

The remnant (**113**) was dissolved in anhydrous CH_2Cl_2 (20 mL) and the solution was cooled to 0 °C. $BF_3{\cdot}OEt_2$ (517 mg, 462 µL, 3.64 mmol, 5.00 equiv.) was added under an argon atmosphere and the mixture was stirred for 1 h at rt. Saturated aqueous NH_4Cl solution (20 mL) was added, stirring was continued for 10 min, and the mixture was extracted with CH_2Cl_2 (3×100 mL). The combined organic layers were dried (Na_2SO_4), concentrated at reduced pressure, and purified by column chromatography (silica gel, n-pentane/CH_2Cl_2 4:1) to yield **115** (378 mg, 474 µmol, 78%) as a pale orange solid. The product was obtained as a mixture of isomers, thus resulting in additional hardly discriminable signals in the spectra. Only the most pronounced signals are given.

R_f = 0.37 (*n*-pentane/CH_2Cl_2 4:1).

^{1}H NMR (400 MHz, $CDCl_3$): δ (ppm) 7.91–7.81 (m, 6 H), 7.70 (m, *J* = 13.8 Hz, 3.0 Hz, 2 H), 7.65–7.56 (m, 2 H), 7.46 (m, *J* = 8.0 Hz, *J* = 2.3 Hz, 2 H), 7.39–7.32 (m, 2 H), 7.29 (m, *J* = 5.9 Hz, *J* = 1.5 Hz, 2 H), 7.22–7.12 (m, 2 H), 6.79–6.57 (m, 3 H), 5.85–5.67 (m, 3 H), 2.96–2.86 (m, 9 H), 2.40–2.27 (m, 9 H), 1.22–0.97 (m, 9 H).

^{13}C NMR (100 MHz, $CDCl_3$): δ (ppm) 147.1 (C), 147.0 (C), 146.9 (C), 146.6 (C), 146.5 (C), 146.4 (C), 146.4 (C), 143.3 (C), 143.2 (C), 143.2 (C), 141.1 (C), 141.1 (C), 141.0 (C), 140.7 (C), 140.6 (C), 140.6 (C), 138.8 (C), 138.3 (C), 138.3 (C), 138.3 (C), 138.1 (C), 137.9 (C), 137.2 (C), 137.1 (C), 136.9 (C), 136.5 (C), 136.4 (C), 136.3 (C), 135.4 (C), 135.3 (C), 135.2 (C), 134.9 (C), 133.2 (C), 131.0 (CH), 130.8 (CH), 130.8 (CH), 130.7 (CH), 129.4 (CH), 129.3 (CH), 129.1 (CH), 128.2 (CH), 128.1 (CH), 127.0 (CH), 126.5 (CH), 125.2 (CH), 123.9 (CH), 119.0 (CH), 116.0 (CH), 115.9 (CH), 115.4 (CH), 49.7 (CH), 49.6 (CH), 49.5 (CH), 22.5 (CH_3), 22.5 (CH_3), 22.2 (CH_3), 21.4 (CH_3), 21.1 (CH_3), 21.1 (CH_3), 18.8 (CH_3), 18.4 (CH_3), 18.1 (CH_3).

IR (ATR) $\tilde{\nu}$ (cm^{-1}) = 3053 (w), 3003 (w), 2951 (w), 2917 (m), 2853 (w), 2731 (w), 1723 (w), 1611 (w), 1579 (vw), 1519 (vw), 1479 (m), 1458 (m), 1431 (m), 1375 (w), 1366 (w), 1307 (s), 1262 (w), 1244 (w), 1197 (w), 1142 (w), 1033 (w), 1016 (w), 933 (w), 887 (m), 860 (w),

844 (m), 816 (vs), 795 (vs), 744 (vs), 698 (w), 595 (w), 564 (w), 543 (w), 516 (w), 492 (w), 466 (s), 424 (w), 409 (w).

MS (ESI): *m/z* (%): 798.4 (1) $[M+2]^+$, 797.4 (3) $[M+1]^+$, 796.4 (5) $[M]^+$; HRMS (ESI): *m/z* calcd for $C_{62}H_{52}$: 796.4069 $[M]^+$; found: 796.4062.

7,10,18-Trimesitylbisbenz[6,7]indeno[1,2-b:2',1'-h]fluorenyl Radical (40)

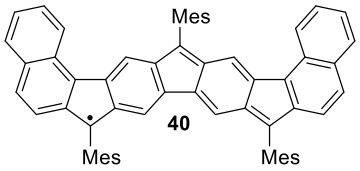

In accordance to a published method,[204] precursor **114** (70.0 mg, 88.0 µmol, 1.00 equiv.) and KO*t*Bu (138 mg, 1.23 mmol, 14.0 equiv.) were dissolved in anhydrous THF (10 mL) under an argon atmosphere and heated for 16 h to 60 °C. The mixture was allowed to cool to rt and *p*-chloranil (86.0 mg, 351 µmol, 4.50 equiv.) was added. After stirring for 10 min, the mixture was concentrated at reduced pressure. The obtained remnant was purified by column chromatography (silica gel, *n*-pentane/CH_2Cl_2 4:1) to yield **40** (67.0 mg, 84.4 µmol, 96%) as a dark green solid.

R_f = 0.30 (*n*-pentane/CH_2Cl_2 4:1).

m.p. 432 °C.

IR (ATR) $\tilde{\nu}$ (cm^{-1}) = 3356 (w), 2953 (m), 2919 (s), 2851 (s), 2728 (w), 1687 (s), 1677 (vs), 1650 (m), 1562 (s), 1520 (m), 1504 (m), 1489 (m), 1456 (m), 1375 (w), 1337 (m), 1316 (w), 1256 (m), 1232 (m), 1210 (m), 1183 (w), 1105 (vs), 1035 (m), 1014 (m), 972 (w), 905 (w), 888 (m), 850 (m), 810 (m), 744 (vs), 711 (vs), 613 (w), 586 (vw), 543 (w), 510 (w), 469 (w), 463 (w), 414 (w).

UV/Vis (CH_2Cl_2): λ_{max} (ε) [nm ($mol^{-1}dm^3cm^{-1}$)] = 295 (39,000), 375 (26,000), 390 (32,000), 495 (2,000), 620 (7,000), 670 (31,000), 735 (5,000), 825 (2,000).

MS (ESI): *m/z* (%): 796.4 (5) $[M+3]^+$, 795.4 (23) $[M+2]^+$, 794.4 (67) $[M+1]^+$, 793.4 (100) $[M]^+$; HRMS (ESI): *m/z* calcd for $C_{62}H_{49}$: 793.3834 $[M]^+$; found: 793.3818.

8,16,19-Trimesitylbisbenz[4,5]indeno[1,2-b:2',1'-h]fluorenyl Radical (41)

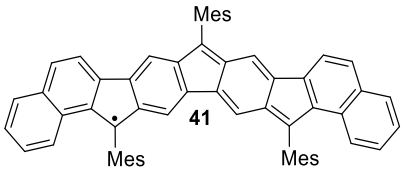

In accordance to a published method,[204] precursor **115** (55.0 mg, 69.0 µmol, 1.00 equiv.) and KO*t*Bu (108 mg, 966 µmol, 14.0 equiv.) were dissolved in anhydrous THF (10 mL) under an argon atmosphere and heated for 16 h to 60 °C. The mixture was allowed to cool to rt and *p*-chloranil (76.4 mg, 311 µmol, 4.50 equiv.) was added. After stirring for 10 min, the mixture was concentrated at reduced pressure. The obtained remnant was purified by column chromatography (silica gel, *n*-pentane/CH_2Cl_2 4:1) to yield **41** (35.0 mg, 44.1 µmol, 64%) as a dark blue solid.

R_f = 0.48 (*n*-pentane/CH_2Cl_2 4:1).

m.p. 422 °C.

IR (ATR) $\tilde{\nu}$ (cm^{-1}) = 3376 (w), 3342 (m), 3330 (m), 3319 (m), 3296 (w), 3043 (w), 2952 (m), 2918 (vs), 2871 (m), 2850 (s), 1725 (vw), 1690 (w), 1626 (vs), 1611 (s), 1596 (m), 1587 (m), 1561 (vs), 1543 (vs), 1483 (m), 1458 (m), 1442 (s), 1384 (s), 1354 (s), 1343 (s), 1303 (vs), 1285 (vs), 1247 (s), 1217 (m), 1205 (s), 1177 (vs), 1154 (vs), 1133 (vs), 1116 (s), 1098 (m), 1089 (m), 1064 (m), 1037 (m), 1010 (s), 1001 (s), 982 (m), 956 (m), 899 (vs), 884 (s), 864 (m), 850 (s), 813 (vs), 795 (m), 790 (m), 782 (m), 771 (s), 747 (vs), 738 (vs), 705 (vs), 657 (m), 636 (w), 628 (w), 609 (m), 579 (m), 571 (m), 541 (m), 509 (m), 467 (m), 459 (m), 401 (w), 388 (m).

UV/Vis (CH_2Cl_2): λ_{max} (ε) [nm ($mol^{-1}dm^3cm^{-1}$)] = 296 (20,000), 362 (58,000), 575 (14,000), 620 (18,000), 660 (20,000).

MS (ESI): *m/z* (%): 796.4 (4) $[M+3]^+$, 795.4 (22) $[M+2]^+$, 794.4 (68) $[M+1]^+$, 793.4 (100) $[M]^+$; HRMS (ESI): *m/z* calcd for $C_{62}H_{49}$: 793.3834 $[M]^+$; found: 793.3850.

1,3-Dibromo-2-iodobenzene (119)

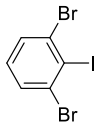

119

Variant A:

Following a published protocol,[147] *n*-BuLi (2.50M; 1.36 g, 8.48 mL, 21.2 mmol, 1.00 eq.) was added dropwise under argon atmosphere to a cooled (-78°C) solution of DIPEA (2.14 g, 2.98 mL, 21.2 mmol, 1.00 eq.) in 50 mL dry THF to generate LDA *in situ*. The resulting solution was stirred for 30 min at -78 °C and 1,3-dibromobenzene (**117**; 2.56 mL, 5.00 g, 21.2 mmol, 1.00 eq.) was added slowly. After stirring for 2 h at -78 °C the mixture was quenched with molecular iodine (5.38 g, 21.2 mmol, 1.00 eq.) in 15 mL dry THF. After the completion of the reaction, excess iodine was quenched with sodium disulfite and the resulting mixture extracted with diethyl ether. The combined organic layers were dried over Na_2SO_4, filtered and concentrated under reduced pressure. The residue was recrystallized from EtOH:H_2O to yield **119** (2.96 g, 8.18 mmol, 39%) as a white solid. The NMR data are in agreement with published data.[147]

Variant B:

Following a published protocol,[149] $NaNO_2$ (6.05 g, 87.7 mmol, 2.20 eq.) in 50 mL H_2O was added portion wise to a cooled (0 °C) solution of 2,6-dibromoaniline (**120**; 10.0 g, 39.9 mmol, 1.00 eq.) in 60 mL H_2SO_4 and stirred vigorously for 3 h at 0 °C. KI (39.7 g, 239 mmol, 6.00 eq.) in 100 mL H_2O was added to this mixture at 0 °C and stirring continued for 16 h while allowing the mixture to warm to rt. solid sodium disulfite was added until the color vanished followed by the addition of EtOAc. The phases were separated and the aqueous phase extracted with EtOAc. The combined organic layers were washed with saturated aqueous $NaHCO_3$, brine, dried over Na_2SO_4 and concentrated under reduced pressure. The obtained crude product was purified by column chromatography (silica gel, *n*-hexane) to yield **119** (13.3 g, 36.7 mmol, 92%) as a white crystalline solid. The NMR data are in agreement with published data.[149]

Variant C:

Following a published protocol,[148] $NaNO_2$ (577 mg, 8.37 mmol, 1.05 eq.) in 10 mL H_2O was added portion wise to a cooled (0 °C) solution of 2,6-dibromoaniline (**120**; 2.00 g, 7.97 mmol, 1.00 eq.) in 20 mL HCl and stirred vigorously for 3 h at 0 °C. KI (662 mg, 3.99 mmol, 0.500 eq.) in 20 mL H_2O was added to this mixture at 0 °C and stirring continued for 16 h while allowing the mixture to warm to rt. solid sodium disulfite was added until the color vanished followed by the addition of EtOAc. The phases were separated and the aqueous phase extracted with EtOAc. The combined organic layers were washed with saturated aqueous $NaHCO_3$, brine, dried over Na_2SO_4 and concentrated under reduced pressure. The obtained crude product was purified by column chromatography (silica gel, *n*-hexane) to yield **119** (1.18 g, 3.26 mmol, 42%) as a white crystalline solid. The NMR data are in agreement with published data.[148]

^{1}H NMR (400 MHz, $CDCl_3$): δ (ppm) 7.55 (dt, J = 8.0, 1.3 Hz, 2H, H-Ar), 7.06 (td, J = 8.0, 1.2 Hz, 1H, H-Ar).

2,2',6,6'-Tetrabromo-1,1'-biphenyl (118)

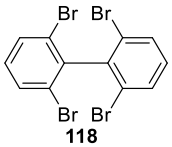

118

Following a published protocol,[149] *n*-BuLi (2.5M; 974 mg, 6.08 mL, 15.2 mmol, 1.10 eq.) was added dropwise under an argon atmosphere over a period of 30 min to a cooled (−78 °C) solution of 1,3-dibromo-2-iodobenzene (**117**; 5.00 g, 13.8 mmol, 1.00 eq.) in 75 mL Et_2O and stirred for 20 min. $CuBr_2$ (4.63 g, 20.7 mmol, 1.50 eq.) was added, stirring continued for 90 min at −78 °C, Nitrobenzene (1.70 g, 1.42 mL, 13.8 mmol, 1.00 eq.) added and the reaction mixture stirred overnight while allowing the temperature to warm to rt. NH_4Cl was added to the crude mixture and the phases separated. The aqueous phase was extracted with Et_2O and the combined organic layers washed with NH_4Cl and H_2O, respectively. After drying over Na_2SO_4 the solvent was evaporated under reduced pressure. Hexane was added and the mixture stored overnight at −30 °C. The resulting crystals were collected and washed with hexane to yield **118** (1.75 g, 3.73 mmol, 27%) as a white crystalline solid. The NMR data are in agreement with published data.[149]

^{1}H NMR (400 MHz, $CDCl_3$): δ (ppm) 7.67 (d, J = 8.1 Hz, 4H, H-Ar), 7.16 (t, J = 8.0 Hz, 2H, H-Ar).

4,5-Dibromo-9*H*-fluoren-9-one (121)

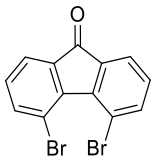

121

Following a published protocol,[93] *n*-BuLi (2.5M; 240 mg, 1.50 mL, 3.75 mmol, 2.20 eq.) was added dropwise under an argon atmosphere to a cooled (−78 °C) solution of 1,3-dibromo-2-(2,6-dibromophenyl)benzene (**119**; 800 mg, 1.70 mmol, 1.00 eq.) in 50 mL anhydrous THF and stirred for 40 min. $ClCO_2Me$ (483 mg, 396 µL, 5.11 mmol, 3.00 eq.) was added to this mixture at −78 °C and stirring continued for 2 h while allowing the mixture to warm to rt. H_2O was added, stirring continued for 10 min and the phases separated. The aqueous phase was extracted with CH_2Cl_2, dried over Na_2SO_4 and concentrated under reduced pressure. The obtained residue was purified by column chromatography (*n*-hexane/CH_2Cl_2 2:1) to yield **121** (374 mg, 1.11 mmol, 65%) as a yellow solid. The NMR data are in agreement with published data.[93]

^{1}H NMR (400 MHz, $CDCl_3$): δ (ppm) 7.73 (m, *J* = 11.7, 7.6, 1.2 Hz, 4H, H-Ar), 7.23 (m, *J* = 8.0, 7.2 Hz, 2H, H-Ar).

4,5-Dibromo-9-mesityl-9*H*-fluorene (122)

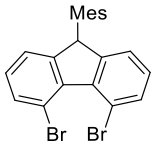

122

Following a published method,[205] Me_3SiCl (63.6 mg, 74.5 µL, 586 µmol, 1.10 eq.) and Et_3SiH (65.6 mg, 90.2 µL, 565 µmol, 1.06 eq.) were added under an argon atmosphere to a solution of 4,5-dibromofluoren-9-one (**121**; 180 mg, 533 µmol, 1.00 eq.) and anhydrous $FeCl_3$ (4.32 mg, 26.6 µmol, 0.05 eq.) in mesitylene (8 mL). The mixture was stirred for 2 h at rt, heated for 18 h to 50 °C, cooled to rt, quenched with H_2O (20 mL) and extracted with CH_2Cl_2 (3×100 mL). The combined organic layers were washed with H_2O (3×100 mL), dried (Na_2SO_4), concentrated at reduced pressure, and purified by column chromatography (silica gel, *n*-hexane) to yield **122** (109 mg, 247 µmol, 46%) as pale orange crystals. The NMR data are in agreement with published data.[205]

^{1}H NMR (400 MHz, $CDCl_3$): δ (ppm) 7.69 – 7.62 (m, 2H, H-Ar), 7.16 – 7.09 (m, 4H, H-Ar), 7.03 – 6.98 (m, 1H, H-Ar), 6.67 (d, J = 1.9 Hz, 1H, H-Ar), 5.50 (s, 1H, CH), 2.62 (s, 3H, CH_3), 2.28 (s, 3H, CH_3), 1.09 (s, 3H, CH_3).

3-Bromo-9,9-dimethyl-9*H*-fluoren-2-amine (128)

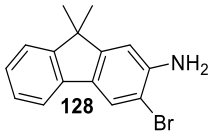

Following a published method,[205] NBS (893 mg, 5.02 mmol, 1.05 eq.) was added portion wise under an argon atmosphere to a cooled solution (0 °C) of 9,9-dimethylfluoren-2-amine (**127**; 1.00 g, 4.78 mmol, 1.00 eq.) in 40 mL CH_2Cl_2 and allowed to warm to rt. After 2 h, the mixture was quenched with $NaHCO_3$, the phases separated and the aqueous phase extracted with CH_2Cl_2. The combined organic layers were dried over Na_2SO_4, filtered and concentrated under reduced pressure. The obtained residue was purified by column chromatography (*n*-hexane/EtOAc 9:1) to yield **128** (1.31 g, 4.56 mmol, 95%) as a beige solid. The obtained NMR data are in agreement with the literature.[205]

R_f = 0.32 (*n*-hexane/EtOAc 9:1).

^{1}H NMR (400 MHz, $CDCl_3$): δ (ppm) 7.8 (s, 1H, H-Ar), 7.5 (dt, *J* = 7.6, 0.9 Hz, 1H, H-Ar), 7.4 – 7.3 (m, 1H, H-Ar), 7.3 (td, *J* = 7.4, 1.3 Hz, 1H, H-Ar), 7.2 (td, *J* = 7.4, 1.3 Hz, 1H, H-Ar), 6.8 (s, 1H, H-Ar), 4.2 (s, 2H, NH_2), 1.4 (s, 6H, CH_3).

3-Bromo-2-iodo-9,9-dimethyl-9*H*-fluorene (129)

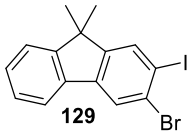

129

Following a published method,[205] 3-bromo-9,9-dimethylfluoren-2-amine (**128**; 1.00 g, 3.47 mmol, 1.00 eq.) was suspended in 10 mL conc. HCl at 0 °C and $NaNO_2$ (527 mg, 7.63 mmol, 2.20 eq.) in 10 mL H_2O was added portion wise over a period of 10 min. The mixture was stirred vigorously for 2 h at 0 °C and subsequently KI (3.46 g, 20.8 mmol, 6.00 eq.) in 20 mL H_2O was added at 0 °C to this mixture and stirring continued over night while allowing the mixture to warm to rt. Solid sodium disulfite was added until the color vanished followed by the addition of CH_2Cl_2. The phases were separated and the aqueous phase extracted with CH_2Cl_2. The combined organic layers were washed with saturated aqueous NaHCO3 solution and brine, dried over Na_2SO_4 and concentrated under reduced pressure. The obtained crude was purified by column chromatography (silica gel, *n*-hexane/CH_2Cl_2 9:1) to yield **129** (844 mg, 2.12 mmol, 61%) as a white solid. The obtained NMR data are in agreement with the literature.[205]

R_f = 0.50 (*n*-hexane/CH_2Cl_2 9:1).

^{1}H NMR (400 MHz, $CDCl_3$): δ (ppm) 8.0 (s, 1H), 7.9 (s, 1H), 7.7 – 7.6 (m, 1H), 7.4 – 7.4 (m, 1H), 7.4 – 7.3 (m, 2H), 1.5 (s, 6H).

3-Bromo-9,9-dimethyl-9*H*-fluorene-2-carbaldehyde (124)

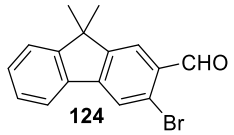

124

Following a published method [127] ^{i}PrMgCl LiCl (2.00M; 61.9 mg, 301 µL, 601 µmol, 1.20 eq.) was added under an argon atmosphere to a cooled solution (−78 °) of 3-bromo-2-iodo-9,9-dimethylfluorene (**129**; 200 mg, 501 µmol, 1.00 eq.) in dry THF (30 mL) and stirred for 15 min. Next, DMF (80.6 mg, 84.8 µL, 1.10 mmol, 2.20 eq.) was added and stirring continued for 1 h while allowing the mixture to warm to rt. NH_4Cl was added, the phases separated, and the aqueous phase extracted with CH_2Cl_2. The combined organic layers were dried over Na_2SO_4, filtered and concentrated under reduced pressure. The obtained crude was purified by column chromatography (silica gel, *n*-hexane/CH_2Cl_2 2:1) to yield **124** (106 mg, 0.35 mmol, 70%) as a light-yellow solid.

R_f = 0.55 (*n*-hexane/CH_2Cl_2 1:2).

^{1}H NMR (400 MHz, $CDCl_3$): δ (ppm) 10.42 (s, 1H, CHO), 7.98 (d, J = 20.3 Hz, 2H, H-Ar), 7.78 – 7.71 (m, 1H, H-Ar), 7.50 – 7.37 (m, 3H, H-Ar), 1.50 (s, 6H, CH_3).

^{13}C NMR (100 MHz, $CDCl_3$): δ (ppm) 192.2 (CHO), 155.3 (C), 153.3 (C), 147.0 (C), 136.6 (C), 131.9 (C), 129.8 (CH), 127.7 (CH), 126.9 (C), 125.2 (CH), 123.9 (CH), 123.2 (CH), 121.6 (CH), 77.2 (C), 47.2 (C), 26.9 (CH3).

IR (ATR) $\tilde{\nu}$ (cm^{-1}) = 2958 (w), 2863 (w), 2849 (w), 1680 (vs), 1596 (vs), 1560 (w), 1472 (m), 1456 (w), 1438 (m), 1391 (s), 1378 (s), 1361 (w), 1295 (w), 1266 (m), 1227 (m), 1217 (m), 1169 (vs), 1082 (m), 1030 (m), 1016 (m), 956 (s), 909 (m), 899 (m), 880 (s), 866 (m), 779 (m), 755 (vs), 731 (vs), 713 (m), 622 (w), 618 (w), 567 (m), 551 (w), 500 (m), 479 (w), 429 (vs), 402 (m), 378 (w).

MS (ESI): *m/z* (%): 303.0 (1) $[M+3]^+$, 302.9 (2) $[M+2]^+$, 301.0 (4) $[M+1]^+$, 300.0 (1) $[M]^+$, HRMS (ESI): *m/z* calcd for $C_{16}H_{13}BrO$: 300.0150 $[M]^+$; found: 300.0102.

9,9-Dimethyl-3-(4,4,5,5-tetramethyl-1,3,2-dioxaborolan-2-yl)-9*H*-fluorene-2-carbaldehyde (130)

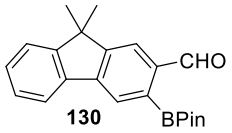

130

PdCl2(dppf) (99.6 mg, 136 µmol, 0.100 eq.) was added under an argon atmosphere to a degassed (ultrasonication, 10 min) solution of 3-bromo-9,9-dimethylfluorene-2-carbaldehyde (**124**; 410 mg, 1.36 mmol, 1.00 eq.), KOAc (401 mg, 4.08 mmol, 3.00 eq.), and B_2Pin_2 (449 mg, 1.77 mmol, 1.30 eq.) in 1,4-dioxane (20 mL) and heated to 80 °C for 48 h. After cooling to rt, the solvent was removed under reduced pressure. EtOAc (50 mL) was added and the solution filtered (Celite), concentrated at reduced pressure, and purified by column chromatography (silica gel, *n*-hexane/EtOAc 9:1) to yield **130** (280 mg, 0.80 mmol, 59%) as a white solid.

R_f = 0.26 (*n*-hexane/EtOAc 9:1).

^{1}H NMR (400 MHz, $CDCl_3$): δ (ppm) 10.66 (s, 1H, CHO), 8.23 (s, 1H, H-Ar), 8.09 (s, 1H, H-Ar), 7.90 – 7.82 (m, 1H, H-Ar), 7.49 – 7.45 (m, 1H, H-Ar), 7.41 – 7.37 (m, 2H, H-Ar), 1.51 (s, 6H, CH_3), 1.43 (s, 12H, CH_3).

^{13}C NMR (100 MHz, $CDCl_3$): δ (ppm) 194.8 (CHO), 156.5 (C), 154.9 (C), 144.2 (C), 140.8 (C), 137.9 (C), 128.9 (CH), 127.4 (CH), 127.4 (CH), 122.9 (CH), 121.9 (CH), 121.5 (CH), 84.6 (C), 47.3 (C), 26.9 (CH3), 25.1 (CH3).

IR (ATR) $\tilde{\nu}$ (cm^{-1}) = 2962 (w), 2924 (w), 1677 (vs), 1599 (s), 1475 (w), 1460 (w), 1445 (w), 1412 (m), 1401 (w), 1381 (s), 1371 (s), 1354 (vs), 1320 (vs), 1292 (s), 1262 (vs), 1234 (m), 1211 (m), 1157 (s), 1140 (vs), 1122 (m), 1111 (s), 1091 (vs), 1048 (vs), 1020 (s), 967 (m), 958 (m), 924 (w), 908 (s), 858 (s), 830 (s), 800 (s), 788 (vs), 764 (vs), 748 (s), 738 (vs), 713 (s), 698 (vs), 669 (m), 647 (w), 612 (w), 578 (w), 569 (s), 555 (w), 484 (w), 433 (s), 426 (m), 392 (m), 382 (m).

MS (ESI): *m/z* (%): 350.2 (23) $[M+2]^+$, 349.1 (100) $[M+1]^+$, 348.2 (14) $[M]^+$, HRMS (ESI): *m/z* calcd for $C_{22}H_{25}BO_3$: 348.1897 $[M]^+$; found: 348.1947.

9'-Mesityl-9,9,9'',9''-tetramethyl-9*H*,9'H,9''*H*-[3,2':7',3''-terfluorene]-2,2''-dicarbaldehyde (131)

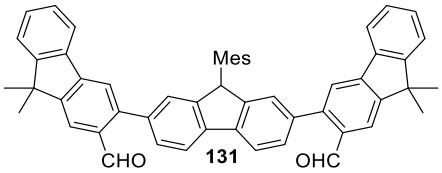

$PdCl_2$(dppf) (7.45 mg, 10.2 µmol, 0.150 eq.) was added under an argon atmosphere to a degassed (ultrasonication, 10 min) mixture of dibromofluorene **46** (30.0 mg, 67.8 µmol, 1.00 eq.), boronate **130** (52.0 mg, 149 µmol, 2.20 eq.), and Cs_2CO_3 (111 mg, 339 µmol, 5.00 eq.) in toluene/H_2O (1:1; 10 mL). The mixture was heated to 105 °C for 18 h, cooled to rt, and the aqueous layer was extracted with CH_2Cl_2 (3×100 mL). The combined organic layers were dried (Na_2SO_4), concentrated at reduced pressure, and purified by column chromatography (silica gel, *n*-hexane/EtOAc 9:1) to yield **131** (136 mg, 188 µmol, 52%) as a beige solid.

R_f = 0.26 (*n*-hexane/EtOAc 9:1).

^{1}H NMR (400 MHz, $CDCl_3$): δ (ppm) 9.99 (s, 2H, CHO), 8.10 (s, 2H, H-Ar), 8.02 (d, *J* = 7.8 Hz, 2H, H-Ar), 7.80 (dd, *J* = 6.9, 1.6 Hz, 2H, H-Ar), 7.76 (s, 2H, H-Ar), 7.51 (ddd, *J* = 14.9, 7.4, 1.7 Hz, 4H, H-Ar), 7.44 – 7.37 (m, 4H, H-Ar), 7.34 (s, 2H, H-Ar), 6.96 (s, 1H, H-Ar), 6.68 (s, 1H, H-Ar), 5.69 (s, 1H, CH), 2.69 (s, 3H, CH_3), 2.23 (s, 3H, CH_3), 1.55 (s, 12H, CH_3), 1.26 (s, 3H, CH_3).

^{13}C NMR (100 MHz, $CDCl_3$): δ (ppm) 192.4 (CHO), 155.4 (C), 153.1 (C), 148.1 (C), 146.4 (C), 144.8 (C), 140.3 (C), 138.0 (C), 137.8 (C), 137.7 (C), 137.6 (C), 136.8 (C), 133.0 (C), 130.9 (C), 129.5 (CH), 129.2 (CH), 127.5 (CH), 126.0 (CH), 123.1 (CH), 122.2 (CH), 121.7 (CH), 121.5 (CH), 120.3 (CH), 50.1 (C), 47.2 (CH), 27.1 (CH_3), 27.1 (CH_3), 22.0 (CH_3), 20.9 (CH_3), 19.1 (CH_3).

IR (ATR) $\tilde{\nu}$ (cm^{-1}) = 2961 (w), 2919 (w), 1677 (s), 1608 (m), 1458 (w), 1443 (w), 1395 (w), 1259 (vs), 1159 (w), 1153 (w), 1146 (w), 1078 (vs), 1014 (vs), 963 (w), 907 (w), 891 (w), 866 (w), 858 (w), 795 (vs), 758 (s), 742 (vs), 727 (m), 707 (m), 671 (m), 633 (w), 615 (w), 601 (w), 569 (w), 557 (w), 548 (w), 500 (w), 482 (w), 432 (m), 402 (s), 387 (s), 382 (s).

MS (ESI): *m/z* (%): 725.3 (15) $[M+1]^+$, 724.4 (1) $[M]^+$, 723.4 (14) $[M-1]^+$, HRMS (ESI): *m/z* calcd for $C_{54}H_{44}O_2$: 724.3341 $[M]^+$; found: 724.3290.

(9'-Mesityl-9,9,9'',9''-tetramethyl-9*H*,9'H,9''*H*-[3,2':7',3''-terfluorene]-2,2''-diyl)bis(mesitylmethanol) (132)

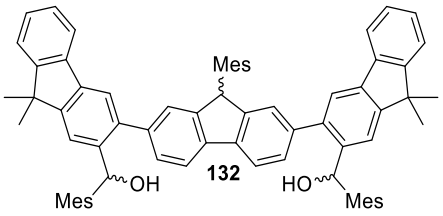

In accordance to a published method,[203] MesMgBr (1.00M in THF; 151 mg, 676 µL, 676 µmol,, 5.00 eq.) was added dropwise under an argon atmosphere to a cooled (0 °C) solution of biscarbaldehye **131** (98.0 mg, 135 µmol, 1.00 eq.) in anhydrous THF (15 mL). After addition was completed, the cooling bath was removed and the mixture was stirred for 15 min at rt. Saturated aqueous NH_4Cl solution (20 mL) was added, stirring was continued for 10 min, and the mixture was extracted with CH_2Cl_2 (3×100 mL). The combined organic layers were dried (Na_2SO_4) and concentrated at reduced pressure.

Radical precursor 133

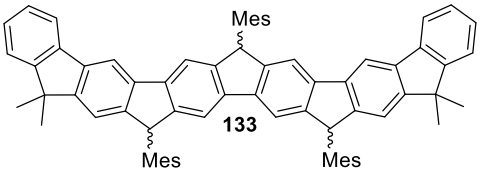

The remnant (**132**) was dissolved in anhydrous CH_2Cl_2 (20 mL) and the solution was cooled to 0 °C. $BF_3{\cdot}OEt_2$ (151 mg, 676 µL, 676 µmol, 5.00 equiv.) was added under an argon atmosphere and the mixture was stirred for 1 h at rt. Saturated aqueous NH_4Cl solution (20 mL) was added, stirring was continued for 10 min, and the mixture was extracted with CH_2Cl_2 (3×100 mL). The combined organic layers were dried (Na_2SO_4), concentrated at reduced pressure, and purified by column chromatography (silica gel, *n*-pentane/CH_2Cl_2 4:1) to yield **133** (127 mg, 137 µmol, quant.) as a pink solid. The product was obtained as a mixture of isomers, thus resulting in additional hardly discriminable signals in the spectra. Only the most pronounced signals are given.

R_f = 0.31 (*n*-pentane/CH_2Cl_2 4:1).

^{1}H NMR (400 MHz, $CDCl_3$): δ (ppm) 8.07 (d, *J* = 9.6 Hz, 2H, H-Ar), 7.76 (d, *J* = 7.3 Hz, 2H, H-Ar), 7.71 (s, 2H, H-Ar), 7.50 (d, *J* = 8.0 Hz, 2H, H-Ar), 7.41 (d, *J* = 7.2 Hz, 2H, H-Ar), 7.35 (s, 2H, H-Ar), 7.23 (s, 2H, H-Ar), 7.09 (m, 3H, H-Ar), 6.68 (m, *J* = 17.9 Hz, 3H), 5.71 (s, 1H, CH), 5.58 (d, *J* = 10.1 Hz, 2H, CH), 2.85 (d, *J* = 54.4 Hz, 9H, CH_3), 2.41 – 2.25 (m, 9H, CH_3), 1.47 (d, *J* = 5.2 Hz, 6H, CH_3), 1.40 (d, *J* = 4.8 Hz, 6H, CH_3), 1.11 (s, 9H, CH_3).

^{13}C NMR (100 MHz, $CDCl_3$): δ (ppm) 154.0 (C), 153.6 (C), 147.8 (C), 146.9 (C), 146.6 (C), 140.7 (C), 140.5 (C), 140.3 (C), 139.5 (C), 138.4 (C), 137.9 (C), 136.3 (C), 134.7 (C), 130.9 (CH), 129.0 (CH), 127.1 (CH), 122.7 (CH), 119.9 (CH), 118.4 (CH), 115.9 (CH), 115.6 (CH), 111.5 (CH), 49.6 (CH), 46.8 (C), 27.5 (CH_3), 22.8 (CH_3), 22.1 (CH_3), 21.1 (CH_3), 18.7 (CH_3), 18.6 (CH_3).

IR (ATR) $\tilde{\nu}$ (cm^{-1}) = 2953 (s), 2919 (vs), 2851 (vs), 1723 (vw), 1609 (w), 1479 (m), 1456 (vs), 1431 (s), 1412 (m), 1377 (m), 1358 (w), 1288 (vs), 1261 (w), 1239 (w), 1221 (m), 1153 (w), 1084 (w), 1028 (m), 1016 (m), 936 (w), 887 (m), 880 (m), 849 (vs), 807 (m), 792 (s), 776 (s), 755 (vs), 744 (vs), 722 (vs), 616 (w), 571 (m), 564 (m), 480 (m), 429 (m), 399 (m), 385 (w), 375 (w).

MS (ESI): *m/z* (%): 931.5 (31) $[M+3]^+$, 930.5 (56) $[M+2]^+$, 929.5 (83) $[M+1]^+$, 928.4 (41) $[M]^+$,
HRMS (ESI): *m/z* calcd for $C_{72}H_{64}$: 928.5008 $[M]^+$; found: 928.4968.

Radical 126

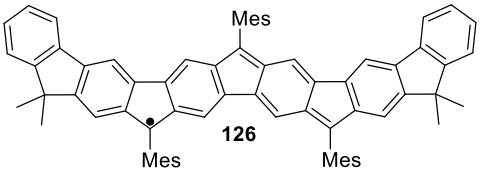

Following a published method,[74] precursor **133** (125 mg, 135 µmol, 1.00 eq.) and KO*t*Bu (211 mg, 1.88 mmol, 14.0 eq.) were dissolved in anhydrous THF (15 mL) under an argon atmosphere and heated for 16 h to 50 °C. The mixture was allowed to cool to rt and *p*-chloranil (149 mg, 605 µmol, 4.50 eq.) was added. After stirring for 10 min, the mixture was concentrated at reduced pressure. The obtained remnant was purified by column chromatography (silica gel, *n*-pentane/CH_2Cl_2 4:1) to yield **126** (101 mg, 109 µmol, 81%) as a dark green solid.

R_f = 0.29 (*n*-pentane/CH_2Cl_2 4:1).

IR (ATR, cm^{-1}): $\tilde{\nu}$ = 2953 (m), 2917 (vs), 2853 (s), 1672 (w), 1568 (w), 1513 (w), 1455 (m), 1436 (m), 1429 (m), 1374 (m), 1358 (m), 1340 (m), 1316 (w), 1290 (m), 1259 (m), 1232 (w), 1215 (w), 1198 (w), 1177 (w), 1154 (w), 1129 (s), 1098 (m), 1085 (m), 1064 (s), 1021 (s), 970 (w), 882 (vs), 863 (m), 849 (s), 803 (s), 781 (s), 749 (vs), 737 (s), 722 (s), 710 (s), 688 (m), 657 (w), 571 (m), 557 (m), 469 (w), 419 (w), 399 (m).

MS (ESI): *m/z* (%): 928.4 (8) $[M+3]^+$, 927.4 (30) $[M+2]^+$, 926.4 (78) $[M+1]^+$, 925.4 (100) $[M]^+$, HRMS (ESI): *m/z* calcd for $C_{72}H_{61}$: 925.4773 $[M]^+$; found: 925.4787.

3-Bromo-9*H*-fluoren-2-amine (135)

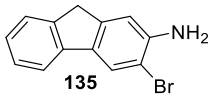

135

Following a published method,[205] NBS (1.03 g, 5.79 mmol, 1.05 eq.) was added portion wise under an argon atmosphere to a cooled solution (0 °C) of 9*H*-fluoren-2-amine (**134**; 1.00 g, 5.52 mmol, 1.00 eq.) in 40 mL CH_2Cl_2 and allowed to warm to rt. After 2 h, the mixture was quenched with $NaHCO_3$, the phases separated, and the aqueous phase extracted with CH_2Cl_2. The combined organic layers were dried over Na_2SO_4, filtered and concentrated under reduced pressure. The obtained residue was purified by column chromatography (silica gel, *n*-hexane/EtOAc 9:1) to yield **135** (1.03 g, 3.96 mmol, 72%) as a beige solid.

R_f = 0.16 (*n*-hexane/EtOAc 9:1).

^{1}H NMR (400 MHz, $CDCl_3$): δ (ppm) 7.81 (s, 1H, H-Ar), 7.60 (d, *J* = 7.5 Hz, 1H, H-Ar), 7.46 (d, *J* = 7.4 Hz, 1H, H-Ar), 7.32 (t, *J* = 7.5 Hz, 1H, H-Ar), 7.22 (td, *J* = 7.4, 1.1 Hz, 1H, H-Ar), 6.96 (d, *J* = 1.3 Hz, 1H, H-Ar), 4.14 (s, 2H, NH_2), 3.78 (s, 2H, CH_2).

^{13}C NMR (100 MHz, $CDCl_3$): δ (ppm) 144.3 (C), 143.0 (C), 142.5 (C), 141.2 (C), 134.4 (C), 127.0 (CH), 125.9 (CH), 125.0 (CH), 124.0 (CH), 119.0 (CH), 112.4 (CH), 108.4 (C), 36.7 (CH_2).

IR (ATR) $\tilde{\nu}$ (cm^{-1}) = 3439 (w), 3421 (w), 3353 (w), 3336 (w), 3313 (w), 3040 (w), 3033 (w), 3013 (w), 1612 (m), 1564 (w), 1446 (m), 1412 (s), 1391 (m), 1346 (w), 1307 (w), 1278 (m), 1248 (m), 1227 (w), 1197 (w), 1176 (w), 1160 (w), 1137 (w), 1101 (w), 1084 (w), 1028 (w), 1021 (w), 1009 (m), 959 (m), 949 (m), 924 (w), 871 (s), 858 (s), 830 (w), 758 (vs), 728 (vs), 704 (m), 680 (m), 667 (m), 642 (m), 636 (m), 615 (m), 588 (s), 572 (vs), 554 (s), 548 (s), 538 (s), 528 (s), 509 (s), 493 (s), 476 (s), 469 (s), 455 (s), 443 (m), 424 (vs), 391 (s), 385 (s), 380 (s).

MS (ESI): *m/z* (%): 260.9 (97) $[M+2]^+$, 258.9 (100) $[M]^+$, HRMS (ESI): *m/z* calcd for $C_{13}H_{10}BrN$: 258.9997 $[M]^+$; found: 258.9991.

3-Bromo-2-iodo-9*H*-fluorene (136)

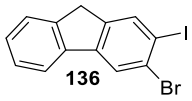

Following a published method,[205] 3-bromo-9*H*-fluoren -2-amine (**135**; 500 mg, 1.92 mmol, 1.00 eq.) was suspended in 5 mL conc. HCl at 0 °C and $NaNO_2$ (292 mg, 4,23 mmol, 2.20 eq.) in 10 mL H_2O was added portion wise over a period of 10 min. The mixture was stirred vigorously for 2 h at 0 °C and subsequently KI (1.91 g, 11.5 mmol, 6.00 eq.) in 20 mL H_2O was added at 0 °C to this mixture and stirring continued over night while allowing the mixture to warm to rt. Solid sodium disulfite was added until the color vanished followed by the addition of CH_2Cl_2. The phases were separated and the aqueous phase extracted with CH_2Cl_2. The combined organic layers were washed with saturated aqueous NaHCO3 solution and brine, dried over Na_2SO_4 and concentrated under reduced pressure. The obtained crude was purified by column chromatography (silica gel, *n*-hexane/CH_2Cl_2 9:1). Recrystallization by EtOH yielded **136** (596 mg, 1.61 mmol, 84%) as a white crystalline solid.

R_f = 0.50 (*n*-hexane/CH_2Cl_2 9:1).

^{1}H NMR (400 MHz, $CDCl_3$): δ (ppm) 8.04 (d, *J* = 2.1 Hz, 2H, H-Ar), 7.73 (d, *J* = 6.6 Hz, 1H, H-Ar), 7.54 (dt, *J* = 7.0, 1.2 Hz, 1H, H-Ar), 7.38 (m, *J* = 7.4, 1.5 Hz, 2H, H-Ar), 3.82 (s, 2H, CH_2).

^{13}C NMR (100 MHz, $CDCl_3$): δ (ppm) 144.0 (C), 143.9 (C), 143.3 (C), 139.9 (C), 136.7 (CH), 128.1 (CH), 128.0 (CH), 127.3 (C), 125.3 (CH), 124.0 (CH), 120.4 (CH), 98.2 (C), 36.3 (CH_2).

IR (ATR) $\tilde{\nu}$ (cm^{-1}) = 3048 (w), 3017 (w), 2953 (w), 2919 (m), 2850 (w), 1714 (w), 1595 (w), 1567 (w), 1473 (w), 1460 (w), 1436 (s), 1408 (m), 1390 (m), 1360 (m), 1307 (w), 1273 (w), 1264 (w), 1230 (w), 1191 (w), 1174 (w), 1166 (w), 1152 (w), 1106 (w), 1095 (w), 1084 (w), 1071 (w), 1055 (m), 1027 (m), 1010 (m), 956 (w), 946 (w), 919 (w), 878 (m), 864 (m), 850 (m), 806 (s), 764 (vs), 734 (vs), 725 (vs), 688 (m), 670 (w), 660 (m), 628 (w), 579 (s), 486 (m), 441 (w), 415 (vs).

MS (ESI): *m/z* (%): 371.8 (98) $[M+2]^+$, 370.8 (14) $[M+1]^+$, 396.8 (100) $[M]^+$,HRMS (ESI): *m/z* calcd for $C_{13}H_8BrI$: 369.8854 $[M]^+$; found: 369.8851.

2-Amino-9*H*-fluoren-9-one (138)

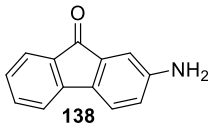

138

Following a published method,[206] Cs_2CO_3 (10.8 g, 33.1 mmol, 3.00 eq.) was added to a solution of 9*H*-fluoren-2-amine (2.00 g, 11.0 mmol, 1.00 eq.) in 50 mL DMSO and stirred for 16 h at rt. Water was added and the formed precipitate filtered, washed with water and dried to yield **138** (1.95 g, 9.99 mmol, 91%) as a red solid. The NMR data are in agreement with published data.[207]

^{1}H NMR (400 MHz, DMSO-*d6*): δ (ppm) 7.46 – 7.41 (m, 3H, H-Ar), 7.37 (d, *J* = 8.0 Hz, 1H, H-Ar), 7.13 (ddd, *J* = 7.4, 5.6, 2.9 Hz, 1H, H-Ar), 6.81 (d, *J* = 2.2 Hz, 1H, H-Ar), 6.68 (dd, *J* = 8.0, 2.3 Hz, 1H, H-Ar), 5.64 (s, 2H, NH_2).

3-Bromo-2-iodo-9*H*-fluoren-9-one (137)

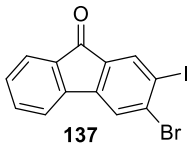

137

Variant A:

Following a published method,[195] KOH (90.0 mg, 1.60 mmol, 1.00 eq.) was added to 3-bromo-2-iodo-9*H*-fluorene (**136**; 595 mg, 1.60 mmol, 1.00 eq.) in 10 mL THF and stirred at rt for 16 h. Water was added and the formed precipitate filtered, washed with small amount of water and dried to yield **137** (522 mg, 1.36 mmol, 85%) as a yellow solid.

Variant B:

Following a published protocol,[208] $NaNO_2$ (189 mg, 2.74 mmol, 1.50 eq.) in 10 mL H_2O was added portion wise to cooled (0 °C) solution of 2-amino-3-bromofluoren-9-one (**139**; 500 mg, 1.82 mmol, 1.00 eq.) in 10 mL HCl and stirred vigorously for 2 h at 0 °C. KI (908 mg, 5.47 mmol, 3.00 eq.) in 15 mL H_2O was added to this solution, stirring continued for 16 h while allowing the mixture to warm to rt. Solid sodium disulfite was added until the color vanished followed by the addition of CH_2Cl_2. The organic layer was separated and the aqueous phase extracted with CH_2Cl_2. The combined organic layers were washed with saturated aqueous $NaHCO_3$, brine, dried over Na2SO4 and concentrated under reduced pressure. The obtained crude product was purified by column chromatography (silica gel, *n*-hexane/EtOAc 4:1) to yield **137** (121 mg, 314 µmol, 17%) as a yellow solid. The NMR data are in agreement with published data.[208]

^{1}H NMR (400 MHz, $CDCl_3$): δ (ppm) 8.11 (s, J = 3.6 Hz, 1H, H-Ar), 7.81 (s, 1H, H-Ar), 7.68 (d, J = 7.4, 1.0 Hz, 1H, H-Ar), 7.52 (m, J = 3.9, 3.4, 0.9 Hz, 2H, H-Ar), 7.38 (m, J = 7.4, 5.6, 2.9 Hz, 1H, H-Ar).

^{13}C NMR (100 MHz, $CDCl_3$): δ (ppm) 191.5 (CO), 145.3 (C), 142.9 (C), 136.6 (C), 135.7 (CH), 135.3 (CH), 134.1 (C), 133.8 (C), 130.3 (CH), 124.9 (CH), 124.8 (CH), 120.9 (CH), 101.0 (CH).

IR (ATR) $\tilde{\nu}$ (cm^{-1}) = 3077 (w), 3064 (w), 2924 (w), 1707 (vs), 1604 (m), 1594 (m), 1585 (s), 1561 (m), 1434 (m), 1349 (m), 1295 (w), 1259 (w), 1237 (w), 1184 (m), 1129 (m), 1081 (m),

1060 (w), 1030 (w), 1004 (w), 928 (m), 898 (m), 880 (m), 813 (m), 761 (vs), 730 (vs), 666 (s), 636 (w), 591 (w), 469 (w), 409 (m).

MS (ESI): *m/z* (%): 385.3 (17) $[M+2]^+$, 384.3 (25) $[M+1]^+$, 383.3 (100) $[M]^+$,HRMS (ESI): *m/z* calcd for $C_{13}H_6BrIO$: 383.8647 $[M]^+$; found: 383.8636.

2-Amino-3-bromo-9*H*-fluoren-9-one (139)

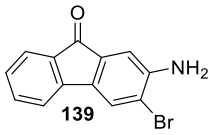

139

Following a published protocol,[208] NBS (915 mg, 5.14 mmol, 1.05 eq.) was added portion wise to a cooled solution (0 °C) of 2-aminofluoren-9-one (**138**; 956 mg, 4.90 mmol, 1.00 eq.) in 30 mL CH_2Cl_2, allowed to warm to rt and stirred for 16 h. $NaHCO_3$ was added, the phases separated and the aqueous phase extracted with CH_2Cl_2. The combined organic layers were dried over Na_2SO_4, filtered and concentrated under reduced pressure. The obtained residue was purified by column chromatography (silica gel, CH_2Cl_2) to yield **139** (1.18 g, 4.29 mmol, 88%) as a red solid. The NMR data are in agreement with published data.[208]

^{1}H NMR (400 MHz, $CDCl_3$): δ (ppm) 7.59 (dt, *J* = 7.4, 1.0 Hz, 1H, H-Ar), 7.56 (s, 1H, H-Ar), 7.42 (dd, *J* = 7.4, 1.2 Hz, 1H, H-Ar), 7.34 (dt, *J* = 7.4, 0.9 Hz, 1H, H-Ar), 7.19 (td, *J* = 7.4, 1.0 Hz, 1H, H-Ar), 7.05 (s, 1H, H-Ar), 4.31 (s, 2H, NH_2).

3-Bromo-2-iodo-9-mesityl-9*H*-fluorene (141)

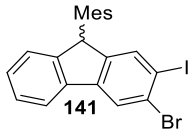

Following a published method,[125] Me_3SiCl (57.4 mg, 67.2 µL, 529 µmol, 1.10 eq.) and Et_3SiH (59.2 mg, 81.4 µL, 509 µmol, 1.06 eq.) were added under an argon atmosphere to a solution of 3-bromo-2-iodofluoren-9-one (**137**; 185 mg, 481 µmol, 1.00 eq.) and anhydrous $FeCl_3$ (3.90 mg, 24.0 µmol, 0.05 eq.) in mesitylene (5 mL). The mixture was stirred for 2 h at rt, heated for 18 h to 50 °C, cooled to rt, quenched with H_2O (20 mL) and extracted with CH_2Cl_2 (3×100 mL). The combined organic layers were washed with H_2O (3×100 mL), dried (Na_2SO_4), concentrated at reduced pressure, and purified by column chromatography (silica gel, *n*-hexane) to yield **141** (215 mg, 440 µmol, 91%) as a white solid.

R_f = 0.21 (*n*-hexane).

^{1}H NMR (400 MHz, $CDCl_3$): δ (ppm) 8.08 (s, 1H, H-Ar), 7.78 (dt, *J* = 7.7, 1.0 Hz, 1H, H-Ar), 7.69 (d, *J* = 1.1 Hz, 1H, H-Ar), 7.40 (tt, *J* = 7.5, 1.1 Hz, 1H, H-Ar), 7.30 (td, *J* = 7.5, 1.2 Hz, 1H, H-Ar), 7.19 (dd, *J* = 7.5, 1.0 Hz, 1H, H-Ar), 7.02 (d, *J* = 2.1 Hz, 1H, H-Ar), 6.71 – 6.64 (m, 1H, H-Ar), 5.39 (s, 1H, CH), 2.65 (s, 3H, CH_3), 2.29 (s, 3H, CH_3), 1.11 (s, 3H, CH_3).

^{13}C NMR (100 MHz, $CDCl_3$): δ (ppm) 147.9 (C), 147.4 (C), 143.1 (C), 138.9 (C), 137.8 (C), 137.8 (C), 136.9 (C), 135.7 (CH), 132.6 (C), 130.8 (CH), 129.1 (CH), 128.6 (CH), 128.0 (CH), 127.4 (CH), 124.4 (CH), 124.2 (CH), 120.6 (CH), 98.9 (C), 49.3 (CH), 21.9 (CH_3), 21.0 (CH_3), 18.9 (CH_3).

IR (ATR) $\tilde{\nu}$ (cm^{-1}) = 2963 (w), 2949 (w), 2915 (m), 2851 (w), 1609 (w), 1477 (w), 1456 (m), 1432 (vs), 1375 (w), 1353 (m), 1307 (w), 1292 (w), 1271 (m), 1244 (w), 1232 (w), 1221 (w), 1203 (w), 1173 (w), 1154 (w), 1084 (w), 1027 (m), 1009 (m), 939 (w), 897 (s), 881 (s), 858 (m), 846 (vs), 829 (w), 805 (w), 788 (m), 765 (vs), 739 (vs), 724 (vs), 674 (m), 639 (w), 622 (m), 602 (w), 581 (w), 565 (m), 551 (s), 540 (w), 516 (w), 493 (w), 463 (w), 435 (w), 419 (s), 394 (w).

MS (ESI): *m/z* (%): 489.9 (96) $[M+2]^+$, 488.9 (20) $[M+1]^+$, 487.9 (100) $[M]^+$,HRMS (ESI): *m/z* calcd for $C_{22}H_{18}BrI$: 487.9637 $[M]^+$; found: 487.9632.

3-Bromo-9-mesityl-9*H*-fluorene-2-carbaldehyde (125)

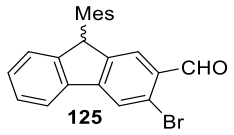

125

Following a published method,[127] ^{i}PrMgCl LiCl (1.3M in THF; 134 mg, 708 µL, 920 µmol, 1.50 eq.) was added under an argon atmosphere to a cooled solution (−78 °) of 3-bromo-2-iodo-9-mesityl-9*H*-fluorene (**141**; 300 mg, 613 µmol, 1.00 eq.) in dry THF (15 mL) and stirred for 30 min. Next, dry DMF (98.6 mg, 104 µL, 1.35 mmol, 2.20 eq.) was added and stirring continued for 1 h while allowing the mixture to warm to rt. NH_4Cl was added, the phases separated and the aqueous phase extracted with CH_2Cl_2. The combined organic layers were dried over Na_2SO_4, filtered and concentrated under reduced pressure. The obtained crude was purified by column chromatography (silica gel, *n*-hexane/CH_2Cl_2 2:1) to yield **125** (242 mg, 619 µmol, quant.) as a light-yellow solid.

R_f = 0.66 (*n*-hexane/CH_2Cl_2 2:1).

^{1}H NMR (400 MHz, $CDCl_3$): δ (ppm) 10.43 (d, J = 43.4 Hz, 1H, CHO), 8.07 (s, 1H, H-Ar), 7.88 – 7.84 (m, 1H, H-Ar), 7.76 (d, J = 1.3 Hz, 1H, H-Ar), 7.45 (t, J = 7.4 Hz, 1H, H-Ar), 7.37 (td, J = 7.4, 1.3 Hz, 1H, H-Ar), 7.28 – 7.24 (m, 1H, H-Ar), 7.02 (d, J = 1.9 Hz, 1H, H-Ar), 6.64 (d, J = 2.0 Hz, 1H, H-Ar), 5.48 (d, J = 11.1 Hz, 1H. CH), 2.66 (s, 3H, CH_3), 2.28 (s, 3H, CH_3), 1.06 (s, 3H, CH_3).

^{13}C NMR (100 MHz, $CDCl_3$): δ (ppm) 192.0 (CHO), 190.0 (CHO), 149.4 (C), 148.3 (C), 147.0 (C), 138.4 (C), 137.8 (C), 137.5 (C), 137.0 (C), 132.1 (C), 131.8 (C), 130.8 (CH), 129.7 (CH), 129.3 (CH), 127.6 (CH), 126.5 (C), 125.3 (CH), 125.3 (CH), 124.7 (CH), 121.6 (CH), 49.7 (CH), 21.9 (CH_3), 21.0 (CH_3), 18.9 (CH_3).

IR (ATR) $\tilde{\nu}$ (cm^{-1}) = 3513 (w), 3004 (w), 2949 (w), 2914 (w), 2859 (w), 1680 (vs), 1598 (vs), 1554 (w), 1479 (w), 1459 (s), 1449 (m), 1436 (s), 1387 (vs), 1343 (w), 1309 (w), 1293 (w), 1251 (w), 1232 (m), 1183 (s), 1142 (m), 1115 (m), 1096 (w), 1030 (m), 1014 (m), 993 (w), 969 (s), 959 (m), 942 (w), 932 (w), 902 (m), 885 (w), 875 (m), 866 (m), 847 (s), 819 (w), 805 (m), 765 (s), 756 (vs), 737 (vs), 725 (vs), 703 (m), 677 (m), 640 (w), 622 (w), 606 (w), 598 (w), 581 (w), 572 (w), 544 (m), 516 (w), 496 (m), 475 (w), 462 (w), 441 (m), 421 (vs), 390 (w).

MS (ESI): *m/z* (%): 394.0 (24) $[M+4]^+$, 393.0 (99) $[M+3]^+$, 392.0 (25) $[M+2]^+$, 391.0 (100) $[M+1]^+$,HRMS (ESI): *m/z* calcd for $C_{23}H_{19}BrO$: 390.0619 $[M]^+$; found: 391.0695 $[M+1]^+$.

9-Mesityl-3-(4,4,5,5-tetramethyl-1,3,2-dioxaborolan-2-yl)-9*H*-fluorene-2-carbaldehyde (142)

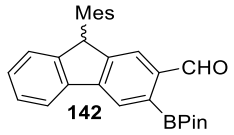

PdCl2(dppf) (37.4 mg, 51.1 µmol, 0.100 eq.) was added under an argon atmosphere to a degassed (ultrasonication, 10 min) solution of **141** (200 mg, 511 µmol, 1.00 eq.), KOAc (150 mg, 1.53 mmol, 3.00 eq.), and B_2Pin_2 (169 mg, 664 µmol, 1.30 eq.) in 1,4-dioxane (15 mL). The mixture was heated to 80 °C for 48 h. After cooling to rt, the solvent was removed at reduced pressure. EtOAc (50 mL) was added and the solution was filtered (Celite), concentrated at reduced pressure, and purified by column chromatography (silica gel, *n*-hexane/EtOAc 9:1) to yield **142** (70.0 mg, 160 µmol, quant.) as a brown oil.

R_f = 0.82 (*n*-hexane/EtOAc 9:1).

^{1}H NMR (400 MHz, $CDCl_3$): δ (ppm) 10.52 (s, 1H, CHO), 8.29 (s, 1H, H-Ar), 7.96 (dd, *J* = 8.1, 4.5 Hz, 1H, H-Ar), 7.83 (s, 1H, H-Ar), 7.42 (t, *J* = 7.3 Hz, 1H, H-Ar), 7.35 – 7.30 (m, 1H, H-Ar), 7.02 (d, *J* = 1.8 Hz, 1H, H-Ar), 6.62 (s, 1H, H-Ar), 5.53 (s, 1H, CH), 2.68 (s, 3H, CH_3), 2.27 (s, 3H, CH_3), 1.45 (s, 12H, 4x CH_3), 1.01 (s, 3H, CH_3).

^{13}C NMR (100 MHz, $CDCl_3$): δ (ppm) 194.6 (CHO), 150.0 (C), 148.8 (C), 140.5 (C), 139.6 (C), 137.9 (C), 136.8 (C), 130.7 (CH), 129.2 (CH), 128.8 (CH), 127.3 (CH), 127.0 (CH), 124.5 (CH), 123.9 (CH), 121.6 (CH), 84.6 (C), 50.1 (CH), 25.1 (CH_3), 21.9 (CH_3), 21.0 (CH_3), 18.8 (CH_3).

IR (ATR) $\tilde{\nu}$ (cm^{-1}) = 2978 (w), 2919 (w), 2857 (w), 1681 (vs), 1604 (m), 1578 (w), 1551 (w), 1470 (m), 1446 (m), 1411 (m), 1390 (w), 1371 (s), 1354 (vs), 1317 (vs), 1288 (s), 1271 (s), 1234 (m), 1211 (m), 1193 (m), 1180 (m), 1167 (m), 1140 (vs), 1120 (s), 1111 (m), 1099 (m), 1052 (vs), 1031 (m), 1018 (m), 979 (m), 960 (m), 933 (w), 908 (s), 854 (vs), 832 (s), 810 (m), 768 (s), 749 (s), 734 (vs), 718 (vs), 693 (m), 674 (m), 666 (m), 646 (m), 620 (m), 603 (w), 579 (m), 571 (w), 550 (m), 531 (w), 523 (w), 506 (w), 501 (w), 489 (w), 469 (w), 456 (w), 445 (w), 416 (m), 401 (w), 385 (w).

MS (ESI): *m/z* (%): 441.2 (5) $[M+3]^+$, 440.2 (30) $[M+2]^+$, 439.2 (100) $[M+1]^+$, 438.2 (23) $[M]^+$,HRMS (ESI): *m/z* calcd for $C_{29}H_{31}BO_3$: 438.2366 $[M]^+$; found: 438.2394.

2,2'-(9-Mesityl-9*H*-fluorene-2,7-diyl)bis(4,4,5,5-tetramethyl-1,3,2-dioxaborolane) (146)

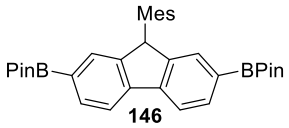

146

PdCl2(dppf) (41.4 mg, 56.5 µmol, 0.05 eq.) was added under an argon atmosphere to a degassed (ultrasonication, 10 min) solution of fluorene **46** (500 mg, 1.13 mmol, 1.00 eq.), KOAc (555 mg, 5.65 mmol, 5.00 eq.), and B_2Pin_2 (718 mg, 2.83 mmol, 2.50 eq.) in 1,4-dioxane (20 mL). The mixture was heated to 80 °C for 48 h. After cooling to rt, the solvent was removed at reduced pressure. EtOAc (50 mL) was added and the solution was filtered (Celite), concentrated at reduced pressure, and purified by column chromatography (silica gel, *n*-hexane/EtOAc 9:1) to yield **146** (320 mg, 597 µmol, 53%) as a white solid.

R_f = 0.41 (*n*-hexane/EtOAc 9:1).

^{1}H NMR (400 MHz, $CDCl_3$): δ (ppm) 7.86 (d, *J* = 0.9 Hz, 4H, Ar-H), 7.65 (d, *J* = 1.1 Hz, 2H, Ar-H), 7.26 (s, 1H, Ar-H), 7.01 (d, *J* = 2.0 Hz, 1H, Ar-H), 6.66 – 6.57 (m, 1H, Ar-H), 5.49 (s, 1H, CH), 2.69 (s, 3H, CH_3), 2.28 (s, 3H, CH_3), 1.33 (s, 24H, 4 x CH_3), 1.07 (s, 3H, CH_3).

^{13}C NMR (100 MHz, $CDCl_3$): δ (ppm) 147.1 (C), 143.7 (C), 138.2 (C), 138.1 (C), 136.1 (C), 133.8 (C), 130.6 (CH), 130.4 (CH), 129.0 (CH), 119.9 (CH), 83.9 (C), 49.7 (CH), 25.1 (CH_3), 24.9 (CH_3), 22.1 (CH_3), 21.0 (CH_3), 18.8 (CH_3).

IR (ATR, cm^{-1}): $\tilde{\nu}$ = 2973 (w), 2927 (w), 1605 (w), 1572 (w), 1475 (w), 1417 (m), 1388 (m), 1378 (m), 1371 (m), 1344 (vs), 1310 (vs), 1290 (s), 1268 (s), 1252 (s), 1208 (w), 1166 (m), 1142 (vs), 1123 (vs), 1108 (s), 1075 (vs), 1037 (m), 1014 (w), 1006 (w), 963 (s), 936 (w), 919 (m), 901 (w), 851 (vs), 826 (vs), 798 (s), 749 (w), 737 (w), 722 (vs), 700 (m), 669 (m), 654 (vs), 620 (m), 578 (m), 557 (w), 541 (w), 518 (w), 475 (w), 455 (w), 449 (w), 429 (w), 409 (w), 398 (w).

MS (ESI): *m/z* (%): 538.3 (30) $[M+2]^+$, 537.3 (100) $[M+1]^+$, 536.3 (40) $[M]^+$, 535.3 (4) $[M-1]^+$, HRMS (ESI): *m/z* calcd for $C_{34}H_{42}B_2O_4$: 536.3269 $[M]^+$; found: 536.3307.

9,9',9''-Trimesityl-9*H*,9'H,9''H-[3,2':7',3''-terfluorene]-2,2''-dicarbaldehyde (143)

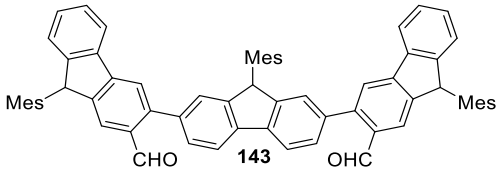

Variant A:

$PdCl_2$(dppf) (6.70 mg, 9.16 µmol, 0.150 eq.) was added under an argon atmosphere to a degassed (ultrasonication, 10 min) mixture of dibromofluorene **46** (27.0 mg, 61.1 µmol, 1.00 eq.), boronate **142** (58.9 mg, 134 µmol, 2.20 eq.), and Cs_2CO_3 (99.5 mg, 305 µmol, 5.00 eq.) in toluene/H_2O (1:1; 10 mL). The mixture was heated to 105 °C for 18 h, cooled to rt, and the aqueous layer was extracted with CH_2Cl_2 (3×100 mL). The combined organic layers were dried (Na_2SO_4), concentrated at reduced pressure, and purified by column chromatography (silica gel, *n*-hexane/EtOAc 9:1) to yield **143** (2.30 mg, 2.54 µmol, 4%) as a beige solid.

Variant B:

$Pd(PPH_3)_2Cl_2$ (9.82 mg, 14.0 µmol, 0.150 eq.) was added under an argon atmosphere to a degassed (ultrasonication, 10 min) mixture of boronate **146** (50.0 mg, 93.2 µmol, 1.00 eq.), 3-bromo-9-mesityl-9*H*-fluorene-2-carbaldehyde **125** (80.3 mg, 205 µmol, 2.20 eq.), SPhos (11.5 mg, 28.0 µmol, 0.300 eq.) and Cs_2CO_3 (152 mg, 466 µmol, 5.00 eq.) in toluene/H_2O (1:1; 10 mL). The mixture was heated to 105 °C for 18 h, cooled to rt, and the aqueous layer was extracted with CH_2Cl_2 (3×100 mL). The combined organic layers were dried (Na_2SO_4), concentrated at reduced pressure, and purified by column chromatography (silica gel, *n*-hexane/EtOAc 9:1) to yield **143** (7.50 mg, 8.29 µmol, 9%) as a beige solid.

R_f = 0.21 (*n*-hexane/EtOAc, 9:1).

^{1}H NMR (400 MHz, $CDCl_3$): δ (ppm) 9.98 (s, 1H, CHO), 9.89 – 9.83 (m, 1H, CHO), 8.00 – 7.80 (m, 8H, H-Ar), 7.73 (m, *J* = 1.1 Hz, 1H, H-Ar), 7.47 – 7.40 (m, 3H, H-Ar), 7.39 – 7.31 (m, 4H, H-Ar), 7.28 (m, *J* = 1.2 Hz, 2H, H-Ar), 7.08 – 7.00 (m, 3H, H-Ar), 6.72 – 6.63 (m, 3H, H-Ar), 5.60 (m, *J* = 39.6 Hz, 3H, 3x CH), 2.71 (m, *J* = 15.0 Hz, 9H, CH_3), 2.32 – 2.26 (m, 9H, CH_3), 1.18 – 1.04 (m, 9H, CH_3).

^{1}H NMR (400 MHz, $CDCl_3$): δ (ppm) 9.96 (d, *J* = 3.1 Hz, 2H, CHO), 8.03 (d, *J* = 7.7 Hz, 2H, H-Ar), 7.93 – 7.89 (m, 2H, H-Ar), 7.89 – 7.84 (m, 4H, H-Ar), 7.54 (dd, *J* = 8.5, 3.8 Hz, 2H, H-Ar), 7.43 (t, *J* = 7.4 Hz, 2H, H-Ar), 7.40 – 7.34 (m, 4H, H-Ar), 7.28 (d, *J* = 7.5 Hz, 2H, CH), 7.04 (d, *J* = 1.9 Hz, 2H, CH), 7.00 (s, 1H, CH), 6.72 (q, *J* = 3.1 Hz, 1H, CH), 6.65 (s, 2H, CH), 5.71 (d, *J* = 3.3 Hz, 1H, CH), 5.58 (s, 2H, CH), 2.71 (d, *J* = 8.4 Hz, 9H, CH_3), 2.27 (d, *J* = 12.9 Hz, 9H, CH_3), 1.29 (d, *J* = 5.5 Hz, 3H, CH_3), 1.11 (d, *J* = 1.7 Hz, 6H, CH_3).

^{13}C NMR (100 MHz, $CDCl_3$): δ (ppm) 192.3 (CHO), 149.3 (C), 148.1 (C), 148.0 (C), 146.8 (C), 146.2 (C), 146.0 (C), 146.0 (C), 140.3 (C), 139.4 (C), 138.0 (C), 138.0 (C), 137.9 (C), 137.8 (C), 137.6 (C), 137.6 (C), 136.9 (C), 136.8 (C), 133.1 (C), 132.9 (C), 132.9 (C), 132.8 (C), 132.8 (C), 130.9 (CH), 130.7 (CH), 129.8 (CH), 129.7 (CH), 129.2 (CH), 129.1 (CH), 127.3 (CH), 126.0 (CH), 125.9 (CH), 124.6 (CH), 123.2 (CH), 122.3 (CH), 121.5 (CH), 120.3 (CH), 50.1 (CH), 49.8 (CH), 22.0 (CH_3), 21.9 (CH_3), 21.0 (CH_3), 19.1 (CH_3), 19.0 (CH_3), 19.0 (CH_3).

IR (ATR) $\tilde{\nu}$ (cm^{-1}) = 2955 (w), 2919 (s), 2851 (m), 1684 (vs), 1605 (vs), 1571 (w), 1554 (w), 1480 (w), 1445 (s), 1425 (m), 1395 (m), 1377 (m), 1343 (w), 1298 (w), 1283 (w), 1256 (m), 1232 (m), 1196 (s), 1142 (m), 1109 (m), 1091 (m), 1058 (w), 1026 (m), 1014 (m), 1006 (m), 979 (w), 965 (w), 955 (w), 945 (w), 933 (w), 907 (m), 881 (m), 850 (s), 832 (m), 807 (s), 768 (vs), 728 (vs), 681 (m), 666 (w), 642 (w), 615 (s), 601 (w), 584 (w), 571 (w), 544 (w), 499 (w), 470 (m), 456 (m), 446 (w), 433 (w), 419 (m), 401 (m), 388 (w), 381 (m).

MS (ESI): *m/z* (%): 905.4 (25) $[M+1]^+$, 904.4 (70) $[M]^+$, 903.4 (100) $[M-1]^+$, HRMS (ESI): *m/z* calcd for $C_{68}H_{56}O_2$: 904.4280 $[M]^+$; found: 904.4250.

(9,9',9''-Trimesityl-9*H*,9'H,9''*H*-[3,2':7',3''-terfluorene]-2,2''-diyl)bis(mesitylmethanol) (147)

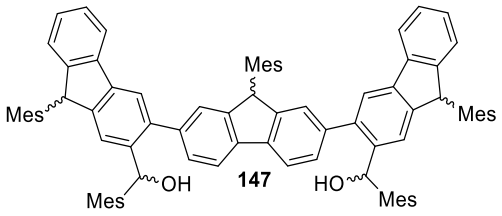

In accordance to a published method,[203] MesMgBr (1.00M in THF; 9.26 mg, 41.4 µL, 41.4 µmol,, 5.00 eq.) was added dropwise under an argon atmosphere to a cooled (0 °C) solution of biscarbaldehye **143** (7.50 mg, 8.29 µmol, 1.00 eq.) in anhydrous THF (5 mL). After addition was completed, the cooling bath was removed and the mixture was stirred for 15 min at rt. Saturated aqueous NH_4Cl solution (20 mL) was added, stirring was continued for 10 min, and the mixture was extracted with CH_2Cl_2 (3×100 mL). The combined organic layers were dried (Na_2SO_4) and concentrated at reduced pressure.

Radical precursor 148

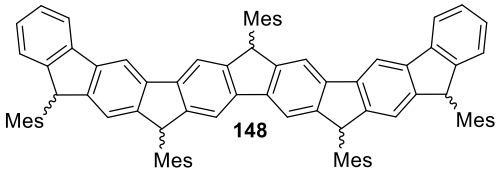

The remnant (**147**) was dissolved in anhydrous CH_2Cl_2 (20 mL) and the solution was cooled to 0 °C. $BF_3{\cdot}OEt_2$ (4.65 mg, 4.15 µL, 32.7 µmol, 5.00 equiv.) was added under an argon atmosphere and the mixture was stirred for 1 h at rt. Saturated aqueous NH_4Cl solution (20 mL) was added, stirring was continued for 10 min, and the mixture was extracted with CH_2Cl_2 (3×100 mL). The combined organic layers were dried (Na_2SO_4), concentrated at reduced pressure, and purified by column chromatography (silica gel, *n*-pentane/CH_2Cl_2 4:1) to yield **148** (6.40 mg, 4.15 µL, 5.77 µmol, 88%) as a beige solid. The product was obtained as a mixture of isomers, thus resulting in additional hardly discriminable signals in the spectra. Only the most pronounced signals are given.

R_f = 0.18 (*n*-pentane/CH_2Cl_2 4:1).

^{1}H NMR (400 MHz, $CDCl_3$): δ (ppm) 8.24 – 8.14 (m, 1H, H-Ar), 7.96 – 7.68 (m, 5H, H-Ar), 7.51 – 7.33 (m, 4H, H-Ar), 7.20 (m, *J* = 7.5 Hz, 3H, H-Ar), 7.11 (m, *J* = 7.0 Hz, 3H, H-Ar), 6.98 (m, *J* = 18.9, 2.4 Hz, 4H, H-Ar), 6.80 – 6.51 (m, 6H, H-Ar), 5.74 – 5.40 (m, 5H, CH), 2.86 (d, *J* = 36.8 Hz, 3H, CH_3), 2.75 – 2.56 (m, 10H, CH_3), 2.53 – 2.36 (m, 4H, CH_3), 2.24 (m, *J* = 13.1, 4.4 Hz, 13H, CH_3), 1.21 – 1.08 (m, 15H, CH_3).

IR (ATR) $\tilde{\nu}$ (cm^{-1}) = 2955 (s), 2922 (vs), 2854 (s), 2201 (w), 1925 (w), 1460 (m), 1380 (w), 1288 (w), 1261 (w), 1095 (w), 1020 (w), 874 (w), 847 (w), 810 (w), 790 (w), 764 (w), 742 (w), 727 (w), 592 (w), 571 (w), 530 (w), 493 (w), 482 (w), 398 (w), 394 (m), 380 (m).

MS (ESI): *m/z* (%): 1110.6 (26) $[M+2]^+$, 1109.6 (64) $[M+1]^+$, 1109.5 (75) $[M]^+$, HRMS (ESI): *m/z* calcd for $C_{86}H_{76}$: 1108.5947 $[M]^+$; found: 1108.5969.

Radical 42

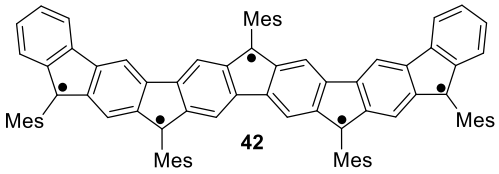

Following a published method,[74] precursor **148** (6.40 mg, 5.77 µmol, 1.00 eq.) and KO*t*Bu (9.06 mg, 80.7 µmol, 14.0 eq.) were dissolved in anhydrous THF (5 mL) under an argon atmosphere and heated for 16 h to 50 °C. The mixture was allowed to cool to rt and *p*-chloranil (6.38 mg, 26.0 µmol, 4.50 eq.) was added. After stirring for 10 min, the mixture was concentrated at reduced pressure. The obtained remnant was purified by column chromatography (silica gel, *n*-pentane/CH_2Cl_2 4:1) to yield **42** in traces as a violet solid.

R_f = 0.29 (*n*-pentane/CH_2Cl_2 4:1).

IR (ATR) $\tilde{\nu}$ (cm^{-1}) = 2955 (m), 2921 (vs), 2851 (vs), 1711 (m), 1460 (w), 1377 (w), 1261 (w), 1196 (m), 1074 (vs), 1068 (vs), 1038 (vs), 1030 (vs), 847 (w), 793 (s), 727 (w), 613 (w), 469 (s), 463 (s), 442 (m), 421 (w), 404 (w).

3,6-Dibromo-9,9-dimethyl-9*H*-fluorene-2,7-diamine (151)

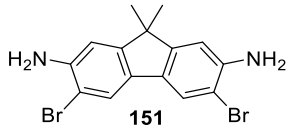

151

In variation to a published method,[127] NBS (1.67 g, 9.36 mmol, 2.10 eq.) was added portion wise to a cooled (0 °C) solution of 9,9-dimethylfluorene-2,7-diamine (**150**; 1.00 g, 4.46 mmol, 1.00 eq.) in 30 mL CH_2Cl_2 and stirred for 18 h, while allowing the mixture to warm to rt. $NaHCO_3$ was added, the phases separated and the aqueous phase extracted with CH_2Cl_2 (3 x 100 mL). The combined organic layers were dried over Na_2SO_4, filtered and concentrated under reduced pressure. The obtained residue was purified by column chromatography (silica gel, *n*-hexane/EtOAc 9:1) to yield **151** (270 mg, 705 µmol, 16%) as a red solid.

R_f = 0.48 (*n*-hexane/EtOAc 1:1).

^{1}H NMR (400 MHz, $CDCl_3$): δ (ppm) 7.58 (s, 2H, H-Ar), 6.78 (s, 2H, H-Ar), 4.10 (s, 4H, NH_2), 1.38 (s, 6H, CH_3).

^{13}C NMR (100 MHz, $CDCl_3$): δ (ppm) 153.8 (C), 142.5 (C), 131.0 (C), 123.1 (CH), 110.3 (CH), 108.2 (C), 46.5 (C), 27.5 (CH_3).

IR (ATR) $\tilde{\nu}$ (cm^{-1}) = 3468 (m), 3451 (m), 3363 (s), 3285 (w), 3183 (w), 3174 (w), 3165 (w), 2976 (w), 2963 (m), 2922 (w), 2866 (w), 2856 (w), 1612 (vs), 1565 (m), 1466 (vs), 1417 (vs), 1409 (vs), 1361 (m), 1307 (vs), 1249 (m), 1220 (m), 1079 (m), 1024 (s), 967 (m), 901 (w), 888 (w), 877 (vs), 861 (vs), 827 (w), 816 (w), 802 (w), 790 (w), 772 (w), 758 (m), 731 (m), 710 (vs), 686 (m), 662 (s), 639 (vs), 601 (s), 584 (s), 569 (s), 537 (vs), 518 (vs), 514 (vs), 503 (vs), 484 (vs), 459 (vs), 441 (vs), 422 (vs), 415 (vs), 408 (vs), 398 (vs), 392 (vs).

MS (ESI): *m/z* (%): 384.9 (4) $[M+5]^+$, 383.9 (48) $[M+4]^+$, 382.9 (22) $[M+3]^+$, 381.9 (99) $[M+2]^+$, 380.9 (2) $[M+1]^+$, 379.9 (48) $[M]^+$,HRMS (ESI): *m/z* calcd for $C_{15}H_{14}Br_2N_2$: 379.9524 $[M]^+$; found: 379.9518.

3,6-Dibromo-2,7-diiodo-9,9-dimethyl-9*H*-fluorene (152)

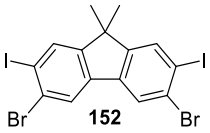

152

In slight variation to a published protocol,[127] $NaNO_2$ (127 mg, 1.85 mmol, 3.00 eq.) in 10 mL H_2O was added portion wise to cooled (0 °C) solution 3,6-dibromo-9,9-dimethyl-9*H*-fluorene-2,7-diamine (**151**; 235 mg, 615 µmol, 1.00 eq.) in 10 mL HCl and stirred vigorously for 2 h at 0 °C. KI (613 mg, 3.69 mmol, 6.00 eq.) in 15 mL H_2O was added to this solution, stirring continued for 16 h while allowing the mixture to warm to rt. Solid sodium disulfite was added until the color vanished followed by the addition of CH_2Cl_2. The organic layer was separated and the aqueous phase extracted with CH_2Cl_2. The combined organic layers were washed with saturated aqueous $NaHCO_3$, brine, dried over Na2SO4 and concentrated under reduced pressure. The obtained crude product was purified by column chromatography (silica gel, *n*-hexane/CH_2Cl_2 9:1) to yield **152** (112 mg, 186 µmol, 30%) as a beige solid.

R_f = 0.59 (*n*-hexane/CH_2Cl_2 9:1).

^{1}H NMR (400 MHz, $CDCl_3$): δ (ppm) 7.92 (s, 2H, H-Ar), 7.89 (s, 2H, H-Ar), 1.44 (s, 6H, CH_3).

^{13}C NMR (100 MHz, $CDCl_3$): δ (ppm) 153.8 (C), 139.3 (C), 134.8 (CH), 128.5 (C), 124.5 (CH), 100.6 (C), 46.8 (C), 26.8 (CH_3).

IR (ATR) $\tilde{\nu}$ (cm^{-1}) = 2956 (s), 2918 (m), 2856 (m), 1732 (w), 1594 (w), 1550 (w), 1459 (s), 1434 (vs), 1378 (m), 1349 (vs), 1265 (vs), 1235 (w), 1220 (w), 1201 (w), 1142 (w), 1089 (vs), 1016 (w), 935 (w), 870 (vs), 834 (vs), 725 (w), 639 (w), 606 (w), 578 (w), 438 (s), 399 (m).

HRMS (ESI): *m/z* calcd for $C_{15}H_{10}Br_2I_2$: 601.7239 $[M]^+$; found: 604.4050 $[M+3]^+$.

3,6-Dibromo-9,9-dimethyl-9*H*-fluorene-2,7-dicarbaldehyde (149)

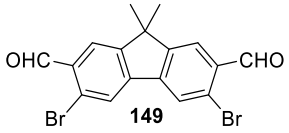

149

Following a published method [127] ^{i}PrMgCl LiCl (1.3M in THF; 59.3 mg, 314 µL, 408 µmol, 1.50 eq.) was added under an argon atmosphere to a cooled solution (−78 °) of 3,6-dibromo-2,7-diiodo-9,9-dimethylfluorene (**152**; 112 mg, 185 µmol, 1.00 eq.) in dry THF (15 mL) and stirred for 30 min. Next, dry DMF (59.7 mg, 62.8 µL, 816 µmol, 4.40 eq.) was added and stirring continued for 1 h while allowing the mixture to warm to rt. NH_4Cl was added, the phases separated, and the aqueous phase extracted with CH_2Cl_2. The combined organic layers were dried over Na_2SO_4, filtered and concentrated under reduced pressure. The obtained crude was purified by column chromatography (silica gel, *n*-hexane/CH_2Cl_2 2:1) to yield **149** (11.0 mg, 26.9 µmol, 15%) as a light-yellow solid.

R_f = 0.42 (*n*-hexane/CH_2Cl_2, 2:1).

^{1}H NMR (400 MHz, $CDCl_3$): δ (ppm) 10.44 (s, 2H, CHO), 8.02 (d, J = 2.1 Hz, 4H, H-Ar), 1.52 (s, 6H, CH_3).

^{13}C NMR (100 MHz, $CDCl_3$): δ (ppm) 191.8 (CHO), 154.6 (C), 143.7 (C), 133.5 (C), 126.7 (CH), 124.3 (CH), 47.5 (C), 26.6 (CH_3).

IR (ATR) $\tilde{\nu}$ (cm^{-1}) = 2961 (m), 2921 (s), 2880 (m), 2866 (m), 2853 (m), 1677 (vs), 1596 (vs), 1562 (m), 1468 (vs), 1446 (s), 1390 (vs), 1361 (m), 1293 (m), 1279 (m), 1238 (s), 1231 (s), 1167 (vs), 1115 (m), 1086 (vs), 1054 (m), 1031 (s), 1001 (m), 975 (m), 926 (vs), 907 (vs), 890 (vs), 846 (m), 834 (m), 826 (m), 772 (s), 745 (vs), 734 (vs), 718 (s), 657 (m), 628 (vs), 618 (s), 589 (s), 568 (m), 543 (m), 526 (m), 518 (m), 501 (m), 492 (m), 483 (m), 475 (m), 441 (vs), 416 (vs), 405 (m), 391 (w), 382 (w).

MS (ESI): *m/z* (%): 410.9 (50) $[M+5]^+$, 409.9 (18) $[M+4]^+$, 408.9 (100) $[M+3]^+$, 407.9 (9) $[M+2]^+$, 406.9 (52) $[M+1]^+$,HRMS (ESI): *m/z* calcd for $C_{17}H_{12}Br_2O_2$: 405.9204 $[M]^+$; found: 406.9286 $[M+1]^+$.

9,9-Dimethyl-3,6-diphenyl-9*H*-fluorene-2,7-dicarbaldehyde (154)

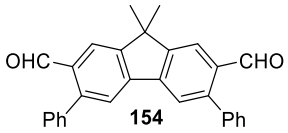

154

$PdCl_2$(dppf) (2.96 mg, 4.04 µmol, 0.15 eq.) was added under an argon atmosphere to a degassed (ultrasonication, 10 min) mixture of **149** (11.0 mg, 27.0 µmol, 1.00 eq.), phenylboronic acid (**153**; 7.23 mg, 59.3 µmol, 2.20 eq.), and Cs_2CO_3 (43.9 mg, 135 µmol, 5.00 eq.) in toluene/H_2O (1:1; 10 mL). The mixture was heated to 105 °C for 18 h, cooled to rt, and the aqueous layer was extracted with CH_2Cl_2 (3×50 mL). The combined organic layers were dried (Na_2SO_4), concentrated at reduced pressure, and purified by column chromatography (silica gel, *n*-hexane/EtOAc 9:1) to yield **154** (6 mg, 14.9 µmol, 55%) as a beige solid.

R_f = 0.28 (*n*-hexane/EtOAc 9:1).

^{1}H NMR (400 MHz, $CDCl_3$): δ (ppm) 10.02 (s, 2H, CHO), 8.18 (s, 2H, H-Ar), 7.84 (s, 2H, H-Ar), 7.51 – 7.43 (m, 10H, H-Ar), 1.64 (s, 6H, CH_3).

^{13}C NMR (100 MHz, $CDCl_3$): δ (ppm) 192.4 (CHO), 154.5 (C), 146.3 (C), 143.0 (C), 138.0 (C), 134.1 (C), 130.3 (CH), 128.7 (CH), 128.4(CH), 123.5 (CH), 122.0 (CH), 47.5 (C), 27.0 (CH_3).

Dimethyl 2,5-dibromoterephthalate (160)

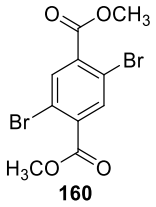

160

Following a published protocol,[209] 5-dibromoterephthalic acid (**159**; 2.00 g, 6.17 mmol, 1.00 eq.) was dissolved in 35 mL of MeOH and refluxed for 30 min. Subsequently, $SOCl_2$ (14.0 g, 8.52 mL, 117 mmol, 19.0 eq.) was added carefully and the final mixture refluxed for 12 h. The mixture was allowed to cool to rt, water was added, the precipitate filtered and dried under vacuum to yield **160** (2.07 g, 5.90 mmol, 96%) as a pale-yellow solid. The NMR data of the product are in agreement with published data.[209]

^{1}H NMR (400 MHz, $CDCl_3$): δ (ppm) 8.1 (s, 2H, Ar-H), 4.0 (s, 6H, CH_3).

Dimethyl 2,5-di((E)-styryl)terephthalate (161)

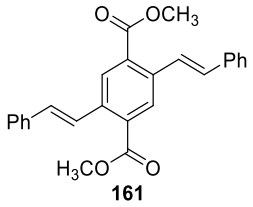

161

$Pd(OAc)_2$ and triphenylphosphane (37.3 mg, 142 µmol, 0.100 eq.) were added to a degassed mixture of dimethyl 2,5-dibromobenzene-1,4-dicarboxylate (**160**; 500 mg, 1.42 mmol, 1.00 eq.), styrene (888 mg, 975 µL, 8.52 mmol, 6.00 eq.) and triethylamine (1.44 g, 1.97 mL, 14.2 mmol, 10.0 eq.) in anhydrous DMF (10 mL). The resulting mixture was stirred for 20 min at rt and subsequently heated to 110 °C for 4 h. After cooling to rt, the mixture was treated with water and extracted with EtOAc. The organic layers were combined and washed with 6M HCl solution, water and brine, respectively. After drying over Na_2SO_4 and evaporating the solvent under reduced pressure the obtained crude was purified by column chromatography (silica gel, *n*-pentane/CH_2Cl_2 2:1 -> 1:1) to yield **161** (376 mg, 944 mmol, 66%) as a yellow solid.

R_f = 0.41 (*n*-pentane/CH_2Cl_2 2:1).

^{1}H NMR (400 MHz, $CDCl_3$): δ (ppm) 8.3 (s, 2H, H-Ar), 7.9 (d, J = 16.3 Hz, 2H, H-Ar), 7.6 – 7.5 (m, 4H, H-Ar), 7.4 – 7.4 (m, 4H, H-Ar), 7.3 – 7.3 (m, 2H, CH_2), 7.1 (d, J = 16.2 Hz, 2H, CH_2), 4.0 (s, 6H, CH_3).

^{13}C NMR (100 MHz, $CDCl_3$): δ (ppm) 167.4 (**C**$OOCH_3$), 137.5 (C), 137.3 (C), 132.3 (CH), 131.6 (C), 129.2 (CH), 128.9 (CH), 128.3 (CH), 127.1 (CH), 126.1 (CH), 52.7 (CH_3).

IR (ATR) $\tilde{\nu}$ (cm^{-1}) = 3078 (w), 3063 (w), 3021 (w), 3012 (w), 3003 (w), 2945 (w), 2904 (w), 2885 (w), 2837 (w), 1715 (vs), 1622 (w), 1595 (w), 1574 (w), 1494 (m), 1448 (w), 1434 (s), 1298 (m), 1278 (s), 1228 (vs), 1190 (s), 1166 (s), 1095 (vs), 1028 (m), 984 (w), 955 (vs), 908 (s), 897 (m), 851 (m), 834 (m), 793 (m), 778 (vs), 744 (vs), 690 (vs), 611 (m), 596 (s), 562 (m), 537 (w), 523 (m), 493 (m), 465 (m), 438 (w), 431 (w), 415 (m), 405 (m), 385 (w).

MS (ESI): *m/z* (%): 400.1 (14) $[M+2]^+$, 399.1 (57) $[M+1]^+$, 398.1 (86) $[M]^+$, HRMS (ESI): *m/z* calcd for $C_{26}H_{22}O_4$: 398.1518 $[M]^+$; found: 398.1519.

Dimethyl 2,5-diphenethylterephthalate (162)

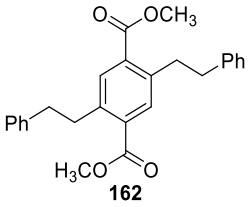

162

Following a published method,[154] 10% Pd/C (64.1 mg, 602 µmol, 0.50 eq.) and 16 mL of MeOH were added to a solution of dimethyl 2,5-di((E)-styryl)terephthalate (**161**; 480 mg, 1.20 mmol, 1.00 eq.) in 20 mL CH_2Cl_2. The final mixture was purged with H2 and kept under an atmosphere of H2 while stirring at rt for 16 h. Next, the mixture was filtered through a pad of Celite and the filtrate concentrated under reduced pressure. The obtained crude was purified by column chromatography (silica gel, *n*-hexane/CH_2Cl_2/EtOAc 20:5:1) to yield **162** (461 mg, 1.15 mmol, 95%) as a white crystalline solid.

R_f = 0.32 (*n*-hexane/CH_2Cl_2/EtOAc 20:5:1).

^{1}H NMR (400 MHz, $CDCl_3$): δ (ppm) 7.74 (s, 2H, H-Ar), 7.33 – 7.27 (m, 4H, H-Ar), 7.25 – 7.19 (m, 6H, H-Ar), 3.91 (s, 6H, CH_3), 3.27 – 3.20 (m, 4H, CH_2), 2.92 – 2.85 (m, 4H, CH_2).

^{13}C NMR (100 MHz, $CDCl_3$): δ (ppm) 167.5 ($COOCH_3$), 141.8 (C), 141.1 (C), 133.4 (CH), 132.6 (C), 128.7 (CH), 128.5 (CH), 126.1 (CH), 52.3 (CH_3), 38.2 (CH_2), 36.4 (CH_2).

IR (ATR) $\tilde{\nu}$ (cm^{-1}) = 3065 (w), 3024 (w), 2996 (w), 2946 (w), 2922 (m), 2887 (w), 2860 (w), 2840 (w), 1717 (vs), 1599 (w), 1581 (w), 1494 (m), 1453 (m), 1446 (m), 1435 (s), 1279 (vs), 1245 (vs), 1190 (vs), 1157 (w), 1142 (m), 1098 (vs), 1072 (s), 1034 (m), 1011 (m), 987 (m), 962 (s), 911 (s), 861 (w), 824 (w), 781 (vs), 756 (m), 735 (vs), 696 (vs), 669 (w), 622 (m), 612 (m), 562 (m), 521 (w), 483 (m), 438 (w), 422 (w), 414 (w), 411 (w), 394 (w), 387 (w).

MS (ESI): *m/z* (%): MS (ESI): *m/z* (%): 404.1 (27) $[M+2]^+$, 403.1 (95) $[M+1]^+$, 402.1 (21) $[M]^+$, HRMS (ESI): *m/z* calcd for $C_{26}H_{26}O_4$: 402.1831 $[M]^+$; found: 402.1754.

2,5-Diphenethylterephthalic acid (163)

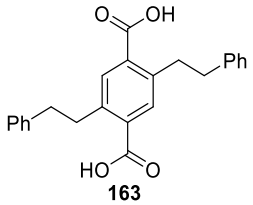

163

To a solution of **162** (2.00 g, 4.97 mmol, 1.00 eq.) in 100 mL EtOH was added NaOH (2.23 g, 55.7 mmol, 11.2 eq.) and refluxed for 16 h. After cooling to rt, the solvent was removed under reduced pressure. The obtained residue was acidified with a 10% aqueous HCl solution. The formed precipitate was filtered, washed with water and small amount of *n*-hexane, and dried under reduced pressure to yield **163** (1.85 g, 4.93 mmol, 99%) as a white solid.

^{1}H NMR (400 MHz, DMSO-*d6*): δ (ppm) 13.19 (s, 2H, COOH), 7.73 (s, 2H, H-Ar), 7.31 – 7.23 (m, 8H, H-Ar), 7.21 – 7.16 (m, 2H, H-Ar), 3.20 – 3.10 (m, 4H, CH_2), 2.86 – 2.75 (m, 4H, CH_2).

^{13}C NMR (100 MHz, DMSO-*d6*): δ (ppm) 168.4 (COOH), 141.7 (C), 140.0 (C), 133.2 (C), 132.5 (CH), 128.4 (CH), 126.0 (CH), 37.4 (CH_2), 35.5 (CH_2).

IR (ATR) $\tilde{\nu}$ (cm^{-1}) = 3084 (w), 3063 (w), 3024 (w), 3000 (w), 2992 (w), 2980 (w), 2929 (w), 2907 (w), 2893 (w), 2866 (w), 2800 (w), 2741 (w), 2643 (w), 2578 (w), 2544 (w), 2530 (w), 2520 (w), 2468 (w), 1693 (vs), 1680 (vs), 1602 (w), 1494 (m), 1453 (w), 1408 (m), 1383 (w), 1316 (w), 1283 (vs), 1251 (vs), 1196 (m), 1156 (w), 1139 (m), 1118 (w), 1072 (w), 1028 (w), 939 (m), 918 (s), 805 (w), 786 (m), 765 (s), 739 (s), 696 (vs), 618 (w), 565 (m), 545 (w), 516 (w), 497 (m), 483 (m), 441 (w), 428 (w), 421 (w), 412 (w), 398 (w), 388 (w).

MS (ESI): *m/z* (%): 376.2 (1) $[M+2]^+$, 375.1 (1) $[M+1]^+$, 374.3 (2) $[M]^+$, HRMS (ESI): *m/z* calcd for $C_{24}H_{22}O_4$: 374.1518 $[M]^+$; found: 374.3626.

7,8,15,16-Tetrahydrobisbenzo[4,5]cyclohepta[1,2-a:1',2'-d]-benzene-5,13-dione (157)

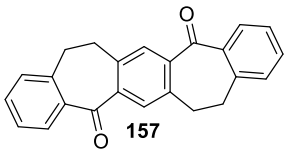

157

Variant A:

Following a published protocol,[155] polyphosphoric acid (6.00 g, 2.91 mL, 61.2 mmol, 229 eq.) was added to 2,5-bis(2-phenylethyl)terephthalic acid (**163**; 100 mg, 267 µmol, 1.00 eq.) and stirred at 155 °C for 18 h. After cooling to rt, 50 mL of ice water was added to this mixture. The resulting suspension was extracted with CH_2Cl_2 and the combined organic layers washed with H_2O, $NaHCO_3$ and H_2O, respectively. After drying over Na_2SO_4, filtering and concentration under reduced pressure, the obtained crude product was purified by column chromatography (silica gel, *n*-hexane:CH_2Cl_2) to yield **157** (48.0 mg, 142 µmol, 53%) as a yellow solid. The NMR data of the product are in agreement with published data.[155]

Variant B:

Following a published procedure,[157] to **163** (1.00 g, 2.67 mmol, 1.00 eq.) in 20 mL dry CH_2Cl_2 was added 3 mL thionyl dichloride and 3 drops of dry DMF. The resulting mixture was refluxed overnight until the starting material fully dissolved. After cooling to rt, the solution was concentrated under reduced pressure and the obtained crude dissolved in 20 mL of dry CH_2Cl_2 and cooled to 0 °C. Next, $AlCl_3$ (1.42 g, 10.7 mmol, 4.00 eq.) was added to this mixture and the resulting solution stirred at rt overnight. The mixture was quenched with an aq. 10% HCl solution and extracted with CH_2Cl_2. The organic layers were washed with H_2O, dried over Na_2SO_4, filtered and concentrated under reduced pressure. The obtained crude product was purified by column chromatography (silica gel, *n*-hexane/ CH_2Cl_2 1:1) to yield **157** (865 mg, 2.56 mmol, 96%) as a yellow solid.

^{1}H NMR (400 MHz, $CDCl_3$): δ (ppm) 8.02 (dd, J = 7.9, 1.5 Hz, 2H, H-Ar), 7.87 (s, 2H, H-Ar), 7.46 (td, J = 7.4, 1.5 Hz, 2H, H-Ar), 7.34 (td, J = 7.6, 1.3 Hz, 2H, H-Ar), 7.26 – 7.23 (m, 2H, H-Ar), 3.24 (d, J = 2.3 Hz, 8H, CH_2).

Bisbenzo[4,5]cyclohepta[1,2-a:1',2'-d]benzene-5,13-dione (158)

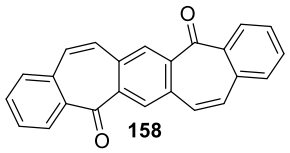

158

In slight modification to a published protocol,[155] diketone **157** (160 mg, 473 µmol, 1.00 eq.), NBS (185 mg, 1.04 mmol, 2.20 eq.) and DBPO (11.5 mg, 47.3 µmol, 0.100 eq.) in 20 mL CCl_4 was refluxed (80 °C) for 5 h. After cooling to rt, the mixture was filtered and the solvent removed under reduced pressure. The obtained crude was redissolved in 5 mL DMF and DBU (180 mg, 176 µL, 1.18 mmol, 2.50 eq.) was added while cooling to 0 °C. After warming to rt, the mixture was heated to 80 °C for 5 h, cooled to rt, diluted with water and the formed precipitate filtered. The obtained crude product was dried and purified by column chromatography (silica gel, *n*-hexane/CH_2Cl_2 2:1 -> 1:3). Recrystallization by toluene yielded **158** (73.0 mg, 218 µmol, 46%) as yellow crystals. The NMR data of the product are in agreement with published data.[155]

^{1}H NMR (400 MHz, $CDCl_3$): δ (ppm) 8.41 (s, 2H, H-Ar), 8.25 (dd, *J* = 8.2, 1.5 Hz, 2H, H-Ar), 7.67 (dd, *J* = 7.2, 1.6 Hz, 2H, H-Ar), 7.60 – 7.55 (m, 4H, H-Ar), 7.22 (d, *J* = 12.1 Hz, 2H, H-Ar), 7.12 (d, *J* = 12.1 Hz, 2H, H-Ar).

Diol (164)

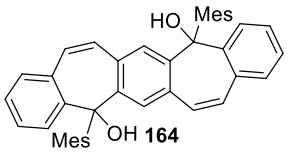

164

Following a published method,[155] *n*-BuLi (1,6M in THF; 69.0 mg, 673 µL, 1.08 mmol, 6.00 eq.) was added to a solution of 2-bromo-1,3,5-trimethylbenzene (214 mg, 162 µL, 1.08 mmol, 6.00 eq.) in 10 mL dry THF at −78 °C under an argon atmosphere and stirred for 1 h at −78 °C. To this mixture was added diketone **158** (60.0 mg, 179 µmol, 1.00 eq.) under an argon atmosphere and the resulting mixture allowed to warm to rt. After stirring for 5 h at rt, the reaction mixture was quenched with water and extracted with Et_2O. The combined organic layers were washed with brine, dried over Na_2SO_4, filtered and concentrated under reduced pressure. The obtained residue was purified by column chromatography (silica gel, *n*-hexane/Et_2O 10:1 -> 3:1) to yield **164** (132 mg, 230 µmol, quant.) as a yellow solid. The product was obtained as a mixture of isomers; reasonable NMR spectra could thus not be measured. The product was confirmed by mass spectrometry.

R_f = 0.40 (*n*-hexane/Et_2O 10:1).

MS (ESI): *m/z* (%): 574.2 (2) $[M]^+$, 573.2 (4) $[M-1]^+$, 571.2 (1) $[M-3]^+$, HRMS (ESI): *m/z* calcd for $C_{42}H_{38}O_2$: 574.2872 $[M]^+$; found: 574.2816.

Dimethyl 2-amino-3-bromoterephthalate (167)

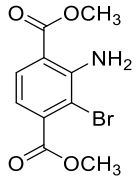

167

Following a published protocol,[93] acetic acid (151 mg, 144 µL, 2.51 mmol, 1.05 eq.) and NBS 425 mg, 2.39 mmol, 1.00 eq.) were added to a solution of dimethyl 2-aminobenzene-1,4-dicarboxylate (**166**; 500 mg, 2.39 mmol, 1.00 eq.) in toluene (50 mL) and stirred for 96 h at rt. Aq. $NaHCO_3$ solution was added to the mixture, the layers separated, and the aq. layer extracted with EtOAc. The combined organic layers were washed with a sat. brine solution, dried over Na_2SO_4 and concentrated under reduced pressure. The crude product was purified by column chromatography (silica gel, *n*-hexane/Et_2O 10:1) to yield **167** (213 mg, 741 µmol, 31%) as a yellow solid. The obtained data are in agreement with published data.[93]

^1H NMR (400 MHz, $CDCl_3$): δ (ppm) 7.9 (d, J = 8.3 Hz, 1H, H-Ar), 6.9 (d, J = 8.3 Hz, 1H, H-Ar), 6.6 (s, 2H, NH_2), 3.9 (s, 3H, CH_3), 3.9 (s, 3H, CH_3).

Dimethyl 2-bromo-3-iodoterephthalate (168)

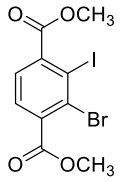

168

Following a published protocol,[93] a solution of $NaNO_2$ (128 mg, 1.85 mmol, 2.50 eq.) in 5 mL H_2O was added dropwise to a cooled (0 °C) suspension of dimethyl 2-amino-3-bromobenzene-1,4-dicarboxylate (**167**; 213 mg, 741 µmol, 1.00 eq.) in a mixture of conc. HCl and H_2O (1:1 5 mL) and stirred for 30 min. Subsequently, the mixture was added slowly to a cooled (0 °C) solution of KI (738 mg, 4.44 mmol, 6.00 eq.) in 10 mL H_2O and stirred vigorously for 18 h at rt. $Na_2S_2O_3$ was added to the mixture until the color vanished followed by the addition of EtOAc. The organic layer was separated and the aqueous layer extracted with EtOAc. The combined organic layers were washed with saturated aqueous $NaHCO_3$ solution, brine and dried over Na_2SO_4. The solvent was removed under reduced pressure and the crude product purified by column chromatography (silica gel, *n*-hexane/EtOAc 6:1->5:1) to yield **168** (141 mg, 353 µmol, 48%) as a yellow solid. The obtained data is in agreement with published data.[93]

^{1}H NMR (400 MHz, $CDCl_3$): δ (ppm) 7.6 (s, 1H, H-Ar), 7.5 (d, J = 7.8 Hz, 1H, H-Ar), 4.0 (s, 3H, $COCH_3$), 3.9 (s, 3H, $COCH_3$).

6.4 Calculated UV/Vis Data

The calculated data for radical **40** (**Table 8**) indicate a vanishingly small calculated absorption at 1201 nm (1.03 eV, oscillator strength f = 0.0002) which is mainly due to a SOMO → LUMO (94%) transition of the β spin. A weak absorption at 825 nm, which is similarly visible in the measured spectrum, (1.50 eV, f = 0.027) can be attributed to the H–1 → LUMO transition of the α spin and the SOMO → L+1 transition of the β spin. Pronounced absorptions at 736 nm (1.68 eV, f = 0.36), 678 nm (1.83 eV, f = 0.58) and 403 nm (3.08 eV, f = 0.12) can essentially be ascribed to transitions of the α spin (SOMO → LUMO, 42%; H–1 → LUMO, 19%; and SOMO → L+2, 27%) and of the β spin (H–1 → LUMO, 19%; SOMO → L+1, 18%; H–1 → L+2, 17%). A similar trend is observed for radical **41** (**Table 8**): A barely existing calculated absorption at 1107 nm (1.12 eV, f = 0.0000) is mainly due to SOMO → LUMO transition (94%) of the β spin. A weak absorption at 792 nm (1.56 eV, f = 0.06) induced by H–1 → LUMO transition (61%) of the α spin and SOMO → L+1 transition (23%) of the β spin is hardly visible in the measured spectra due to the broad absorption in this region. Again, a pronounced absorption at 754 nm (1.64 eV, f = 0.55) can be assigned to SOMO → LUMO transition (94%) of the α spin and H–1 → LUMO transition (16%) of the β spin. There is hardly any visible contribution of the mesityl groups in these low energy transitions; only π-orbitals of the nonacyclic core are involved here.

Table 6: Calculated absorptions and their corresponding transitions for compounds **40** (top) and **41** (bottom)

Calculated transition of 40				
Energy [eV]	**Wavelength [nm]**	**Oscillator strength, *f***	**Transition *α* spin**	**Transition β spin**
1.03	1201	0.0002	–	SOMO → LUMO (94%) H−2 → L+1 (3%)
1.50	825	0.027	H−1 → LUMO (33%)	SOMO → L+1 (26%)
1.68	736	0.36	H−1 → LUMO (33%) SOMO → LUMO (42%)	H−1 → LUMO (14%) SOMO → L+1 (3%)
1.83	678	0.58	H−1 → LUMO (19%) SOMO → LUMO (15%) H−1 → L+1 (3%)	H−2 → LUMO (21%) H−1 → LUMO (19%) SOMO → L+1 (18%)
3.08	403	0.12	H−2 → L+1 (23%) SOMO → L+2 (27%)	H−1 → L+2 (17%) H−2 → L+1 (9%)
3.21	387	0.88	H−1 → L+1 (18%)	SOMO → L+2 (30%)
3.26	380	0.95	H−1 → L+1 (19%)	SOMO → L+2 (21%)
Calculated transition of				
Energy [eV]	**Wavelength [nm]**	**Oscillator strength, *f***	**Transition α spin**	**Transition β spin**
1.12	1107	0.0000	–	SOMO → LUMO (94%) H–2 → L+1 (3%)
1.56	792	0.06	H–1 → LUMO (61%)	SOMO → L+1 (23%)
1.64	754	0.55	H–1 → LUMO (17%) SOMO → LUMO (57%)	H–1 → LUMO (16%)
1.90	652	0.51	H–1 → LUMO (18%)	H–2 → LUMO (14%) H–1 → LUMO (15%) SOMO → L+1 (38%)
3.27	378	0.14	H–1 → L+1 (3%) SOMO → L+1 (3%) SOMO → L+3 (5%)	SOMO → L+2 (6%)
3.38	366	1.34	H–1 → L+1 (22%)	H–3 → L+1 (10%) SOMO → L+2 (26%)
3.40	365	1.00	H–1 → L+1 (16%)	SOMO → L+2 (18%)

6.5 XRD Data

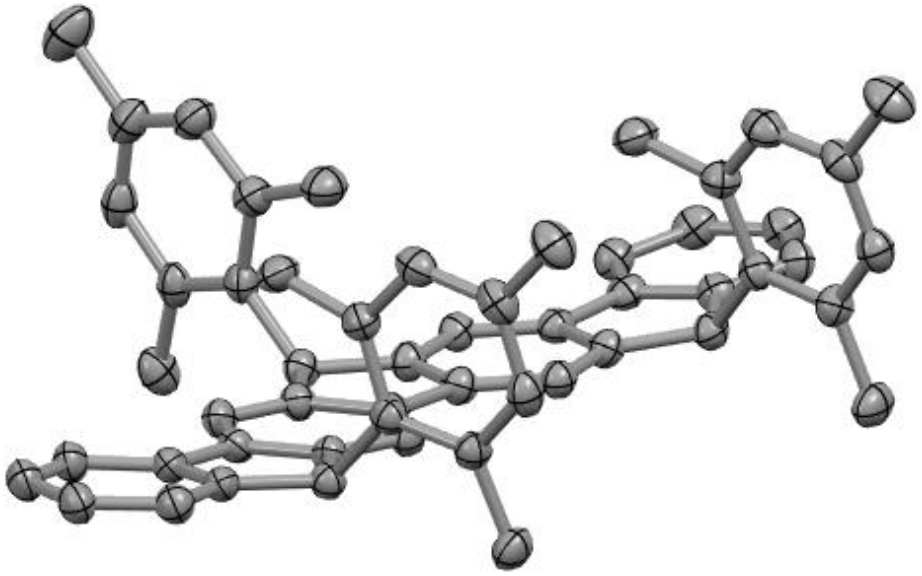

Compound	**all-*cis*-39·$CHCl_3$**
CCDC #	2406041
empirical formula	$C_{55}H_{49}Cl_3$
formula weight	816.29
temperature/K	180
crystal system	orthorhombic
space group	$Pca2_1$
a / Å	17.3253(4)
b / Å	11.0231(3)
c / Å	22.1754(7)
α / °	90
β / °	90
γ / °	90
volume / $Å^3$	4235.0(2)
Z	4
P_{calc} / g/cm^3	1.280
μ / mm^{-1}	1.461
F(000)	1720.0
crystal size / mm^3	0.15 × 0.117 × 0.1
radiation	Ga-Kα (λ = 1.34143 Å)
$2\Theta_{min} – 2\Theta_{max}$ / °	6.936 to 124.994

reflections collected	42210
independent reflections	10115
R_{int}	0.0437
R_{sigma}	0.0280
data/restraints/parameters	10115/1/533
GooF	1.020
R_1	0.0898
wR_2	0.2443
R_1(all)	0.1107
wR_2(all)	0.2641
ρ_{e-} max/ρ_{e-} min / e Å^{-3}	0.61/-0.89

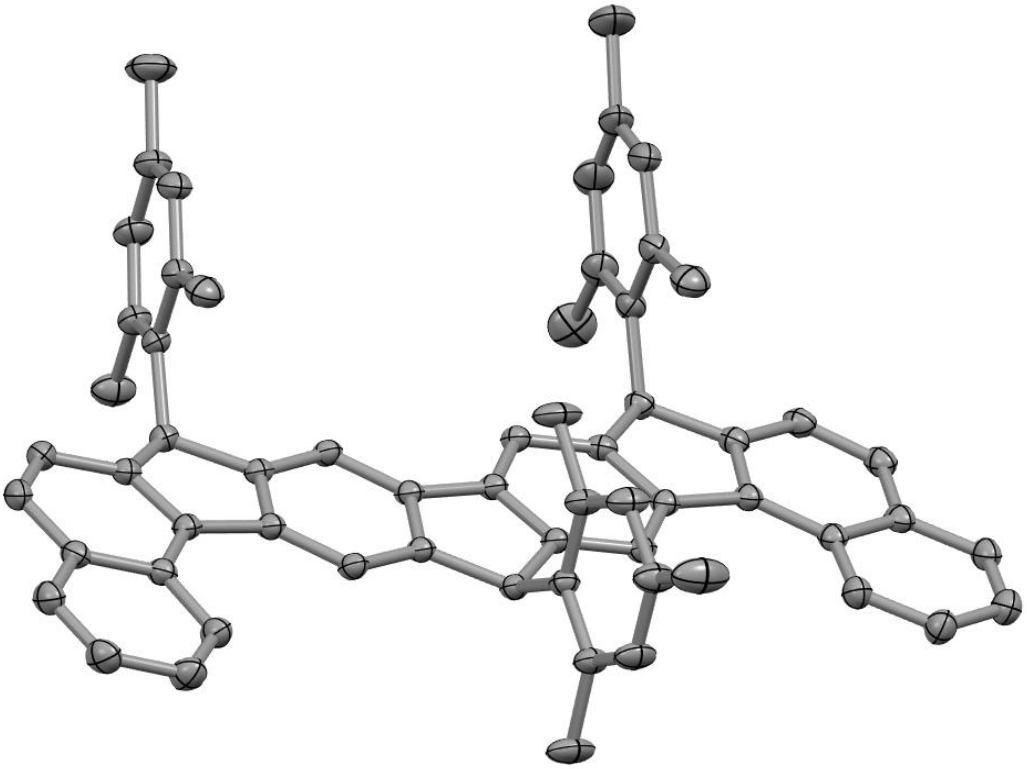

Compound	**40**
CCDC #	2454301
empirical formula	$C_{69}H_{60}$ (**40**·toluene)
formula weight	889.17
temperature/K	150
crystal system	triclinic
space group	$P\bar{1}$
a / Å	15.5622(3)
b / Å	19.2581(5)
c / Å	19.6678(4)
α / °	114
β / °	90
γ / °	106
volume / Å^3	5120.7(2)
Z	4
P_{calc} / g/cm^3	1.153
μ / mm^{-1}	0.27

$F(000)$	1896.0
crystal size / mm^3	0.15 × 0.09 × 0.00
radiation	Ga-Kα (λ = 1.34143 Å)
$2\Theta_{min} – 2\Theta_{max}$ / °	4.314 to 119.996
reflections collected	79575
independent reflections	22795
R_{int}	0.0405
R_{sigma}	0.0386
data/restraints/parameters	22795/24/1220
GooF	1.071
R_1	0.0521
wR_2	0.1421
R_1(all)	0.0791
wR_2(all)	0.1553
ρ_{e-} max/ρ_{e-} min / e $Å^{-3}$	0.18/–0.23

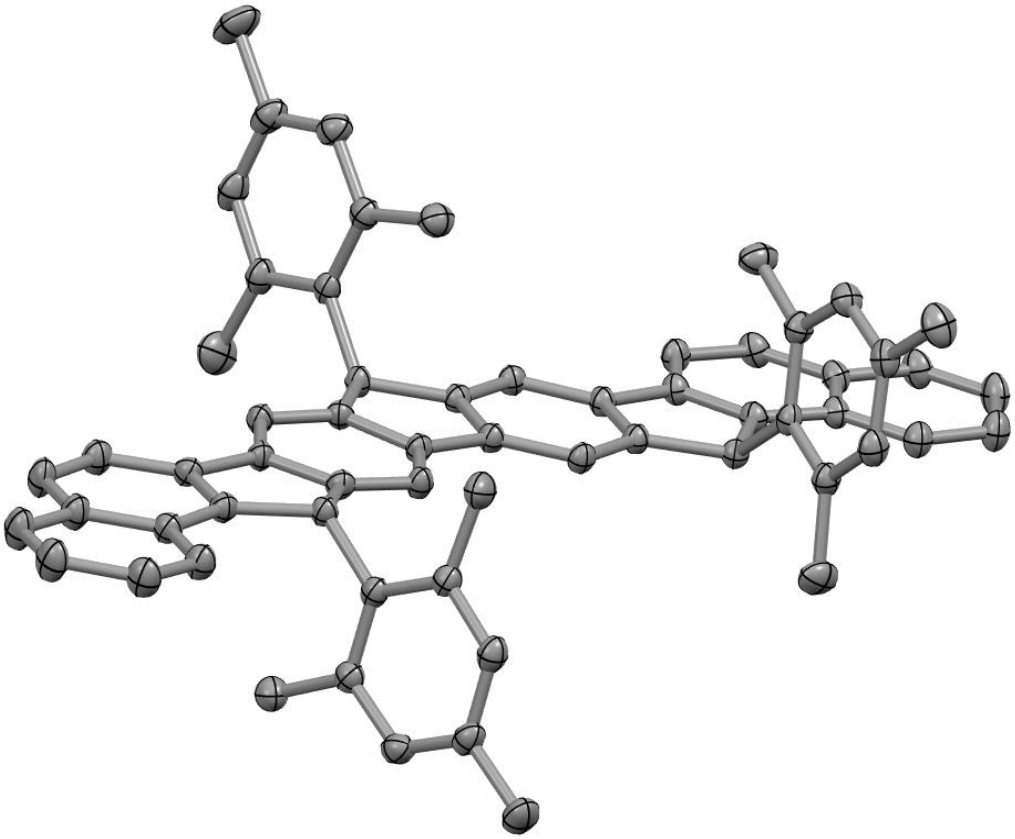

Compound	**41**
CCDC #	2454300
empirical formula	$C_{76}H_{68}$ (**41**·toluene)
formula weight	981.3
temperature/K	150
crystal system	monoclinic
space group	$P2_1/c$
a / Å	12.4754(7)
b / Å	27.6562(16)
c / Å	14.9989(10)
α / °	90
β / °	92
γ / °	90
volume / Å^3	5170.9(5)
Z	4
P_{calc} / g/cm^3	1.261
μ / mm^{-1}	0.27

$F(000)$	2096.0
crystal size / mm^3	0.15 × 0.117 × 0.10
radiation	Ga-Kα (λ = 1.34143 Å)
$2\Theta_{min} – 2\Theta_{max}$ / °	6.168 to 124.994
reflections collected	43090
independent reflections	12229
R_{int}	0.0357
R_{sigma}	0.0346
data/restraints/parameters	12229/0/568
GooF	1.075
R_1	0.0484
wR_2	0.1473
R_1(all)	0.0726
wR_2(all)	0.1606
ρ_{e-} max/ρ_{e-} min / e $Å^{-3}$	0.28/–0.22

7 Abbreviation Index

Å	Ångström
Ac	Acetyl
ACID	Anisotropy of the Induced Current Density
aq.	Aqueous
conc.	Concentrated
CP-PAH	Cyclopenta-fused Polycyclic Aromatic Hydrocarbon
CV	Cyclic Voltammetry
Cw	Continuous wave
DBPO	Benzoyl peroxide
DDQ	2,3-Dichloro-5,6-dicyano-1,4-benzoquinone
DFT	Density Functional Theory
DMAP	4-Dimethylaminopyridine
DMF	Dimethylformamide
DMSO	Dimethyl sulfoxide
EI	Electron ionization
EPR	Electron Paramagnetic Resonance
Eq.	Equivalent
Et	Ethyl
et al.	Et alii
EtOAc	Ethyl acetate
ESI	Electrospray ionization
eV	Electronvolt
e.g.	exempli gratia
FAB	Fast Atom Bombardment
Fc/Fc^+	Ferrocene/Ferrocenium
FET	Field-effect transistors
GGA	Generalized Gradient Approximation
HF	*Hartree Fock*
HOMO	Highest Occupied Molecular Orbital
HONO	Highest Occupied Natural Orbital
HOMA	Harmonic Oscillator Model of Aromaticity

HPLC	High-Performance Liquid Chromatography
HRMS	High Resolution Mass Spectrometry
Hz	Hertz
IF	Indenofluorene
IR	Infrared
LCAO	Linear Combination of Atomic Orbitals
LDA	Local Density Approximation / Lithium diisopropylamide
LUMO	Lowest Unoccupied Molecular Orbital
LUNO	Lowest Unoccupied Natural Orbital
Mes	Mesitylene
MO	Molecular Orbital
MS	Mass spectrometry
NBO	Natural Bond Orbital
NBS	*N*-Bromosuccinimide
NICS	Nucleus-Independent Chemical Shift
NIR	Near-infrared spectroscopy
nm	Nanometer
NMR	Nuclear Magnetic Resonance Spectroscopy
NO	Natural orbital
NOON	Natural Orbital Occupation Number
Norm.	Normalized
OLED	Organic Light-Emitting Diodes
OPV	Organic Photovoltaic Cells
PA	Polyarenes
PAH	Polycyclic Aromatic Hydrocarbon
Ph	Phenyl
ppm	parts per million
QDM	Quinodimethane
s	Symmetric
Sat.	Saturated
SCF	Self-Consistent Field
SOMO	Singly Occupied Molecular Orbital
STO	*Slater*-type Orbital

TD	Time-dependent
TLC	Thin Layer Chromatography
UHF	Unrestricted *Hartree-Fock*
UV	Ultraviolet
Vis	Visible

8 References

[1] R. G. Harvey, *Polycyclic aromatic hydrocarbons: chemistry and carcinogenicity*, CUP Archive, **1991**.
[2] E. Clar, R. Schoental, *Polycyclic hydrocarbons, Vol. 1*, Springer, **1964**.
[3] K.-H. Kim, S. A. Jahan, E. Kabir, R. J. C. Brown, *Environ. Int.* **2013**, *60*, 71-80.
[4] J. Wu, W. Pisula, K. Müllen, *Chem. Rev.* **2007**, *107*, 718-747.
[5] M. Iyoda, J. Yamakawa, M. J. Rahman, *Angew. Chem. Int. Ed.* **2011**, *50*, 10522-10553.
[6] T. J. Müller, U. H. Bunz, *Functional organic materials: syntheses, strategies and applications*, John Wiley & Sons, **2007**.
[7] Y.-T. Wu, J. S. Siegel, *Polyarenes I* **2014**, 63-120.
[8] R. Zahradník, *Angew. Chem. Int. Ed. Engl.* **1965**, *4*, 1039-1050.
[9] D. Peters, *J. Chem. Soc.* **1958**, 1023-1028.
[10] D. Peters, *J. Chem. Soc.* **1958**, 1028-1039.
[11] B. Pigulski, K. Shoyama, F. Würthner, *Angew. Chem. Int. Ed.* **2020**, *59*, 15908-15912.
[12] J. Reinhold, *Quantentheorie der Moleküle: Eine Einführung*, Springer, **2006**.
[13] Y. Tobe, *Chem. Rec.* **2015**, *15*, 86-96.
[14] K. Müllen, U. Scherf, *Organic light emitting devices: synthesis, properties and applications*, John Wiley & Sons, **2006**.
[15] M. M. Haley, R. R. Tykwinski, *Carbon-rich compounds: from molecules to materials*, John Wiley & Sons, **2006**.
[16] J. E. Anthony, A. Facchetti, M. Heeney, S. R. Marder, X. Zhan, *Adv. Mater.* **2010**, *22*, 3876-3892.
[17] M. Bendikov, F. Wudl, D. F. Perepichka, *Chem. Rev.* **2004**, *104*, 4891-4946.
[18] J. E. Anthony, *Chem. Rev.* **2006**, *106*, 5028-5048.
[19] J. E. Anthony, *Angew. Chem. Int. Ed.* **2008**, *47*, 452-483.
[20] P. Herwig, C. W. Kayser, K. Müllen, H. W. Spiess, *Adv. Mater.* **1996**, *8*, 510-513.
[21] M. Kastler, W. Pisula, D. Wasserfallen, T. Pakula, K. Müllen, *J. Am. Chem. Soc.* **2005**, *127*, 4286-4296.
[22] F. L. De La Puente, J.-F. Nierengarten, *Fullerenes: principles and applications*, Royal Society of Chemistry, **2011**.
[23] A. Shimizu, S. Nobusue, H. Miyoshi, Y. Tobe, *Pure and Applied Chemistry* **2014**, *86*, 517-528.
[24] A. G. Fix, D. T. Chase, M. M. Haley, in *Polyarenes I* (Eds.: J. S. Siegel, Y.-T. Wu), Springer Berlin Heidelberg, Berlin, Heidelberg, **2014**, pp. 159-195.
[25] S. Gabriel, *Berichte der deutschen chemischen Gesellschaft* **1884**, *17*, 1389-1396.
[26] L. Chardonnens, R. Ritter, *Helv. Chim. Acta.* **1955**, *38*, 393-396.
[27] L. Chardonnens, B. Laroche, W. Sieber, *Helv. Chim. Acta.* **1974**, *57*, 585-599.
[28] L. Chardonnens, J. Häger, *Helv. Chim. Acta.* **1974**, *57*, 1472-1477.
[29] L. Chardonnens, S. Bitsch, J. Häger, *Helv. Chim. Acta.* **1975**, *58*, 503-507.
[30] S. Merlet, M. Birau, Z. Y. Wang, *Org. Lett.* **2002**, *4*, 2157-2159.
[31] C. Weizmann, E. Bergmann, L. Haskelberg, *J. Chem. Soc.* **1939**, 391-397.
[32] W. Deuschel, *Helv. Chim. Acta.* **1951**, *34*, 2403-2416.
[33] Y. Altman, D. Ginsburg, *J. Chem. Soc.* **1961**, 1498-1505.
[34] H. Usta, A. Facchetti, T. J. Marks, *Org. Lett.* **2008**, *10*, 1385-1388.

[35] H. Usta, A. Facchetti, T. J. Marks, *J. Am. Chem. Soc.* **2008**, *130*, 8580-8581.
[36] H. Usta, C. Risko, Z. Wang, H. Huang, M. K. Deliomeroglu, A. Zhukhovitskiy, A. Facchetti, T. J. Marks, *J. Am. Chem. Soc.* **2009**, *131*, 5586-5608.
[37] J. E. Anthony, J. S. Brooks, D. L. Eaton, S. R. Parkin, *J. Am. Chem. Soc.* **2001**, *123*, 9482-9483.
[38] J. E. Anthony, D. L. Eaton, S. R. Parkin, *Org. Lett.* **2002**, *4*, 15-18.
[39] A. Vollmer, H. Weiss, S. Rentenberger, I. Salzmann, J. P. Rabe, N. Koch, *Surf. Sci.* **2006**, *600*, 4004-4007.
[40] Q. Miao, T.-Q. Nguyen, T. Someya, G. B. Blanchet, C. Nuckolls, *J. Am. Chem. Soc.* **2003**, *125*, 10284-10287.
[41] D. T. Chase, B. D. Rose, S. P. McClintock, L. N. Zakharov, M. M. Haley, *Angew. Chem. Int. Ed.* **2011**, *50*, 1127-1130.
[42] G. I. Warren, K. Młodzikowska-Pieńko, S. Jalife, I. S. Demachkie, J. I. Wu, M. M. Haley, R. Gershoni-Poranne, *Chem. Sci.* **2025**, *16*, 575-583.
[43] C. Poriel, J.-J. Liang, J. Rault-Berthelot, F. Barrière, N. Cocherel, A. M. Z. Slawin, D. Horhant, M. Virboul, G. Alcaraz, N. Audebrand, L. Vignau, N. Huby, G. Wantz, L. Hirsch, *Chem. Eur. J.* **2007**, *13*, 10055-10069.
[44] C.-P. Chen, S.-H. Chan, T.-C. Chao, C. Ting, B.-T. Ko, *J. Am. Chem. Soc.* **2008**, *130*, 12828-12833.
[45] N. Cocherel, C. Poriel, J. Rault-Berthelot, F. Barrière, N. Audebrand, A. M. Z. Slawin, L. Vignau, *Chem. Eur. J.* **2008**, *14*, 11328-11342.
[46] W. Zhang, J. Smith, R. Hamilton, M. Heeney, J. Kirkpatrick, K. Song, S. E. Watkins, T. Anthopoulos, I. McCulloch, *J. Am. Chem. Soc.* **2009**, *131*, 10814-10815.
[47] W. Zhang, J. Smith, S. E. Watkins, R. Gysel, M. McGehee, A. Salleo, J. Kirkpatrick, S. Ashraf, T. Anthopoulos, M. Heeney, I. McCulloch, *J. Am. Chem. Soc.* **2010**, *132*, 11437-11439.
[48] W. S. Trahanovsky, S. P. Lorimor, *J. Org. Chem.* **2006**, *71*, 1784-1794.
[49] T. Kubo, *Chem. Lett.* **2014**, *44*, 111-122.
[50] A. E. Tschitschibabin, *Berichte der deutschen chemischen Gesellschaft* **1907**, *40*, 1810-1819.
[51] C. K. Frederickson, B. D. Rose, M. M. Haley, *Acc. Chem. Res.* **2017**, *50*, 977-987.
[52] Q. Zhou, P. J. Carroll, T. M. Swager, *J. Org. Chem.* **1994**, *59*, 1294-1301.
[53] H. Reisch, U. Wiesler, U. Scherf, N. Tuytuylkov, *Macromol.* **1996**, *29*, 8204-8210.
[54] A. Shimizu, M. Uruichi, K. Yakushi, H. Matsuzaki, H. Okamoto, M. Nakano, Y. Hirao, K. Matsumoto, H. Kurata, T. Kubo, *Angew. Chem. Int. Ed.* **2009**, *48*, 5482-5486.
[55] S. Moles Quintero, M. M. Haley, M. Kertesz, J. Casado, *Angew. Chem. Int. Ed.* **2022**, *61*, e202209138.
[56] J. J. Dressler, A. Cárdenas Valdivia, R. Kishi, G. E. Rudebusch, A. M. Ventura, B. E. Chastain, C. J. Gómez-García, L. N. Zakharov, M. Nakano, J. Casado, M. M. Haley, *Chem* **2020**, *6*, 1353-1368.
[57] R. Nieman, N. J. Silva, A. J. A. Aquino, M. M. Haley, H. Lischka, *J. Org. Chem.* **2020**, *85*, 3664-3675.
[58] J. E. Barker, J. J. Dressler, A. Cárdenas Valdivia, R. Kishi, E. T. Strand, L. N. Zakharov, S. N. MacMillan, C. J. Gómez-García, M. Nakano, J. Casado, M. M. Haley, *J. Am. Chem. Soc.* **2020**, *142*, 1548-1555.
[59] J. E. Barker, C. K. Frederickson, M. H. Jones, L. N. Zakharov, M. M. Haley, *Org. Lett.* **2017**, *19*, 5312-5315.

[60] M. Gomberg, *J. Am. Chem. Soc.* **1900**, *22*, 757-771.
[61] S. Leisering, C. A. Schalley, *Tutorium Reaktivität und Synthese*, Springer, **2017**.
[62] U. Neuenschwander, I. Hermans, *J. Catal.* **2012**, *287*, 1-4.
[63] A. Shimizu, T. Kubo, M. Uruichi, K. Yakushi, M. Nakano, D. Shiomi, K. Sato, T. Takui, Y. Hirao, K. Matsumoto, *J. Am. Chem. Soc.* **2010**, *132*, 14421-14428.
[64] A. Konishi, Y. Hirao, M. Nakano, A. Shimizu, E. Botek, B. Champagne, D. Shiomi, K. Sato, T. Takui, K. Matsumoto, *J. Am. Chem. Soc.* **2010**, *132*, 11021-11023.
[65] A. Shimizu, R. Kishi, M. Nakano, D. Shiomi, K. Sato, T. Takui, I. Hisaki, M. Miyata, Y. Tobe, *Angew. Chem. Int. Ed.* **2013**, *52*, 6076-6079.
[66] D. Doehnert, J. Koutecky, *J. Am. Chem. Soc.* **1980**, *102*, 1789-1796.
[67] K. Yamaguchi, *Chem. Phys. Lett.* **1975**, *33*, 330-335.
[68] M. Nakano, *Chem. Rec.* **2017**, *17*, 27-62.
[69] A. Das, T. Müller, F. Plasser, H. Lischka, *J. Phys. Chem. A.* **2016**, *120*, 1625-1636.
[70] K. Kamada, K. Ohta, A. Shimizu, T. Kubo, R. Kishi, H. Takahashi, E. Botek, B. Champagne, M. Nakano, *J. Phys. Chem. Lett.* **2010**, *1*, 937-940.
[71] C. C. J. Roothaan, *Rev. Mod. Phys.* **1951**, *23*, 69-89.
[72] J. A. Pople, R. K. Nesbet, *J. Chem. Phys.* **1954**, *22*, 571-572.
[73] T. Stuyver, B. Chen, T. Zeng, P. Geerlings, F. De Proft, R. Hoffmann, *Chem. Rev.* **2019**, *119*, 11291-11351.
[74] X. Yang, D. Zhang, Y. Liao, D. Zhao, *J. Org. Chem.* **2020**, *85*, 5761-5770.
[75] A. R. Birge, M. J. Piper, K. J. Painter, G. T. Sazama, *Results in Chemistry* **2022**, *4*, 100393.
[76] X. Zhang, Z. Tong, S. Dong, *Chin. J. Chem.* **2025**, *43*, 536-542.
[77] T. Nishinaga, *Organic redox systems: Synthesis, Properties, and applications*, John Wiley & Sons, **2015**.
[78] D. Griller, K. U. Ingold, *Acc. Chem. Res.* **1976**, *9*, 13-19.
[79] Q. Miao, *Polycyclic arenes and heteroarenes: synthesis, properties, and applications*, John Wiley & Sons, **2015**.
[80] K. Fukuda, J.-y. Fujiyoshi, H. Matsui, T. Nagami, S. Takamuku, Y. Kitagawa, B. Champagne, M. Nakano, *Org. Chem. Front.* **2017**, *4*, 779-789.
[81] H. Yeo, S. Debnath, B. P. Krishnan, B. W. Boudouris, *RSC Appl. Polym.* **2024**, *2*, 7-25.
[82] M. Deumal, S. Vela, M. Fumanal, J. Ribas-Arino, J. J. Novoa, *J. Mater. Chem. C* **2021**, *9*, 10624-10646.
[83] C. Nicolaides, F. Bazzi, E. Vouros, D. F. Flesariu, N. Chrysochos, P. A. Koutentis, C. P. Constantinides, T. Trypiniotis, *Nano Lett.* **2023**, *23*, 4579-4586.
[84] K. Kato, A. Osuka, *Angew. Chem. Int. Ed.* **2019**, *58*, 8978-8986.
[85] N. Jux, Y. Rubin, K. Holczer, *Angew. Chem. Int. Ed. Engl.* **1996**, *35*, 1986-1990.
[86] K. Ogawa, K. Komatsu, T. Kitagawa, *J. Org. Chem.* **2011**, *76*, 6095-6100.
[87] Z. Zeng, Y. M. Sung, N. Bao, D. Tan, R. Lee, J. L. Zafra, B. S. Lee, M. Ishida, J. Ding, J. T. López Navarrete, Y. Li, W. Zeng, D. Kim, K.-W. Huang, R. D. Webster, J. Casado, J. Wu, *J. Am. Chem. Soc.* **2012**, *134*, 14513-14525.
[88] C. Harnack, W. Krull, M. Lehnig, W. P. Neumann, A. K. Zarkadis, *J. Chem. Soc.* **1994**, 1247-1252.
[89] B. Liu, T. Yoshida, X. Li, M. Stępień, H. Shinokubo, P. J. Chmielewski, *Angew. Chem. Int. Ed.* **2016**, *55*, 13142-13146.
[90] C. Koelsch, *J. Am. Chem. Soc.* **1957**, *79*, 4439-4441.

[91] K. Goto, T. Kubo, K. Yamamoto, K. Nakasuji, K. Sato, D. Shiomi, T. Takui, M. Kubota, T. Kobayashi, K. Yakusi, J. Ouyang, *J. Am. Chem. Soc.* **1999**, *121*, 1619-1620.
[92] T. Kubo, Y. Katada, A. Shimizu, Y. Hirao, K. Sato, T. Takui, M. Uruichi, K. Yakushi, R. C. Haddon, *J. Am. Chem. Soc.* **2011**, *133*, 14240-14243.
[93] S. Herzog, A. Hinz, F. Breher, J. Podlech, *Org. Biomol. Chem.* **2022**, *20*, 2873-2880.
[94] A. S. Acan, J. O. Wenzel, F. Breher, J. Podlech, *Chem. Eur. J.* **2025**, *31*, e202403670.
[95] M. Solà, A. I. Boldyrev, M. K. Cyrañski, T. M. Krygowski, G. Merino, **2022**.
[96] G. Merino, M. Solà, I. Fernández, C. Foroutan-Nejad, P. Lazzeretti, G. Frenking, H. L. Anderson, D. Sundholm, F. P. Cossío, M. A. Petrukhina, J. Wu, J. I. Wu, A. Restrepo, *Chem. Sci.* **2023**, *14*, 5569-5576.
[97] M. Faraday, *Philos. Trans. Royal Soc.* **1825**, 440-466.
[98] E. Hückel, *Z. Phys.* **1931**, *70*, 204-286.
[99] R. BRESLOW, *Chemical & Engineering News Archive* **1965**, *43*, 90-100.
[100] R. Breslow, J. Brown, J. J. Gajewski, *J. Am. Chem. Soc.* **1967**, *89*, 4383-4390.
[101] M. J. S. Dewar, in *Advances in Chemical Physics*, **1965**, pp. 64-131.
[102] E. Heilbronner, *Tetrahedron Lett.* **1964**, *5*, 1923-1928.
[103] H. E. Zimmerman, *J. Am. Chem. Soc.* **1966**, *88*, 1564-1565.
[104] S. Winstein, *J. Am. Chem. Soc.* **1959**, *81*, 6524-6525.
[105] R. V. Williams, *Chem. Rev.* **2001**, *101*, 1185-1204.
[106] I. Fernández, G. Frenking, *Faraday Discussions* **2007**, *135*, 403-421.
[107] M. K. Cyrański, *Chem. Rev.* **2005**, *105*, 3773-3811.
[108] R. Gershoni-Poranne, A. Stanger, *Chem. Sci. Rev.* **2015**, *44*, 6597-6615.
[109] F. Feixas, E. Matito, J. Poater, M. Solà, *J. Comput. Chem.* **2008**, *29*, 1543-1554.
[110] J. Pople, *Mol. Phys.* **1958**, *1*, 175-180.
[111] M. Hesse, H. Meier, B. Zeeh, *(No Title)* **2008**.
[112] P. v. R. Schleyer, C. Maerker, A. Dransfeld, H. Jiao, N. J. van Eikema Hommes, *J. Am. Chem. Soc.* **1996**, *118*, 6317-6318.
[113] P. v. R. Schleyer, M. Manoharan, Z.-X. Wang, B. Kiran, H. Jiao, R. Puchta, N. J. R. van Eikema Hommes, *Org. Lett.* **2001**, *3*, 2465-2468.
[114] A. Stanger, *Eur. J. Org. Chem.* **2020**, *2020*, 3120-3127.
[115] A. Stanger, *J. Org. Chem.* **2006**, *71*, 883-893.
[116] R. Gershoni-Poranne, A. Stanger, *Chem. Eur. J.* **2014**, *20*, 5673-5688.
[117] R. Herges, D. Geuenich, *J. Phys. Chem. A* **2001**, *105*, 3214-3220.
[118] D. Geuenich, K. Hess, F. Köhler, R. Herges, *Chem. Rev.* **2005**, *105*, 3758-3772.
[119] P. Senn, *Journal of Chemical Education* **1992**, *69*, 819.
[120] T. M. Krygowski, M. K. Cyrański, *Chem. Rev.* **2001**, *101*, 1385-1420.
[121] T. M. Krygowski, *Journal of Chemical Information and Computer Sciences* **1993**, *33*, 70-78.
[122] D. Püschner, *Quantitative Rechenverfahren der Theoretischen Chemie*, Springer, **2017**.
[123] B. M. Rode, T. S. Hofer, M. D. Kugler, *The basics of theoretical and computational chemistry* **2007**.
[124] F. Jensen, *Introduction to computational chemistry*, John wiley & sons, **2017**.
[125] R. Savela, M. Majewski, R. Leino, *Eur. J. Org. Chem.* **2014**, *2014*, 4137-4147.
[126] H. Sharma, P. K. Sharma, S. Das, *Chem. Commun.* **2020**, *56*, 11319-11322.
[127] M. A. Majewski, T. Lis, J. Cybińska, M. Stępień, *Chemical Communications* **2015**, *51*, 15094-15097.

[128] H. Phan, T. S. Herng, H. Xudong, L. K. Nguyen, V. T. La, C. D. Huynh, J. Ding, J. Wu, *RSC Adv.* **2024**, *14*, 16945-16950.
[129] in *Spektroskopische Methoden in der organischen Chemie*, 9. Auflage ed. (Eds.: S. Bienz, L. Bigler, T. Fox), Thieme, **2016**.
[130] M. M. Roessler, E. Salvadori, *Chem. Sci. Rev.* **2018**, *47*, 2534-2553.
[131] J. Hioe, H. Zipse, *Org. Biomol. Chem.* **2010**, *8*, 3609-3617.
[132] T. Constantin, F. Juliá, N. S. Sheikh, D. Leonori, *Chem. Sci.* **2020**, *11*, 12822-12828.
[133] J. M. Spruell, *PAC* **2010**, *82*, 2281-2294.
[134] B. Prajapati, M. D. Ambhore, D.-K. Dang, P. J. Chmielewski, T. Lis, C. J. Gómez-García, P. M. Zimmerman, M. Stępień, *Nat. Chem.* **2023**, *15*, 1541-1548.
[135] F. Gerson, W. Huber, *Electron spin resonance spectroscopy of organic radicals*, John Wiley & Sons, **2003**.
[136] P. Karafiloglou, *J. Chem. Educ.* **1989**, *66*, 816.
[137] Q. Jiang, H. Tang, Y. Peng, Z. Hu, W. Zeng, *Chem. Sci.* **2024**, *15*, 10519-10528.
[138] H. Sharma, N. Bhardwaj, S. Das, *Org. Biomol. Chem.* **2022**, *20*, 8071-8077.
[139] J.-B. Bongui, A. Elomri, D. Cahard, F. Tillequin, ccedil, ois, B. Pfeiffer, Pierr, eacute, Alain, E. Seguin, *Chem. Pharm. Bull.* **2005**, *53*, 1540-1546.
[140] S. Staniland, R. W. Adams, J. J. W. McDouall, I. Maffucci, A. Contini, D. M. Grainger, N. J. Turner, J. Clayden, *Angew. Chem. Int. Ed.* **2016**, *55*, 10755-10759.
[141] D. Li, B. Zhao, E. J. LaVoie, *J. Org. Chem.* **2000**, *65*, 2802-2805.
[142] Z.-T. Du, J. Lu, H.-R. Yu, Y. Xu, A.-P. Li, *J. Chem. Res.* **2010**, *34*, 222-227.
[143] B. S. Kumar, K. Ravi, A. K. Verma, K. Fatima, M. Hasanain, A. Singh, J. Sarkar, S. Luqman, D. Chanda, A. S. Negi, *Bioorg. Med. Chem.* **2017**, *25*, 1364-1373.
[144] Z.-T. Du, J. Lu, H.-R. Yu, Y. Xu, A.-P. Li, *J. Chem. Res.* **2010**, *34*, 222-227.
[145] Q. Perron, A. Alexakis, *Adv. Synth. Catal.* **2010**, *352*, 2611-2620.
[146] A. S. Acan, J. O. Wenzel, J. Podlech, *Chem. Eur. J.*, *n/a*, e02467.
[147] T. Dumslaff, B. Yang, A. Maghsoumi, G. Velpula, K. S. Mali, C. Castiglioni, S. De Feyter, M. Tommasini, A. Narita, X. Feng, K. Müllen, *J. Am. Chem. Soc.* **2016**, *138*, 4726-4729.
[148] M. R. Witten, E. N. Jacobsen, *Org. Lett.* **2015**, *17*, 2772-2775.
[149] T. W. Greulich, E. Yamaguchi, C. Doerenkamp, M. Lübbesmeyer, C. G. Daniliuc, A. Fukazawa, H. Eckert, S. Yamaguchi, A. Studer, *Chem. Eur. J.* **2017**, *23*, 6029-6033.
[150] F. R. Leroux, R. Simon, N. Nicod, *Lett. Org. Chem.* **2006**, *3*, 948-954.
[151] R. Holzwarth, R. Bartsch, Z. Cherkaoui, G. Solladié, *Eur. J. Org. Chem.* **2005**, *2005*, 3536-3541.
[152] R. Huisgen, J. Sauer, *Angew. Chem.* **1960**, *72*, 91-108.
[153] I. Agranat, D. Avnir, *J. Am. Chem. Soc.* **1974**, 1155-1161.
[154] X. Yang, X. Shi, N. Aratani, T. P. Gonçalves, K.-W. Huang, H. Yamada, C. Chi, Q. Miao, *Chem. Sci.* **2016**, *7*, 6176-6181.
[155] X. Yang, D. Liu, Q. Miao, *Angew. Chem. Int. Ed.* **2014**, *53*, 6786-6790.
[156] C.-Y. Hsu, C.-J. Zheng, Y.-Y. Wu, W.-H. Fan, C.-H. Lin, *ACS Omega* **2022**, *7*, 21505-21527.
[157] B. Kobin, F. Bianchi, S. Halm, J. Leistner, S. Blumstengel, F. Henneberger, S. Hecht, *Adv. Funct. Mater.* **2014**, *24*, 7717-7727.
[158] Y. Tian, K. Uchida, H. Kurata, Y. Hirao, T. Nishiuchi, T. Kubo, *J. Am. Chem. Soc.* **2014**, *136*, 12784-12793.

[159] A. G. Fix, P. E. Deal, C. L. Vonnegut, B. D. Rose, L. N. Zakharov, M. M. Haley, *Org. Lett.* **2013**, *15*, 1362-1365.
[160] B. D. Rose, L. E. Shoer, M. R. Wasielewski, M. M. Haley, *Chem. Phys. Lett.* **2014**, *616-617*, 137-141.
[161] N. G. Connelly, W. E. Geiger, *Chem. Rev.* **1996**, *96*, 877-910.
[162] A. D. Zdetsis, *J. Phys. Chem. C.* **2018**, *122*, 17526-17536.
[163] G. I. Warren, J. E. Barker, L. N. Zakharov, M. M. Haley, *Org. Lett.* **2021**, *23*, 5012-5017.
[164] A. Minsky, A. Y. Meyer, M. Rabinovitz, *Tetrahedron* **1985**, *41*, 785-791.
[165] M. Nendel, B. Goldfuss, K. Houk, K. Hafner, *J. Mol. Struct.* **1999**, *461*, 23-28.
[166] K. Hafner, B. Stowasser, H.-P. Krimmer, S. Fischer, M. C. Böhm, H. J. Lindner, *Angew. Chem. Int. Ed.* **1986**, 630-632.
[167] J. D. Dunitz, C. Krüger, H. Irngartinger, E. F. Maverick, Y. Wang, M. Nixdorf, *Angew. Chem. Int. Ed. Engl.* **1988**, *27*, 387-389.
[168] W. C. Still, M. Kahn, A. Mitra, *The Journal of Organic Chemistry* **1978**, *43*, 2923-2925.
[169] J. E. Silver, C. A. Bailey, R. L. Lewis, S. R. Paeschke, *Abstr Pap Am Chem S* **2013**, *246*.
[170] R. Beckert, E. Fanghänel, K. Schwetlick, *Organikum: organisch-chemisches Grundpraktikum*, 23. ed., Wiley VCH, Weinheim, **2009**.
[171] V. Kotlyar, *J. Org. Chem.* **1997**.
[172] J. Koziskova, F. Hahn, J. Richter, J. Kozisek, *Acta Chim. Slovaca* **2016**, *9*, 136.
[173] O. V. Dolomanov, L. J. Bourhis, R. J. Gildea, J. A. Howard, H. Puschmann, *J. Appl. Cryst.* **2009**, *42*, 339-341.
[174] G. Sheldrick, *Struct. Chem.* **2015**, *71*, 3.
[175] J. Koziskova, F. Hahn, J. Richter, J. Kožíšek, *Acta Chimica Slovaca* **2016**, *9*, 136-140.
[176] *Journal of Applied Crystallography* **2009**, *42*, 339--341.
[177] *Acta Crystallographica Section A* **2015**, *71*, 3--8.
[178] *Acta Crystallographica Section C* **2015**, *71*, 3--8.
[179] M. e. Frisch, G. Trucks, H. B. Schlegel, G. Scuseria, M. Robb, J. Cheeseman, G. Scalmani, V. Barone, G. Petersson, H. Nakatsuji, Gaussian, Inc. Wallingford, CT, **2016**.
[180] S. Grimme, S. Ehrlich, L. Goerigk, *J. Comput. Chem.* **2011**, *32*, 1456-1465.
[181] F. Weigend, R. Ahlrichs, *Phys. Chem. Chem. Phys.* **2005**, *7*, 3297-3305.
[182] F. Weigend, *Phys. Chem. Chem. Phys.* **2006**, *8*, 1057-1065.
[183] R. Dennington, T. Keith, J. Millam, *Semichem Inc., Shawnee Mission, KS* **2019**.
[184] V. Barone, M. Cossi, *J. Phys. Chem. A* **1998**, *102*, 1995-2001.
[185] M. Cossi, N. Rega, G. Scalmani, V. Barone, *J. Comput. Chem.* **2003**, *24*, 669-681.
[186] H. Fliegl, S. Taubert, O. Lehtonen, D. Sundholm, *Phys. Chem. Chem. Phys.* **2011**, *13*, 20500-20518.
[187] J. Jusélius, D. Sundholm, J. Gauss, *J. Chem. Phys.* **2004**, *121*, 3952-3963.
[188] A. D. Becke, *J. Chem. Phys.* **1993**, *98*, 5648-5652.
[189] P. J. Stephens, F. J. Devlin, C. F. Chabalowski, M. J. Frisch, *J. Phys. Chem.* **1994**, *98*, 11623-11627.
[190] A. Stanger, *J. Org. Chem.* **2010**, *75*, 2281-2288.
[191] M. Frisch, G. Trucks, H. Schlegel, G. Scuseria, M. Robb, J. Cheeseman, G. Scalmani, V. Barone, B. Mennucci, G. Petersson, Inc, **2013**.
[192] R. Krishnan, J. S. Binkley, R. Seeger, J. A. Pople, *J. Chem. Phys.* **1980**, *72*, 650-654.

[193] C. C. J. Roothaan, *Rev. Mod. Phys.* **1951**, *23*, 69.
[194] M. R. Niazi, E. Hamzehpoor, P. Ghamari, I. F. Perepichka, D. F. Perepichka, *Chem. Commun.* **2020**, *56*, 6432-6435.
[195] X. Zhang, X. Ji, S. Jiang, L. Liu, B. L. Weeks, Z. Zhang, *Green Chem.* **2011**, *13*, 1891-1896.
[196] S. Alvi, R. Ali, *Org. Biomol. Chem.* **2021**, *19*, 9732-9745.
[197] K. K. Park, L. K. Tsou, A. D. Hamilton, *Synth.* **2006**, *2006*, 3617-3620.
[198] R. K. Arafa, R. Brun, T. Wenzler, F. A. Tanious, W. D. Wilson, C. E. Stephens, D. W. Boykin, *J. Med. Chem.* **2005**, *48*, 5480-5488.
[199] L. R. Holloway, P. M. Bogie, Y. Lyon, R. R. Julian, R. J. Hooley, *Inorg. Chem.* **2017**, *56*, 11435-11442.
[200] S. Mushtaq, S. Bi, F. Zhang, M. M. Naseer, *New J. Chem.* **2022**, *46*, 17374-17385.
[201] G. C. Vougioukalakis, M. M. Roubelakis, M. Orfanopoulos, *J. Org. Chem.* **2010**, *75*, 4124-4130.
[202] K. Urakawa, M. Sumimoto, M. Arisawa, M. Matsuda, H. Ishikawa, *Angew. Chem. Int. Ed.* **2016**, *55*, 7432-7436.
[203] H. Sharma, P. K. Sharma, S. Das, *Chem. Commun.* **2020**, *56*, 11319-11322.
[204] X. Yang, D. Zhang, Y. Liao, D. Zhao, *J. Org. Chem.* **2020**, *85*, 5761-5770.
[205] K. Horii, R. Kishi, M. Nakano, D. Shiomi, K. Sato, T. Takui, A. Konishi, M. Yasuda, *J. Am. Chem. Soc.* **2022**, *144*, 3370-3375.
[206] I. H. Bae, H. S. Kim, Y. You, C. Chough, W. Choe, M. K. Seon, S. G. Lee, G. Keum, S. K. Jang, B. Moon Kim, *Eur. J. Med. Chem.* **2015**, *101*, 163-178.
[207] Y. Xie, Z. Li, X. Xu, H. Jiang, K. Chen, J. Ou, K. Liu, Y. Zhou, K. Luo, in *Molecules, Vol. 29*, **2024**.
[208] X. Zhu, F. Liu, X. Ba, Y. Wu, *Org. Lett.* **2022**, *24*, 5851-5854.
[209] J. J. Dressler, S. A. Miller, B. T. Meeuwsen, A. M. S. Riel, B. J. Dahl, *Tetrahedron* **2015**, *71*, 283-292.

9 List of Publications

- Ali S. Acan, Jonas O. Wenzel, Frank Breher, Joachim Podlech, A Stable Carbon-Centered Radical Showing Six Amphoteric Redox States, *Chem. Eur. J.* **2025**, 31, e202403670.
- Ali S. Acan, Jonas O. Wenzel, Joachim Podlech, Cyclopenta-Fused Polyaromatic Hydrocarbon (CP-PAH) Radicals: Synthesis, Characterization, and Quantum Chemical Calculations, *Chem. Eur. J.* e02467.

10 Acknowledgements

Mein aufrichtiger Dank gilt zuallererst Herrn Prof. Dr. Joachim Podlech. Ich danke ihm herzlich dafür, dass er mich in seine Arbeitsgruppe aufgenommen und mir die Möglichkeit gegeben hat, diese Arbeit im Rahmen meiner Promotion anzufertigen. Seine stets offene und zugewandte Art, seine Bereitschaft, fachliche Fragen jederzeit mit Geduld und Klarheit zu beantworten, sowie die vertrauensvolle und produktive Arbeitsatmosphäre, die er geschaffen hat, haben meine Zeit in der Arbeitsgruppe maßgeblich geprägt. Für sein kontinuierliches Vertrauen, seine fachliche Unterstützung und die wertvolle Freiheit, eigene Ideen zu verfolgen, bin ich ihm besonders dankbar.

Mein besonderer Dank gilt auch meinen Kolleginnen und Kollegen, die mich auf dem langen Weg der Promotion begleitet haben. Ich danke Inka Marten für die freundliche Aufnahme in die Arbeitsgruppe und für die coole Zeit, die wir gemeinsam auf der Konferenz in Toronto verbringen konnten. Ein großes Dankeschön geht auch an Felix Schumann für seine Offenheit und stetige Hilfsbereitschaft. Er war oft meine erste Anlaufstelle bei Fragen, Problemen oder den etwas ungewöhnlicheren Ideen im Labor. Zudem danke ich ihm für das Korrekturlesen dieser Arbeit. Zuletzt bedanke ich mich bei Jonas Springer, unserem letzten Neuzugang in der Gruppe.

An dieser Stelle möchte ich mich auch herzlich bei meinen ehemaligen Kollegen bedanken. Mein besonderer Dank gilt Maximilian Gutsche für die freundliche Aufnahme im Labor 405. Ich habe seine jederzeit angebotene Unterstützung sowie die unterhaltsamen Gespräche zwischendurch sehr geschätzt. Ebenso danke ich Stefan Herzog, meinem Vorgänger im Thema der Radikale. Seine Hilfsbereitschaft, auch über seine Promotionszeit hinaus, war für mich von großem Wert. Ich bin ihm dankbar für sein anhaltendes Interesse an meinem Fortschritt und den fachlichen Austausch, selbst nach seiner Zeit am KIT. Mein letzter Dank gilt Victor Vallejos González. Auch wenn unsere gemeinsame Zeit im Labor nur kurz war, danke ich ihm für die freundliche Aufnahme in die Arbeitsgruppe und die angenehme Zusammenarbeit.

Auch meinen Studenten möchte ich herzlich danken, sie haben maßgeblich zur Fertigstellung dieser Arbeit beigetragen. Mein besonderer Dank gilt dabei Rabea Schneider, meiner Vertieferstudentin, sowie Caitlin Möller, meiner Bachelorstudentin, für ihre engagierte Mitarbeit und wertvolle Unterstützung. Mein Dank geht außerdem an

Peter Mosur, meinen Auszubildenden, dessen praktische Unterstützung im Labor und bei der Synthese viele Aufgaben deutlich erleichtert hat.

Darüber hinaus möchte ich mich bei Jonas Wenzel bedanken, mit dem ich die Ehre hatte, zwei gemeinsame Publikationen zu veröffentlichen. Ich schätze die stets angenehme und erfolgreiche Zusammenarbeit sowie seine Unterstützung. Mein Dank gilt auch Mathis Mitha für seine Hilfe bei der Aufnahme der Fluoreszenzspektren, Johannes Werner für die Aufzeichnung der EPR-Spektren, sowie Fabian Rang für das Messen der DSC/TGA-Daten.

Mein Dank gilt der ebenso der Analytikabteilung des IOC – insbesondere Angelika Mösle und Lara Hirsch aus der Massenspektrometrie sowie Andreas Rapp aus der NMR-Abteilung – für ihre stets zuverlässige und kompetente Unterstützung.

Diese Arbeit wäre ohne die Unterstützung vieler nicht in dieser Form möglich gewesen. Ein herzliches Dankeschön geht an Patrick Kern, Dr. Julian Brückel, Savumiga Shanmugamani, Felix Schumann, Caroline Röttger und Milada Mergel und Aulona Sahiti. Danke, dass ihr euch die Zeit genommen habt, meine Arbeit aufmerksam zu lesen und mir mit konstruktivem Feedback zur Seite zu stehen. Eure Hilfe war von unschätzbarem Wert.

Ohne bestimmte Menschen, die mich nicht nur während der Promotion und des Studiums, sondern auch weit darüber hinaus begleitet und unterstützt haben, wäre dieser Abschluss nur halb so wertvoll. Mein besonderer Dank gilt dabei meinen beiden Mitbewohnern – Ahmet Acan, meinem Bruder, und Mehmet Güler, meinem Kumpel seit der fünften Klasse. Danke, dass ihr in guten wie in schwierigen Zeiten an meiner Seite wart. Eure Freundschaft und Unterstützung bedeutet mir sehr viel. Darüber hinaus möchte ich Aulona Sahiti für ihre warmherzige und fürsorgliche Art danken, Milada Mergel für ihre unbeabsichtigt humorvolle Art, die mich immer wieder zum Lachen bringt, Yuting Li für ihre Warmherzigkeit, die sie immer wieder auf besondere Weise zum Ausdruck bringt, sowie Lisa Wanner für ihre Live-Musik-Sessions im Labor – ein Erlebnis, das mir sicher in Erinnerung bleiben wird, auch wenn ich es nicht vermissen werde. Savumiga Shanmugamani danke ich für ihre ruhige Art, ihre Bescheidenheit und ihr offenes Ohr. Sie war oft eine meiner ersten Anlaufstellen bei Fragen, Problemen und vielen meiner Anliegen. Aleksandra Vranić, meiner Schreibnachbarin, die somit das gleiche Schicksal wie ich geteilt hat, danke ich herzlich für die wunderbare Schreibzeit, die von guter Unterhaltung und tiefgründigen Gesprächen geprägt war, auch wenn diese uns

nicht selten vom eigentlichen Schreiben abgehalten haben. Caroline Röttger danke ich für ihre positive Ausstrahlung und ihre humorvolle Art, mit der sie die Menschen um sich herum begeistert. Ich schätze die vielen bereichernden Gespräche und ihr stets offenes Ohr für meine Probleme sehr. Zuletzt möchte ich mich bei Patrick Kern bedanken. Seine lustige Art, die er nicht nur im Labor, sondern auch privat gezeigt hat, war für mich stets eine große Aufmunterung. Ich danke ihm für die tolle gemeinsame Zeit auf unserer langen Reise durch die Promotion. Ein Freund, mit dem ich viele Erfolge teilen durfte – sei es unsere Herausforderungen im Gym oder unser gemeinsam gemeistertes Ziel: der Marathon. Jedes dieser Erlebnisse hat mich geprägt und bleibt mir unvergesslich.

Abschließend möchte ich meiner Familie, darunter meiner Mutter, meinem Vater, meinem Bruder und meiner Schwester von Herzen danken. Ihr seid mir auf diesem langen Weg immer zur Seite gestanden und habt mich mit all eurer Kraft unterstützt. Danke für euer unerschütterliches Vertrauen, es hat mir mehr bedeutet, als Worte ausdrücken können.